MULTI-SCALE FATE AND TRANSPORT OF LNAPL UNDER VARYING SUBSURFACE FLOW CONDITIONS

Ph.D. THESIS

by

PANKAJ KUMAR GUPTA

DEPARTMENT OF HYDROLOGY
INDIAN INSTITUTE OF TECHNOLOGY ROORKEE
ROORKEE - 247 667 (INDIA)
AUGUST, 2018

MULTI-SCALE FATE AND TRANSPORT OF LNAPL UNDER VARYING SUBSURFACE FLOW CONDITIONS

A THESIS

Submitted in partial fulfilment of the requirements for the award of the degree

of

DOCTOR OF PHILOSOPHY

in

HYDROLOGY

by

PANKAJ KUMAR GUPTA

DEPARTMENT OF HYDROLOGY
INDIAN INSTITUTE OF TECHNOLOGY ROORKEE
ROORKEE – 247 667 (INDIA)
AUGUST, 2018

INDIAN INSTITUTE OF TECHNOLOGY ROORKEE
ROORKEE

CANDIDATE'S DECLARATION

I hereby certify that the work which is being presented in the thesis entitled "**MULTI-SCALE FATE AND TRANSPORT OF LNAPL UNDER VARYING SUBSURFACE FLOW CONDITIONS**" in partial fulfilment of the requirements for the award of the Degree of Doctor of Philosophy and submitted in the Department of Hydrology of the Indian Institute of Technology Roorkee is an authentic record of my own work carried out during a period from July, 2014 to August, 2018 under the supervision of Dr. Brijesh Kumar Yadav, Associate Professor, Department of Hydrology, Indian Institute of Technology Roorkee, Roorkee.

The matter presented in this thesis has not been submitted by me for the award of any other degree of this or any other institution.

(PANKAJ KUMAR GUPTA)

This is to certify that the above statement made by the candidate is correct to the best of my knowledge.

Dated: **(BRIJESH KUMAR YADAV)**
Supervisor

The Ph.D. Viva-Voce Examination of Mr. Pankaj Kumar Gupta, Research Scholar, has been held on……...

Chairman, SRC **Signature of External Examiner**

This is to certify that the student has made all the corrections in the thesis.

Signature of Supervisor **Head of the Department**
Date:

Acknowledgements

I express my deep sense of gratitude for all those helped me, supported me and cooperated with me in thesis work, not just for customary but with feelings starting with my foremost guiding person, my thesis supervisor Dr. Brijesh Kumar Yadav. Five years ago I had the pleasure of meeting Dr. Yadav in summer internship program at IIT Delhi. Since then, he has become my mentor. Over that time, he has pushed me to become a better academician and most importantly a better person and for that I am eternally grateful to him. I deeply express my gratitude to him for valuable guidance, constant support and immense patience that inspired me to work smoothly in completion of the thesis. His deep knowledge in the field and fruitful discussions brought many ideas in carrying out my research in this very attractive field since starting of the work. He supported me in every possible way without which this thesis could not be in its present form.

I wish to extend my sincere thanks to the past and present heads of the Department of Hydrology for the facilities extended to me. I thank the members of my S.R.C. Prof. N.K Goel, Prof. Himanshu Joshi and Prof. Sudipta Sarkar (Civil Engineering Dept.) for sparing their valuable suggestions and time. I want to record my gratitude to Prof. M. Perumal (D.R.C. Chairman), Prof. D.S. Arya, Dr. Manoj Kumar Jain and Dr. Sumit Sen for their help and giving me an opportunity to carry out this research work here. I express my regards and thanks to Prof. D.C. Singhal (Retired Professor) for his motivational support and providing me an opportunity to work with him in field. Thanks are also due to the staffs of Department, specially Shri Raj Kumar, Mr. Shayam, Mr. Deepak Kumar for providing me helpful co-operation throughout this research work.

I would like to thank to all my co-authors Dr. Basant Yadav (Cranfield University), Prof. P.N. Lens (IHE Delft), Dr. Hassana I. Mustapha (Federal University of Technology Minna), Dr. Shreejita Basu (Sustainable Northwest, Portland), Dr. Svetlana Sushkova (Southern Federal University), Mr. Abhishek (IIT Roorkee) for an opportunity of collaborative research works. I am also thankful to Prof. S. Majid Hassanizadeh (Utrecht University) for pre-submission review and his insightful and constructive comments and suggestions for improving a manuscript of this thesis work. I would also like to thank Mr. Jahangeer, Ms. Shachi, Mr.

Shashi Ranjan, Anooja Thomas, Ms. Anuradha Garg, Mr. Subhan Tiwari, Mr. Manik Goel and other fellow research scholars for their support, co-operation, friendship, and for making my time enjoyable.

Since starting I have had an enormous amount of support from Dr. Devesh Sharma (CURaj), Prof. K.C. Sharma (CURaj), Prof. M.M. Salunkhe (Former Vice-Chancellor, CURaj), Prof. Neeraj Gupta (CURaj), Prof.A.B.Gupta (MNIT), Dr. Baskhar Singh (CUJ), Dr. Deepak Kumar (GBPUAT), Dr. Vivek Agarwal (CDC), Dr. M.K. Sharma (NIH), Dr. Gopal Krishanan (NIH). I am thankful to you all.

I am thankful to the University Grant Commission (UGC) New Delhi for providing the financial support as Junior/Senior Research Fellowship (JRF/SRF), for this research work. I am equally thankful to Department of Science and Technology (DST) for proving research funding as Ramanujan Fellow award to Dr. Brijesh K Yadav. I am also thankful to AGU and IIT Roorkee for providing travel grants to attend AGU Fall Meeting 2017 and JpGU for JpGU meeting 2018 during this research work. I take this opportunity to thank SWINDON SEA-DAAD program and regional coordinator Prof. M.S. Babel (AIT Thailand) for providing full financial supports to attend international workshop at AIT Thailand.

Also, I would like to express my sincerest love and gratitude to my parents, wife and brothers, for their endless love and unflagging support, throughout my studies. Furthermore, I am also thankful to in-lows family members, and all others who directly or indirectly co-operated with me during this work.

Last, but not the least, I thank all those who inspired and helped me throughout my research.

Date Pankaj Kumar Gupta

Abstract

Pollution of soil-water resources by release of hydrocarbons such as light non-aqueous phase liquids (LNAPL) is of major concern because of their high water solubility and wide coverage under dynamic subsurface conditions. The rate of biodegradation of LNAPL is significantly governed by site prevailing environmental conditions and groundwater dynamics. Therefore, the focus of this study is to investigate LNAPL fate and transport under varying subsurface conditions using multi-scale laboratory experiments and numerical modeling.

A series of microcosms experiments were first performed to see the biodegradation capability of indigenous microbiota at different initial substrate conditions. A wide range of initial dissolved toluene (10-250 ppm), the selected LANPL, was taken in microcosms and periodically analysed for toluene concentration using GC-MS. The results show that LNAPL degradation increases with increasing initial dissolved LNAPL concentration up to about 50 ppm and remain maximum till about 100 ppm before started decreasing with increment in the LNAPL concentration. Microcosm experiments were then conducted to investigate the role of soil moisture and temperature on biodegradation of LNAPL. Each set of sterile and live microcosms having a different level of soil moisture content (20, 40, 60, 80% of θ_s) was kept at prevailing high room temperature (30±2°C) while the other was incubated at low soil-water temperature (10±0.5°C). It was found that biodegradation rate was high in case of high moisture contents i.e. 60-80% at 30°C than the microcosms having low moisture contents (40-20%) at the same soil-water temperature level. Results show that temperature of soil-water system was more sensitive to temperature at high moisture content as compared to the low moisture level.

Role of varying groundwater temperature on dissolution and biodegradation was also investigated in a continuous system of column setup. The column experiments were performed at four levels of groundwater temperature (4^0C, 20^0C, 28^0C and 36^0C) separately. Results of the column experiments show that accelerated dissolution rate of LNAPL at 36^0C temperature was observed followed by 28^0C, 20^0C and 4^0C cases. The biodegradation rates of LNAPL were found 0.002, 0.008, 0.012 and 0.015 mg-L/hr at groundwater temperature of 4^0C, 20^0C, 28^0C and 36^0C, respectively. Microbial number was found high in region of 140 ppm-150 ppm

dissolved toluene concentration at 28^0C and 36^0C temperature. Thereafter, the role of plant on different LNAPL compounds was investigated using treatment wetlands planted with and without *P. australis*. It was found that the plant significatly remove the LNAPL componts from root zone from plated treatment wetlands.

Thereafter, fate and transport of LNAPL under dynamic groundwater table was investigated using 2D sand tank setup having a dimension of 125cm-L × 90cm-H × 10cm-W integrated with an auxiliary column. Initially, tracer experiments were performed to determine soil-water flow and solute transport parameter for different groundwater fluctuation cases. The LNAPL transport experiment was then conducted under stable groundwater table condition followed by rapid, general and slow groundwater table fluctuation cases by rising/falling the groundwater table in 2, 4 and 8 hours, respectively. Numerically runs were conducted for the LNAPL transport under varying groundwater conditions for the experimental domain. The results show that a large LNAPL pool under fluctuating groundwater conditions contributes to high concentration of dissolved LNAPL plume in saturated zone. The transport of dissolved LNAPL plume was comparatively fast in case of rapid fluctuating groundwater case resulting in closely spaces concentration isolines of toluene contaminated plume. A high biodegradation rate was observed in regions having LNAPL concentration ranging from 140 - 160 ppm. The response of microbial community was found to be increasing as plume moved away from the pure phase pool.

To see the role of varying groundwater flow regimes, laboratory experiments and numerical runs were conducted using 3D sand tank setup. A constant water flux was allowed to flow through homogeneously packed 3D sand tank first for maintaining a base flow velocity of 1.2 m/day in the horizontal direction. The flow velocity was then increased/decreased by changing the water flux passing through the saturated zone by keeping the water table location at the same height. The LNAPL mass transfer coefficient was found to increase linearly with velocity and was estimated for the selected groundwater flow regimes varying from 0.083 to 0.129 cm/h. The observed high rate of degradation of toluene for faster flow velocities shows the dependency of the degradation kinetics on dissolved LNAPL concentration. The breakthrough curves at different ports showed that horizontal and transverse transport of the LNAPL was more prominent as compared to its vertical movement. The concentration of

dissolved toluene compared well with the simulated curves for the three cases of groundwater flow conditions.

Finally, a simulation-optimization approach was to evaluate the performance of bioremediation system with respect to its remediation time and cost. Design of in-situ bioremediation system consisted of three injection wells to provide oxygen/nutrients to polluted saturated zone and one extraction well to control toluene plume spreading. The extracted groundwater was used to recharge polluted unsaturated zone which significantly enhanced the removal of toluene by maintaining optimal soil moisture content. The biodegradation rates estimated in laboratory experiments having different combination of soil moisture and temperature were incorporated as sink of toluene in unsaturated zone. While BIOPLUME III was used to estimate the biodegradation rate in saturated zone by considering additional oxygen and nutrient supply by injection wells. These degradation rates were used in HYDRUS 3D to simulate the saturated and vadose zone soil-moisture flow and toluene transport. The data generated from simulation runs were used in Extreme Learning Machine (ELM)-Particle Swarm Optimization (PSO) tools to achieve the minimum remediation time and cost. Spreading of toluene was more through vadose zone having soil moisture level higher than 60% at 30°C than 10°C. A minimum cost of $106,570 and $107,245 was achieved when the soil moisture was 80% and 60%, respectively, at 30°C during one year. A small difference of remediation cost clearly demonstrate the effect of vadose zone recharge on accelerated biodegradation. However, for soil moisture content of 40% and 20%, the optimized cost was $120,306 and $126,905 in time frame of 1 year and 3 months and 1.5 years, respectively. The total cost estimated by the ELM-PSO approach was found minimum after fulfilling all the regulatory constraints of the contaminated site. Findings of this study are of direct use in applying engineered bioremediation techniques in field having dynamic subsurface conditions.

Keywords: Subsurface pollution, LNAPL, Bioremediation, Soil Moisture, Temperature, Groundwater Flow Regimes, Laboratory Experiments, Simulation-Optimization

Contents

List of Figures

List of Tables

Nomenclature

Symbols	*Meaning*
n	Porosity of soil
S_f	Fluid saturation in pore space
ρ_f	Fluid density
Q_f	Source or sink term
κ	Permeability tensor
k_{rf}	Relative permeability
μ_f	Fluid viscosity
g	Acceleration due to gravity
z	Elevation
p_f	Fluid pressure
f	Fluid which can be NAPL, water, and air
C_{if}	LNAPL compound in *f* phase
q_f	Discharge
D_{if}	Hydrodynamic dispersion coefficient
K_{if}	The dissolution rate of LNAPL
s	Biodegradation rate as sink term
τ	Tortuosity
D_L	Longitudinal hydrodynamic dispersion coefficient
D_T	Transvers hydrodynamic dispersion coefficient
V_x	Groundwater velocities
K	Saturated hydraulic conductivity
e	Effective porosity
C	Concentration of LNAPL
α_L	Longitudinal dynamic dispersivity
α_T	Transverse dynamic dispersivity
D^*	Diffusion coefficient
S_{max}	Adsorbed LNAPL concentration
K_L	Langmuir adsorption coefficient
K_{dis}	dissolution rate constant
$C_{\max}$	Equilibrium concentration
X	Mole fractions

μ_{max}	Maximum specific growth rate
C_0	The initial LNAPL concentration
X_0	Contaminate required to produce initial microbial density
C_w / C_{Liq}	Liquid LNAPL concentration
C_{gas}	Measured LNAPL vapour concentration
H_e	Henry's constant
k^*	LNAPL mass transfer coefficient
C_s	Effective solubility
R	Retardation factor
l_c	Characteristics LNAPL pool length
λ_{BIO}	Biodegradation decay term
μ_{max}	Maximum growth rate
K_V	Unsaturated hydraulic conductivity
θ_s	saturated soil water content
D_{LV}	Vadose zone longitudinal hydraulic dispersivity
D_{TV}	Vadose zone traverse hydraulic dispersivity
D_{WS}	Molecular diffusion coefficient in saturated zone
D_{WV}	Molecular diffusion coefficient in Vadose zone
F	Total cost of in-situ bioremediation system
W_F	Factor used to convert injection/extraction to their present value
e	Index denoting a potential injection/extraction locations
p_e	Injection/extraction rate at the location e
C_{pe}	Cost coefficient of injection/extraction
N_w	Total number of injection and extraction well
C_{lpe}	Installation cost of the well
I_{pe}	Zero-one integer for well existence
N_e	Total number of extraction well
i_r	Discount rate
C_{st}	Clean-up standard in observation well
H_e	Hydraulic head in a well at location e
Hi_{max}	Maximum hydraulic head allowed at injection well
Hi_{min}	Minimum hydraulic head allowed at injection well
$H_{e\,max}$	Maximum hydraulic head allowed at extraction well

$H_{e\min}$	Minimum hydraulic head allowed at extraction well
$p_{\min}$	Minimum injection rate
$p_{\max}$	Maximum extraction rate
N_0	Number of observation wells
C_{pi}	Injection cost
C_{pe}	Extraction cost

Acronyms and Abbreviations

POM	Polyoxymethylene
NAPL	Non-Aqueous Phase Liquids
DNAPL	Dense Non-Aqueous Phase Liquids
LNAPL	Light Non-Aqueous Phase Liquids
AST	Above Ground Storage Tank
UST	Below Gound Storage Tank
USEPA	United States Environmental Protection Agency
DRO	Diesel Range Organics
VF CWs	Vertical Flow Constructed Wetland
HFF	Horizontal Flow Constructed Wetland
HRRL	HPCL Rajasthan Refinery Limited
IOCL	Indian Oil Corporation Limited
HPCL	Hindustan Petroleum Corporation Limited
MRPL	Mangalore Refinery and Petrochemicals Limited
BPCL	Bharat Petroleum Corporation Limited
CPCL	Chennai Petroleum Corporation Limited
ONGC	Oil and Natural Gas Corporation Limited
NRL	Numaligarh Refinery Limited
BTCs	Break through Curves
MPNG,GOI	Ministry of Petroleum and Natural Gas, Government of India
BTEX	Benzene ,Toluene, Ethyl benzene, and Xylene
EUGRIS	European Groundwater and Contaminated Land Remediation Information System
MTBE	Methyl tert-butyl ether
ELM	Extreme Learning Machine
SVM	Support Vector Machine
SLFN	Single Hidden Layer Feed Forward Neural Network
PSO	Particle Swarm Optimization
SEM	Scanning Electron Microscopy

Chapter 1

Introduction

1.1 General

Pollution of natural resources due to release of several contaminants including hydrocarbons is a key human and ecological health concern. The hydrocarbons like non-aqueous phase liquids (NAPL), are of particular concern under varying environmental conditions because of their high sensitivity to subsurface variability, which enables them to spread widely in subsurface (Oostrom et al. 2000; Kim and Corapcioglu, 2003). The NAPL are not freely missible in water, but a small quantity of NAPL gets dissolved with water is sufficient enough to seriously degrade its quality. Based on their density, NAPL are classified as light and dense NAPL, known as LNAPL and DNAPL, respectively. The LNAPL are the most commonly encountered organic contaminants in subsurface due to their pervasive use, poor historic disposal practices, accidental releases during handling, storage or transfer at fuel manufacturing facilities, refineries, bulk product terminals, gas stations, airports, military bases, and from smaller scale storage at domestic properties, industrial facilities and farms (Essaid et al. 2015; Kumar et al. 2016; Srivastava et al. 2018). Typically, the main sources of LNAPL contaminants are above-ground storage tanks (AST) or underground storage tanks (UST) holding petrochemical products, generally occurs near petroleum and natural gas production sites, petrol stations (USEPA 2006a).

When released in ample amount at (sub)-surface, the LNAPL moves downward through the unsaturated zone and are mostly retained by the water table due to their lighter density as shown in (figure 1.1). While, DNAPL penetrate water table and continues moving downwards until any bed/hard rock is encountered (Yadav and Hassanizadeh, 2011). The LNAPL pool retained at the water table, starts dissolving with groundwater and subsequently moves to surrounding locations due to advection, diffusion and dispersion mechanisms of mass transport (Chrysikopoulos, 1995; Narayanan et al. 1998a, b; Fagerlund et al. 2008; Yadav et al 2013). Groundwater flow regimes play a significant role in the dissolution and spreading of pure phase LNAPL and in movement of dissolved LNAPL to the surrounding locations (Soga et al. 2004; Sulaymon and Gzar, 2011). Dynamic nature of groundwater table causes spreading of LNAPL in smear zone,

which considerably increases the LNAPL-water interphase area resulting in accelerated dissolution of the pure phase LNAPL in surrounding groundwater resource (Nambi and Powers, 2000; Dobson et al. 2007). The dissolved LNAPL moves along with groundwater which forms a plume features with varying concentration of LNAPL compounds (Vasudevan et al. 2014; 2015). Thus, it is important to understand the fate and transport of LNAPL thoroughly under varying subsurface conditions in order to frame a suitable engineered remediation strategy for these contaminants.

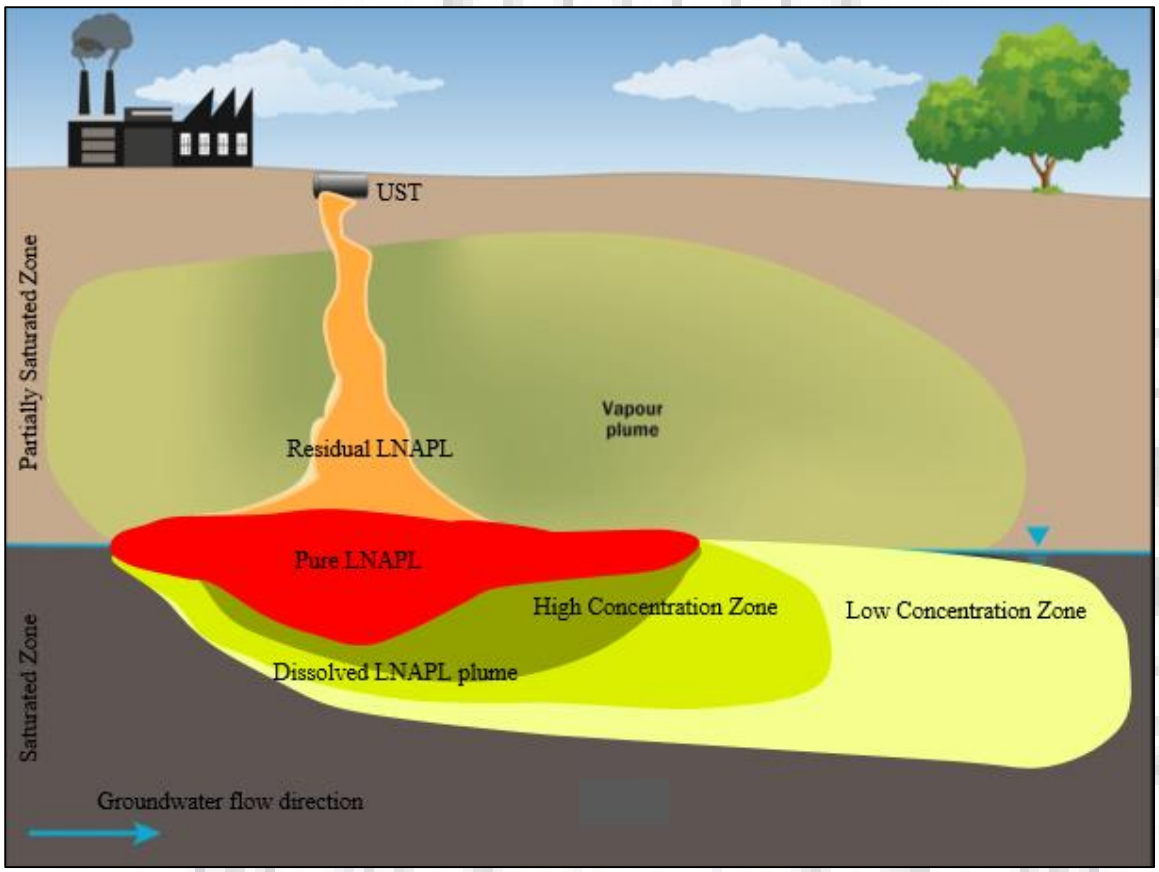

Figure 1.1. Illustrative diagram of LNAPL release from a source nearby to surface and its subsequent movement in variably saturated zone.

Amongst the physical, chemical and biological methods used for the treatment of LNAPL contaminated sites, bioremediation is considered as one of the most environmental benign remediation options. Though the natural bioremediation is safer and less disruptive treatment technique than other conventional technologies, it takes considerably long time to restore the polluted site under prevailing site environmental conditions (Yadav et al. 2012; Basu et al. 2015). Therefore, engineered bioremediation techniques like biostimulation and bioaugmentation are gaining popularity due to their faster remediating

rates. In engineered bioremediation, microbial population and their surrounding environmental conditions are technically modified for hastening the process of biodegradation which is achieved by maintaining favourable environmental conditions, addition of nutrients, and/or bacterial strain to the polluted site. Out of several environmental factors, temperature variations, soil moisture content, nutrients and oxygen availability play very crucial role in maintaining the biodegradation rate of LNAPL compounds in subsurface (Yadav and Hassanizadeh 2011; Kamaruddin et al. 2011).

Fate and transport of LNAPL in subsurface are highly affected by soil moisture level governed by fluctuating groundwater table and evaporation/precipitation fluxes at top boundary. Variation in groundwater table significantly affects the behaviors of LNAPL transport in subsurface. Dynamic groundwater flow regimes enhance the dissolution, volatilization and mobilization of LNAPL in smear zone which may causes large polluting (un)saturated zones. The hydraulic force from fluctuating groundwater table also remobilizes the residual LNAPL present in vadose zone. It also leads to enhanced volatilization, dissolution and subsequent advective transport of LNAPL in the contaminated subsurface system (Kim and Corapcioglu, 2003). Conversely, these fluctuations can provide additional oxygen which significantly enhances microbial activities in polluted zones. Aerobic biodegradation of LNAPL generally increases due to favourable amended subsurface conditions (Dobson et al. 2007).

The soil moisture content and its distribution also regulates the water film thickness which affects the diffusion of substrate, oxygen and nutrients to the microbes which are mostly attached to the soil partcles. A high soil moisture content accelerates the aqueous mass transfer and increases the bioavailability of LNAPL along with a high concentration load to the underlying groundwater resources. Conversely, high moisture contents intercept the oxygen flux which may considerably affect microbial biodegradation of LNAPL pollutants in vadose zone (Yadav and Hassanizadeh, 2011). On the other hand, optimal temperature range helps in moderating physiological behavior of potential microbes which support accelerated biodegradation (Kulkarni et al. 2017). While, a low soil temperature generally decreases the enzyme production rate which is a complementary part of the metabolic pathway of LNAPL degradation in the cellular tissues. Low temperature also reduces the fluidity and permeability of the cellular membrane which hinders the nutrient, oxygen and contaminant uptake. Most of the studies on LNAPL biodegradation are conducted at near-optimal soil moisture conditions

and constant room temperature and very limited studies have been conducted on biodegradation of LNAPL contaminated subsurface having varying soil moisture content and temperature conditions. Moreover, the impact of soil moisture and temperature variations on biodegradation rate has been reported separately and their integrated impact is need to be investigated (Garg et al. 2017).

Plants can also provide a suitable bioremediation environment by maintaining favourable conditions for metabolism of microorganisms (Yadav et al. 2013). Plants at polluted sites can improve the pollutant removal efficiency by enhancing the microbial diversity and their metabolic activity. Plants play important role in improving microbial activity by improved supply of oxygen, direct uptake, and release of root exudates in the rhizospheric zone which ultimately enhance the degradation rate of LNAPL (Boonsaner et al. 2011, Mustapha et al. 2018a, b). Experiments are required to understand the dynamics and functions of the soil-plant-atmospheric continuum which can help in improving the conevtional bioremdiation systems.

For maintaining favourable conditions for engineered bioremediation, injection wells are commonly used to supply electron acceptors, nutrients laden water, hot air, along with seeding of potential microbes in the contaminated zone. Extraction wells are used in such systems for controlling LNAPL plume spreading in down-gradient locations (Shieh and Peralta, 2005; Prasad et al. 2008; 2009; Kumar et al. 2013, 2015; Yadav et al. 2016). Maintaining desired environmental balance of these parameters directly in the field is quite costly and a very difficult task for large scale sites. The cost for installation/operation and maintenance of injection and extraction wells requires a substantial budget in designing bioremdiation system for such types of polluted sites. Thus, the optimum injection and extraction pumping rates to achieve the desired treatment performance in minimum time and cost is a key issue in designing bioremediation systems (Kumar et al 2013; Yadav et al. 2017). Thus, a better understanding of fate and transport of LNAPL contaminants and its bioremediation under varying subsurface conditions will help in optimal designing and implementation of bioremedial measures under site prevailing conditions.

1.2 Research Gaps

Majority of the earlier works focused on fate and transport of dissolved LNAPL in subsurface either using small scale laboratory experiments or numerically by considering simplified conditions (Essaid et al.2015; Tomlinson et al. 2015). Variation in subsurface conditions affects soil-water parameters, LNAPL pool behaviour and to the dissolved LNAPL plume in under/over-lying (un)saturated zone. Impact of vadose zone factors like temperature, soil moisture, oxygen and nutrient levels have been investigated individually. However, combined impacts of these environmental parameters on subsurface processes are still awaited. Impact of dynamic groundwater flow regimes on LNAPL fate and transport is not investigated in subsurface. Further, most of the earlier studies related to designing the bioremediation system were limited to saturated zone and have used mostly data based optimization approaches (Yadav et al. 2016; 2017). One cannot ignore the role of vadose zone in treating the saturated zone as most of the LNAPL leakages take place nearby to surface before polluting the underlying saturated zone. Thus, it is important to investigate the performance of a designed bioremediation system for the entire subsurface by considering role of vadose zone variables. Further, upscaling of the microcosm findings to continuous experimental setups like column and tank scale experiments are required to study the fate and transport of LNAPL in real field like conditions. Consideration of the entire subsurface system as a whole along with the integrated role of different subsurface environmental conditions can also contribute immensely in understanding of fate and transport of LNAPL in subsurface.

Thus, this thesis is novel as the impact of soil moisture content and temperature of groundwater on biodegradation of LNAPL were studied earlier too, however attention to their combined effect was not considered in the past. The present study considers their combined effect on biodegradation of dissolved toluene through a series of microcosm experiments. An extensive study is conducted to investigate the impact of water table dynamics on LNAPL transport using 2-D sand tank experiments. Fluctuations in the water table due to various reasons including tidal effects have a profound influence on the spatial distribution, dissolution and biodegradation of LNAPL in the subsurface environment. Similarly, the effect of changes in groundwater flow velocity and flow regimes have significant effect on the fate and transport of LNAPL, the same has been studied using 3-D sand tank and experimental results are compared well with simulated

results for three cases of flow conditions. Further, the role of plants on bioremediation of LNAPL studied using treatment wetlands adds to the novelty. The experiments were conducted using a column setup along with a small scale treatment wetland, with and without plants. Furthermore, the study considers both vertical as well as horizontal/transverse flow LNAPL in the vadose and saturated zones respectively. This coupled effect has not been addressed adequately in the previous studies. Likewise, the use of injection/extraction wells to enhance biodegradation has been studies for saturated medium only in the past, however, in this study, the unsaturated zone has also been considered taking various soil moisture content at different temperature to determine the remedial cost and remediation time. Lastly, the knowledge acquired in this study contributes extensively towards understanding the impact of dynamic subsurface conditions on engineered bioremediation techniques.

1.3 The Objectives of the Study

The focus of this study is to investigate the behaviour of LNAPL and its bioremediation under varying subsurface conditions using a series of laboratory experiments and numerical runs. The specific objectives of this research are:

1. Understanding fate and transport of LNAPL in variably saturated subsurface environment.
2. To investigate the release dynamics of pure phase LNAPL in subsurface.
3. To investigate the impact of water table dynamics on fate and transport of LNAPL in subsurface.
4. To investigate the impact of varying groundwater velocities on dissolution and movement of pure phase LNAPL in multi-dimension zones.
5. To investigate the role of vadose zone conditions on fate and transport of LNAPL in subsurface.

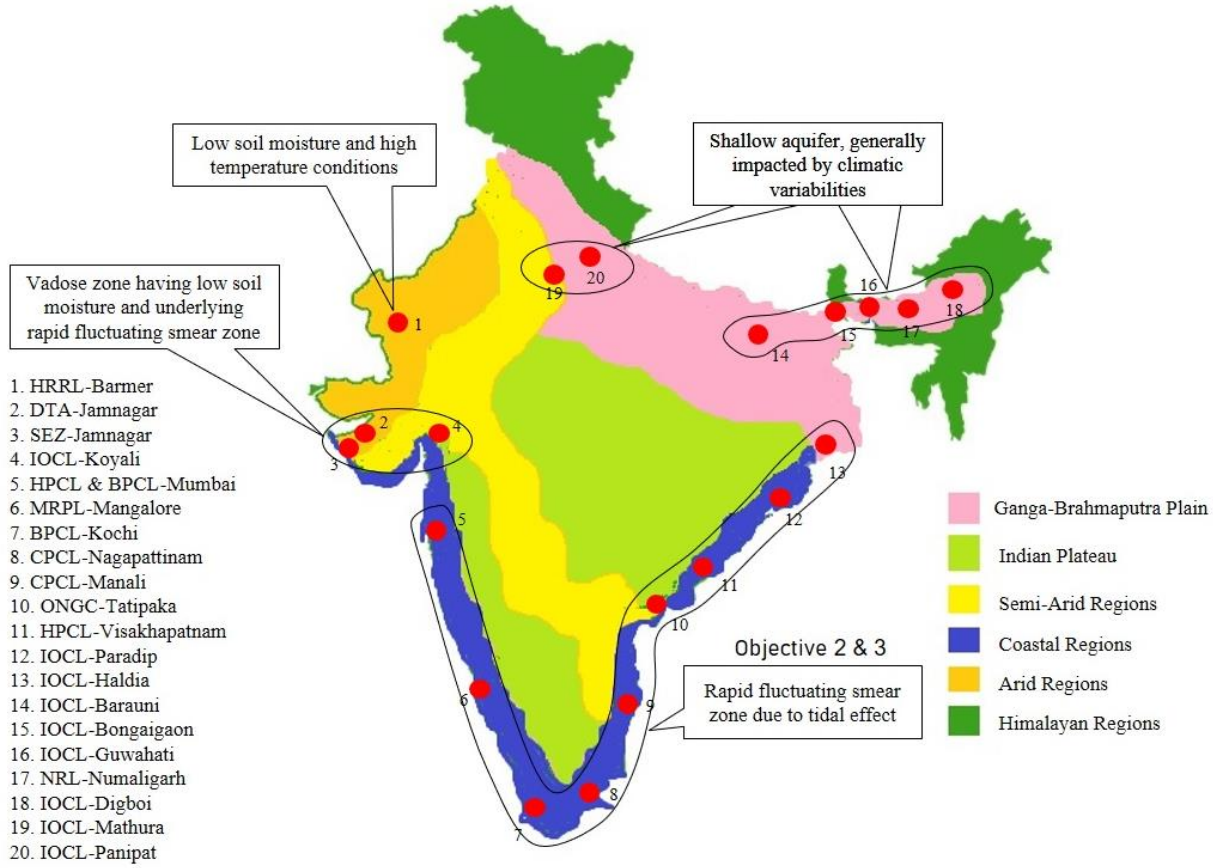

Figure 1.2: Scope of this study to various potential sites due to existing petrochemical industries and refineries located in the different climatic zone of India.

1.4 Scope of the Work

Identification of suitable remedial measures for LNAPL polluted sites require a better understanding of fate and transport of target pollutants under varying subsurface conditions. Therefore, in this study, behaviour of LNAPL from the release point to the downgradient receptors and its degradation is investigated under varying subsurface conditions. In context to India, the petroleum production and refineries are increaseing very fast. According to annual report 2017-18 of the Ministry of Petroleum and Natural Gas, Government of India, 247.6 million metric tons per year addition capacity of all refineries of India was developed in 2017. Most of the petroleum production industries and refineries are located in coastal zones having arid and semi-arid climatic conditions where the dynamic soil moisture level and temperature conditions significantly affects the

groundwater flow regimes. Figure 1.2 highlights distribution of refineries and petrochemical industries. the results of this study can help in designing cost-effective treatment technique of bioremediation at hydrocarbon polluted sites including.

1.5 Organization of Thesis

The thesis includes five chapters in addition to this introductory chapter. In introductory chapter, the background and focus of the study along with the different objectives and scope of the research work is discussed.

Chapter 2: An overview of literature pertaining to fate and transport of LNAPL in subsurface under varying subsurface conditions is presented. The basis of soil-water flow and mass transport processes are discussed first followed by a discussion on role of varying subsurface conditions. A review of literature on multi-scale laboratory investigations and numerical modeling of governing mechanisms is conducted next. Thereafter, previous research work and their findings of bioremediation of LNAPL polluted sites are highlighted.

Chapter 3: A detailed methodology adopted to fulfil the objectives of this study is presented in chapter 3. Materials and methods followed by analytical tools and microbiological assessment used in different laboratory experiments are presented first. Microcosms experiments used for the estimation of biodegradation rates at different initial substrate concentrations are then discussed along with description of microcosms experiments conducted to investigate combined role of soil moisture and soil temperature conditions. One dimensional column experiments are presented next to investigate the role of groundwater temperature in continuous system followed by role of plant in treatment wetland to decontaminate LNAPL contaminated water. Thereafter, methodology related to fate and transport of LNAPL under dynamic groundwater table using two dimensional sand tank setup is presented in detail. Impact of groundwater flow velocity on LNAPL behaviour is described next using the three dimensional sand tank experiments. Subsequently, simulation-optimization approach to remediate LNAPL contaminated vadose and saturated zones is described in detail for varying soil moisture and temperature conditions.

Chapter 4: In this chapter, results and discussions of different laboratory experiments and numerical runs used to investigate the fate and transport of LNAPL under varying subsurface conditions are presented. The results of microcosms experiments performed to investigate impact of substrate concentration, soil moisture level and temperature on biodegradation of dissolved LNAPL are highlighted. Next, the findings of one-dimensional column experiments and numerical runs are presented to discuss the role of varying groundwater temperature on fate and transport of LNAPL in continuous system. Later on, the performance of plant to decontaminate LNAPL polluted sites is discussed based of laboratory and modelling results.

Thereafter, the fate and transport of LNAPL under stable and fluctuating groundwater table conditions is discussed based on results of two-dimensional sand tank experiments and numerical modelling. Movement of dissolved LNAPL plume under different groundwater table fluctuation conditions are emphasized along with biodegradation rates and microbial growth. Similarly, the behaviour of LNAPL under varying subsurface flow conditions is discussed on the basis of results of three dimensional sand tank experiments in the later part of this chapter. Finally, a bioremediation system design to decontaminate LNAPL polluted vadose zone having varying soil moisture contents and temperature along with the polluted saturated zone is presented. Bioremediation efficiency is discussed in last with respect to optimize injection and extraction rates to minimize the remediation cost and maximize the removal of LNAPL from subsurface.

Chapter 5: It summarizes the research contributions with conclusions, suggestions for future research in this area. The background information related to this study, such as experimental setups used to investigate fate and transport of LNAPL have been placed in appendices. Furthermore, pictures of plates of microbial counting during column and two dimensional sand tank experiments are presented next. Methods and calibration curves of GC-MS and random generated injection and extraction rates have been placed in last.

Chapter 2

Literature Review

In this chapter, a state of art of literatures are presented on LNAPL fate and transport under varying subsurface conditions. LNAPL sources, its types and their toxicity is discussed first. Fate and transport of LNAPL in subsurface is presented next followed by details of governing mechanism. Thereafter, a detail literature on factors affecting biodegradation of LNAPL is discussed with emphasis of impact of soil moisture levels and temperature condition. Earlier studies on LNAPL movement under dynamic groundwater table conditions and groundwater flow velocities are discussed next. Then, details of bioremediation along with treatment wetlands for LNAPL removal are presented followed by highlights of research gaps.

2.1 LNAPL: Sources, Types and Toxicity

Petroleum hydrocarbons are the natural mixes of crude oils, containing hydrogen and carbon in straight and fragrant chain. These chemicals are the most extensive pollutant of soil and groundwater systems which are categorized as Dense- or Light Non Aqueous Phase Liquid (DNAPL and LNAPL respectively) based on their relative density (Margesin et al. 2000). The LNAPL include benzene, toluene, ethylbenzene and xylene (BTEX), fluorine, styrene, naphthalene and other nonaromatic constituents of petroleum products (Kumar et al. 2015). Table 2.1 presents the chemical and physical characteristics of some LNAPL compounds reported in groundwater. Refinery and petrochemical industrial discharges are the main sources of these hydrocarbons in subsurface (Kurniawan et al. 2006; Fuentes et al. 2014). LNAPL are also utilized in other industries in form of industrial feedstock, part in fuel and as a solvent in paints, coatings, gums, pitches etc. (Nema and Gupta, 1999; Shpiner et al. 2009).

Release of LNAPL in subsurface significantly affects the soil-water functions resulting in the continuous loss of sustaining living organisms (Wipfler et al. 2004). The LNAPL are immiscible in nature and even a small amount is enough to degrade the quality of groundwater (Jha et al. 1999; Babel and Kurniawan, 2003; Nema and Gupta, 2003; Saien and Shahrezaei, 2012; Mohanty et al. 2013; Machiwal and Jha, 2015;

Chabakdhara et al. 2016) and can alter the human metabolism if exposed to more than permissible limit. These contaminants are reported as neurotoxic and carcinogenic in nature (Tormoehlen et al. 2014). The LNAPL compounds are detrimental to the environment and disrupting to the habitats of potential micro-biota in soil-water systems. Therefore, LNAPL are of serious concern for safe drinking water production and ecological sustainability (Essaid et al. 2015).

Table 2.1: Physicochemical properties of some LNAPL compounds polluting soil-water systems.

Property	*Benzene*	*Toluene*	*Ethyl benzene*	*o,m,p Xylene*
Molecular weight (g mol^{-1})[a]	78.1	92.1	106.2	106.2
Water Solubility (mg L^{-1})[b]	1780	535	152	175,135,198
Density (liquid) (g cm^{-3})[c] at 293K	0.88	0.87	0.87	0.88, 0.88, 0.86
Henry's constant (dimensionless) at 298K[d]	0.23	0.26	0.345	0.2084, 0.3139, 0.3139
Log (K_{ow})[a]	2.13	2.69	3.15	3.12, 3.20, 3.20

[a] Boonsaner et al. 2011;[b] EUGRIS; [c]Weast and Astle 1981; [d]Yadav et al. 2012

2.2 Fate and Transport of LNAPL in Subsurface

When LNAPL are released into soil-water system, they can percolate through the unsaturated zone and eventually reach the capillary fringe before accumulating over the water table (Wipfler et al. 2004). In partially saturated zone, LNAPL show a complex three-phase (gas, water, and organic liquid) flow behaviours which is affected by factors such as heterogeneity in soil matrix and, spatial and temporal variability in soil water saturations, temperature and water table dynamics (Yang et al. 2017). Their transport in groundwater systems is governed by gravity, viscous forces, and capillary forces. Multiphase behaviors of LNAPL in soil may vary in different porous media depending upon their pore structure and wetting tendencies (Gharedaghloo and Price, 2017). The soil

water content of vadose zone also controls the migration and spatial distribution of LNAPL in unsaturated zone (Singh et.al. 2011). The soil water content varies with time due to spatial variability of soil properties and also with recharge from precipitation. Hence, following a spill, a fraction of LNAPL is trapped in soil matrix known as residual saturation in the form of isolated ganglia (Kechavarzi et al. 2008). For large spills, the LNAPL head dominates the combined forces of buoyancy and capillarity displacing water from the capillary fringe and can penetrates the water table (Das et at. 2002; 2004; Rahman, 2008; Raoof and Hassanizadeh, 2013; Shuai et al. 2014; D'Alessio et al. 2014; 2015). The formation of LNAPL lens also depends on the water table fluctuations and underlying groundwater flow conditions (Kim and Corapcioglu, 2003). The LNAPL pool then starts dissolving into groundwater and subsequently moves to surrounding downgradient locations (Das, 2002; Das and Nassei, 2003; Das and Mizzaei, 2012; Vasudevan et al. 2014). Transport of the dissolved LNAPL through inter-connected pores is predominantly governed by hydrodynamic dispersion under dynamic groundwater flow regimes (Rahman et.at. 2007; 2009; 2013). While, LNAPL vapour moves through unsaturated zone causing upward movement of contaminants which is also affected by groundwater table fluctuation (Wang et al. 2003; Baedecker et al. 2011). Movement of LNAPL under varying subsurface conditions are poorly understood for soil-water systems. Thus, it is required to investigate the fate and transport of LNAPL in subsurface from release point to the saturated zone considering.

2.3 Governing Mechanisms of LNAPL Movement

LNAPL into soil-water resources create a multi-phase flow system. The Darcy's equation coupled with mass balance results in a following multiphase flow equation used for describing the LNAPL transport in subsurface (Essaid et al. 2015).

$$\frac{\partial}{\partial t}(nS_f\rho_f) = \nabla.(\rho_f \frac{\kappa k_{rf}}{\mu_f}(\nabla p_f + \rho_f g \nabla z)) \pm Q_f \qquad (2.1)$$

Where n is porosity of soil [L^3L^{-3}], S_f is fluid saturation in pore space [L^3L^{-3}], ρ_f is the fluid density [ML^{-3}], Q_f is sink or source term [$ML^{-3}T^{-1}$] (source resulted from remobilization), κ is the permeability tensor [L^{-2}], k_{rf} is the relative permeability [-], μ_f is the fluid viscosity [$ML^{-1}T^{-1}$], g is acceleration due to gravity [LT^{-2}], z is elevation [L],

p_f is fluid pressure [$ML^{-1}T^{-2}$], f is fluid which can be air, water or LNAPL. While dissolved phase LNAPL transport in saturated zone as (Essaid et al. 2015):

$$\frac{\partial}{\partial t}(\phi S_f C_{if}) = -\nabla.(q_f C_{if}) + \nabla.(nS_f D_{if}.\nabla C_{if}) + K_{if} - S \tag{2.2}$$

Where C_{if} is NAPL compound in f phase [ML^{-3}], q_f is discharge through soil profile [LT^{-1}], While K_{if} is the dissolution rate of LNAPL [$ML^{-3}T^{-1}$] can be observed using characteristic length of LNAPL pool and equilibrium concentration in dissolved phase. Likewise, S is biodegradation rate [$ML^{-3}T^{-1}$] (as sink term) can be obtained using (control and live) microcosms experiments. D_{if} is hydrodynamic dispersion [L^2T^{-1}] which can be obtained using breakthrough curves (BTCs) of tracer transport experiment. Mechanisms wise simplified governing mass transport equations are listed below:

Advective Flux: Advection is the movement of the contaminant due to the flow velocity of aqueous phase. Mathematically, the advective flux as (Fetter 1994; Fetter et al. 2017):

$$J_{adv} = v\theta C_{if} = q_f C_{if} \tag{2.3}$$

Where v is the pore-water velocity [LT^{-1}], and θ is the volumetric water content [L^3L^{-3}].

Diffusive Flux: Diffusion is described by Fick's law which states that the net rate of contaminant transport is proportional to the negative gradient of its concentration. For the unsaturated porous medium, Fick's law can be modified as:

$$J_{diff} = -\tau D_O \theta \frac{\partial c_{if}}{\partial z} = -D_m \theta \frac{\partial c_{if}}{\partial z} \tag{2.4}$$

Where τ is tortuosity, generally defined as the ratio of the average length of all particle path lines passing through a given cross sectional area during a unit time period to the width of the sample. D_m and D_o are the molecular diffusion coefficients and free water diffusivity, respectively [L^2T^{-1}].

Dispersive Flux: At a microscopic scale, the dispersion occurs because of the velocity variations within the pores and also due to the tortuous movement of the fluid around the

soil grains. At macroscopic scale, dispersion results from the inter fingering of the materials of different permeability. Mathematically, dispersion (mechanical) is given in the same way as (molecular) diffusion by the Fick's law as:

$$J_{dis} = -\alpha_L v \frac{\partial C_{if}}{\partial z} = -\alpha_L \frac{q}{\theta} \frac{\partial C_{if}}{\partial z} = D_{if} . \nabla C_{if} \tag{2.5}$$

where, α_L is the longitudinal dispersivity [L] of porous media in the flow direction and v is the pore velocity. D_{if} is hydrodynamic dispersivity which is the summation of molecular diffusion and mechanical dispersion flux as:

$$D_{if} = \tau D_* + D_x \tag{2.6}$$

The diffusive flux can be estimated by the product of the tortuosity of the medium i.e. 1.43 and the coefficient of diffusion of toluene i.e. 6.3×10^{-6} [cm^2 s^{-1}] by. Furthermore, D_{if} can be obtained (Perkins and Johnston, 1963; Sulaymon and Gzar 2011) using equation 2.7 by applying BTCs of tracer transport experiment.:

$$D_{if} = 0.5\left[\frac{t_{84} - t_{16}}{2t_{50}}\right] v \tag{2.7}$$

Where t_{84}, t_{16}, t_{50} is time corresponding to 86%, 16% and 50% respectively of relative concentration of BTCs. Ratio of LNAPL transported by advection and by mechanical dispersion or diffusion known as Peclet number (P_e) (dimensionless). It can use to evaluate the relative contribution of hydrodynamic dispersion and diffusion to LNAPL transport as (equation 2.8):

$$P_e = \frac{v \times r}{D_{if}} \tag{2.8}$$

Where r is radius or length of LNAPL pool. Likewise, Sherwood number (S_h) (dimensionless) is ratio of dissolution rate and diffusion as:

$$S_h = \frac{k_{if}}{D_*} \tag{2.9}$$

k_{if} can be estimated as:

$$k_{if} = n\sqrt{\frac{4D_{if}v}{\pi l_c}} \tag{2.10}$$

Where l_c is characteristic length of LNAPL pool. The LNAPL can be partitioning into gas phase i.e. volatilization, aqueous phase i.e. dissolution, and solid phase i.e. sorption. Furthermore, biodegradation of LNAPL in subsurface is governed by natural agents like microbes, plants. An overview of governing processes used to simulate fate of LNAPL is listed in Table 2.2.

Sink term in flow and transport equation of LNAPL represent the attenuation and biodegradation by microbes and plant of these contaminants in soil-water system. Efforts has been made in past to increase the rate of removal using various techniques. Conventionally, physic-chemical treatments are used to decontaminate the polluted sites which are reviewed in detail by Khan et al. (2004). Soil washing, soil flushing, air sparging or SVE (soil vapor extraction), and pump-and-treat are common physical treatment methods for LNAPL polluted sites (Albergaria et al. 2012). In soil flushing, polluted soil can be treated with water or reagents while in soil washing water is used with other physical separation/scrubbing tools. Concentrated soil fraction containing the LNAPL can be treated effectively by this method. In pump-and-treat method, polluted groundwater is extracted from saturated zone and treated at surface using appropriate treatment techniques (Boarden et al. 1992). It is one of the most popular techniques of LNAPL remediation but it depresses the groundwater level and leaves residuals sorbed to the soil. Likewise, air stripping is technique in which (hot)-air injected in polluted saturated zone. Air sparging or commonly known as SVE is an *in-situ* remediation technique, mainly for LNAPL polluted sites. It basically involves the injection of air into the saturated zone and allowing venting through the unsaturated zone to remove LNAPL contaminants (Frutos et al. 2010).

In chemical treatment methods like oxygen releasing compounds (calcium peroxide, urea peroxide, and magnesium peroxide) are injected (Bianchi et al. 1994) for treatment of LNAPL polluted zones. Chemical oxidation using permanganate are another potential technique for treating LNAPL polluted sites (Forsey et al. 2010). Certain chemicals (oxidants or other amendments) are injected directly into the contaminated zone (Franzetti et al.2008; Tobiszewski et al. 2012). These chemicals destroy LNAPL constituents in place and forms by products such as carbon dioxide, water, and chlorides. Commonly used chemical oxidants for LNAPL treatment are potassium permanganate,

Table 2.2: Overview of mathematical expressions used to simulate LNAPL fate mechanism in subsurface.

<table>
<tr><th>Mechanisms</th><th>Governing Equations</th><th>Descriptions</th></tr>
<tr><td>Volatilization</td><td>$C_{gas} = H\frac{C_{liq}}{RT}$</td><td>H = Henry's constant [Pa L mol^{-1}], R = Universal gas constant (8.31 J mol^{-1}K^{-1}), T = absolute temperature [K].</td></tr>
<tr><td>Dissolution</td><td>$\frac{\partial C}{\partial t} = K_{dis}(C_{max} - C_w)$
$C_{max} = SX$</td><td>K_{dis}= Dissolution rate constant [T^{-1}], C_{max} = Equilibrium concentration [ML^{-3}], C_w= LNAPL concentration in water [ML^{-3}], S = Solubility limits, X = mole fractions.</td></tr>
<tr><td>Biodegradation
$-\frac{\partial C}{\partial t} = \mu_{max} C\left(\frac{Co+Xo-C}{Ks+C}\right)$
Kinetics model | Condition | Equation | Rate constant
Zero order (Constant) | X_o>>C_o; C_o>>K_s | $-\frac{\partial C}{\partial t} = k_o$ | $k_o = \boldsymbol{\mu}_{max}X_o$
First order (Linear) | X_o>>C_o; K_s>> C_o | $-\frac{\partial C}{\partial t} = k_1 C$ | $k_1 = \boldsymbol{\mu}_{max}X_o/ K_s$
Monod | X_o>>C_o | $-\frac{\partial C}{\partial t} = k_m C/(K_s+C)$ | $k_m = \boldsymbol{\mu}_{max}X_o$
Logistic | K_s>> C_o | $-\frac{\partial C}{\partial t} = k_1 C/(C_o+ X_o-C)$ | $k_1 = X_o/ K_s$
Logarithmic | K_s>> C_o | $-\frac{\partial C}{\partial t} = k /(C_o+ X_o-C)$ | $K = \boldsymbol{\mu}_{max}$</td><td>$\boldsymbol{\mu}_{max}$ =Maximum specific growth rate, C = pollutant's concentration (at time = t), C_o = pollutant's concentration (at time = 0) and X_o = Contaminate concentration needed to produce initial microbial density, $\boldsymbol{\mu}_{max}$ and K_m = kinetics parameters, K_s = Substrate affinities constant, $Y_{s/x}$ and S_{min} = stoichiometric parameters.</td></tr>
</table>

hydrogen peroxide, sodium permanganate and ozone. However, these techniques are expensive and sometimes disturb the indigenous biota (Chabukdhara et al. 2016) Moreover, these techniques might result in incomplete mass removal and are often infeasible in remote locations (Van Stempvoort and Biggar, 2008; Olson and Sale 2015). Hence, environmental benign techniques like bioremediation is needed to be investigated thoroughly under prevailing site conditions.

As natural attenuation of LNAPL compounds in contaminated soil-water systems is quite slow in degrading the contaminants to reach upto the acceptable level, especially under the stressed environmental conditions (Shimp et al. 1993; Schnoor et al. 1995; Chapelle, 1999; Raifai et al. 2005; Yadav et al. 2013, Gupta and Yadav, 2017). Bioremediation has been used to remove LNAPL without affecting further environmental damage (Rifai et al. 2000). Engineered bioremediation techniques are gaining popularity due to their faster-remediating rates particularly for sites facing extreme environmental conditions (Bento et al. 2005). The engineered bioremediation is achieved by maintaining favorable environmental conditions like soil moisture level, pH, salinity and temperature of the target site (Yadav and Hassanizadeh, 2011). This can be performed by applying surface recharge, providing oxygen/nutrients, using plants at the contaminated sites (Dzantor, 2007) which help to maintain favorable bioremediation conditions (Basu et al. 2015). These alterations at target sites influence the microbial activities and their neighbouring environmental condition for accelerating the biodegradation rate and categorized as bioaugmentation and biostimulation (Popp et al. 2006; Suthersan et al. 2015; Sudrajat et al. 2016; Poi et al. 2018). In bioaugmentation, microorganism seeding is practiced for cultivating the volume of a LNAPL degrader grown independently in favourable conditions (He et al. 2003a, b; 2006; Farhadian et al. 2008). Da Silva and Alvarez (2004) investigated enhanced biodegradation of NAPLs in microbial seeded aquifer columns and showed an increase of up to 88 % in LNAPL mass removal rates.

In biostimulation, biodegradation rate is enhanced by addition of nutrients, electron acceptors, oxygen and other relevant compounds to the polluted sites for increasing the (co)-metabolic actions of the microbes (Alvarez et al. 1991; 1994; Eckert and Appelo, 2002). Generally, the oxygen releasing compounds like H_2O_2. MgO_2, O_2, NO_3, SO_4, Mn(IV), Fe(III) are used to stimulate the LNAPL polluted sites. These electron acceptors significantly increase the oxygen level which helps in maintaining the aerobic condition. Alvarez et al. (1995) used nitrate as electron acceptor to incubate NAPL degrader in batch system. The addition of nitrate to soil enhanced the denitrification

causing increased oxygen level ultimately enhancing the degradation of the NAPL mass. Similarly, Roling et al. (2002) investigated the impact of nutrient amendment on activities of bacterial communities responsible for NAPL biodegradation and found that the nutrient amendment significantly increases the bacterial population and improved biodegradation up to 92% of initial NAPLs mass. Yadav et al. (2013) conducted a series of microcosm experiments, by adding the domestic wastewater to polluted groundwater for raising the nutrients level. However, no impact was observed due to presence of sufficient nutrients in the polluted groundwater site.

Selective plant species are also used for enhancing the natural degradation rate termed as Plant assistant bioremediation (Mathur and Yadav, 2008, 2009; Yadav et al. 2009, 2011; Abou-Elela et al. 2013). This technique uses the plant-geochemical interaction to modify the polluted site and also supply (micro)-nutrient, oxygen etc. into subsurface for better performance of LNAPL degraders on targeted pollutants (Susarla et al. 2002). The plant–geochemical interaction enhances the 1) physical and chemical properties of sites 2) nutrient supply by releasing root exudates (Shimp et al. 1993) 3) the aeration by transfer the oxygen (Burken et al. 1998) 4) interception and retardation the movements of chemicals 5) the plant enzymatic transformation 6) resistant to the vertical and lateral migration of pollutants (Narayanan et al. 1998a, b). Similarly, the plant-microbe's interaction increase 1) mineralization in rhizosphere 2) numbers of degraders and shorter the lag phase until disappearance of the compound (Chavan and Mukharji, 2008; Imfeld et al. 2009). Some key factors to consider when choosing a plant include: root system, toxicity of pollutant to plant, plant survival and its adaptability to prevailing environmental conditions, plant growth rate, resistant to diseases and pests (Sushkova et al.2018).

The deep root systems of plant improve the aeration in subsurface, which maintain the oxygen level in deep vadose zone. The root exudates, dead root hair and fine root serves as an important sources of the carbon for microbial growths (Shimp et al. 1993). The root exudates also help to accelerate the enzyme synthesis of microbial metabolisms (Dzantor et al. 2007; Azubuike et al. 2016). The role of plants on LNAPL removal using pot scale setup planted with *Canna generalis* under controlled conditions were investigated by Basu et al. (2015). The total removal time of the LNAPL was found to be highest in the unplanted followed by planted mesocosm and degradation rate were found higher in planted pot setups. Different bioremediation techniques used in LNAPL treatment are presented in figure 2.1.

Treatment wetlands are a cost effective and potential techniques for decontaminate LNAPL pollution from polluted sites. The processes that help in removal of LNAPL from wetland are sorption, microbial degradation, and volatilization (Dittmer et al. 2005; Henrichs et al. 2007). TWs cab be classified in two types horizontal flow (HF) and vertical subsurface flow (VF) wetlands on the basis of their water flow through system (Vymazal, 2005a, b; 2009). An integration of both horizontal flow and vertical flow wetlands are refer as hybrid wetlands or duplex wetlands.

Salmon et al. (1998) computed complete removal of LNAPL in free water surface mesocosm setup. In the system cultivated with *Typha latifolia*, natural growth of Lemna minor occurred. The overall 90% removal of LNAPL was reported in this study. Likewise, Giraud et al. (2001) developed an experimental constructed wetland for subsurface flow. There were two beds that were operated in series and a detention period of 3 days. LNAPL was decomposed efficiently by microbial species capable of eradicating LNAPL by around 70%. For peat soils, LNAPL removal capability was tested in HSSF wetland (Moore et al. (2000a). The system planted with *T. Latifolia* and *P. Australis* showed reduction of 40-60% achieved in a period of 14 days with no aeration. If aeration was performed, it resulted in complete removal in the matching detention period. Inlet flow rates varied from 7-33L/min whereas inlet concentration varied from 4.5 mg/L to 12.1 mg/L. Anaerobic and aerobic biological degradation of LNAPL in wetland system was estimated by Moore et al. (2002). Aerobic degradation was computed from removal of iron, manganese, nitrate and sulphate which are electron acceptors whereas aerobic degradation was computed using oxygen consumption and carbon dioxide emission. Similarly, Chang et al. (2001) found that degradation was rapid for LNAPL constituents due to consumption of benzene, toluene and ethyl benzene as carbon sources whereas xylene removal due to co-metabolism by potential microbes. Later on, Lee et al. (2004) conveyed in the study how first order constant of removal rate for LNAPL compounds. Keefe et al. (2004) investigated performance of wetland of area 1.4-hectare free water surface of depth 60 cm and a detention time of 3.9 days. Around 80% decrease of toluene degradation was reported by wetland. A summary of different studies related to treatment wetland used for removal of LNAPL polluted soil-water system are listed in table 2.3.

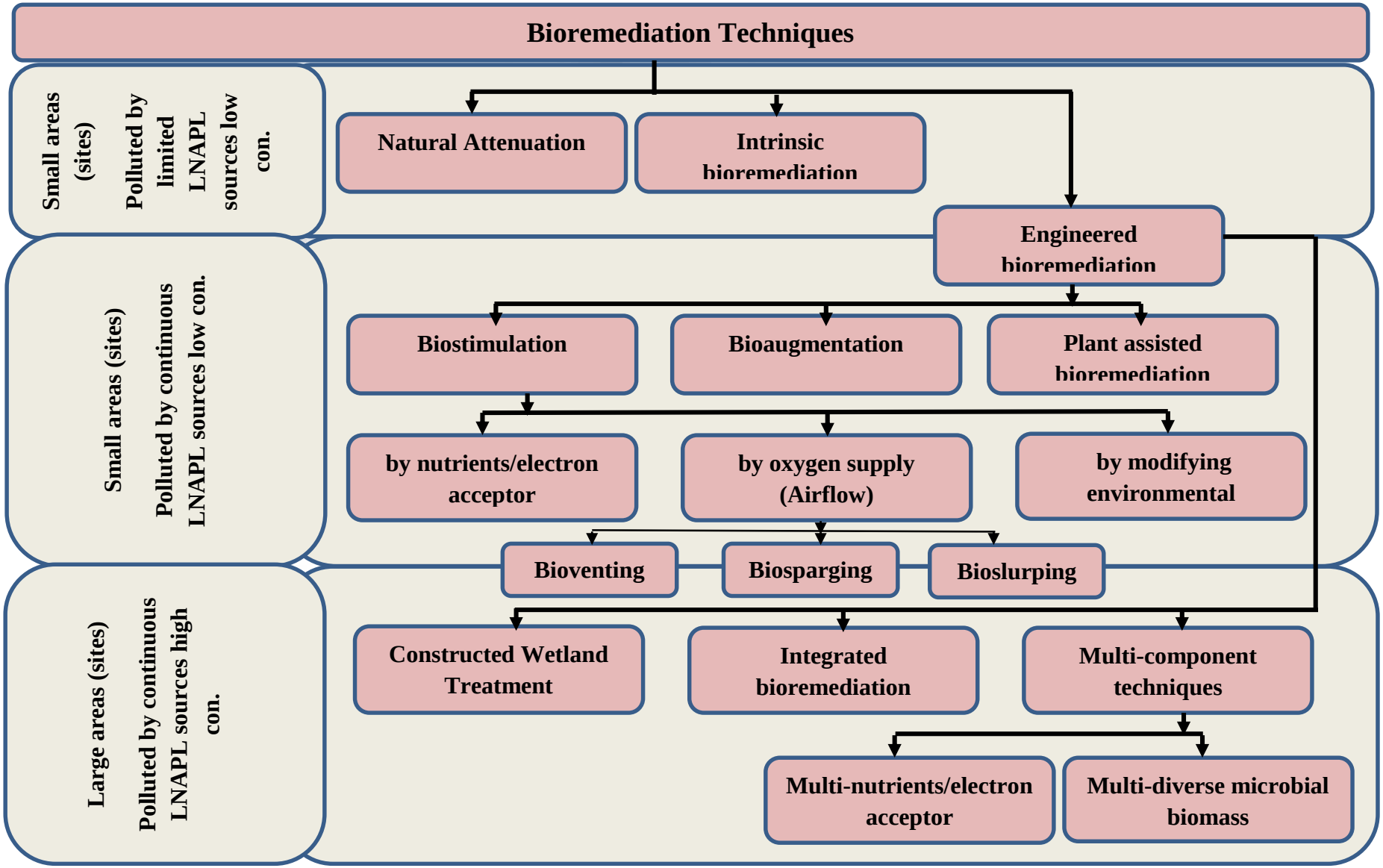

Figure 2.1: Different bioremediation techniques generally used to decontaminate LNAPL polluted sites.

Table 2.3: Summary of studies on treatment wetlands used for removal of LNAPL polluted soil-water system.

Reference	Types of study	Types of CWs	Conditions	Experimental setups	Plant Species	Removal	Highlight
Bedessem et al. 2007	Practical	Vertical flow and Horizontal flow	With and without aeriation	Treatment Cell: 7 × 1.7 × 1.1 m	Willows (Salix), reed (Phragmites), bulrush (Scirpus), rash (Juncus), and dogwood (Cornu)	BTEX: >88%	Aeration significantly improved by 13-21%.
Eke et al. 2008	Practical	Vertical Flow	Field condition/ Scotland UK	Pot Scale: 61-75 cm	*Phragmites*	Benzene: >85%	More than 80% nutrient removal was reported
van Afferden et al. 2011	Practical	Vertical Flow (Two stage filters)	Field condition	Pilot Scale Treatment Facility: 2.3 × 1.75 × 1.75 m	*Salix alba*	Benzene: >98%	70% removal for MTBE also reported
Chen et al. 2012	Practical	Horizontal Flow	Field Condition: Germany	Pot Scale: 5 × 1.1 × 0.6 m	*Phragmites australis*	Benzene: 22-100%	Volatilization contributes 3-15% to total removal
Seeger et al. 2011; 2013	Practical	Horizontal Flow	Site Condition/ Germany	Pot Scale: 5 × 1.1 × 0.6 m	*Phragmites australis*	Benzene:>98	Filter additives (charcoal and ferric oxides did not improve contaminant depletion.
Ranieri et al. 2013	Pilot Study	Horizontal Flow	Field condition	Wetland Area: 4.80×7.15m	*Phragmites australis* *Typha latifolia*	BTEX:46-55%	The average removal in the *Phragmites* field was 5% higher than the *Typha* field and 23% higher than the unplanted field.
Al-Baldawi et al. 2013; 2015	Practical	Horizontal Flow	Field condition	Pot Scale: 30 × 30 × 30 cm	*Scirpus grossus*	TPH: 80.2-91.5%	Subsurface flow CWs are better than Free flow CWs
Martínez-Lavanchy et al. 2015	Practical	Horizontal Flow	Additional Nutrients ($NH4^+$)	Pot Scale Cylindrical	*Juncus effuses*	Benzene: > 81%	Monooxygenation pathway of toluene biodegradation was investigated
Basu et al. 2015; 2017	Practical & Numerical	Horizontal Flow	Domestic wastewater used as carbon source	Pot Scale: 28 cm diameter and 30 cm height	*Canna generalis*	BTEX: >98%	First order kinetics of BTEX biodegradation
Ballesteros et al. 2016	Practical	Horizontal Flow	Field condition	Pot Scale: 1 × 0.6 × 0.8 m	*Phragmites australis*	Benzene: 48%	Unplanted CWs shows 31% removal efficiency
Stefanakis et al. 2016	Practical	Horizontal Flow	Site Condition/ Germany	Pilot Scale: 5.9 × 1.1 × 1.2 m	*Phragmites australis*	Benzene: 100%	Ammonium removal was also higher in the planted bed (40.7%).
Mustapha et al. 2018	Practical	Free water surface flow	Site Condition	Pilot Scale: Area 50 m^2	*Phragmites and Typha*	B (92.6%), T(93.4%), E(98.3%), m-p-X (91.3%) and o-xylene (87.4%)	First order kinetics of biodegradation of BTEX was reported

2.4 Factors Affecting LNAPL in Subsurface

The LNAPL are affected by soil characteristics, environmental conditions (substrata concentration, soil moisture and temperature), groundwater dynamics (table fluctuation and flow velocities) and its release dynamics (Alvarez and Vogel, 1991). Deep and Alvarez (1999) performed experiments to understand the impact of substrate concentration on biodegradation of LNAPL compounds. They found that biodegradation of LNAPL pollutants by *Rhodococcus rhodochrous,* increases with high initial individual substrate concentrations while decreases in case of mixed substrate concentrations. Reardon et al. (2000) reported that toluene substrate concentration inhibits the biodegradation of other pollutants like phenol in subsurface. Most of these studies are limited to low range of substrate, thus three is need to investigate impact of wide range of substrate on biodegradation of LNAPL in subsurface. Likewise, fate and transport behaviours of LNAPL are highly affected by soil temperature and soil moisture level. Soil moisture and temperature in subsurface is governed by atmospheric flux and act as sensitive variables to the existing biota. Soil moisture paly significant role in diffusion of oxygen and nutrient in subsurface which regulate its supply to microbes. On the other hand, temperature play important role in microbial growth and their microbial activities. Most of the earlier studies are limited to investigation on impact of soil moisture and soil temperature separately on LNAPL fate and transport in subsurface (Yadav and Hassanizadeh 2011).

Groundwater dynamics including its table fluctuation and flow regimes affects the LNAPL movement in subsurface. A fluctuation in groundwater table also alter its flow regimes which significantly modify the behaviour of LNAPL in saturated zone. Moreover, groundwater fluctuation provides additional oxygen to vadose zone which considerably affects the biodegradation rates of LNAPL (Dobson et al. 2007). Groundwater flow pattern is an important parameter which considerably accelerate dissolution and movement of LNAPL in saturated zone (Vasudevan et al. 2014). On the other hand, LNAPL introduction and its movement through subsurface zone might affect the microbial communities responsible for biodegradation (Zhou et al. 2015). Most of the earlier studies are conducted at steady state conditions and at base groundwater velocity. A better understanding of different environmental variables and groundwater dynamics on fate and transport of LNAPL is required in order to frame an effective remediation technique. Accurate estimation of LNAPL movement under varying groundwater regimes may help to forecast future pollution load and range of coverage. Impact of soil moisture and temperature

conditions along with role of groundwater table dynamics and flow velocities are presented in detail in forthcoming section.

The soil water content and soil temperature are the pivotal subsurface variables, which directly and indirectly affects the biodegradation of LNAPL pollutants (Coulon et al.2007). The variations in both subsurface parameters are reported at most of the polluted sites (Pramer and Bartha, 1972). The soil moisture level and its distribution regulates the diffusion of oxygen and nutrient to the microbes. The higher soil moisture level fills the pore spaces and enhance the advective flow and diffusion of oxygen and nutrient to microbiota in subsurface (Shaw and Burns 2003). This influences the bioavailability of dissolved phase LNAPL pollutants (Zhou et al. 2015). A high soil water content of vadose zone also enhances the LNAPL load to under lying groundwater resources (Papendick and Campbell 1981). Conversely, high moisture content intercept the oxygen flux which may considerably affects microbial biodegradation of LNAPL pollutants in vadose zone (Prado et al. 1999). However, at low water content, the LNAPL may be stunted by adsorption onto mineral and/or organic components of soil solids (Petersen et al. 1994) which will inhibit metabolic actions of the microbes. Thus, it is important to maintain the soil water potential optimum at polluted sites for achieving a faster biodegradation rates.

Few studies are performed on behaviour of LNAPL in subsurface with varying soil moisture contents (Yadav and Hassanizadeh, 2011) and most of the other studies are conducted at near optimal soil-moisture conditions (Dibble and Bartha 1979; Bossert et al. 1984; Harms 1996; Davis and Madsen, 1996; Holden et al. 1997; 2001 and Chen et al. 2007). Holman and Tsang (1995) showed that a water content of 50–70% of field capacity was optimal for biodegradation of aromatic hydrocarbons. Pramer and Bartha (1972) conducted batch scale experiments and showed that removal of organic matter in soil is generally highest at 50% - 70% of soil's field capacity. Whereas, optimum soil water content in between 30% and 90% of soil's field capacity is reported by Dibble and Bartha (1979). Later, Harms (1996) confirmed that the degradation rates of a LNAPL contaminated media varies with the effective diffusivity which is further proportional to the soil moisture level.

Likewise, subsurface temperature significantly affects the LNAPL-water mass transfer rates, sorption and biodegradation of dissolved phase mass (Atlas 1991; Margesin and Schinner, 2001). Earlier, Mulkins-Phillips and Stewart (1974) conducted a series of batch experiments to study the impact of temperature on the biodegradation of LNAPL contaminated soils. This study suggested that 52% and 85% of pollutants were removed

from batch setup incubated at 5°C and 15°C, respectively. The enzymatically moderated physiological behavior of potential microbes were found to be very sensitive to the temperature changes (Corseuil and Weber, 1994). A low soil temperature generally decreases the enzyme production rate which is a complementary part of the metabolic pathway of LNAPL degradation in the cellular tissues. It also reduces the fluidity and permeability of the cellular membrane which hinders the nutrient, oxygen and contaminant uptake (Corseuil and Alvarez, 1996; Alvarez and Illman, 2006). While, higher soil temperature reduces the LNAPL adsorption to soil particles, which in turn affects their bioavailability to the indigenous microbes (Perfumo et al. 2007). Furthermore, Deeb and Alvarez-Cohen (1999) investigated the role of soil temperature on LNAPL biodegradation by *Rhodococcus rhodochrous* derived from the aquifer media contaminated with gasoline. The results showed that the microbial growth on toluene increased when the temperature was kept between 7-35°C, however, it decreased sharply in the range of 36-40°C, and was inhibited entirely at temperatures above 45°C. Likewise, Margesin and Schinner, (2001) reported that the elevated temperature enhances dissolution and bioavailability, which help to remediate LNAPL polluted sites effectively. Recently Yadav et al. (2012) investigated biodegradation kinetics of toluene under diurnal and seasonal fluctuations of soil-water temperature using a series of batch experiments. The results of batch experiments showed that diurnal and seasonal fluctuations of soil-water temperature strongly affect the degradation time of toluene. The degradation rate is enhanced almost two-times for every 10°C rise in soil-water temperature.

To sum up, there is a paucity of knowledge on the combined impact of soil moisture and temperature conditions on behaviour of LNAPL in subsurface. Studies are reported in literature on biodegradation of LNAPL under different range of soil moisture and temperature conditions. Thus, a better understanding of behaviors of LNAPL under varying soil moisture and temperature is needed to regulate the subsurface condition for maintaining the optimal conditions during the in-situ bioremediation of polluted sites. In this study, a series of microcosms experiments are performed to investigate the combined impact of different soil moisture levels and temperature on biodegradation of LNAPL in subsurface. Furthermore, another series of column experiments were performed to investigate impact of groundwater temperature on LNAPL in a continuous soil-water system.

2.5 Bioremediation and Dynamic Groundwater Flow Regimes

Variations in groundwater table and flow velocities, particularly in shallow unconfined aquifers are expected due to climate variability and changes, tidal effects in coastal areas, changes in extraction patterns and surface recharge. Kruger et al. (2001) predicted a 30% reduction in recharge rate due to climate change of a lowland aquifer in Germany. MacDonald et al. (2016) observed the significant groundwater variations in some areas of Indus, Brahmaputra and Ganges basins during 2000 -2012. Variations of groundwater not only cause changes in the soil-water system, but also impact LNAPL behaviors in (un)-saturated zones. A high concentration of LNAPL plume shall originates from accelerated dissolution of LNAPL due to dynamic groundwater table conditions. Dobson et al. (2007) investigated the impact of water table fluctuations on LNAPL dissolution and movement using two-dimensional sand tank experiments. They concluded that the water table fluctuation resulted in entrapment of LNAPL below the water table causing enhanced dissolution and increased the vertical extent of the LNAPL pool (Aral and Liao, 2002; Kumar et al. 2011). When water table falls, LNAPL lying in smear zone also follows the falling water table trajectory. As the LNAPL moves down it leave a trail of LNAPL in unsaturated zone in form of isolated ganglia. Subsequently, when the water table rises the LNAPL move upwards leaving behind a trapped amount of LNAPL in form of disconnected blobs in the saturated zone (Lenhard et al. 2004; Kechavarzi et al. 2005). A part of the residual LNAPL in the unsaturated zone may get mobilized again when the water table rises. Such water-table fluctuations affect the spatial distribution of LNAPL and oxygen in polluted subsurface, particularly in the vertical direction (Rolle et al. 2009). This may increase the aqueous-phase plume size and the biodegradation rate because of increased availability of electron acceptors, nutrients and enhanced bioavailability of the LNAPL compounds (Zhang et al. 2014). Further, groundwater fluctuation enhances the oxygen diffusion (Legout et al. 2009) and accelerate the transverse mixing in deeper subsurface. Whereas, groundwater fluctuation is most influencing factor to dissolution and its subsequent transport in variably saturated zones in real field conditions (Yadav and Hassanizadeh, 2011). Only few studies have reported the impact of water-table dynamics on LNAPL fate and transport in subsurface as listed in table 2.4.

Groundwater velocity is also expected to vary significantly under changing climate, tidal effects, recharge/extraction pattern of groundwater. Changes in flow velocity can strongly affect the fate and transport of LNAPL in subsurface (Powers et al. 1992; Barker

et al. 2000; Dobson et al. 2007; Yadav et al. 2012). Dissolution and volatilization of LNAPL increases with increasing length of LNAPL pool and its plume under high groundwater flow velocities (Brusseau et al.2002; Chrysikopoulos et al. 2003; Valsala and Govindarajan, 2018). Furthermore, advective transport plays a crucial role in elongation and re-distribution of LNAPL under varying flow velocity (Saba and Illangasekare, 2000). Voudrias and Yeh, (1994) conducted a two-dimensional sand tank experiment to investigate the impact of groundwater velocity on the dissolution of pure LNAPL phase in subsurface. Miller et al. (1990) investigated dissolution of LNAPL mass and concluded that mass transfer rate increase sharply with groundwater velocity. Kim and Corapcioglu, (2003) developed a two-dimensional LNAPL migration model for investigating dissolution and volatilization under varying subsurface flow conditions. Recently, Sulaymon and Gzar, (2011) conducted experiments for LNAPL dissolution under different groundwater velocities and concluded that aqueous mass transfer rate increased with groundwater velocity. Table 2.5 listed various laboratory and simulation experiments showing the impact of groundwater velocity on LNAPL dissolution and movements in subsurface. Thus, LNAPL mass-transfer from pure phase to dissolved phase and its subsequent attenuation under varying groundwater flow velocity are not addressed adequately (Seagren et al. 1999; Sookhak Lari et al. 2016). A better understanding of fate and transport of LNAPL under dynamic groundwater conditions is required to effectively design a remediation plan and the associated cost.

Table 2.4: Summary of studies to investigate the impact of water table dynamics on LNAPL fate and transport in subsurface.

References	Experimental Design/Setup	Methodology	Remark
Dobson et al. (2007)	2D sand tank 80 cm× 51 cm× 3.3cm	The water and solute were pumped in dry sand packed model aquifer, and pumping time (on/off) used to maintain water table dynamics.	The water-table fluctuation increased dissolution of LNAPL components in the model aquifer.
Rühle et al. 2015	1D Column Plexiglas Column (14cm inner diameter and 50 cm long)	Vertical flow experiments were performed by applying water and tracer from top to maintain periodical lowering and raising of the water table in the dynamic column.	Transport parameters changes were caused by the temporal and spatial variation of water contents and/or flow velocities within the zone of fluctuation.

Table 2.5: Summary of earlier studies showing the impact of groundwater velocities on LNAPL behaviour in subsurface.

References	Experimental Design/Setup	Methodology	Results/Comments/Gaps
Imhoff and Miller 1996	2D sand cell	NAPL pumped in from the lower port at a high flow rate. The dissolve concentration was analyzed and different dissolution was investigated.	The heterogeneous media leads to the heterogeneous dissolution and distribution of LNAPL in the cell and depends on the groundwater flux.
Powers et al. 1994	1D column (8.5cm x 6.86 cm) and 2D (10 cm x 17.8 cm) experiments having heterogeneous pattern.	Fine sand was packed in the 1/2D cell and different groundwater velocities were maintained.	Rate-limited dissolution becomes important for low-LNAPL saturations ($S_n < \sim 0.05–0.15$)
Sulaymon and Gzar 2011	3D saturated sand tank (100 cm × 40 cm × 35 cm)	Ten dissolution experiments were performed in the 3D tank with the water flow from the storage tank. The constant head tank was transferred by gravity.	The studies concluded that dissolution experiments do not reach the maximum value (1770 mg L^{-1}) because the higher dissolution rates can be associated with: (1) increased contact area between LNAPL and water (2) higher LNAPL saturation in the porous media, and (3) higher interstitial velocity.

2.6 Multi-Scale Studies on Fate and Transport of LNAPL

Theories of single phase and multiphase subsurface flow, hydrodynamic dispersion, and kinetics of LNAPL degradation were started around 1965. The groundwork upon which the quantitative study of these LNAPL transport in subsurface was established during 1965-1980. The classical advection-dispersion equation of solute transport in subsurface was introduced by Bachmat and Bear (1964) followed by introduction of two phase flow equation (Nelson, 1966). Numerical solutions for these solute transport equations and their subsequent applications began to appear by researchers in 1970s. By the early 1980s, research findings of multiphase flow, contaminant transport with biodegradation, and mass transfer was well progressive (Mercer and Cohen, 1990; Illangasekare et al. 1995). Particularly in 1990-2000, attention was more on analytical and numerical solutions for LNAPL behaviours in subsurface followed by field investigations (Bao et al. 2003; Oostrom et al. 2007). Researchers used many analytical solution (Cardiff et al. 2010) and

modeling tools like BIONAPL 3D, MODFLOW (Prommer et al. 2003), HYDRUS (Horel et al. 2015), FREEWAT (Borsi et al. 2015) and pore network modeling (Raoof and Hassanizadeh, 2012) to simulate LNAPL transport in subsurface.

A summary of selected multi-scale studies related to fate and transport of LNAPL in subsurface is listed in tables 2.6-2.9. The Table 2.6 highlights the microcosms studies with specific focus of soil moisture and temperature impact on bioremediation of LNAPL. Similarly, table 2.7 presents studies of column experiments for investigating biodegradation of LNAPL at constant temperature. Multi-dimensional studies on fate and transport of LNAPL in subsurface are listed in tables 2.8 -2.9.

2.7 Bioremediation System Designs

The remediation system design for the LNAPL contaminated sites has been attempted by some researchers considering various simulation and optimization techniques. Minsker and Shoemaker (1998a, b) designed the remediation system and optimized the well location and pumping rates to achieve the minimum remediation cost for a hypothetical site contaminated with Phenol. Similarly, Wang and Zheng, (1998); Yoon and Shoemaker, (1999); Aly and Peralta, (1999); Shieh and Peralta, (2005); Kumar et al., (2013) and Yadav et al. (2016, 2017) designed the optimal bioremediation system for sites contaminated with organic compounds in the saturated zone.

Physical simulator like BIOPLUME II, BIOPLUME III have been coupled with the optimization techniques for the selection of a cost-effective remediation strategy (Shieh and Peralta, 2005; Nesheli et al. 2015; Yadav et al. 2016). Later, Prasad and Mathur (2008) suggested a data-based simulation-optimization approach by developing a hybrid Neural Network-Monte Carlo based system replacing the BIOPLUME III model with a data-based simulator to optimize the well locations for in-situ bioremediation. For maintaining favourable conditions for bioremediation, injection wells are mostly used to supply electron acceptors, nutrients laden water, hot air, along with seeding of potential microbes in the contaminated zone (Cunningham et al. 2001). Extraction wells are used in such systems for controlling plume spreading in down-gradient locations (Shieh and Peralta, 2005; Kumar et al. 2013, 2015; Yadav et al. 2016). Application of data based simulator in bioremediation system design was further extended using advanced techniques like Support Vector Machine (SVM) and Extreme Learning Machine (ELM) (Kumar et al. 2013; Yadav et al. 2016, 2017).

Table 2.6: Overview of recent microcosms scale studies (reported after year 2000) on fate and transport of LNAPL in subsurface.

Types	Reference	Contaminant Source	Concentration level	Temp.	Water Saturation	Experimental setups	Governing processes	Highlight
Batch Laboratory studies	Reardon et al. 2000	Benzene, Toluene, and Phenol	43 ppm	C (30ºC)	F	Batch bottles: 2L	Biodegradation (using *P. putida* F1)	Observed Monod kinetics with K_s values 32 mg/L
	Holden et al. 2001	Dissolved Toluene	Vapor	C (25ºC)	100-50%	Batch bottles: 40 mL vials 10 g soil	Biodegradation	0.03 L^{-1} h^{-1} biodegradation rate
	Hoehener et al. 2003	VOCs, Dissolved Toluene	___	C (23ºC)	F	Batch bottles: 63 mL	Biodegradation	0.12 L^{-1} h^{-1} biodegradation rate
	Shim et al. 2005	BTEX	M:1000 ppm	C (25ºC)	F	Batch bottles: 95mL	Biodegradation (enhanced by H_2O_2)	Biodegradation rate without H_2O_2: 0.991; with H_2O_2: 1.319 mg 1^{-1} h^{-1}.
	Jo et al. 2008	BTEX	75 ppm	C(28-30ºC)	F	Batch bottles: 500 mL	Biodegradation	97% removal of B, 93% of T, 90% of E, 98% of X in 50 h.
	Wolicka et al. 2009	BTEX	M: 500 ppm	C	F	5 g soil in 300 mL Flasks	Biodegradation	Benzene: 914 µM L^{-1} d^{-1}; toluene: 771 µM L^{-1} $d^{-1,}$ xylene: 673 µM L^{-1} d^{-1} and ethylbenzene: 644 µM L^{-1} d^{-1}
	Mazzeo et al. 2010	BTEX	-----	C (21ºC)	F	Batch bottles	Biodegradation	20.4-100 % removal of BTEX
	Morlett-Chávez et al. 2010	BTEX	M: 50 ppm	C (36ºC)	F	Batch bottles: 500 mL	Biodegradation	80% removal of B, 81% of T, 80% of E, 25% of X in 60 h
	Robledo et al. 2011	BTEX	30-90 ppm	C (30ºC)	F	Erlenmeyer flasks 250 mL	Biodegradation	100% removal of BT, 60% of E and 80% of X in 6-14 h
	Di Martino et al. 2012	BTX	___	C (30ºC)	F	Batch bottles: 50 mL	Biodegradation & Characterization of potential microbes	*Pseudomonas* sp. isolated and reported high efficiency to degrade BTX compounds
	Yadav et al. 2012	Dissolved Toluene	1 ppm	10ºC-21ºC-30ºC	F	Batch bottles: 120 mL	Biodegradation at 10ºC-21ºC-30ºC	An increment of biodegradation to twice for every 10°C rise in soil-water temperature.
	Picone et al. 2013	Dissolved Toluene	5-8 ppm	C (20ºC)	6–30 %	Batch bottles: 250 mL	Biodegradation	Observed first-order biodegradation constants that increased with water filled porosity
	Yadav et al. 2013	Dissolved Toluene	8 ppm	C (21ºC)	F	Batch bottles: 120 mL	Biodegradation enhanced by nutrients, plants	Natural degradation ≃ biostimulation < plant-assisted biostimulation << combination of bioaugmentation and biostimulation.
	Nagarajan, K., and Loh, K. C. (2015)	BTEX	140-220 ppm	C (25ºC)	F	Erlenmeyer flasks: 500 mL	Biodegradation using *Pseudomonas putida F1 and P. stutzeri* OX1 (PsOX1)	100% removal was reported by *P. putida F1* (PpF1) *and P. stutzeri* OX1 (PsOX1) in 24 h.
	Khodaei et al. 2017	BTEX	250 ppm	C (37ºC)	F	Batch bottles: 150 mL	Biodegradation using *Pseudomonas* sp. BTEX-30	1.5 L^{-1} h^{-1} biodegradation rates for ethylbenzene and m-xylene and 2.8 and 2.7 L^{-1} h^{-1} biodegradation rates for benzene and toluene respectively.

C= Constant; F= Fully Saturated; M= Mixed; RT= Room Temperature

Table 2.7: Overview of recent 1D column studies on fate and transport of LNAPL in subsurface.

Types	Reference	Contaminant Source	Concentration level	Temp.	Water Saturation	Experimental setups	Governing processes	Highlight
L & N	Da Silva and Alvarez, 2002	MTBE and BTEX	BTEX:1 ppm MTBE:25 ppm	C (22ºC)	F	Glass: 5 cm diameter and 20 cm length	Retardation; Biodegradation (impact of ethanol)	MTBE didn't degraded in biologically active column and did not affect degradation of BTEX, while Ethanol significantly affect biodegradation.
L & N	Sovik et al. 2002	Toluene & o-Xylene	Mix: 50 ppm of both	C (12ºC)	14-15% at top	Glass: 0.5 m length and 10 cm diameters	Volatilization and biodegradation	First order degradation coefficient were estimated in the range of 0.10 to 0.11 d^{-1} for o-xylene and 0.19 to 0.21 d^{-1} for toluene.
L & N	Zheng et al. 2002	Toluene and 1,2,4-trimethylbenzene	Pure phase	C (8-10ºC)	F	Stainless steel: 25 cm length and 2.5 cm diameter	Biodegradation rates and sorption	Zero order biodegradation rates due to Fe(III) reduction.
L & N	Davis et al. 2003	Diesel	Dissolved 337 ppm	RT	Top unsaturated	Glass: 10 cm length Aluminum: 50 cm Plexiglas: 120 cm	Biodegradation rates	An average biodegradation rates was 0.20 mg (Kg d^{-1}.
L & N	Ranck et al. 2005	Toluene	Mix BTEX: 15 ppm	RT	F	Glass: 17.8 cm diameter &122 cm length	Biodegradation (using modified zeolites)	High removal efficiency of BTEX by modified zeolites.
L	Tindall et al. 2005	Toluene	Pure phase	RT	70%	PVC: 30cm diameter and 150 cm length	Biodegradation (using Nitrate and H_2O_2)	Nutrient-enhanced columns degraded significantly more toluene than the control columns.
L	Vogt et al. 2007	Benzene	Dissolved	V (12-20ºC)	F	Stainless: 6 m length 25 cm diameter	Biodegradation under sulfate-reducing conditions	Estimated biodegradation rate was 8–36 µM day^{-1}.
L	Nerantzis & Dyer, 2010	BTEX	Mixed pure phase	C (21ºC)	0-12% from top	PVC: 50 cm length 10 cm diameter	Vapor transport & biodegradation rates	A thin soil layer of high moisture content can significantly obstruct the gaseous transport of BTEX vapor.
L	Filho et al. 2013	Gasoline	Mixed with Ethanol	C (19.9±2.3ºC)	F	Glass: 110 mm high	Advection; Volatilization; Biodegradation	Ethylbenzene and toluene showed the highest volatilizations in the gasoline-ethanol column.
L & N	Picone et al. 2013	Dissolved Toluene	12-21 ppm	C (20ºC)	9-27%	Glass: 3.5cm diameter and 19.5 cm length	Gas advection and biodegradation	Maximum mass removal rates were 0.69±0.09, 0.73±0.04, and 1.06±0.22 mg h^{-1} at 27, 14, and 9 % water saturation, respectively.
L	Zhao et al. 2015	BTEX	B: 8.7 ppm; T: 5.44 ppm; E:0.37 ppm and X:0.38 ppm	RT	F	Glass: 98 cm length 14 cm diameter	Biodegradation rates under nitrate, sulfate and Fe (III) reducing conditions	Degradation of BTEX with four electron acceptors was in order as: nitrate > sulphate > chelated Fe(III) > DO.
L & N	Khan et al. 2016	Toluene	Pure phase	RT	12% of pore space	Chromoflax glass column: 35 cm length 4.1 cm diameter	Biodegradation of toluene vapors	High biodegradation rates of toluene were observed within few centimeters pathway of vapor in column.
L	Yang et al. 2017	Toluene	Pure phase	RT	Unsaturated	Glass: 5 cm length 5 cm diameter	Natural attenuation under fluctuating groundwater conditions	Toluene degradation significantly affected by groundwater table fluctuation.

L=Laboratory experiments; N=Numerical Modeling; C= Constant; F= Fully Saturated; M= Mixed; RT= Room Temperature; V= Varying

Table 2.8: Overview of recent 2D studies on fate and transport of LNAPL in subsurface.

Types	Reference	Contaminant Source	Concentration level	Water Saturation	Experimental setups	Governing processes	Highlight
L & N	Saba et al. 2001	*p*-xylene	Pure phase	Fully Saturated	Glass: 57 cm × 38 cm × 5.08 cm Homogeneous	Dissolution of entrapped LNAPL using surfactant	Effluent concentrations were inversely proportional to the flushing velocity of the surfactant solution through experimental setup.
L& N	Imhoff et al. 2003	Toluene	Pure Phase	Fully Saturated	Plexiglas 228.6 cm × 55.9 cm × 5.9 cm Heterogeneous	Migration of Toluene and DNAPL	Laboratory investigated migration pattern, time and concentrations are upscale and well matched with field data.
L & N	Wipfler et al. 2004	Jet fuel A-1	Pure phase	Partially Saturated at 18ºC	Plexiglas: 40 cm × 40 cm × 2.5 cm Heterogeneous	Infiltration of LNAPL in unsaturated soil	Different results show the redistribution of LNAPL is primarily subjected to the capillarity contrast between sands. A greater contrast accelerates horizontal migrations.
L & N	Kechavarzi et al. 2005	Soltrol 220	Pure phase	Fully Saturated	Glass and Perspex sheet: 2D sand tank Size: 180 cm × 120 cm × 8 cm Homogeneous	Multiphase flow	Established a constitutive pressure-saturation relations
L & N	Oostrom et al. 2006	90% Peacock lard oil and 10% 1-iodoheptane	Pure phase	Fully Saturated	1.02 m × 0.75 m × 0.055 m Homogeneous	Behavior of a Viscous LNAPL Under Variable Water Table Conditions	Capillary fringes played important role in multiphase flow of LNAPL
L & N	Dobson et al. 2007	Synthetic BTEX compound	Pure phase	Fully Saturated at 25ºC	Glass and POM sheeting 80 cm × 51 cm × 3.3 cm Homogeneous	Fate and transport of LNAPL under dynamic groundwater table conditions	Groundwater table fluctuation significantly affects the biodegradation and dissolution of LNAPL compounds.
L & N	Fagerlund et al. 2007	Soltrol 220	Mix with iodoheptane (10% w/w)	Fully Saturated	Plexiglas: 70.5 cm × 53 cm × 4.7 cm Heterogeneous	Migration and entrapment of LNAPL in heterogeneous media.	LNAPL entrapment depends on saturation history and significantly affected by heterogeneity.
L & N	Kechavarzi et al. 2008	Soltrol 220	Pure phase	Fully Saturated	Glass and Perspex sheet: 2D sand tank Size: 180 cm × 120 cm × 8 cm Heterogeneous	Multiphase flow and LNAPL transport in subsurface	LNAPL entrapment depends on initial water saturation, water pressures and texture contrasts between layers, which lead to permeability and capillary barrier effects.
L & N	Mobile et al. 2012	NAPL	Pure phase	Fully Saturated	Glass: 5.5 × 4.5 × 2.2 m Homogeneous	Dissolution of NAPL	Obtained dissolution rate coefficient ranges 0.082-2.0 d^{-1}

L=Laboratory experiments; N=Numerical Modeling; C= Constant; F= Fully Saturated; M= Mixed; RT= Room Temperature; V= Varying

Table 2.9: Overview of recent 3D studies (reported after year 2000) on fate and transport of LNAPL in subsurface.

References	Experimental Design/Setup	Pollutants	Methodology	Results/Comments/Gaps
Abreu L.D.V., Robert Ettinger 2009	3D numerical domain	BTEX Vapor phase	Steady-state conditions and homogeneous soil properties were simulated which incorporating the natural attenuation from source points.	The vapor intrusion depends upon the source-surface distances and biodegradation was significant for low concentration.
Ozgur Bozkurt, Kelly G. Pennell 2009	3D numerical domain	BTEX Vapor phase	The importance of factors influencing the vapor intrusion under the non-homogeneity of soils was estimated using a 3D finite element model.	In layered geological structures, rates of vapor intrusion often limit a lower diffusivity and permeability soil layer between source and building, even if a higher permeability layer near the foundation permits increased soil-gas flow rates into the building.
Sulaymon and Gzar, 2011	3D saturated sand tank :100 cm × 40 cm × 35 cm	Pure phase Benzene	A 3D tank was used for experimentation considering the flow of water from storage tank due to gravity with constant head.	The conclusion of these studies shows that maximum value was not attained by the dissolution experiments due to the higher rates of dissolution can be associated with: (1) increased contact area between LNAPL and water, (2) higher LNAPL saturation in the porous media, and (3) higher interstitial velocity.
Luo et al. 2015	2D/3D Heterogeneous domain Modelling	Not specific	In heterogeneous carrier beds hydrocarbon migration pathways formation was simulated with the help of MigMOD mode.	The heterogeneous property of reservoir was main reason for the irregular distribution of hydrocarbons in the study domain and other oilfields.

The LNAPL fate and transport is estimated for both vertical as well as horizontal/transverse directions in vadose and saturated zones which were not addressed in earlier studies. In the design of such bioremediation system, the cost for installation/operation and maintenance of injection and extraction wells requires a substantial budget. Thus, the optimum injection and extraction pumping rates to achieve the highest treatment performance in minimum time and cost is a (Prasad and Mathur, 2007; Kumar et al 2013; Yadav et al. 2017). This study is a significant extension and integration of the developed techniques to investigate fate and transport of LNAPL through vadose zone and saturated zones and its in-situ bioremediation under varying soil moisture and temperature conditions. Experimental observations are integrated here for the effective designing of a bioremediation system. The designed system can be used for applying engineered bioremediation technique in field for remediating polluted unsaturated zone having different soil moisture and temperature conditions along with the saturated zone.

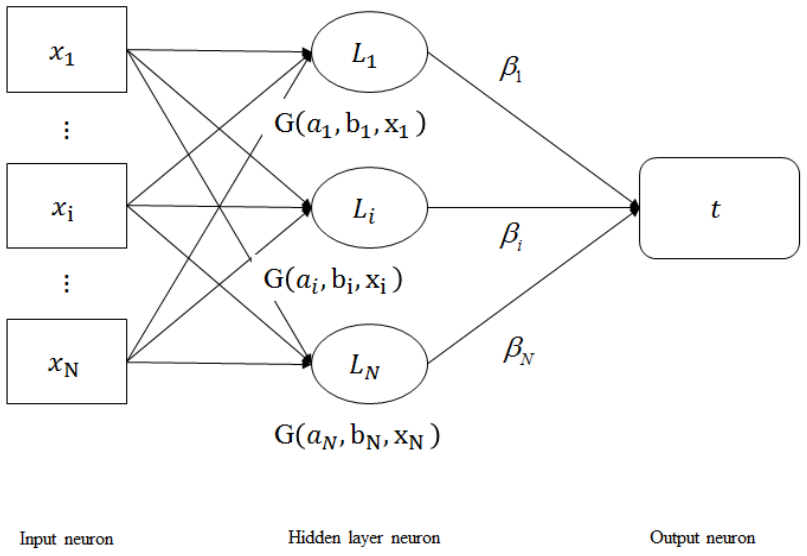

Figure 2.2: Structure of a typical ELM.

ELM was developed by Huang et al., (2006) as an improved learning algorithm for a single feed-forward neural network architecture with a fast learning speed compared to a traditional algorithm that also provides a better generalization performance. ELM randomly chooses and fixes the input weight and hidden layers based on a continuous probability density function. It

then analytically calculates the weights between the hidden and output layers through a simple generalized inverse operation of the hidden layer output matrices (figure 2.2). The proposed method is fast and overcomes the traditional requirement of all parameters for tuning. The theoretical structure of ELM comprises a single hidden-layer feed forward neural network (SLFN) with a randomly chosen input weight matrix and an analytically determined output weight matrix (Huang et al. 2004; 2006; Liang et al. 2005).

Swarm Optimization, like genetic algorithms, is an evolutionary technique based on the metaphor of social behavior. Particle Swarm Optimization (PSO) is the tool of a wide category of swarm intelligence based methods used for solving global optimization problems. It is an evolutionary computation technique based on the simulation of simplified social models, such as bird flocking, fish schooling and swarm theory. In PSO algorithms, the solution in a random space is determined by simulating the movement of a bird or fish. It searches a space by adjusting the trajectory of an individual vector called 'particle'. The trajectories depend upon their own performance and also on the performance of their neighboring companions. It can also be defined in terms of birds searching for food and considering two factors for achieving goal: their own best previous experience and the best experience of all other members. This is similar to the human behavior of making decisions based on their own best past experience or that of the other people around them.

In PSO algorithms, a system is initialized with a population of particles and that particles represent the potential solution. To find a new position for each particle at every iteration (time step), a velocity term is computed on the basis of the experience of the particles. Each particle keeps track of its coordinates in the problem space associated with the best solution (fitness) it has achieved so far (the fitness value is also stored), which is called pbest. Another best value is tracked by the global version of the particle swarm optimizer is the overall best value and its location obtained so far by any particle in the population, called as gbest.

2.8 Summery and Research Gaps

Groundwater pollution due to release of LNAPL is of major concern under varying subsurface conditions because of their higher water solubility and wide coverage in subsurface. The LNAPL migrate laterally as an immiscible phase predominantly in direction of groundwater flow. Though LNAPL are not freely missible in water, a small quantity of LNAPL gets dissolved with water to seriously degrade its quality.

Most of the industries and refineries are located in arid and semi-arid coastal regions which may be a potential site of LNAPL pollution. Arid and semi-arid coastal regions are very sensitive and characterized by specific environmental extremes; soil moisture contents, varying low and high temperatures, groundwater table dynamics, and varying groundwater velocity by tidal effects. LNAPL pollution at these site is highly sensitive to site prevailing environmental conditions. While, the impact of soil moisture and temperature on biodegradation rate has been reported separately and their integrated impact is not investigated so far. Similarly, impact of varying groundwater temperature on fate ad transport of LNAPL in continuous system is not investigated adequately. Furthermore, dynamic nature of groundwater table and flow regimes significantly affects the LNAPL pool movement and its dissolution in subsurface. There is a paucity of knowledge on the impact of dynamic groundwater table conditions on LNAPL behaviors in subsurface. Likewise, behaviour LNAPL in subsurface is poorly understood under varying groundwater flow regimes. Most of the earlier studies have focused on LNAPL mass transfer and transport under steady state subsurface flow conditions. These studies were either conducted numerically or in laboratory considering simplified soil water-flow and solute transport parameters in small-scale laboratory experiments using zero/one-dimensional domain. A better understanding of combined impact of soil moisture contents and temperature conditions is important to design bioremediation system for polluted vadose zones. Understanding of fate and transport of LNAPL under fluctuating groundwater table conditions is also required for effective designing of the remediation strategies and for predicting clean-up time and associated cost. Likewise, the relationship between groundwater flow and mass transfer could help in estimating spread of pure and dissolved LANPL pool around a source.

LNAPL transport through subsurface zones might affect the microbial communities responsible for biodegradation of their aqueous phase concentrations. Presence of LNAPL alter microbial populations and diversity is unclear till the date. So, in order to enhance the

degradation rate, engineered bioremediation is practiced using additives to the polluted site and or manipulating subsurface parameters. Since subsurface parameters are difficult to control directly in the field conditions indirectly they can be modified using plants that aid in the overall bioremediation process. For maintaining favourable conditions in enhanced bioremediation, injection wells are used to supply both aerobic and/or anaerobic electron acceptors along with the nutrients and potential microbes in the contaminated zone, while extraction wells are used for controlling plume spreading in down-gradient locations. Installation/operation and maintenance of these injection and extraction wells in field require substantial budget. Further determining optimum injection and extraction pumping rates to achieve the highest treatment performance in minimum time and cost is a key issue in such types of bioremediation systems. Earlier studies on these bioremediation system designs are only for saturated zone and were purely based on numerical analysis. Therefore, there is a need of a bioremediation design for LNAPL polluted vadose zone having varying soil moisture level and temperature conditions along with the saturated zone.

Chapter 3

Methodology

In this chapter, a detail methodology of laboratory experiments and numerical runs used to investigate the LNAPL behaviour in subsurface under varying subsurface conditions are presented. The capability of native microbes to degrade different initial LNAPL concentrations was investigated using a series of microcosm scale experiments. Subsequently, a series of another microcosm experiments were performed to investigate impact of soil moisture and temperature conditions on bioremediation of toluene. In microcosms experiments A series of one dimensional (1-D) column experiments were also performed to investigate LNAPL dissolution and biodegradation under varying temperature conditions. Role of plants on LNAPL remediation was in then investigated using a set of column experiments integrated with treatment wetland. Data set of a duplex constructed wetland was then analysed to see the role of plant and nutrient loading on various compounds of LNAPL removal from polluted root zone. Thereafter, role of groundwater table dynamics was investigated using a series of two dimensional (2-D) sand tank experiments and numerical runs. Three dimensional (3-D) sand tank experiments were also conducted to investigate the behaviour of LNAPL under varying groundwater flow conditions. Finally, simulation-optimization approach was used to design a bioremediation system to LNAPL polluted vadose and saturated zones under varying soil moisture and temperature conditions. The overall methodology of this study is shown in figure 3.1.

3.1 Materials and Methods

3.1.1 Experimental Media

The Indian standard (IS) clean sand 650 grade-II having less than 1 mm and greater than 0.5 mm particle distribution size was used as the experimental porous media. Before use experimental media, the sand was washed and oven dried at 100°C before using in microcosms, column and tank setups.

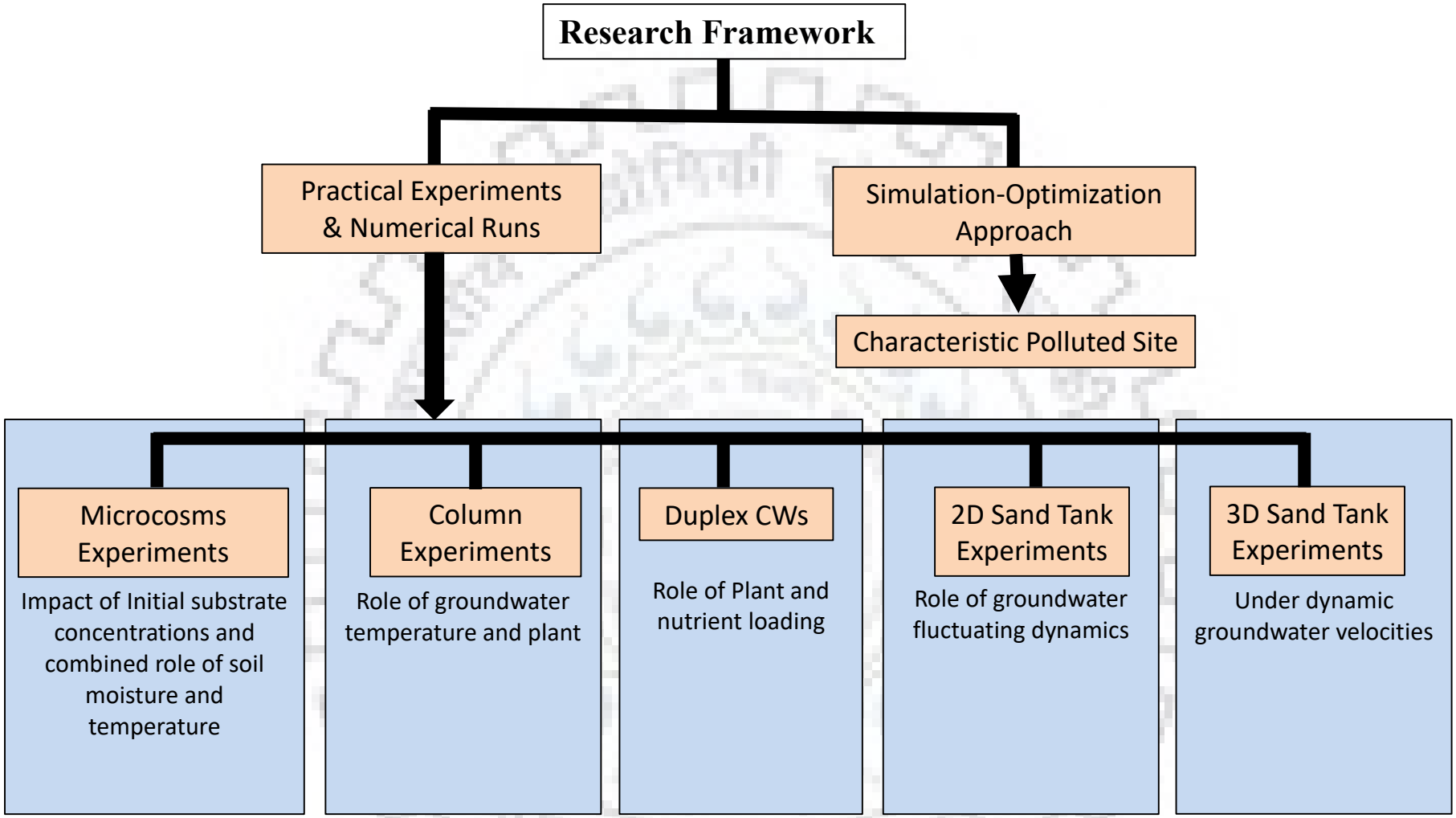

Figure 3.1: The overview of methodology adopted in this study to investigate the fate and transport of LNAPL and its bioremediation under varying subsurface conditions.

3.1.2 Toluene and Other Chemicals

Pure phase toluene (Fischer Scientific) was used in column and 2-D/3-D sand tank experiments of this study. While in microcosms experiments, a stock solution was prepared to dissolve toluene with 99.99% purity in Millipore water to its solubility limit (≃ 490 ppm at 20°C) at actual room temperature. The stock solution was incubated on an orbital shaker for 24 hours using a magnetic stirrer (REMI 10 MHL Plus). Solution of Sodium chloride (Merck) was used in different tracer experiments in column and sand tank experiments. In the sterile microcosms, $HgCl_2$ (Merck) was used to prevent the biotic losses. While, a mixture of dissolved phase BTEX and DRO compounds were used in duplex wetland study.

3.1.3 Experimental and Sampling Tools

Batches of 120 mL capacity were used in microcosms experiments. The Viton stoppers were used for seal using crimp seal to prevent any loss from batches. Similarly, certified screw top vial (Agilent 5183-2067) closed with Blue Screw Cap; PTFE/Red Si Septa (Agilent 5190-1599) were used during samples collections. The sterile dispo Van syringe (5mL, 10mL) manufactured as per IS: 10258/ ISO: 7886-1 were used for water sampling. Gas samples were collected using gold standard attached needles syringes (Agilent 9301-0713). GC syringes were provided by Agilent (part no: 9301-0713) attached with autoclave PTFE needles.

VDRL (Venereal Disease Research Laboratory) rotator/shaker was used for the mixing of chemicals during the batch experiment. The shaker was orbital rotator having speed range 70 to 210 RPM under platform (325×325 mm) with holder clamp and springs. Peristaltic pump (Model RH-P100VS-100-2H of Ravel Hitecks Pvt. Ltd. India) having dimension of 115 mm×225 mm×280 mm were used in different the experiment having a roller cage driven pumping mechanism (Anodized Aluminium) fitted with a stepper motor. The flow rate rang of the pump was 1 to 500ml/hr. The nozzles (3 mm inner diameter) were used to connect the tubing at both sides of the roller. The Viton tubes having inner diameter 3.6 mm were used with peristaltic pump during this study. The USP Class VI autoclavable carboy with stopcock (Tarsons Product Private Ltd.

India, Code 583280) having 10 litters storage capacity was used as water storage tanks during 3D sand tank experiments.

3.1.4 Polluted Groundwater Collection

The groundwater was collected from the shallow public hand-pump located at petrochemical contaminated sites nearby a refinery in India. Groundwater was collected with standard protocol and was left open under a ventilated hood to remove all volatile organic compounds which was later used as a primary source of potential microbes. Groundwater samples from each container were analyzed to confirm the background concentration of toluene.

3.1.5 Particle Size Analysis

The analytical sieve shaker (400 mm×230 mm ×350 mm) of Retsch (Germany) series AS 200 having measuring range 20µm to 20mm was used in these studies. Mechanical sieve analysis was performed to find the particle size distribution of the sand which is listed in table 3.1 along with other physical parameters.

Table 3.1: Properties of the sand used in laboratory experiments.

Characteristic	Values
Type	Medium Sand
Grain Size	0.5-1 mm
Particle Size > 1 mm	1.71±0.5%
Particle Size 0.5mm-1mm	98.27±0.5%
Particle Size < 0.5 mm	0.02±0.01%
Effective Porosity	0.33±0.02%
Bulk Density	1.52 ±0.1g/cm^3
Grain Density	2.31±0.1 g/cm^3

3.1.6 Sand Packing

The sand was made oversaturated first and then allowed to flow into the experimental setup. A comb-like rectangular metallic sheet was used to remove air bubbles from sand layers. The water filled setups was left for overnight to make the sand packing stable before draining the excess water.

3.1.7 Preliminary Experiments

Preliminary experiments were conducted to characterize the flow and transport parameters. The average porosity (η) of the sand obtained by oven dry and volumetric methods was found to be 0.33. The saturated hydraulic conductivity (K) from the constant head permeameter experiment was 8.15×10^{-5} m/s. For unsaturated hydraulic conductivity, the pressure plate experiments were conducted to estimate soil-water characteristic curve. The longitudinal dispersivity (D_L) resulted from dispersivity flux were estimated on basis of the breakthrough curves (BTCs) obtained from the tracer experiments for different experiments. Time values corresponding to relative concentration ratios of 84%, 50%, and 16% were used in calculating dispersion coefficient (D_L) by equation 2.7. The vertical dispersivity (D_V) were considered 0.1 times of the obtained longitudinal dispersivity (Dobson et al. 2007).

3.1.8 Vapour phase/liquid phase toluene mapping using GC-MS Analysis

The vapour phase samples were collected using air tight syringes from head spaced and unsaturated zone during different experiments of this study. Similarly, liquid phase samples were collected using sterile dispo Van syringe from saturated zone of experimental setups. The aqueous phase toluene concentration in the different microcosms was estimated using Henry's equation and by assuming equilibrium partitioning conditions. Collected samples were analysed using Gas Chromatography Mass Spectrometer (GC-MS), a synergistic combination of two powerful micro analytical techniques. It integrates the Gas Chromatography (GC) and Mass Spectrometer (MS) detector for qualitative and quantitative identification of organic compounds including the selected LNAPL. The GC separates the representative chemical and MSD provides the information that aids in structural identification using mass spectrum of each components. The GC-MS system consisted of the integration of GC system and MS detector equipped with carrier gases, automatic sampler (ALV system) along with work station having mass hunter software for control and data analysis. Annexure-VI describes the component wise specification of GC-MS system used for analysis of toluene throughout this study.

Agilent GC-MS (Model No. 5977) equipped with fast electronics model was used in this study, which can simultaneously acquire Selective Ion Monitoring (SIM) and SCAN

data. In this study, toluene concentrations were analyzed by SIM method, in which only selected ion fragments were monitored in order to obtain maximum sensitivity. The prepared method for toluene analysis was first calibrated for different toluene concentrations. In calibration, standard solutions of 2.5 ppm-100ppm concentration of toluene were prepared using stock solution. Then, these known standard solutions were analyzed in triplicate for area response curve. The obtained area response curves for each standard solutions were used in getting the calibration curve (Annexure-VI). A Chrompack capillary column (30m×0.25mm, Silicone coating of 0.25µm) was used for toluene analysis. Helium (99.999% pure gas from Sigma Gas, New Delhi) was employed as the carrier gas at a flow rate of 25 mL/min. Air and Nitrogen with a flow rate of 20 mL/min are used. The temperature of injection port, oven, and detector port was kept at 150°C, 120°C, and 150°C, respectively, during the measurements.

3.1.9 Microbiological Analysis

The microbiological analysis was performed during 1D column and 2D sand tank experiments. Microbial population was counted using heterotrophic or standard plate count methods (No. 9215C) (APHA, 1989). In this method, colony forming units (CFU) for live heterotrophic bacteria was estimated for collected soil-water samples during laboratory experiments. Immediately, all collected samples were diluted with a factor of 10^{1} to 10^{-5} and before shaking them for 15 seconds. Growth media was prepared using a combination of 20g protease peptone; 1.5g of K_2HPO_4; 1.5 g of $MgSO_4.7H_2O$; and 20g of Agar. Final P^H of media was adjusted to 7.2 by adding 1*N* NaOH, before autoclaving at 121^0C for 15 minutes. The laminar air flow setup was wiped with the 70% ethanol and UV light for the 15 minutes. Well marked (sample number, dilution, and date) plates poured with 30mL prepared growth media and kept still for few minutes to solidify agar surface. Thereafter, diluted samples were inoculated with the help of spreader on agar surface of respective plates. Successively, all the plates were kept for 48 hours at 36±1ºC for incubation. After the incubation, plates were counted manually using the quadrate method. Figure 3.2 shows a stepwise method used in CFU count in this study. Plates having an un-countable number (or too numerous) was considered as overgrowth.

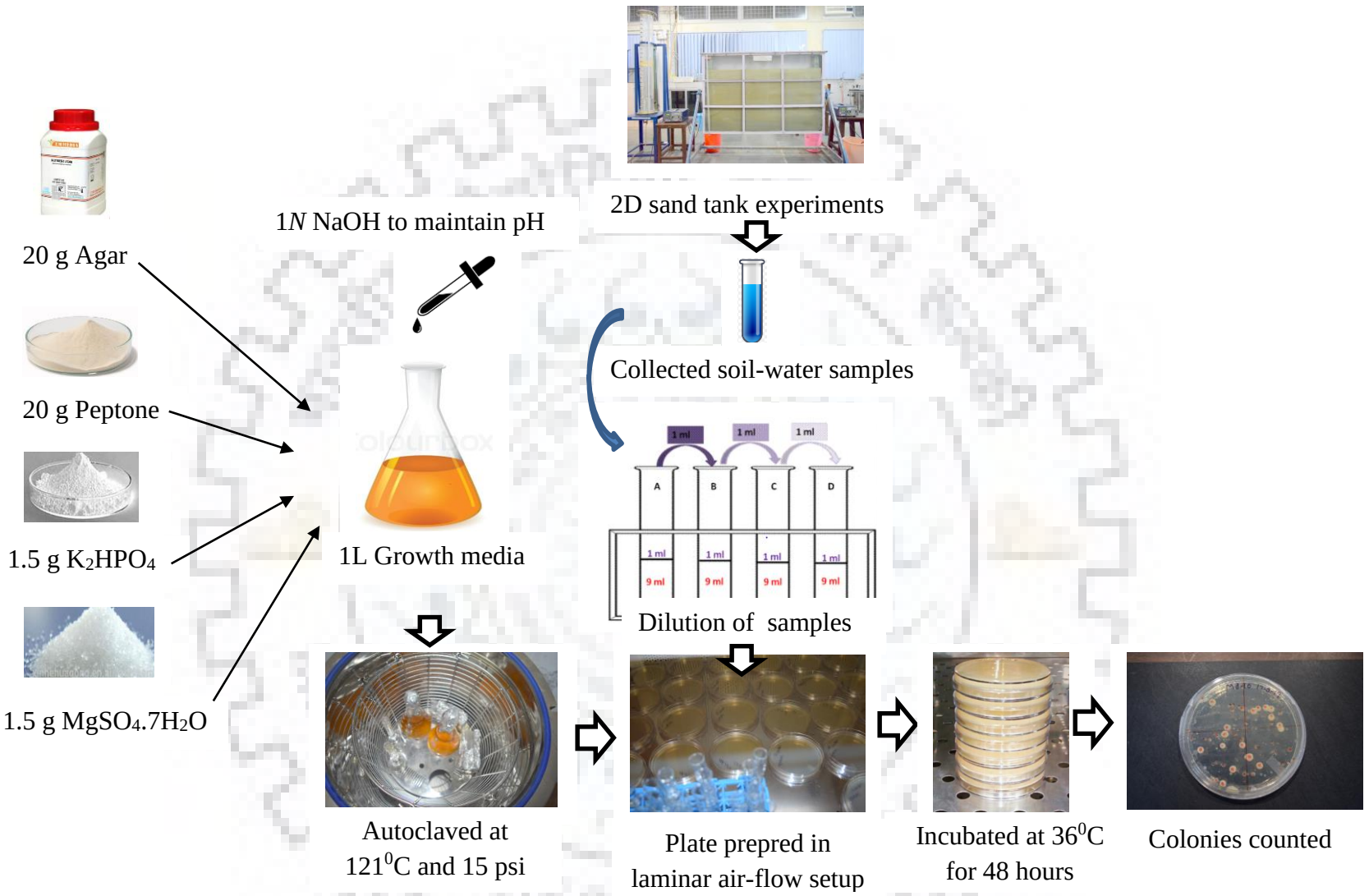

Figure 3.2: Schematic diagram representing the plat count method used in this study.

3.2 Microcosm Experiments

Microcosm experiments were performed using polluted groundwater collected from the refinery to check the capability of indigenous microbes to degrade dissolved toluene, the selected LNAPL. The basic aim of collecting the groundwater from the polluted site was to capture microbial population responsible for degrading the LNAPL pollutants. Batches of 120 mL capacity were assembled by adding 10 g soil along with appropriate volume of groundwater. Based on simple mass balance, a headspace of about 110 mL was provided to maintain aerobic condition throughout the experimental period for degrading the total added toluene in all the batches. Viton stoppers sealed with aluminum crimp were used to close the batches for preventing any leakages of toluene to the atmosphere. Sterile batches were prepared by adding 60 μL of 10 g/L of $HgCl_2$, in order to observe the abiotic losses of the LNAPL. Respective volume of stock toluene solution was injected trough the stopper with a gas-tight syringe to get initial its concentration of 10, 50, 100, 150, 200, 250 mg/L. Head space air and soil water samples were collected periodically and analyzed using GC-MS. The aqueous phase toluene concentration in the different microcosms was estimated using henry's equation and by assuming equilibrium partitioning conditions. Biodegradation rates were calculated using the observed concentration of dissolved toluene of live and sterile batches with progression of time in microcosms experiments. Two consecutive values of toluene concentration were used along with the time interval of the observation for calculating the degradation rate. Biodegradation rates obtained from the microcosm experiment were used in simulating the sink term representing the LNAPL attenuation rate at different substrate concentrations.

Thereafter, another series of microcosm experiments were performed to investigate the combined role of soil moisture and soil temperature conditions on biodegradation of dissolved toluene. Two sets of microcosms of 120 ml capacities were prepared considering four different moisture contents (20, 40, 60 and 80% of θ_s) in 20 g oven dry sand corresponding to about 20ml volume. The volume of void (0.008L) was obtained based on the volume of solids (0.02L) and porosity (40%) of the considered porous media. The remaining headspace (0.120L-0.02L+0.008L) of more than 230 mL with air at atmospheric composition ensured excess oxygen. The amount of soil water ratios for all batches were calculated using the

porosity of the sand (Table 3.2). The microcosm were assembled by adding appropriate amount of the dissolved phase toluene solution. Further, $HgCl_2$ was added in sterile batches to prohibit the microbial activities. In all the batches, a sufficient headspace was provided to maintain aerobic conditions throughout the experimental period. Later, the prepared batches with above mentioned combination of soil moisture contents were maintained at 30±2°C, to see the role of soil moisture conditions on biodegradation at room temperature. Whereas, another set of microcosms having same combination of soil moisture contents were incubated at 10±0.5°C to see the comparative impact of soil temperature along with varying moisture contents. The headspace vapour samples were collected from GC-MS analysis from the different microcosms periodically. Only dissolved phase of Toluene, the selected LNAPL, is used in microcosm experiments for investigating impact of different initial substrate concentration and combined role of temperature and soil moisture level on biodegradation rate. Other by- products and metabolic pathway of the considered LNAPL are not studied here as the main focus of these microcosm experiments was to investigate the impact of different (sub)surface parameters on degradation of the pollutant with progression in time.

Table 3.2: Microcosm setup used to investigate the combined effect of soil moisture and soil temperature on biodegradation of LNAPL.

Total Batch volume [mL]	Soil Volume [g]	Remain headspace [L]	Total Pore volume [L]	Batch Moisture %	Groundwater [L]	Toluene Stock [L]	Total Liquid Volume [L]	Air filled pore volume [L]	Total Batch Gas volume [L]
120	20	0.092	0.008	80	0.0016	0.0016	0.0032	0.0048	0.1148
				60	0.0012	0.0012	0.0024	0.0056	0.1156
				40	0.0008	0.0008	0.0016	0.0064	0.1164
				20	0.0004	0.0004	0.0008	0.0072	0.1172

3.3 One Dimensional (1D) Column Experiments

A one dimensional glass column setup was fabricated and filled homogenously with sand for this purpose. Column was integrated with automatic cold and hot bath to maintain groundwater temperature of 4^0C, 20^0C, 28^0C and 36^0C during experimental phase. Figure 3.3 shows the

schematic diagram of the one dimensional column set having inner diameter if 14.2 cm and a height of 140 cm. Sand was packed up to 70 cm and remaining top 70 cm was kept as head-space to maintain aerobic condition. The water filled column was left for overnight to make the sand and then allowed to drain. Filtration screens were fixed around the inlet and outlet valves to prevent the entrance of the sand particles in the connecting viton tubes. Piezometers were attached to the column to measure the positions of the groundwater table. Similarly, an automatically controlling hot bath was connected to same peristaltic pump to provide high temperature groundwater. The hot water bath was attached with metallic heating rod (non-reactive) to stream water. A thermometer and temperature sensor was attached to cold and hot bath respectively. A flow controlling valve was attached to cold/hot baths before the peristaltic pump to allow the required cold/hot groundwater to flow in the system. Sampling ports (P1-P3) were installed in saturated zone at a difference of 10 cm to each other. One head space sampling port was used to collected vapor phase samples. Entire setup was air tight to conserve the mass of the LNAPL.

Tracer transport experiment was performed first to estimate vertical dispersivity coefficient. A solution of tap water and sodium chloride with an initial concentration of 1000 mg/l was continuously injected to column from bottom. The water samples were collected from port 1 for 6 hours with an interval of 0.5 hour and analysed using portable conductivity meter. The soil water flow and solute transport parameters used in this study are listed in table 3.3. Thereafter, LNAPL fate and transport experiments was started by recirculating cold groundwater at the rate of 1.2 m/day to mimic low temperature at i.e. 4^0C inside the column. Once background column temperature reached at 4^0C, 5mL of Toluene, was spiked from injection port (Fig. 3.3). Subsequently, other three set of experiments were performed at soil-water temperature of 20^0C, 28^0C and 36^0C by recirculating heated water with same flow velocity through the column setup. Groundwater temperature was continuously recorded using thermometer attached with column and cold bath. Soil water and vapour samples were collected from sampling ports to analyses dissolved LNAPL concentrations, microbial populations.

(a)

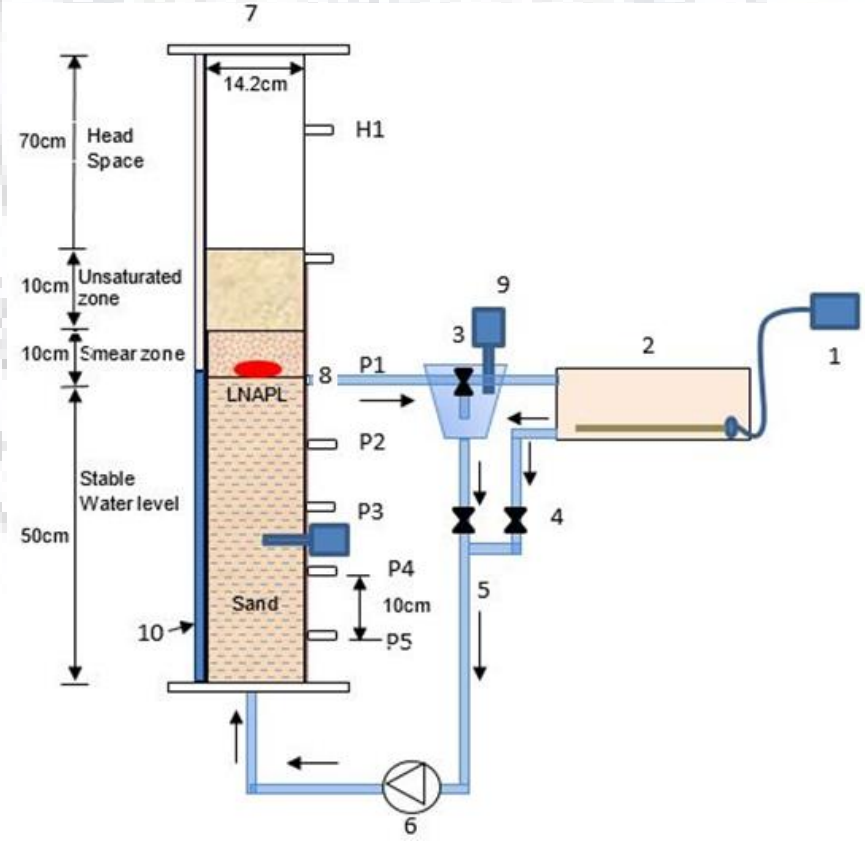
7
14.2cm
70cm
Head Space
H1
10cm
Unsaturated zone
10cm
Smear zone
LNAPL
8
P1
9
3
2
1
P2
Stable Water level
50cm
P3
4
P4
10cm
P5
5
Sand
10
6

(b)

Figure 3.3: (a) Photo of 1D column setup and (b) schematic diagram of the laboratory 1D column setup used to investigate thermally enhanced bioremediation of LNAPL in subsurface. 1: Electric board; 2: Hot water bath; 3: Cold water bath; 4: Flow controlling valve; 5: Viton tube cover with cotton; 6: Peristaltic pump; 7: column setup; 8: Injection port; 9: Thermometer; 10: Piezometer.

Simulation runs were performed using one-dimension LNAPL flow equation for domain having different level of temperatures. A numerical domain similar to 1D column setup was developed and considered as homogenous distribution of sand. The Galerkin finite elements method integrated with Crank-Nicholson iterative scheme is used for the solution. Thus, the total simulation time was taken 60 hours and iteration number was fixed as 40. The biodegradation rates observed in column experiment for respective temperature were incorporated as sink term to numerical domain. Fully saturated porous media upto 50 cm from bottom and no background concentrations was taken as initial condition. A constant concentration boundary condition (Dirichlet) was applied as upper boundary condition. Whereas, the applied groundwater flux was considered at bottom boundary along with zero concentration. Five observation nodes were assigned at a distance of 10 cm to each other from bottom of domain.

Table 3.3: The soil-water and solute transport parameters used to simulate 1D fate and transport of dissolved LNAPL under varying temperature conditions.

Soil-water flow and solute transport parameters	Values	Unit
Porosity (η)	0.33	-
Flow velocity (q)	1.2	m/day
Average bulk density (ρ_b)	1.5	g/cm^3
Vertical dispersivity (D)	2.8	m
Biodegradation rate at 4^{0}C	0.002	mg-L/hr
Biodegradation rate at 20^{0}C	0.008	mg-L/hr
Biodegradation rate at 28^{0}C	0.012	mg-L/hr
Biodegradation rate at 36^{0}C	0.015	mg-L/hr

3.4 Treatment Wetland Investigation

Preliminary, treatment wetland experiments were performed using column setup integrated with a small scale wetland with and without Cana plant. Column setup having inner diameter if 14.2 cm and a height of 140 cm was integrated with wetland setup of dimension 60 cm L × 30 cm W × 30 cm D. Two set of integrated wetland system, one planted and another unplanted, was analysed to see the role of plant. A mixture of polluted groundwater and root zone water was supplied from top surface of sand filled in column. The water samples collected from different ports were analysed for toluene concentration using GC-MS. Experimental data set of duplex CWs performed at IHE delft was collected and analysed to see the role of plant on removal of LNAPL compounds including Diesel ranges organics (DRO). A duplex constructed wetland consists of vertical constructed wetlands (VF-CWs) and horizontal flow filter (HFF) were investigated under three different nutrient amendment conditions. The wetland setup consisted of three evenly spaced laboratory scale duplex-CWs, three influent tanks having a capacity of 200L and made of high-density polyethylene plastic containers located next to the duplex-CWs, and three peristaltic pumps used to pump the influent into the duplex-CWs. The VF of the duplex-CWs had dimensions of 0.6 m L × 0.4 m W × 0.8 m D and planted with common reed *Phragmites australis*, while the HFF had dimensions of 0.6 m L × 0.4 m W × 0.35 m D with a surface area of 0.24 m^2 (L × W) for each set up (figure 3.4). The VF was filled with 10 cm depth of gravel (15 – 30 mm) and was covered with 70 cm fine sand (1–2 mm) on top. The entire depth of the HFF was filled with 35 cm of fine sand. The HRT is calculated using the wetland volume (m^3) divided by average flow rate (m^3/day), while HLR is calculated by average flow rate (m^3/day) divided by wetland area (m^2). The properties of the porous media estimated in primary studies are listed in Table 3.3. The VF and the HFF CWs had an effective volume of 0.0768 m^3 and 0.0336 m^3 and a hydraulic retention time of 4.8 days and 2.1 days, respectively. Before starting the experiments, the duplex-CWs were allowed to acclimatize to an organic loading rate of 0.0660 m^3 m^{-2} day^{-1} for approximately 4 weeks. Thereafter, the data collection was conducted which was done for an additional 8 weeks. All three duplex-CWs were operated under identical conditions. However, nutrient levels were modified after two weeks by adding different concentrations of mineral nitrogen (NH_4Cl) and phosphate (K_2HPO_4) to each of the influent tanks (INF1, INF2, AND INF3), corresponding to

concentrations of 10, 30 and 60 mg/L of NH_4^+-N and 3, 6 and 12 mg/L of PO_4^{3-}, respectively from day 21 to day 56. The hybrid CWs were placed in a climate-controlled greenhouse located at IHE Delft (The Netherlands). The temperature of the greenhouse was kept between 20 and 23^o C and a light intensity between 85 and 100-µmol photons m^{-2} sec^{-1} for 16 h d^{-1} was maintained throughout the experiments. On can find more detail of duplex wetland setup from Mustapha (et al. 2018).

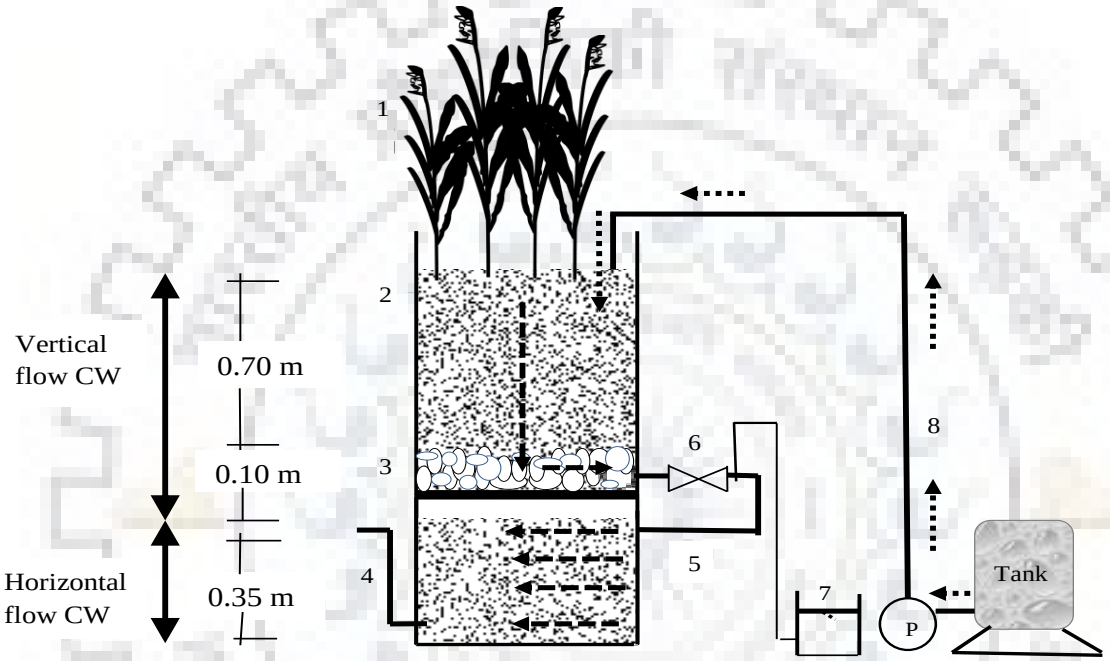

Figure 3.4: Schematic representation of the duplex-CW configuration used in this study. 1-*Phragmites australis*, 2- Sand, 3- Gravel, 4- Outlet pipe, 5- Pipe connecting the compartments, 6- Valve, 7- Effluent collection bucket, 8- Inlet pipe and Tank – Influent tank.

Numerical runs were performed to investigate the biodegradation of LNAPL compounds in a synthetic contaminated wastewater in the duplex constructed wetlands using CW2D. A 2D study domain representing both VF and HFF of duplex-CW was created first to numerically solve the processes of the treatment system. The study domain of the VF CW had dimensions of 0.8 m × 0.4 m, whereas that of the HFF had dimension of 0.35 m × 0.4 m for L×W respectively. The top layer of 0.7 m and undelaying 0.1 m of the VF domain was assigned with sand and gravel characteristics, respectively. Likewise, the entire HFF domain was assigned with sand medium only. The simulation domain was discretized in small fine elements grids of

hexahedral geometry of similar size of media with a stretching factor of unity for solving the governing equations numerically. Three observation nodes situated at the top and outlet of the VF and HFF were considered to represent the sampling ports of the experimental set up. The hydraulic properties of the porous medium were characterized using the van Genuchten-Mualem approach (van Genuchten, 1980). The Crank-Nicholson iterative scheme was used for time weighting solution for every new time step of the nonlinear nature of the governing equations (Simunek et al. 2011). The initial condition for the simulation domain was specified as saturated moisture content of the respective porous media. For the solute transport simulation, zero concentration of the selected pollutants was taken as an initial condition. All three duplex CW were differentiated by its nutrient levels incorporated as initial concentrations of nitrogen and phosphate to each of the influent tanks (INF1, INF2, AND INF3), corresponding to concentrations of 10, 30 and 60 mg/L of NH_4^+-N and 3, 6 and 12 mg/L of PO_4^{3-}, respectively. No flux boundary was taken at lower and side faces of the tank set ups. The outlet point of HFF was considered as a free drainage element. Surrounding greenhouse conditions were taken as the top atmospheric boundary condition of all VF.

Monod type of bio-kinetic model was used in mass balance equation to incorporate the function of these autotrophic and heterotrophic bacteria in all three duplex-CWs. The Monod kinetics can describe degradation rates of hydrocarbons including DRO for varying concentrations to represent zero to first order kinetics (Yadav and Hassanizadeh, 2011) which can be written as equation 3.1:

$$\frac{\partial C}{\partial t} = k_m C/(K_s + C) \tag{3.1}$$

Where rate constant (k_m) was equal to $\mu_{\max} X_0$, K_s was growth limiting concentration and C is target compound concentration at time t. The growth rate depends on the maximum growth rate of the autotrophic/heterotrophic bacteria ($\mu_{\max}$) and concentration required to produces initial biomass concentration (X_0). This kinetic expression was also used to simulate a) the sequential nitrification of ammonium into nitrite and nitrate by *Nitrobacter* and *Nitrosomonas* respectively; b). Nitrite and nitrate based growth of heterotrophs (denitrification); and c). hydrolysis (Langergraber and Šimůnek, 2005). Table 3.4 presents the characteristic of the

practical and simulation experimental domain used to investigate the degradation of LNAPL compounds in the treatment-CWs.

Table 3.4: Characteristics of the practical and simulation experimental domain used to investigate the degradation of LNAPL compounds in the treatment-CWs.

Characteristics	Values	Source
Porosity (gravel)	40%	Determined
Porosity (sand)	34 %	
Effective volume	0.0768 m^3	Calculated
Hydraulic retention time (HRT)	4.85 days	Calculated
Hydraulic loading rate (HLR)	0.0660 $m^3/m^2/day$	Calculated
Diffusivity (D^*)	6.3×10^{-6} [cm^2/sec]	Calculated
Dispersion coefficient (D_i)	3.4±0.2 [cm^2/h]	
Flow rate	0.0158 m^3/day	Calculated
Total simulation time	56 days	Experimental duration
Maximum growth rate μ_{max}	6 [1 d^{-1}]	Langergraber and Šimůnek
Growth limiting concentration K_s	0.5 [mgL^{-1}]	2005

3.5 Two Dimensional (2D) Sand Tank Experiments

In this study, the behaviour of pure phase and dissolved LNAPL plume in subsurface was investigated using a series of 2D sand tank set up. A series of two dimensional sand tank experiments were performed under 1) steady-state groundwater condition and 2) three different dynamic groundwater table fluctuation (rapid, general and slow) conditions. Two dimensional sand tank setup was fabricated having 2.5 mm thick stainless steel formed box with inner dimensions of 150 cm-long × 120 cm-high ×10 cm-deep (Figure 3.5). Two wells were installed at each side of tank and front cover of tank was made of a thick glass sheet for viewing. Sand was packed homogenously between both wells upto 90 cm height. Top 30 cm height of tank was kept as head-space to maintain aerobic condition. The system was then flushed at maximum velocity until the effluent water was free of suspended fine material. After each experiment, the used sand was replaced with fresh sands using same method for each new set of experiment. The integrated wells were used as upstream (high pressure) and downstream (low pressure) reservoir to maintain the water table. An axillary column containing the collected groundwater was connected to the inlet port of upstream well with viton tubes of a

peristaltic pump. This peristaltic pump refers as “upstream pump” was used to supply groundwater to sand tank. The objective of this auxiliary column was to maintain constant pressure of groundwater table (Figure 3.2). Similarly, the outlet of the downstream well was connected to another peristaltic pump (refer as downstream pump) to extract the groundwater and recirculate to axillary column. The flow rate of the pump was adjustable to allow setting of the desired pressure difference in the two reservoirs, thereby controlling the groundwater flow within tank setup. The sampling ports having equal horizontal spacing of 15.5 cm from two horizontal layers situated at 30 and 60 cm from bottom of the tank setup (Figure 3.5). Piezometers were attached to the tank to measure the positions of the groundwater table. Filtration screens were fixed around the inlet and outlet valves to prevent the entrance of the sand particles in the connecting viton tubes. Entire setup was air tight to conserve the mass of the LNAPL. Rapid, general and slow groundwater fluctuations were maintained by raising 5 cm magnitude of fluctuation in 1, 2, and 4 hours respectively. The groundwater table was then lowered in the same manner; a drop of 5 cm in subsequent 1, 2 and 4 hours for rapid, general and slow fluctuation conditions respectively.

(a)

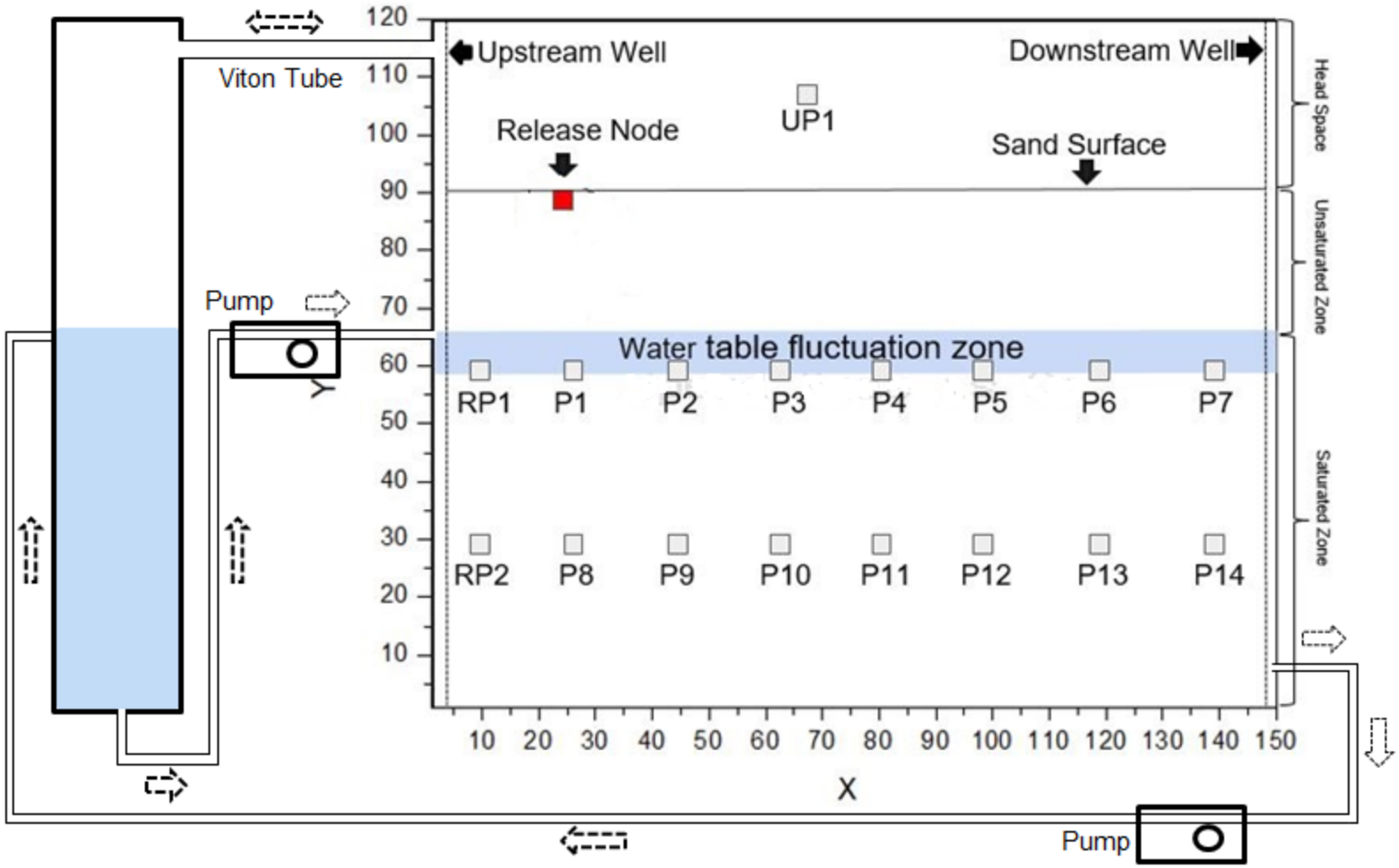

(b)

Figure 3.5: (a) Photo and (b) Schematic diagram of 2D sand tank used to investigate the role of dynamic groundwater table conditions on fate and transport of LNAPL pollutants. Two row of sampling ports are installed at 30 and 60 cm from bottom in back side of tank.

Here “one fluctuation cycle” refers to complete high-low-high groundwater table positions. Groundwater table rising was maintained by pumping water from axillary column to upstream well and closing outflow from downstream well for a target duration of respective fluctuation conditions. Likewise, groundwater falling was maintained by extracting water from downstream well and closing inflow to sand tank from auxiliary column for same duration. Such switching of the peristaltic pump was adjustable and calibrated for a target duration of respective fluctuation conditions. A brief pumping details of different considered cases are listed in table 3.5. To maintain a rise and fall of 5 cm, (150 cm-long × 05 cm-magnitude of fluctuation ×10 cm-deep × 33% porosity) 0.002475 m^3 or 2.475 liters of groundwater was required as inflow and outflow.

Table 3.5: Inflow and outflow pumping strategies of groundwater table fluctuation cases.

Conditions	Inflow Pumping		Outflow pumping		Total Duration	Pumping Rate mL/hr
	Rise	Fall	Rise	Fall		
Rapid fluctuation	1 hour	×	×	1 hour	2 hours	2475.0
General fluctuation	2 hours	×	×	2 hours	4 hours	1237.5
Slow fluctuation	4 hours	×	×	4 hours	8 hours	618.7

× Respective pump was switched-off; *Including rise and falling

Preliminary, a series of tracer transport experiments were performed to determine the longitudinal and vertical dispersivity of sand under rapid, general, slow and stable groundwater table conditions. A solution of tap water and sodium chloride with an initial concentration of 1000 mg/l was continuously injected to tank for the selected groundwater fluctuation cases. The water samples were routinely collected sampling port located at *X:*45; *Y:*50 cm from the injected point. The concentration measurements are done using portable conductivity meter. Subsequently, a series of LNAPL transport experiments were performed conducted using 2D sand tank setup by creating three different groundwater

table fluctuating conditions. Pure phase toluene was released from the top surface of the tank set up to create a pool of the LNAPL above the groundwater table which was fluctuated in the range of 55-60 cm from the tank bottom. The toluene was injected at a constant rate of 02 mL/min for 5 minutes using an air-tight syringe. Thereafter, a small amount of soil water samples from both layers and soil vapor samples from head-space were collected carefully. Soil water samples were collected from all ports with an interval of 1, 2 and 4 hours in rapid, general and slow groundwater fluctuation conditions respectively.

3.6 Three Dimensional (3D) Sand Tank Experiments

Tracer and LNAPL transport experiments were conducted in a three-dimensional air tight tank setup representing a subsurface system of variably saturated zone underlined with shallow unconfined aquifer. Figure 3.6 shows the schematic diagram of the 3D sand tank setup used in this study. The tank setup was made of 7-mm thick glass sheets supported by a stainless steel frame having inner dimensions of 60 cm length, 30 cm width, and 60 cm height. The inlet and outlet ports of the tank setup were connected with 1cm thick water chamber attached with central chamber having sand mass, to ensure the uniform groundwater flow. These chambers are separated from the soil mass by a stainless steel mesh to prevent soil flow in the chambers. The tank setup was embedded with three rows of sampling ports spaced 14 cm apart vertically; two rows in front side and one in backside as shown in the figure 3.6. The square dots in figure 3.6 show the location of the sampling ports (2 cm apart in horizontal direction) embedded in three horizontal layers situated 14 cm apart vertically from each other. Two layers are visible in this photo and the third layer is situated between these two layers on the backside wall of the tank setup. The openings of sampling ports were attached with stainless steel needles of diameter 0.3 mm and were located at 5, 10, 15, 20 and 25 cm depth in the transverse direction and 2 cm away horizontally. The injection port was located at the center point of the upper glass sheet for the introducing of the toluene. Inlet and outlet wells were installed on right and left sides, in order to maintain the groundwater gradient in the tank setup. The tank was filled homogeneously with clean sand which replaced with fresh sands using same method for

each new set of experiment. Filtration screens were fixed around the inlet and outlet valves to prevent the entrance of the sand particles in the connecting viton tubes.

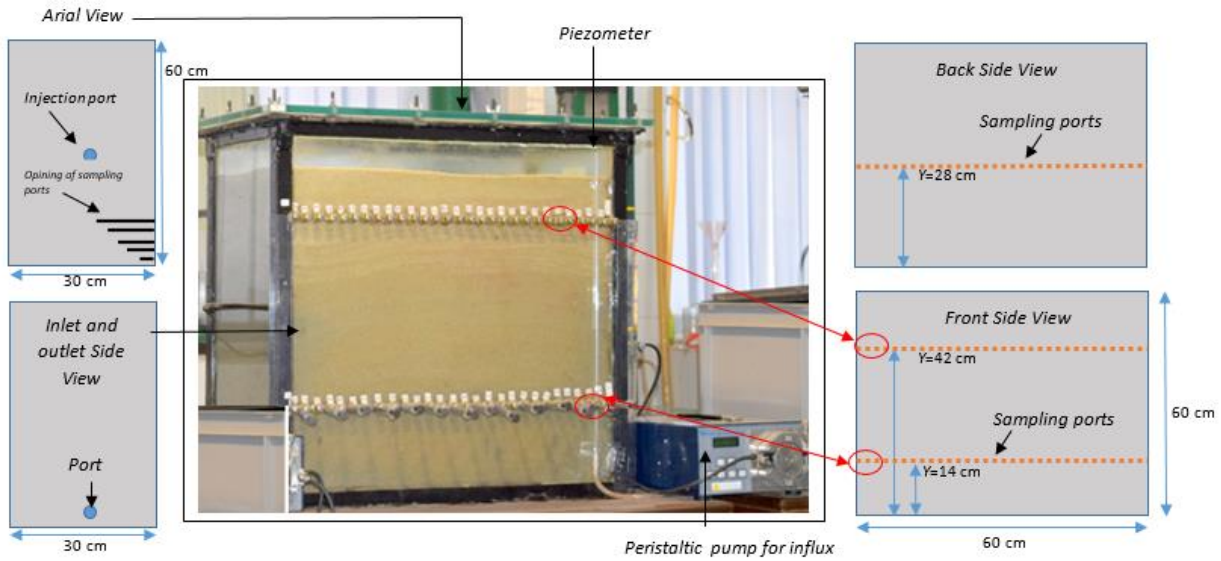

Figure 3.6: Photo of 3D sand tank used to investigate the role of groundwater variation on fate and transport of LNAPL pollutants in subsurface. Groundwater was flowing from right to left. The square dots show the location of the sampling ports (2 cm apart in horizontal direction) embedded in three horizontal layers situated 14 cm apart vertically from each other. Two layers are visible in this photo and the third layer is situated between these two layers on the back side wall of the setup.

A series of tracer transport experiments was performed to determine the longitudinal dispersivity of sand under fast, base and slow groundwater velocities. Sodium chloride with an initial concentration of 1000 mg/l was continuously injected to tank under selected groundwater velocity cases. The water samples were routinely collected at observation point located at *X:*25; *Y:*15; *Z:*28 cm from the injected point. Thereafter, a series of LNAPL transport experiments were performed using 3D sand tank by creating three different groundwater flow regimes. A constant water flux was allowed to flow first for maintaining a flow velocity of 1.2 m/day in the horizontal direction to mimic a groundwater flow regime under high hydraulic gradient conditions. A carboy containing the collected groundwater was connected to the inlet valve with Viton tubes. The outlet of the tank setup was connected to a peristaltic pump to regulate the groundwater flow from

right to left. Pure phase of toluene was released from top surface of the tank setup to create a pool of the LNAPL above the groundwater table which was maintained at 35 cm from the tank bottom. The toluene was injected at a constant rate of 02 mL/min for 5 minutes using an air tight syringe. Separately in another set of experiments the groundwater flow regimes were modified by increasing/decreasing the water flux passing through the saturated zone by keeping the water table location at the same height. Piezometers were attached to the tank to measure the position of the groundwater table. Soil-water samples were collected from different sampling ports and were analyzed for toluene concentration periodically.

3.7 Numerical Modeling of 2-D and 3-D System

Dissolved phase LNAPL transport in saturated zone was simulated using the 2-D or 3-D form of classical solute transport equation 3.2 as-

$$\frac{\partial}{\partial t}(\phi S_f C_{if}) = -\nabla.(q_f C_{if}) + \nabla.(nS_f D_{if}.\nabla C_{if}) + K_{if} - S \qquad (3.2)$$

Where C_{if} is NAPL compound in *f* phase [ML^{-3}], q_f is discharge through soil profile [LT^{-1}], While K_{if} is the dissolution rate of LNAPL [$ML^{-3}T^{-1}$] can be observed using characteristic length of LNAPL pool and equilibrium concentration in dissolved phase. Likewise, S is biodegradation rate [$ML^{-3}T^{-1}$] (as sink term) can be obtained using (control and live) microcosms experiments. D_{if} is hydrodynamic dispersion [L^2T^{-1}] which can be obtained using breakthrough curves (BTCs) of tracer transport experiment. In this study, LNAPL pool dissolution rate (K_{if}) was estimated first using mass transfer relationship (equation 3.3) suggested by Chrysikopoulos et al. (1994).

$$K_{if} = k^*(C_s - C) \qquad (3.3)$$

Where, C is the experimentally observed dissolved LNAPL concentration at time t, and k^* is the dissolution coefficient. C_s is known as effective solubility and equal to $C_0\chi^0$, in

which χ^0 molar fraction of toluene and C_0 subcooled state solubility (Chrysikopoulos, 1995; Saba and Illangasekare, 2000), Dissolution coefficient was estimated using relationship (equation 3.4) suggested by Power and Heermann, (1999).

$$k^* = n\sqrt{4D_L V_x / \pi l_c} \tag{3.4}$$

Where l_c is characteristic LNAPL pool length which is equal to square root of the pool area observed during practical experiments.

The HYDRUS 2-D model was used to solve governing equation for water flow and solute transport (Simunek et al. 1996). A two dimensional numerical domain having similar dimension of sand tank was created to simulate soil water flow and LNAPL transport through saturated zones. The Galerkin finite elements method integrated with Crank-Nicholson iterative scheme was used for the solution. The study domain was given no background concentration of toluene at as initial condition. Saturated moisture content was taken as the initial moisture level of the domain and the top boundary was considered as the water table. Right side boundary was taken as continuous flux by incorporating respective pulse of influx for 1, 2, and 4 hours to maintain groundwater table fluctuation along with base groundwater velocity. Similarly, left side boundary was taken as a pulse out-flux for the respective cases. In case of stable groundwater table condition, constant influx and out-flux was taken without pulse condition. No flux condition was considered as the lower boundary condition. One node in centre of the top boundary was taken as LNAPL release point.

For 3-D sand tank experiments, numerical runs were performed using 3D form of equation 3.2 to solve LNAPL transport under varying groundwater flow velocities. The simulation domain was discretised in small grids of a hexahedral geometry for solving the governing equation numerically. The HYDRUS 3-D is graphical user interface used to solve governing equation for water flow and solute transport (Simunek et al. 1996). A three dimensional numerical domain having similar dimension of sand tank was created to simulate soil water flow and LNAPL transport through saturated zones. The Galerkin finite elements method integrated with Crank-Nicholson iterative scheme is used for the solution

(Šimůnek et al. 2011; 2012). The spatial biodegradation rates were estimated using observed BTCs of dissolved LNAPL transport in 3-D sand tank under varying groundwater flow conditions. The spatial biodegradation rate was calculated using the equilibrium concentration difference between two locations divided by total distance between them. The model input parameters are listed in table 3.6. No background concentration (zero) was taken as initial solute condition for entire the domain. Saturated moisture content was taken as the initial moisture level of the domain and the top boundary was considered as the water table (atmospheric pressure). No flux condition was considered as the lower boundary condition. One node in centre of the top face was taken as LNAPL release point. Right side boundary was taken as constant flux by incorporating respective influx to maintain fast, base and slow groundwater velocity. Similarly, left side boundary was taken as a constant flux for the respective flow velocity case.

Table 3.6: Summary of water flow and solute transport parameters used to simulate LNAPL transport under varying groundwater flow conditions.

Water flow and solute transport parameters	Values
Saturated hydraulic conductivity (K_s)	8.15×10^{-5} m/s
Longitudinal Dispersivity (D_L)	1.42-3.4±0.2 [cm^2/h]
Transverse & Vertical Dispersivity (D_T & D_V)	0.142-0.34±0.02 [cm^2/h]
Diffusion coefficient (D_*)	6.3×10^{-6} [cm^2/sec]
Retardation factor (R)	1
Solubility limit (at 20-25^{0}C)	515 [mg/l]

3.8 Simulation-Optimization Approach for Bioremediation of LNAPL Polluted Subsurface Zones

A characteristics study area of dimension 690m×510m×30m was selected to design bioremediation system to remove toluene from contaminated subsurface comprising unsaturated and saturated zones (figure 3.7). The domain was divided into two vertical layers of 15 m each to represent vadose zone and saturated zone. In which, top 15 m was differentiated by applying varying soil moisture content between 20-80% and the bottom 15 m was incorporated with saturated conditions as selected by Shieh and Peralta (2005) and Yadav et al. (2016) to evaluate the performance of in-situ bioremediation system for polluted groundwater. To maintain groundwater flow in the saturated domain, the western and eastern boundaries were assigned the hydraulic head of 30.5 m and 27.7 m, respectively. Thus, the groundwater flow direction was governed by the initial hydraulic gradient of 0.004 in the west to east direction. The contaminated area of dimension 29 m × 31 m was incorporated with 250 ppm initial dissolved LNAPL concentration at the top surface.

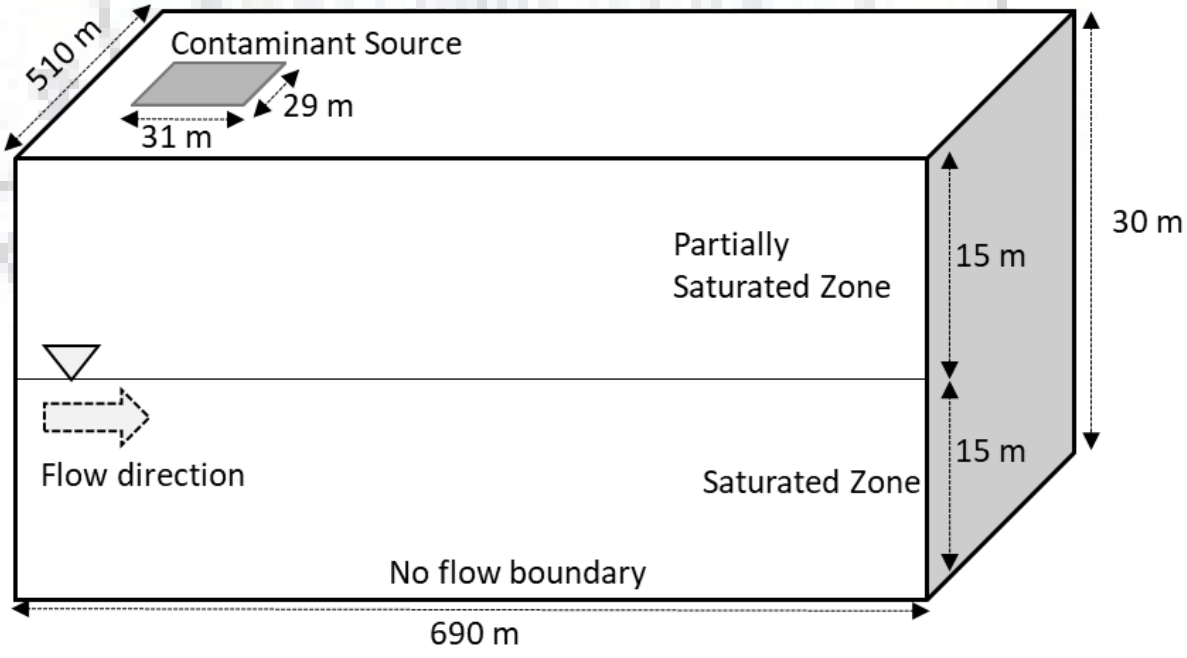

(a)

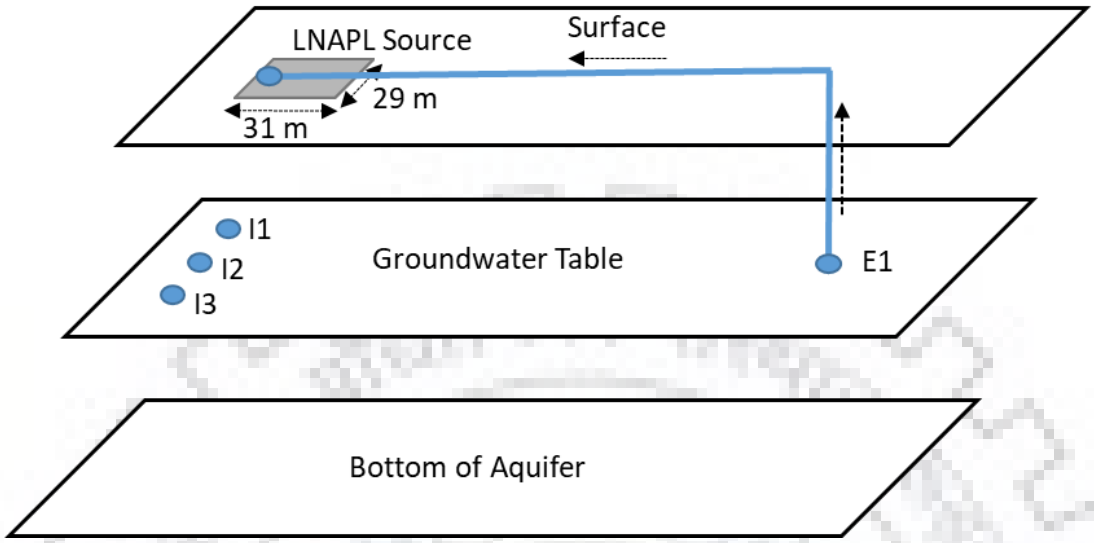

(b)

Figure 3.7: Schematic diagram representing selected study domain. (a) dimensions, layers, and boundary conditions, (b) indicating injection wells used to supply water and electron acceptors and extraction well used to control plume.

To establish bioremediation system, three injection wells and one extraction well were considered in up-gradient and downgradient side, respectively. The injection wells were considered to provide water having high electron acceptor i.e. oxygen, whereas the extraction well was considered to control the dissolved plume. Further, the extracted groundwater was used to recharge top contaminated surface as indicated in the figure 3.4. The designed system was improved in this study by recharging the contaminated unsaturated zone using the extracted groundwater to accelerate biodegradation rate. Recharging vadose zone using extracted water is also not adding any cost to the system, minimizing the overall remediation cost due to high biodegradation in vadose zone. Practical-Simulation-Optimization approach was used to simulate fate and transport of LNAPL in subsurface and to optimize pumping rates for minimum remediation cost and maximum removal of LNAPL from polluted zone. The flowchart shown in figure 3.8 represents the overall methodology adopted in this study. Biodegradation rates observed in

microcosms having different combination of soil moisture and temperature was incorporate here to polluted vadose zone.

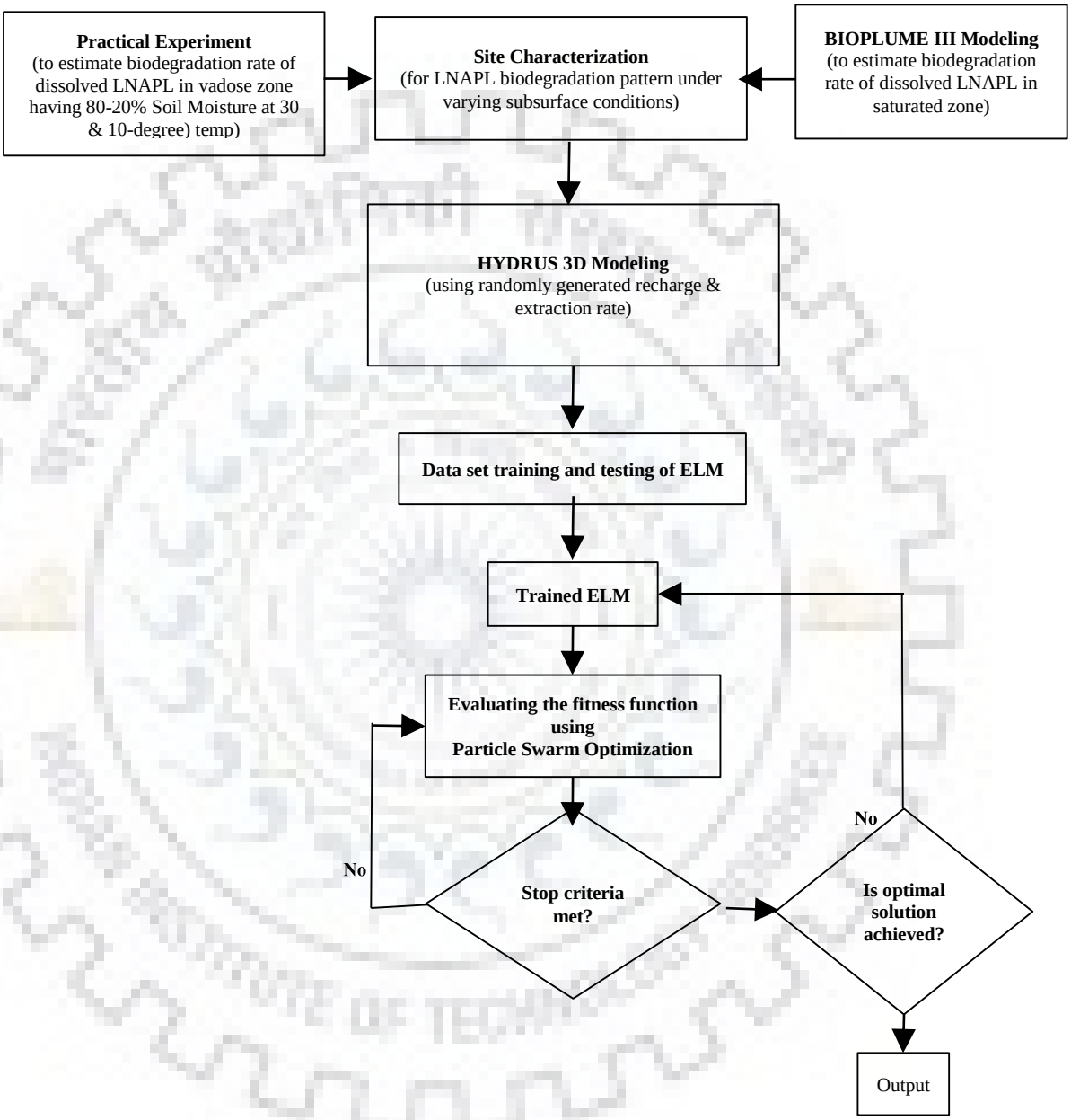

Figure 3.8: Flowchart of the overall methodology adopted to design biodegradation system using a simulation-optimization approach to remove LNAPL from subsurface comprising both unsaturated and saturated zones.

Initially, the numerical simulation was done using BIOPLUME III to estimate the enhanced biodegradation rate of dissolved LNAPL in the saturated zone. The BIOPLUME III model simulates advection, dispersion, sorption, and ion exchange processes. The model simulates both aerobic and anaerobic biodegradation and solves the transport equation for hydrocarbon, oxygen, nitrate, iron (II), sulfate and carbon dioxide using first-order decay or Monod kinetics or instantaneous reaction types of kinetics. In the aerobic biodegradation, oxygen is used as an electron acceptor, however, the anaerobic biodegradation is governed by nitrate, iron (III), sulfate, and carbon dioxide. In this study, only aerobic biodegradation was considered because in the presence of organic substrate and dissolved oxygen, microorganisms capable of aerobic metabolism will predominate over anaerobic forms (Borden and Bedient, 1986). The instantaneous reaction kinetics was used while simulating the aerobic biodegradation of organic compound. For more details about the governing equations, assumptions, and limitations, refer to Rifai et al. (1997).

Thereafter, a series of HYDRUS 3D simulation were performed to investigate the fate and transport of dissolved LNAPL through vadose zone incorporating randomly generated pumping rates for three injections well and one extraction well. The Richards equation coupled with advection-dispersion equation is used for dissolved toluene transport through unsaturated zone as:

$$\frac{\partial \theta}{\partial t} = \frac{\partial}{\partial z}\left[K(h)\left(\frac{\partial h}{\partial z} + 1\right)\right] - S \tag{3.5}$$

where θ is the volumetric water content $\left[L^3L^{-3}\right]$, S is a sink term $\left[T^{-1}\right]$, h is the pressure head $\left[L\right]$, x_i (i=1, 2) are the spatial coordinate $\left[L\right]$, t is time $\left[T\right]$, and *K(h)* is the unsaturated hydraulic conductivity function $\left[LT^{-1}\right]$. To solve this equation, explicit expressions for the soil constitutive relationship between the dependent variable h and the nonlinear terms K and θ are required. Out of the many soil moisture constitutive relationships reported in literature, the most popular ones are by Van Genuchten (1980). The closed form θ-h relationship developed by fitting mathematical equations to field experiments data yields

$$\theta(h) = \begin{cases} \theta_s & h \geq 0 \\ \theta_r + [\theta_s - \theta_r] / \left[1 + |\alpha h|^n\right]^m & h < 0 \end{cases} \quad (3.6)$$

Likewise, Van Genuchten (1980) used the statistical pore size distribution model for the K-h relationship as:

$$K(h) = \begin{cases} K_s & h \geq 0 \\ K_s \dfrac{\left\{1 - (\alpha h)^{n-1}\left[1 + (\alpha h)^n\right]^{-m}\right\}^2}{\left\{1 + (\alpha h)^n\right\}^{m/2}} & h < 0 \end{cases} \quad (3.7)$$

where θs is the saturated water content, θr is the residual water content and K_s is saturated hydraulic conductivity. while h. n, m, α are curve fitting parameters.

A numerical domain of characteristic site was developed and assigned with properties of vadose zone (table 3.7) and undelaying 15-30 m domain with properties of saturated zone. Material distribution and location of injection well in numerical domain is presented in appendix-III. The western and eastern boundary were assigned the hydraulic heads of 30.5 m and 27.7 m, respectively. Thus, the groundwater flows from west to east due to the gradient of 0.004 m (Shieh and Peralta, 2005). The north and south boundaries were assigned as no flow boundary condition. The steady state condition was considered throughout the simulation. Homogeneously distributed sand was considered as porous media. The saturated water content (θ_s) of saturated zone (i.e. between 15-30 m) was 0.33, representing 100% saturation level. Whereas, 0.2, 0.4, 0.6 and 0.8 of θ_s i.e. equal to 0.066, 0.132, 0.198, 0.264 were considered as values of θ_s to represent 20, 40, 60 and 80% moisture contents in vadose zone, respectively. The three injection wells at (*X*:94, *Y*:312, *Z*:15); (*X*:94, *Y*:255, *Z*:15); (*X*:94, *Y*:200, *Z*:15); were used to supply the oxygenated water along with essential nutrients to enhance the microbial activity and the biodegradation rate of LNAPL in saturated zone. The extraction well at (*X*:627, *Y*:226, *Z*:15); established in the downgradient side to control the further migration of plume. The extracted amount of groundwater was then used in surface recharge to accelerate the biodegradation in the vadose zone by maintaining optimal soil moisture content. The top

area covered by four nodes located at (*X*:125, *Y*:255, *Z*:0); (*X*:125, *Y*:226, *Z*:0); (*X*:156, *Y*:226, *Z*:0); (*X*:156, *Y*:255, *Z*:0); were designated as contaminant source of 250 ppm dissolved LNAPL (Figure 3.8). However, the rest of the domain was assigned zero concentration as initial solute condition. The top boundary was considered as atmospheric boundary condition except for one node (*X*:125, *Y*:226, *Z*:0) having recharge flux, whereas bottom was considering as no-flux boundary condition. The van-Genuchten-Mualem single porosity model was selected to simulate the water flow through the domain. The space discretization followed the Galerkin finite elements approaches and time discretization followed Crank-Nicholson scheme for the dissolved LNAPL transport. The observation nodes were established in both zones at marginal locations of the domain. The concentration in the observation nodes should be maintained below a designated or desired water quality level throughout the entire simulation periods.

Thereafter, the simulated data sets were used to develop a surrogate simulator (ELM), which subsequently was coupled with the optimization technique (PSO) to minimize the in-situ bioremediation system cost along with the maximum removal of NAPLs from both vadose and saturated zone. In their approach, the physical simulator (BIOPLUME III) was replaced by a fast and computationally efficient surrogate simulator ELM. ELM was developed by Huang et al. (2006) as an improved learning algorithm for a single feed-forward neural network architecture with a fast learning speed compared to a traditional algorithm that also provides a better generalization performance. Further, the trained surrogate simulator was suitably coupled with the PSO method. Swarm Optimization, like genetic algorithms, is an evolutionary technique based on the metaphor of social behavior.

In total 5000 simulations were conducted with moisture condition varying from 20% to 80% for the two soil temperature combinations (30°C and 10°C). A combination of injection and extraction rates used in this study are listed in appendix-IV. For each combination, a separate ELM model was developed using 70% data for training while 30% for the testing. The trained hybrid data-driven simulator as a surrogate model was then suitably coupled with the optimization technique in a single MATLAB program to develop a hybrid data-driven simulation-optimization modeling approaches.

Table 3.7. Summary of water flow and solute transport parameters used in simulation experiments.

Parameters	Values	Units
Porosity (η)	0.33	-
Residual soil water content (θ_r)	0.0078	-
Saturated soil water content (θ_s)	0.33	-
Saturated hydraulic conductivity (K_s)	6×10^{-5}	m/s
Vadose zone hydraulic conductivity (K_V)	8.15×10^{-5}	m/s
Average bulk density (ρ_b)	1.5	g/cm^3
Saturated longitudinal dispersivity (D_{Ls})	10	m
Saturated transverse dispersivity (D_{Ts})	2	m
Vadose zone longitudinal dispersivity (D_{L_v})	0.34	m
Vadose zone transverse dispersivity (D_{T_v})	0.034	m
Molecular diffusion coefficient in saturated zone (D_{WS})	5E-005	m^2/day
Molecular diffusion coefficient in Vadose zone (D_{WV})	4.15E-005	m^2/day
Retardation factor (R)	1	-
Background Oxygen concentration	5	ppm
Supplying Oxygen concentration	8	ppm
Iteration No	40	-
Remediation Time	1-3	Years

A single objective functions problem was solved to get the minimum remediation cost for the site contaminated with LNAPL. The cost of injection/extraction, installation cost, oxygen/nutrient cost, and treatment facility cost was optimized by a functional equation given by (Shieh and Peralta, 2005).

$$F = W_F \sum_{e=1}^{Nw} C_{p_e} \cdot p_e + \sum_{e=1}^{Nw} C_{Ip_e} \cdot Ip_e + D\left[\sum_{e=1}^{N_i} p_e\right] + E\left[\sum_{e=1}^{N_e} p_e\right] \tag{3.8}$$

$$W_F = \left[(1+i_r)^T - 1\right] \Big/ \left[i_r (1+i_r)^T\right] \tag{3.9}$$

Where, F is the total cost of in-situ bioremediation system ($); W_F is the factor used to convert injection/extraction to their present value; e is the index denoting a potential injection/extraction locations; p_e is the injection/extraction rate at the location e (L^3/T); C_{p_e} is the cost coefficient of injection/extraction ($ per L^3/T); Nw is the total number of injection and extraction well; C_{Ip_e} is installation cost of the well ($ per well) ; Ip_e is the zero-one integer for well existence, respectively, at location e; $D\left[\sum_{e=1}^{N_i} p_e\right]$ is oxygen and nutrient injection facility capital cost; $E\left[\sum_{e=1}^{N_e} p_e\right]$ is the treatment facility capital cost; N_i is total number of injection well; N_e is total number of extraction wells; i_r is the discount rate and T is the total remediation period. The cost coefficient used to optimize the objective function is listed in table 3.8.

The equation (3.8) is subjected to following constraints –

$$0 \le C_{ow} \le C_{st} \qquad \text{For } Ow = 1,2...N_o \tag{3.10}$$

$$H_{i\min} \le H_e \le H_{i\max} \qquad \text{For } e = 1,2...N_i \tag{3.11}$$

$$H_{e\min} \le H_e \le H_{e\max} \qquad \text{For } e = 1,2...N_e \tag{3.12}$$

$$p_{\min} \le p_e \le p_{\max} \qquad \text{For } e = 1,2...Nw \tag{3.13}$$

Where, C_{ow} is the contaminant concentration in the observation wells at the end of the remediation period T [ML^{-3}]; C_{st} is the clean-up standard in observation well [ML^{-3}]; H_e is the hydraulic head in a well at location e [L]; $H_{i\min}$ and $H_{i\max}$ is the minimum and maximum hydraulic head allowed at injection well [L], $H_{e\min}$ and $H_{e\max}$ is the minimum and maximum hydraulic head allowed at extraction well [L], $p_{\min}$ and $p_{\max}$ is the minimum and maximum injection and extraction rates [L^3T^{-1}]. N_o is the number of observation wells. The values of different constraints used to optimize the equation (3.8) is listed in table 3.9.

Table 3.8. Cost coefficient for the objective function

Cost Coefficient	Numerical Value
i_r	0.05
C_{p_e} (Injection cost) (which include oxygen, nutrient, and operation)	4,755 ($ per lps-yr)
C_{p_e} (extraction cost) (it include treatment and pumping operation)	15,850 ($ per lps-yr)
C_{Ip_e}	12,000 ($ per well)
$D_{1.26L/s}$	= $ 20,000
$E_{1.26L/s}$	= $ 30,000

Table 3.9: The values of different constraints used to optimize the objective function.

Constraints	Values
C_{st}	<5ppm
$H_{i\min}$ and $H_{i\max}$	27.7m and 33.5m
$H_{e\min}$ and $H_{e\max}$	24.4m and 30.5m
$p_{\min}$ and $p_{\max}$	0-1.26 L/s

Chapter 4: Results and Discussions

This chapter presents results and discussion of work done to investigate the fate and transport of LNAPL under varying subsurface conditions. Findings of batch experiments are presented first to see the impact of initial substrate concentrations and roles of soil moisture content and temperature on biodegradation of toluene. Findings of column experiments performed at four different soil-water temperature are presented next along with the role of plant (*P. australis*) and nutrient loading on bioremediation of LNAPL. Thereafter, results of tracer experiments used for characterizing flow and transport parameters are presented for two and three dimensional (2D and 3D) sand tank setups. Subsequently, role of dynamic groundwater table and groundwater flow conditions on fate and transport of LNAPL is discussed. Finally, findings of simulation-optimization approach are discussed for a bioremediation system design for a characteristic polluted site.

4.1 Bioremediation and Initial Substrate Concentration

A series of completely mixed microcosm experiments were performed to investigate biodegradation of toluene at its different initial concentrations. Live and sterile set of microcosms were spiked with respective amount of different initial dissolved toluene concentrations. The aqueous phase samples were collected periodically and analysed using GC-MS. Biodegradation rates were calculated using observed concentration of dissolved toluene of live and sterile batches with progression of time in microcosms experiments. Figure 4.1 shows the relative concentration of toluene with progression of time in soil water having varying toluene concentration of 10, 50, 100, 150, 200 and 250 ppm. The continuous and dotted lines depict the relative toluene concentration with time in live and in controlled microcosms respectively. The total time taken for removal of toluene was minimum (22 hours) in microcosms having 100 ppm initial concentration, while, highest time of 30-33 hours was observed in microcosms having lowest initial concentration (10 ppm) of toluene. It was also observed that microcosms having initial toluene concentration beyond 50-100 ppm have taken more time (32-35 hours) to degrade the selected LNAPL. This fortifies the findings of earlier

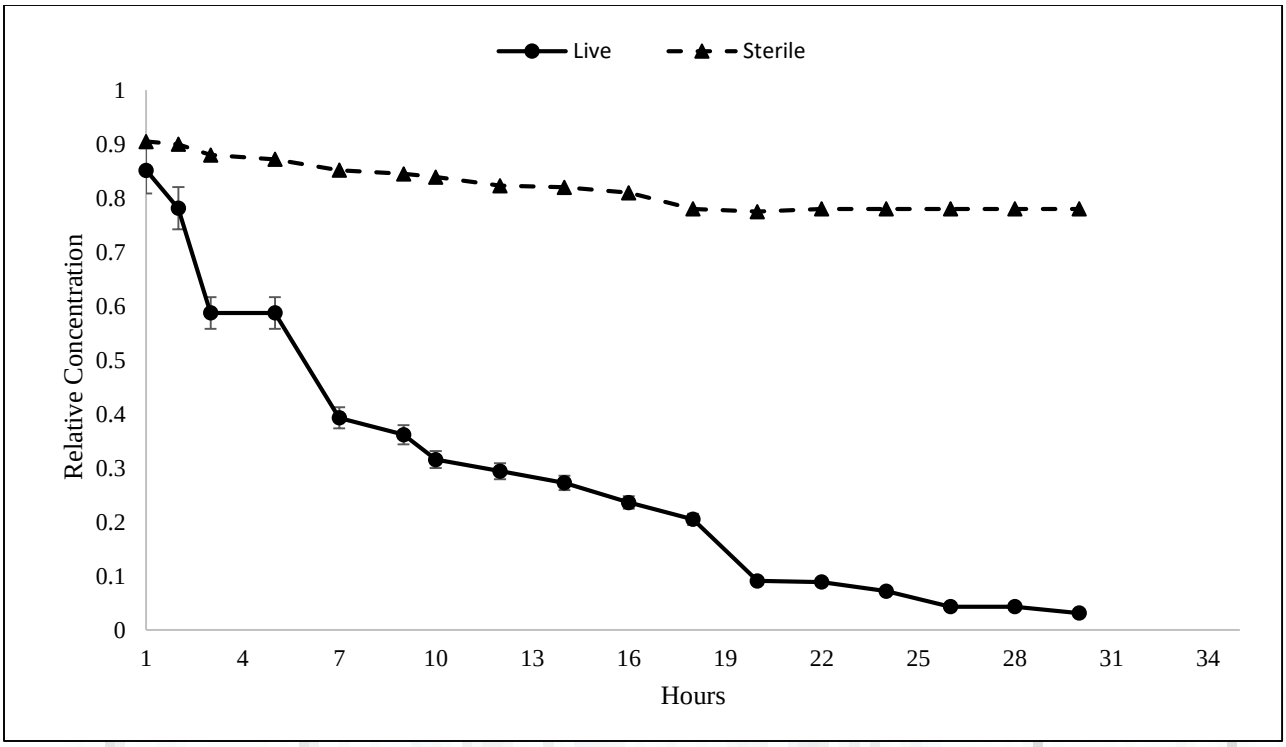

(a) 10 ppm initial LNAPL concentration

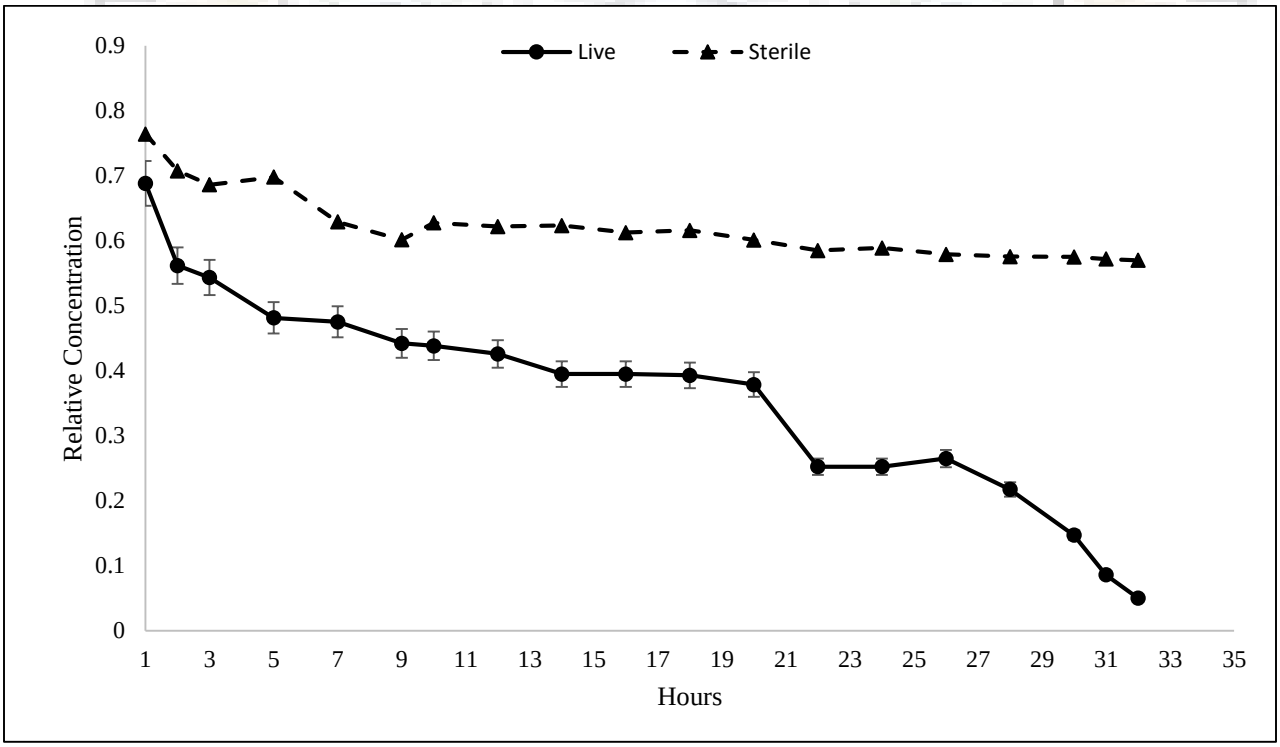

(b) 50 ppm initial LNAPL concentration

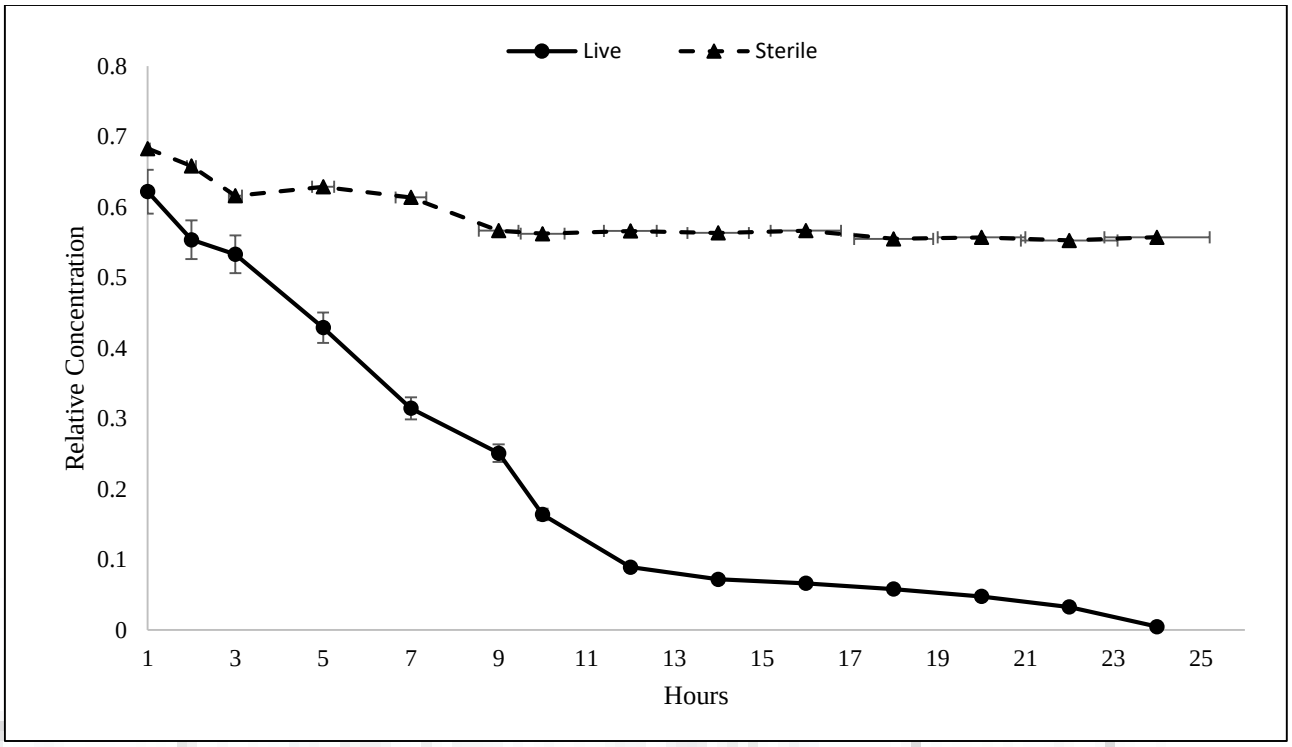

(c) 100 ppm initial LNAPL concentration

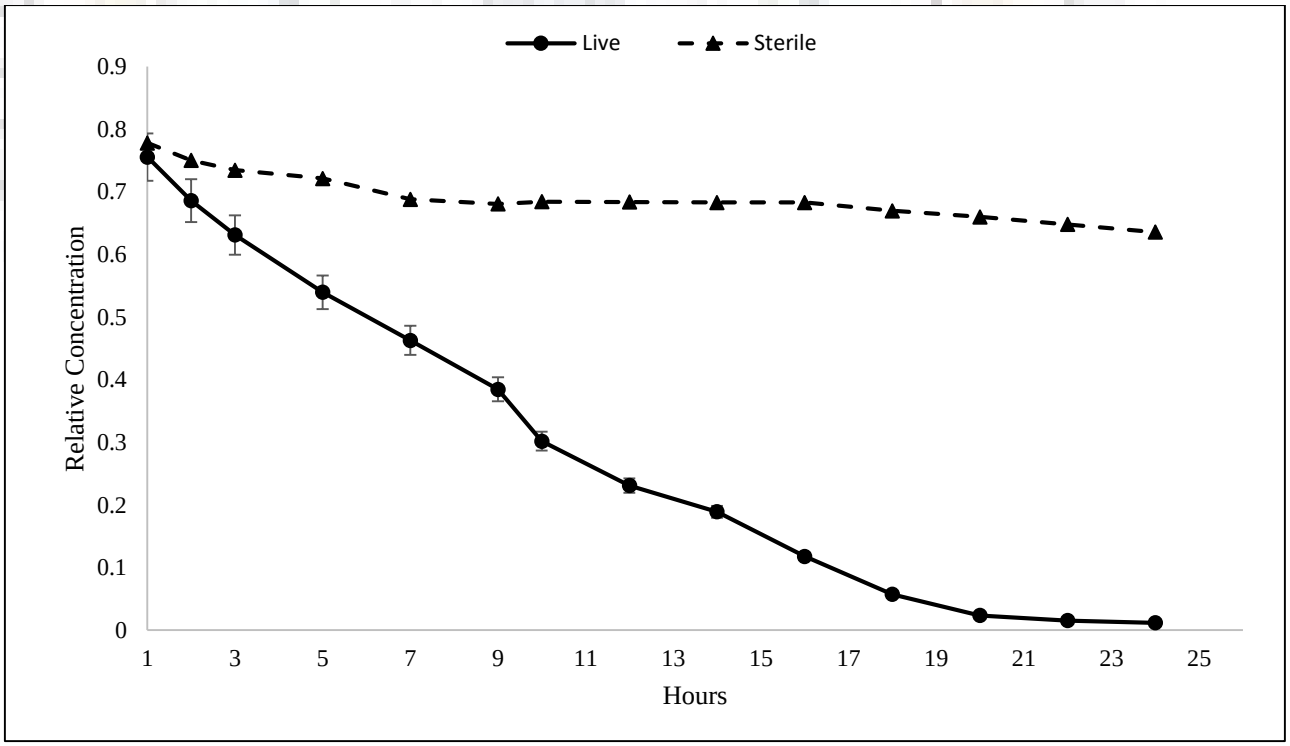

(d) 150 ppm initial LNAPL concentration

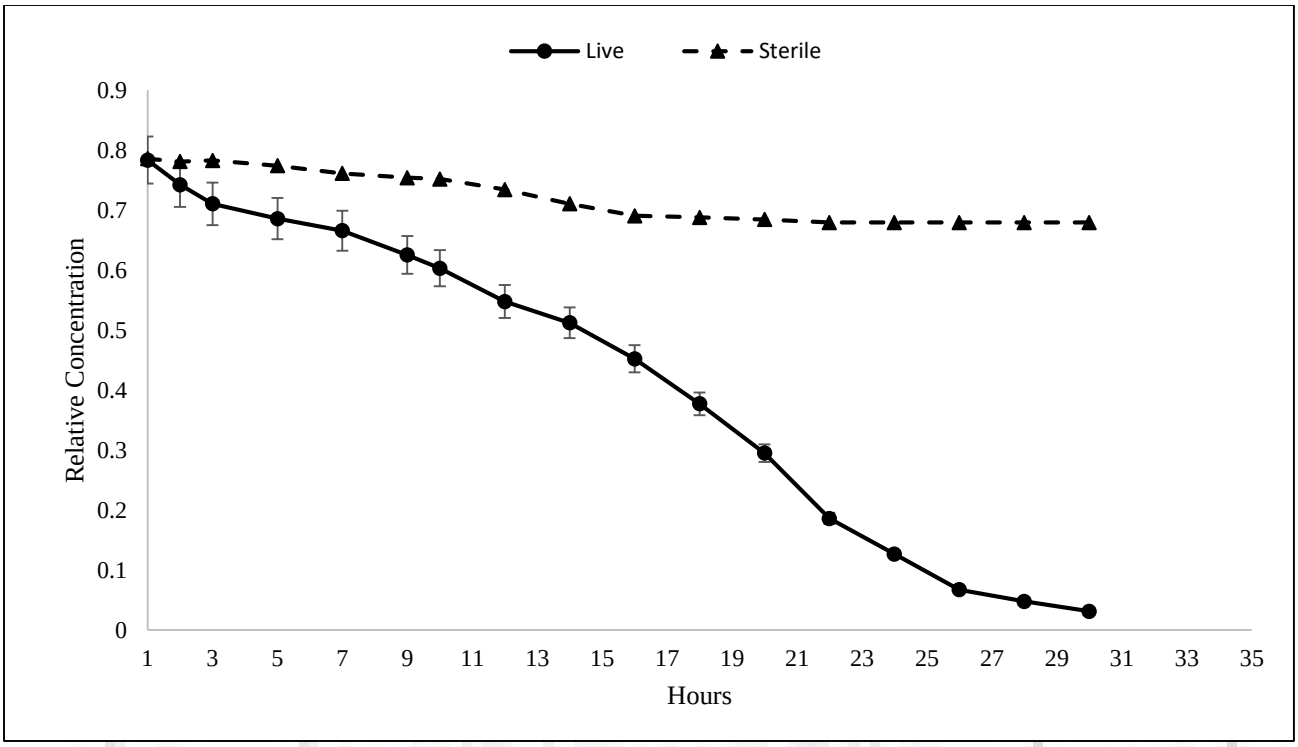

(e) 200 ppm initial LNAPL concentration

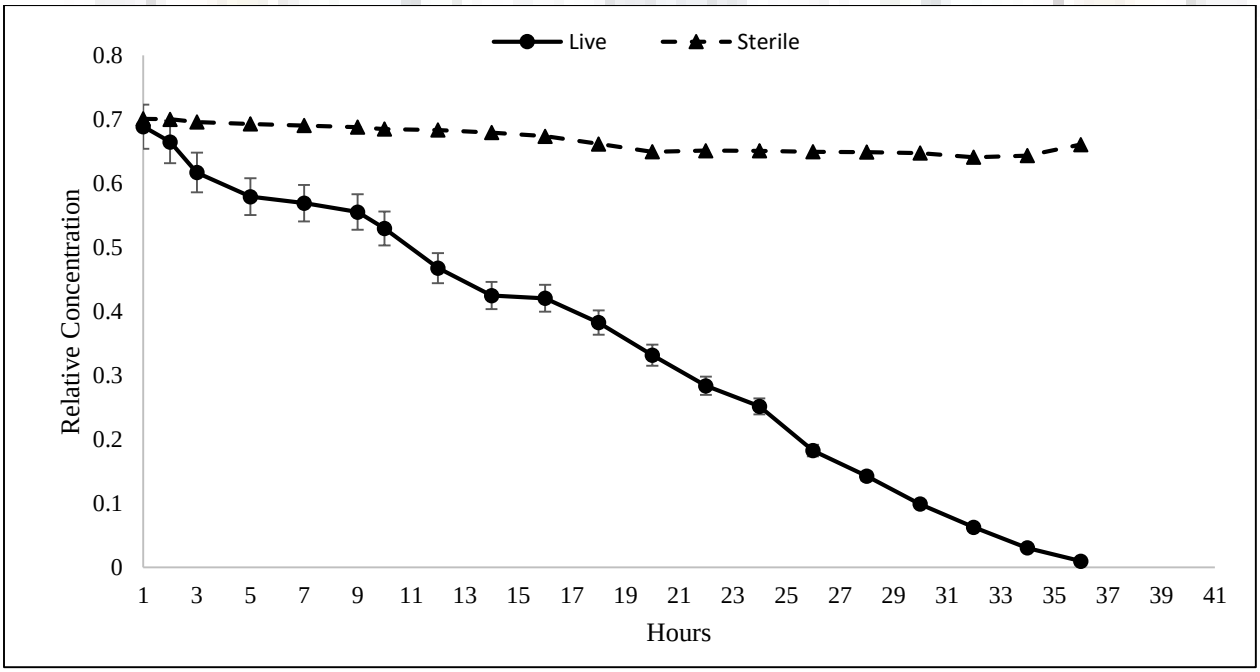

(f)

Figure 4.1: Variation in toluene concentration with time for initial concentration of (a) 10, (b) 50, (c) 100, (d) 150, (e) 200, and (f) 250 ppm. Error bars represent ± standard error for three replicates.

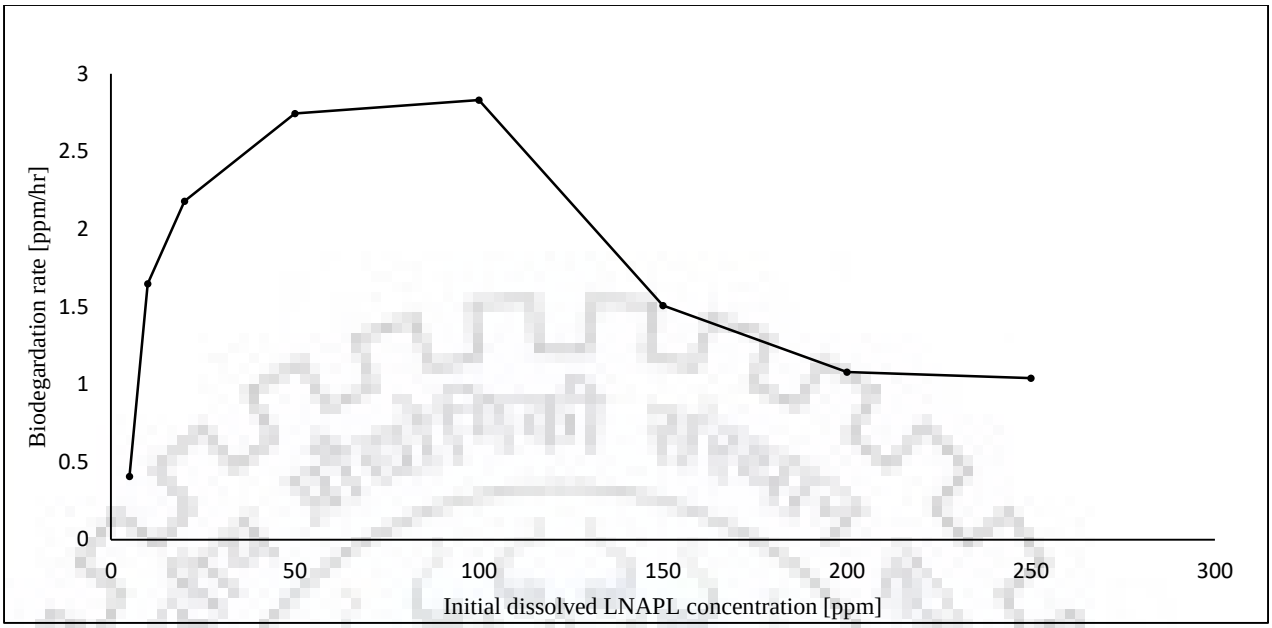

Figure 4.2: Average biodegradation rate at different level of dissolved LNAPL concentrations.

studies (Stroud et al. 2007) showing toxic effect of higher concentration of NAPL on potential microbes present in polluted media. A reduced degradation rate of toluene in microcosms having very low initial concentration seems due to insufficient carbon source to toluene degraders (Basu et al. 2015). Reduction in degradation rate of toluene with time (shown by changing slope of the continuous lines) also confirms this trend in all five microcosms. It is also important to note here the negligible time of acclimatization in all cases which were conducted at fairly high temperature of 28±2ºC. Yadav et al. (2014) also shown a considerable time of acclimatization in batches at low temperature as compared to the high temperature batch cases. Different shape of curvature of the live batches show that degradation pattern of toluene is changing from low to high concentration cases. The estimated avearge degradation rate of toluene at different concentrations is shown in figure 4.2. The figure shows that LNAPL degradation increases with increasing initial concentration of toluene up to about 50 ppm and remain maximum till about 100 ppm before started decreasing with increment in substrate concentration. It has been observed that the rate of degradation is minimum for 10 ppm microcosm (1.02 ppm/hour) and maximum for 100 ppm (7.08 ppm/hour) microcosm. A low degradation rate at high substrate concentration shows the toxic effects of pollutant on toluene degraders.

4.2 Impact of Soil Moisture Content and Temperature

Four sets of sterile and live microcosms having soil moisture content of 20, 40, 60, and 80 percentage of θ_s kept at prevailing high room temperature (30±2°C) while the other sets of same composition of moisture content was incubated at 10±0.5°C to mimic the low soil-water temperature condition. The observed toluene concentration with time in live and sterile microcosms are represented in figures 4.3- 4.6 by dotted and solid lines, respectively. The figures indicate that microcosms having high saturation level at 30°C took 16-17 hours, whereas 35 hours was taken for these microcosms at 10°C to completely degrade the LNAPL mass. Likewise, all other microcosms incubated at 10°C taken about two-fold time than the microcosms at incubated at 30°C. Similarly, the microcosms having $0.2\theta_s$ moisture contents required four-fold time than the $0.8\theta_s$ saturation case. The figure 4.3 representing the biodegradation in microcosms having 80% moisture content shows that the decay was fast until the relative concentration reached below 0.1 which keeps reducing with time. This indicates that the high substrate concentration (C/Co>0.1) provides more carbon source to microbes responsible for biodegradation of toluene. Metabolic activities of the degraders seem hampered when relative concentration of toluene becomes low due to limited availability of the carbon source (Yadav et al. 2013). At t=0 is the initial value which is taken immediately after injection of the stock solution. Because of the temperature variation in headspace different concentration levels of the LANPL are expected as per the Henry's law.

The estimated biodegradation rates along with total removal time of all the microcosms are listed in table 4.1. It can be summarized from the results that the biodegradation rate in microcosms having high moisture contents i.e. 60-80% of θ_s at 30°C was faster (0.0154 and 0.0120 mg/L-hr) than the microcosms having low moisture (40-20%) content at the same soil temperature level. Similarly, a high moisture content in microcosms kept of 60-80% of θ_s at 10°C is found to have high degradation rates (0.0025 and 0.0018 mg/L-hr) than the $0.4\theta_s$-0.2 θ_s moisture content cases (0.0010 and 0.0008 mg/L-hr). In general, the observed biodegradation rates indicate that a high moisture-high temperature combination provides the most favourable conditions for the microbes to degrade the LNAPL. The table 4.1 shows that

the soil-water system is more sensitive to temperature at high levels of moisture content as compared to the dry conditions. By keeping the temperature as a constant environmental parameter, the rate of degradation increases linearly with increment in soil moisture content. However, a nonlinear change in degradation rate was observed by varying the temperature at constant soil moisture level. Similar finding was observed by Holman and Tsang (1995), Yadav and Hassanizadeh, (2011) by conducting separate batch experiments for soil moisture and temperature levels. However, the lower moisture contents reduce the microbial activity due to inadequate moisture content essential for microbial metabolism and for nutrients bioavailability (Yadav et al. 2013).

(i)

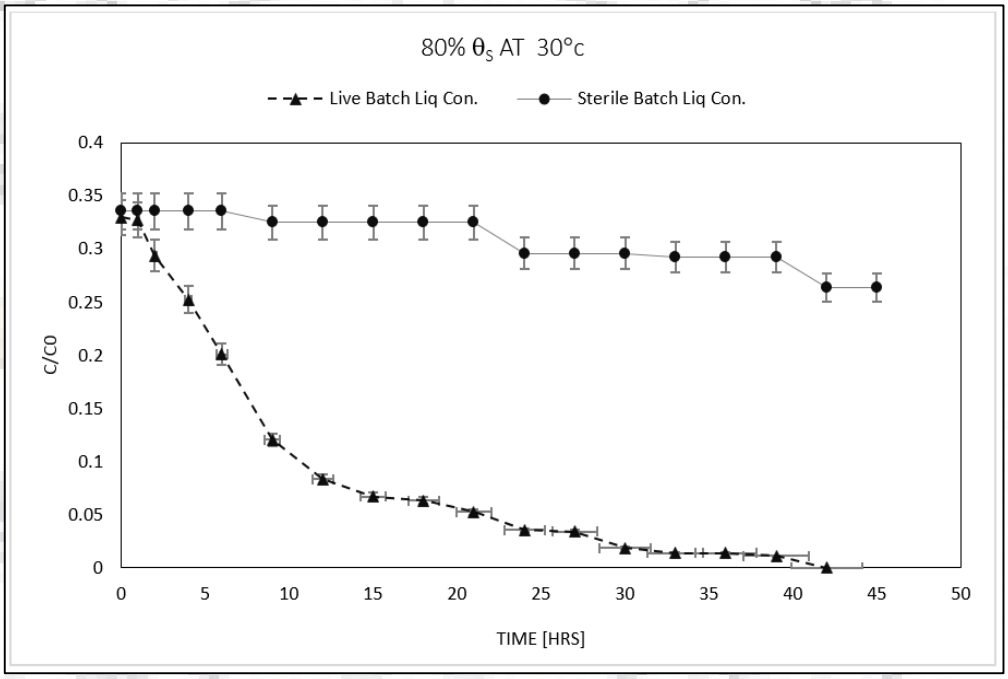

(ii)

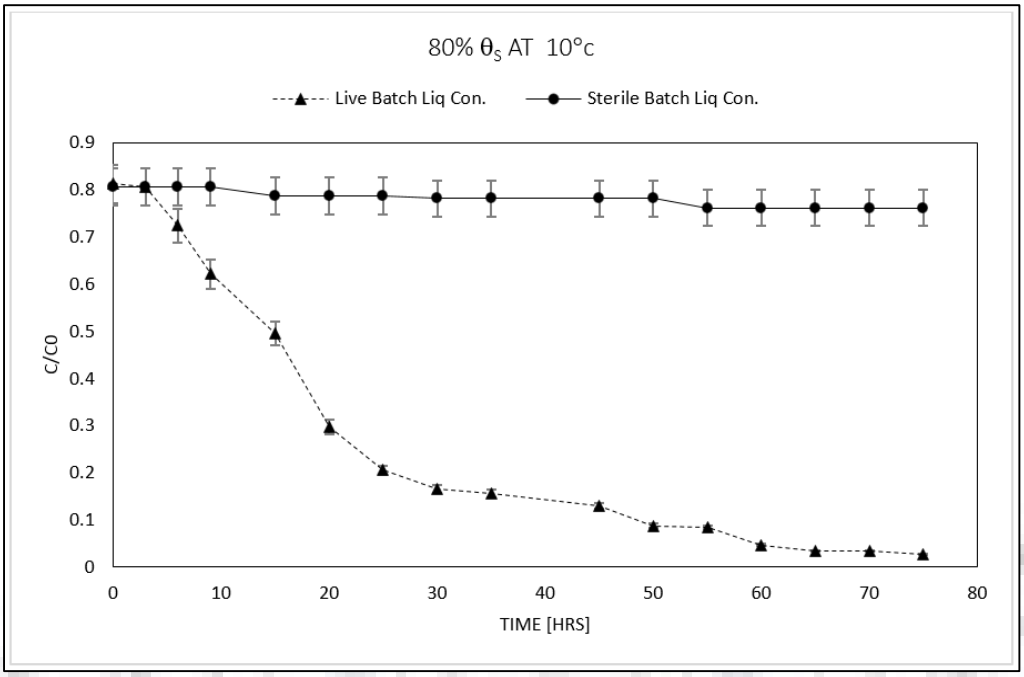

Figure 4.3: Biodegradation of LNAPL with time in microcosms having $0.8\theta_s$ soil moisture contents at (i) 30^0C and (ii) 10^0C. Error bars represent ± standard error for three replicates.

(i)

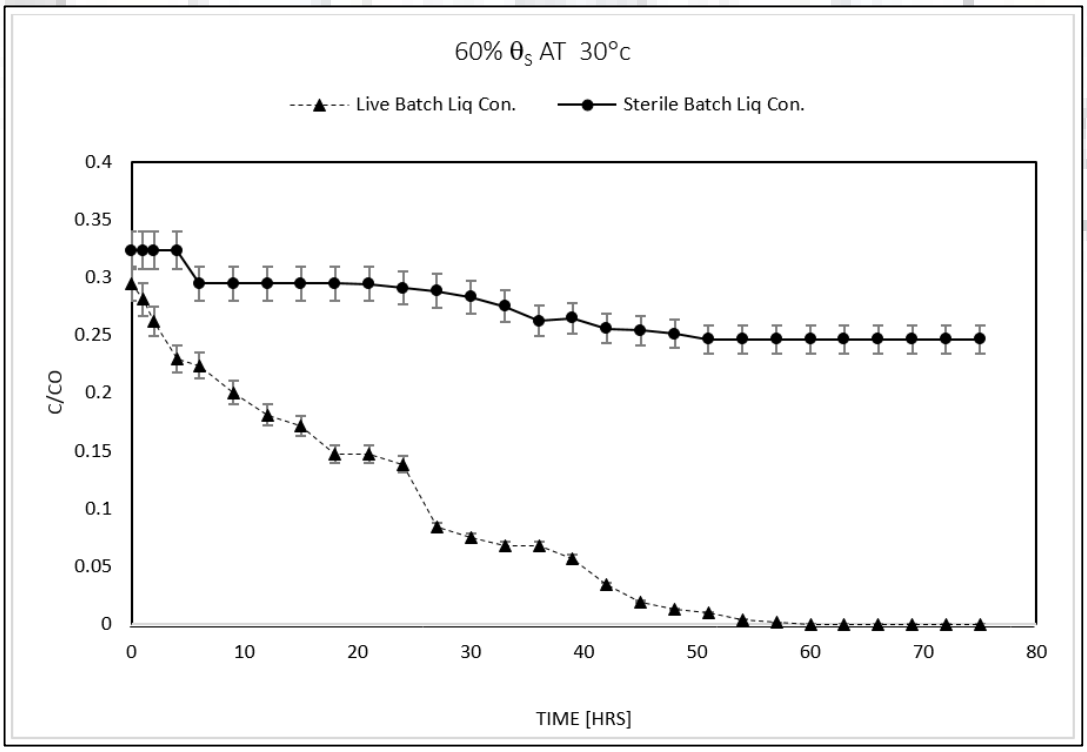

(ii)

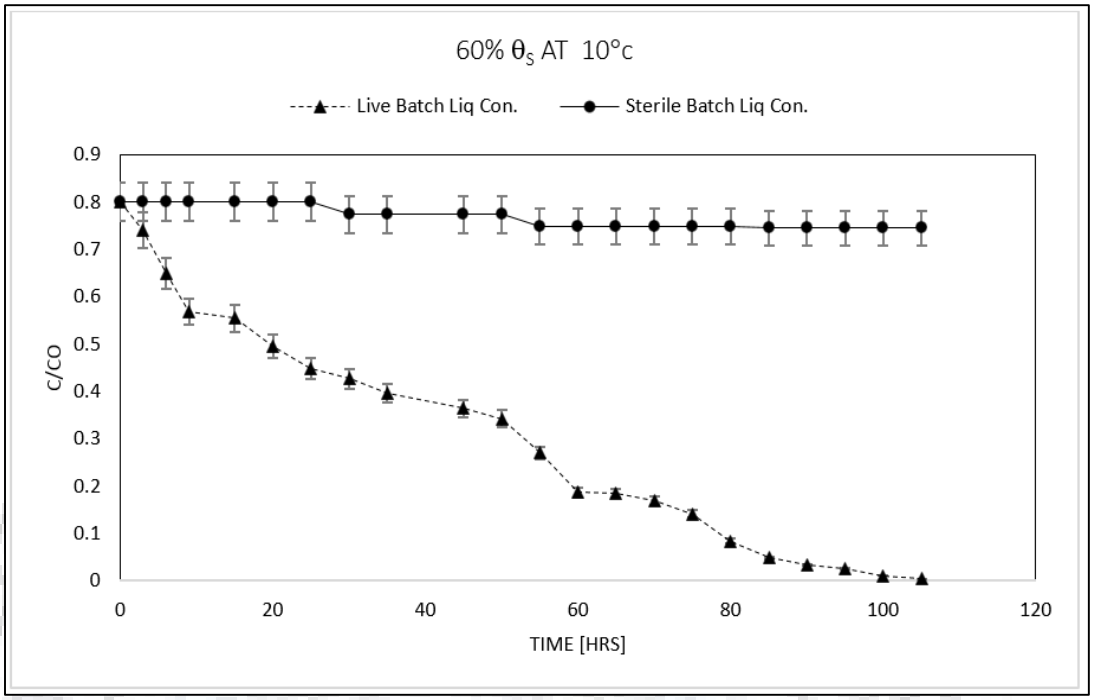

Figure 4.4: Biodegradation of LNAPL with time in microcosms having 0.6θ_s soil moisture contents at (i) 30^{0}C and (ii) 10^{0}C. Error bars represent ± standard error for three replicates.

(i)

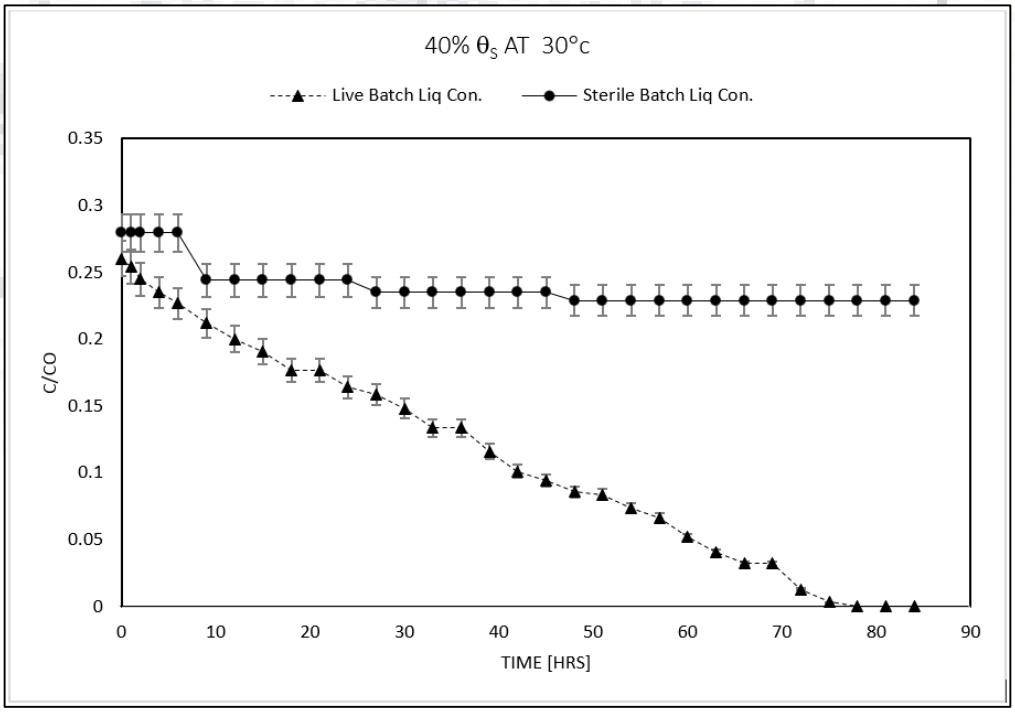

(ii)

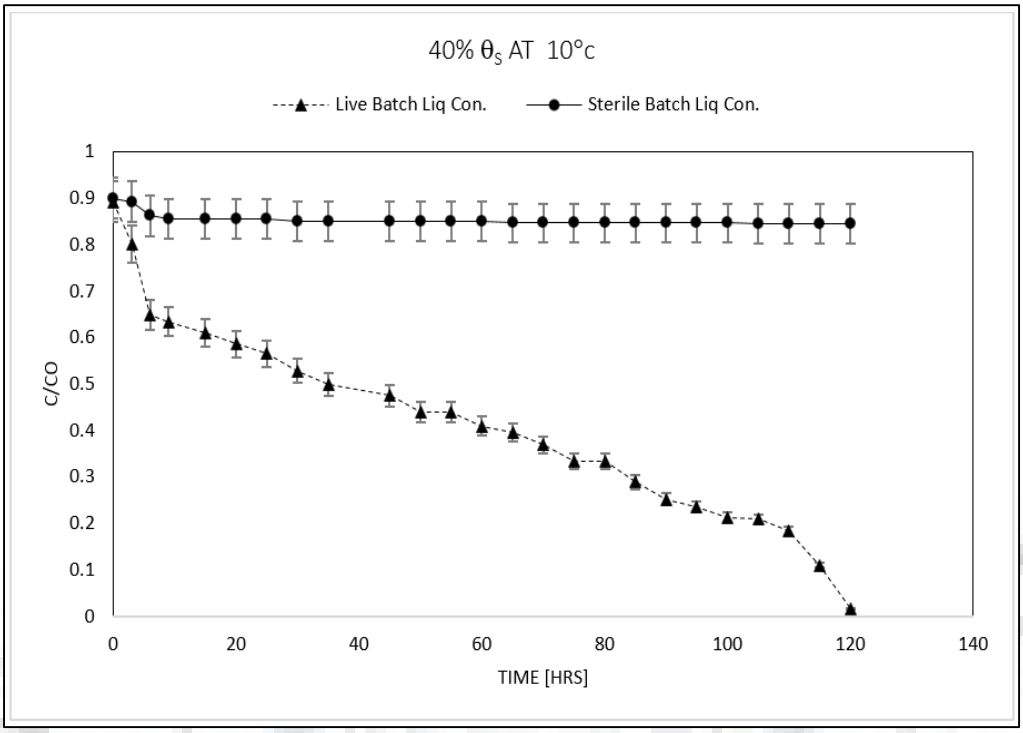

Figure 4.5: Biodegradation of LNAPL with time in microcosms having $0.4\theta_s$ soil moisture contents at (i) 30^0C and (ii) 10^0C. Error bars represent ± standard error for three replicates.

(i)

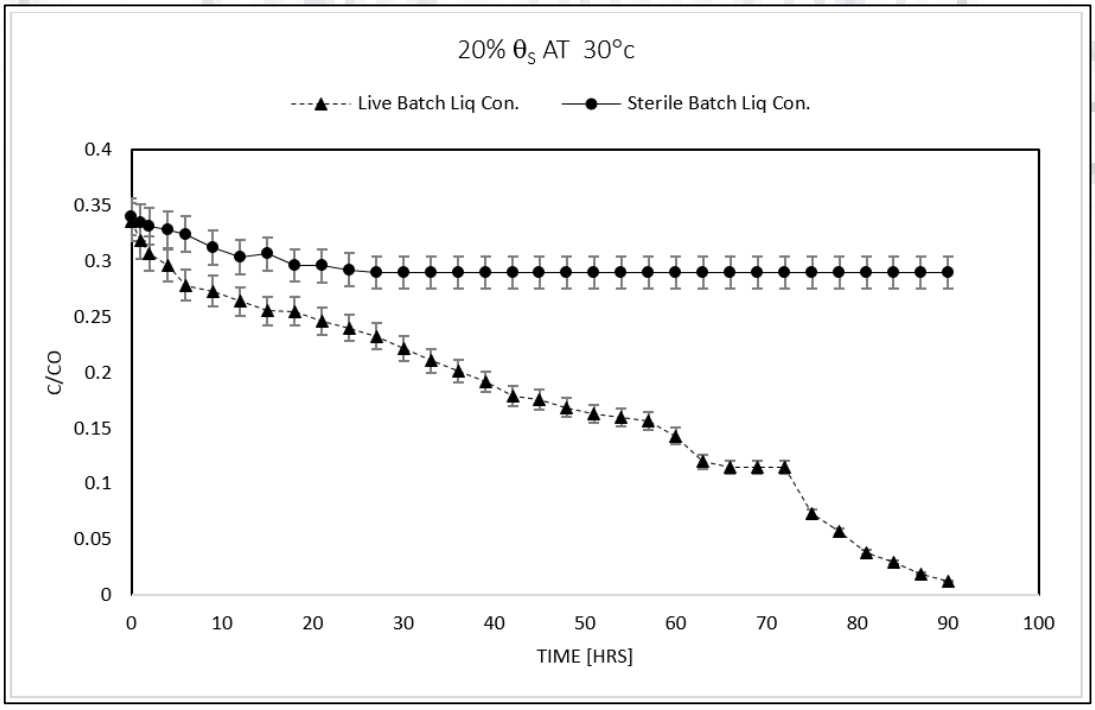

(ii)

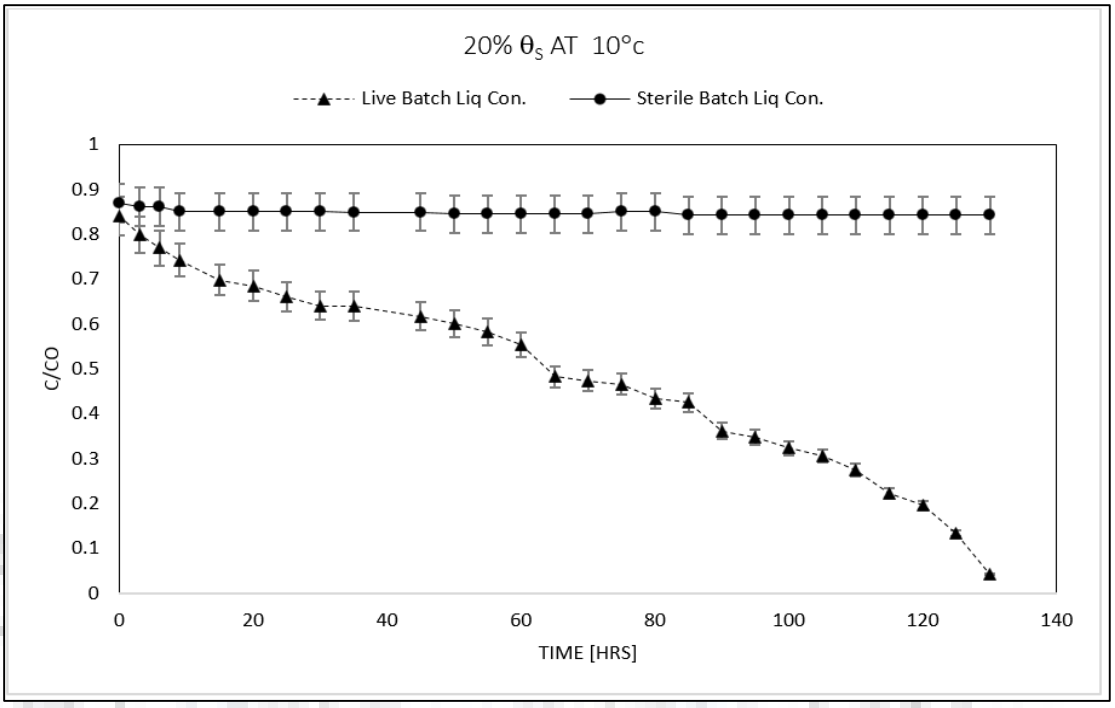

Figure 4.6: Biodegradation of LNAPL with time in microcosms setup having $0.2\theta_s$ soil moisture contents at 30^0C (i) and 10^0C (ii). Error bars represent ± standard error for three replicates.

Table 4.1: Biodegradation rate at different combination of soil moisture and temperature levels.

Soil Moisture Contents	Soil Temperature	Total degradation time [hours]	Rate of Biodegradation [mg/L-hr]
$0.8\theta_s$	10±0.5°C	72	0.0025
	30±2°C	42	0.0154
$0.6\theta_s$	10±0.5°C	105	0.0018
	30±2°C	60	0.0120
$0.4\theta_s$	10±0.5°C	120	0.0010
	30±2°C	84	0.0092
$0.2\theta_s$	10±0.5°C	128	0.0008
	30±2°C	90	0.0028

4.3 Impact of Temperature in Continuous System

Four series of laboratory experiments were performed to investigate the role of different soil-water temperature on toluene biodegradation using a continuous system of column setup. BTCs of LNAPL are presented in figures 4.7- 4.10 for 36^0C, 28^0C, 20^0C and 4^0C cases, respectively. Figures 4.7-4.10 show high equilibrium concentration at upper port (P1) then lower ports (P2 and P3) in all experimental cases. Furthermore, the equilibrium concentration (140-160 ppm) at port 1 (P1) was higher in case of column having 36 ± 2^0C groundwater temperature condition (Figure 4.7). Similarly, the equilibrium concentrations at 28^0C, 20^0C, and 42^0C ranges from 112-120, 80-100, and 40-55 ppm, respectively at the same port. This clearly indicates that the high temperature accelerates the dissolution of LNAPL which significantly contribute high concentration of dissolved LNAPL in soil water plume. The biodegradation rates of LNAPL were 0.002, 0.008, 0.012 and 0.015 mg-L/hour at groundwater temperature 4^0C, 20^0C, 28^0C and 36^0C, respectively. This indicates that higher temperature (28^0C-36^0C) enhanced the biodegradation rates of LNAPL in subsurface. Estimated colony forming units (CFU) listed in table 4.2 shows an increasing microbial number with increasing groundwater temperature (Picture of plates are shown in Appendix-I). Microbial number was high in region of optimal dissolved concentration i.e. 140 -150 ppm at 28^0C and 36^0C temperature. Suarez and Rifai (1999) also reported that at 10-36^0C temperature is suitable for LNAPL degraders. At highly polluted sites, one can modify groundwater temperature by applying steam water/hot air to accelerate microbial activities. The outcomes of this study may help to implement geothermally or solar based surface heating and stream treatment to LNAPL polluted sites.

Table 4.2: Microbial population in column setup having different groundwater temperature.

Temp	0 hour		12 hour	
	P1 (10^4 CFU/mL)	P3 (10^4 CFU/mL)	P1 (10^4 CFU/mL)	P3 (10^4 CFU/mL)
36^0C	28	2.8	120	116
28^0C	3.2	2.6	264	142
20^0C	2.4	0.6	85	72
4^0C	1.2	0.6	8.6	1.4

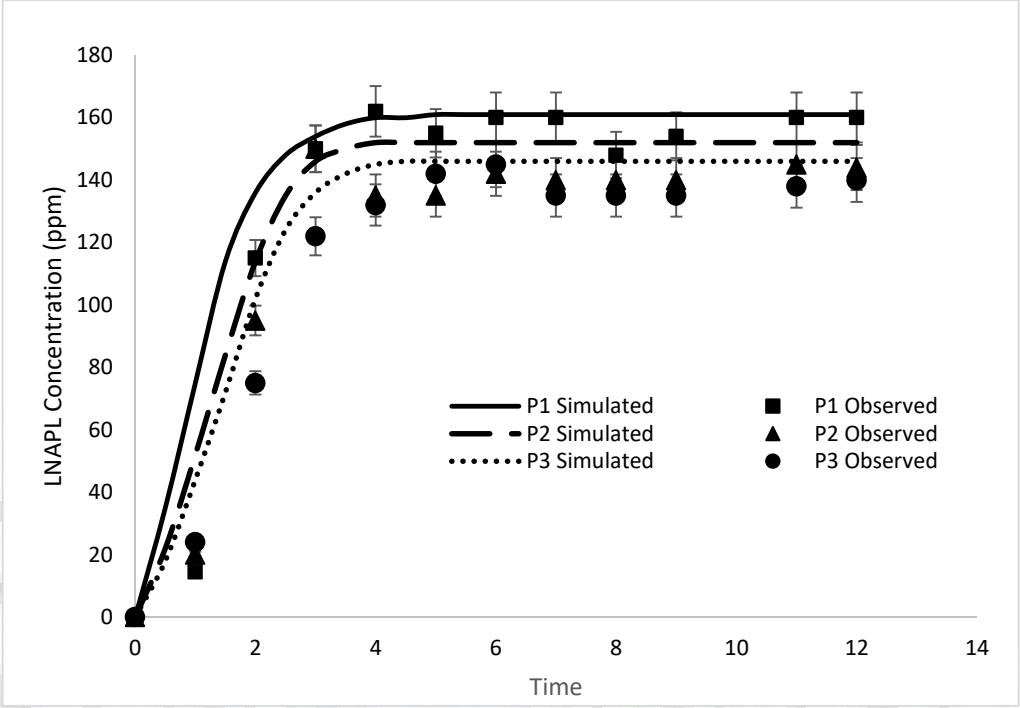

Figure 4.7: Concentration of LNAPL at sampling port P1 (10 cm depth), P2 (20 cm depth), and P3 (30 cm depth) of column setup under groundwater temperature of 36^0C.

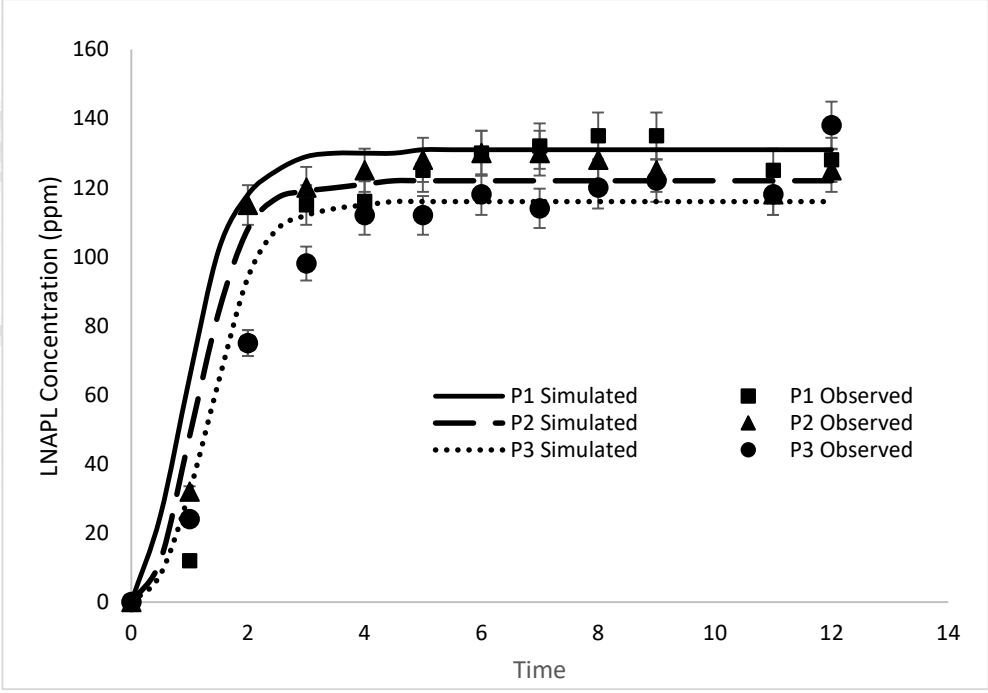

Figure 4.8: Concentration of LNAPL at sampling port P1, P2, and P3 of column setup under groundwater temperature of 28^0C.

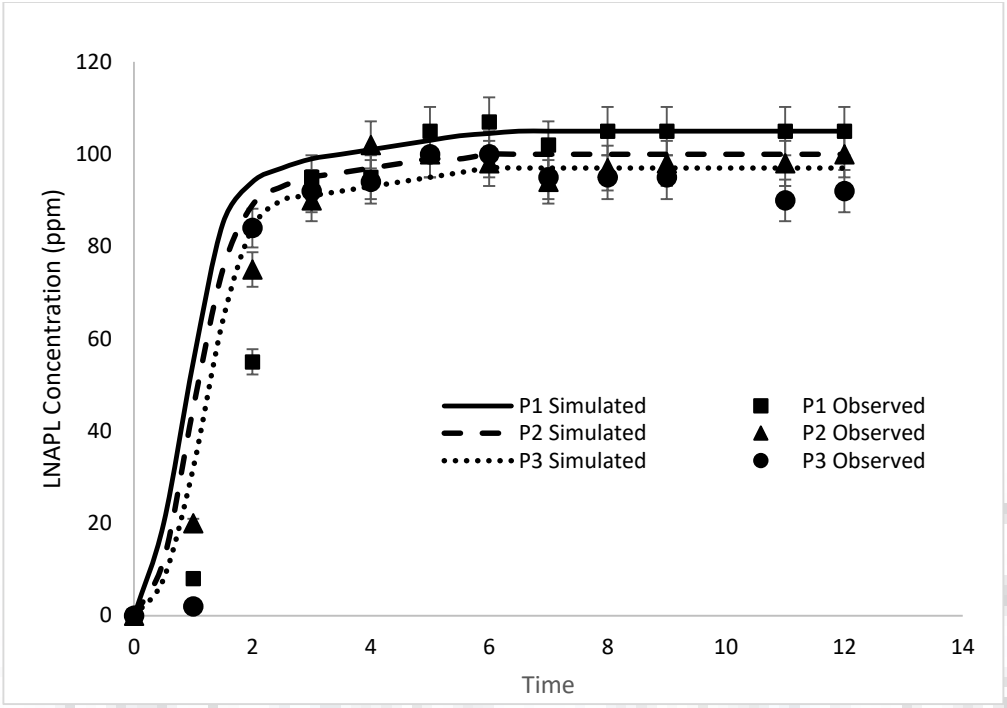

Figure 4.9: Concentration of LNAPL at sampling port P1, P2, and P3 of column setup under groundwater temperature of 20^0C.

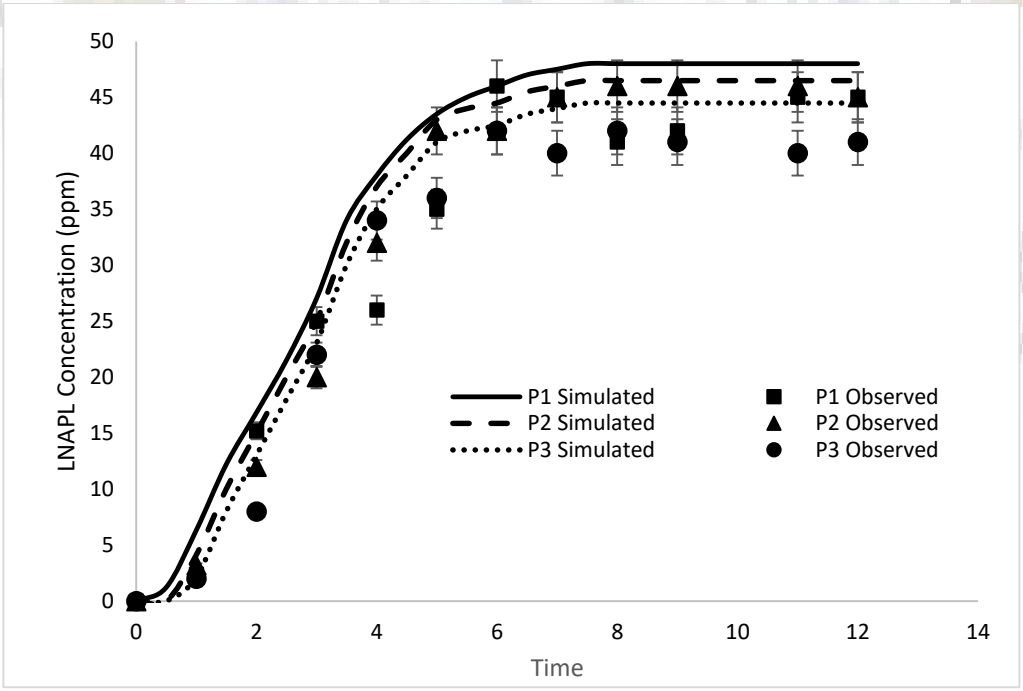

Figure 4.10: Concentration of LNAPL at sampling port P1, P2, and P3 of column setup under groundwater temperature of 4^0C.

4. 4 Role of Plants

The column set up is integrated with a treatment wetland with and without plant. to investigate the role of plants on removal of LNAPL compounds from root zone water. Figures 4.11-4.12 shows the variation in toluene concentration of unplanted and planted cases. It was observed from the BTCs that the equilibrium time was higher for the planted wetland setup as compared to the unplanted one emphasizing the positive role of rhizospheric zone in the process of biodegradation of toluene. The rhizospheric zone is well known as an apt location having significantly large numbers of pollutant degraders than unplanted soils (Basu et al. 2015). Data set of constructed wetlands experiments performed at IHE Delft are utilised here to analyse the t role of plants and nutrients on degradation of LNAPL compounds. The percentage removal efficiency calculated using influent and effluent concentrations of the LNAPL compounds in unplanted and planted wetlands are listed in Tables 4.3-4.4. The corresponding observed removal efficiency is also listed in the tables for initial 20 days in which no nutrient was applied. Removal efficiency of LNAPL compounds after application of nutrients during 21-56 days are listed in the Table 4.4. The quantities of LNAPL compounds were greatly decreased (>90%) in the effluents from the three duplex-CWs. A high removal efficiency (i.e. >95%) was observed in the duplex-CWs domain treating contaminated groundwater.

The VF CW1 showed a 98.4% removal efficiency for benzene followed by 97.4% removal in VF CW2 and 96.2% removal in VF CW3 at the 56^{th} day of the treatment wetland run. Which is considered almost 100% removal of benzene at the 56^{th} day of the treatment run. There was no additional removal of benzene in the HFF (1-3) compartments. The duplex-CWs treatment systems showed a good benzene degradation in the VF compartment. Likewise, all the three VF CWs showed a 100% toluene removal at the 56^{th} day of the treatment, while in the HFF (stage 2) compartments no additional removal was observed by the three duplex-CWs (Table 4.3 and Table 4.4). The duplex CW2 and CW3 showed the highest performance with 88.3 - 89.4% and 100% toluene removal from the experimental and simulation domains, respectively. The domain representing duplex-CW2 and CW3 shows complete degradation of toluene due to the comparatively high nutrient dose as compared to CW1. VF CWs shows high removal efficiency for benzene and toluene causes low concentration load to HFF CWs and therefore HFF shows no additional removal of these pollutants.

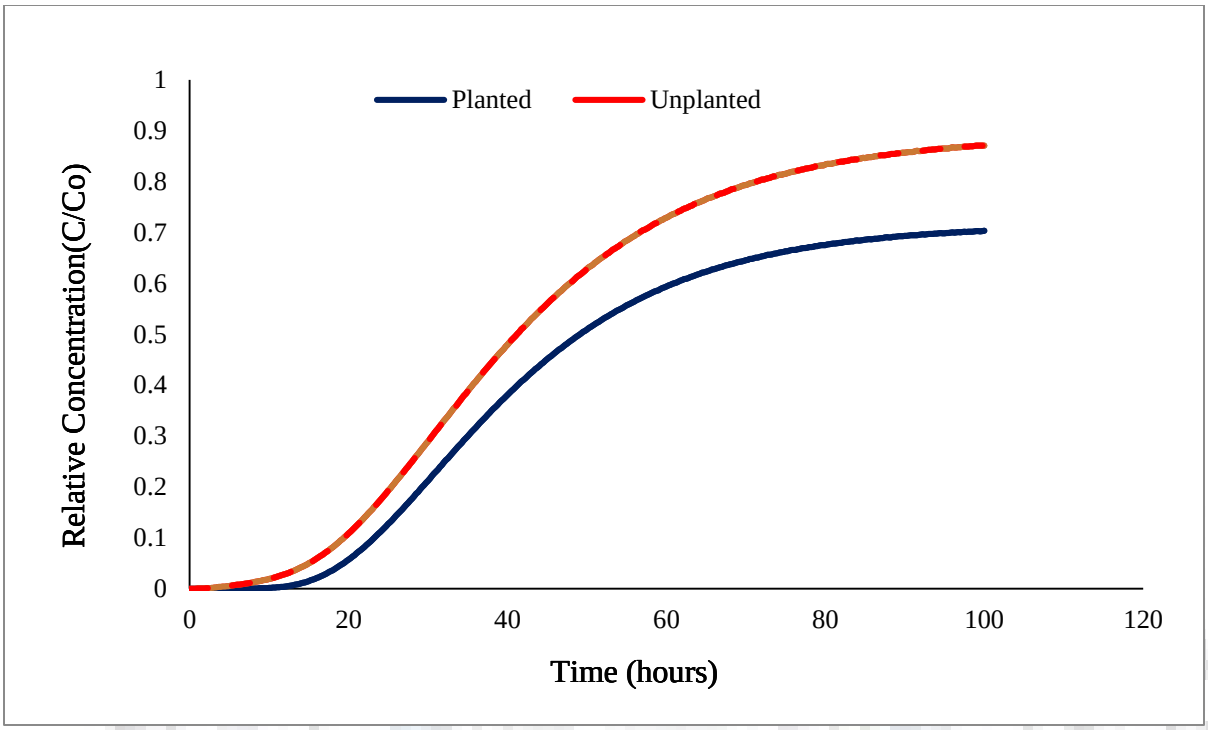

Figure 4.11: Best fitted line of BTC for column attached with unplanted and planted wetland.

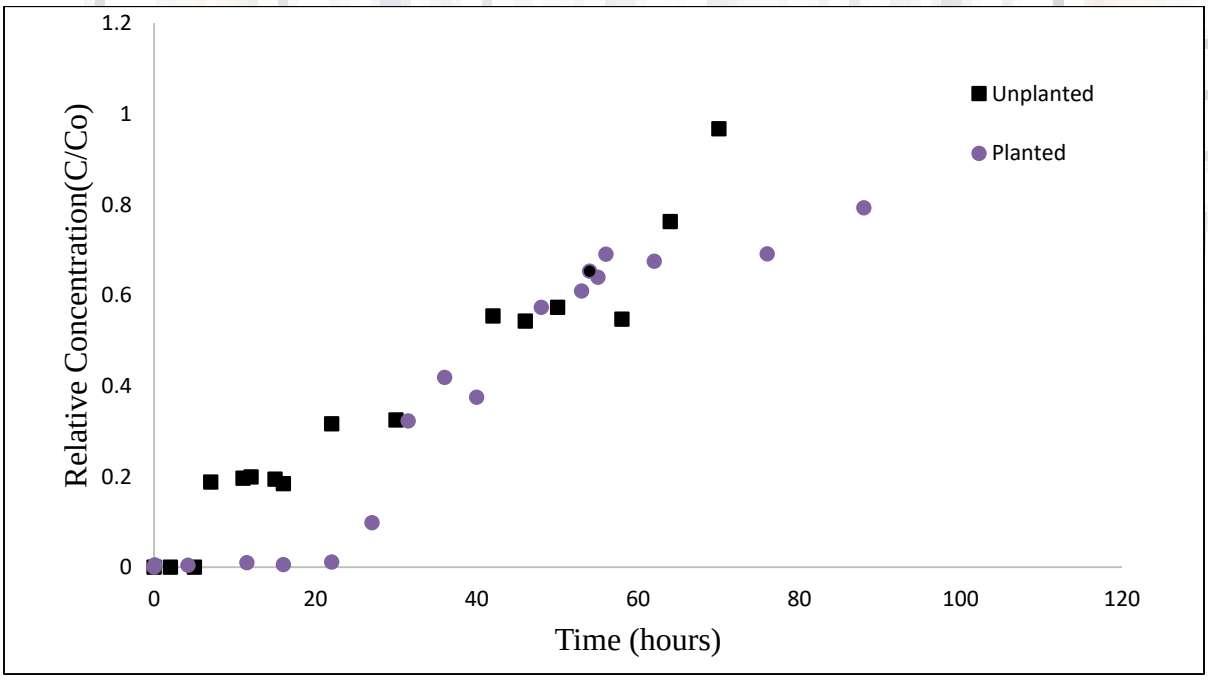

Figure 4.12: Observed values of relative concentration of toluene in column attached with unplanted and planted wetland.

In case of ethylbenzene, the removal efficiencies ranged from 64.9 (± 56.3) % to 100 (± 0.0) % for the first stage (VF CWs). The VF CW1 had a 100% ethylbenzene removal efficiency from day 42 to day 56, while VF CW2 and VF CW3 had 100% removal efficiencies at day 56. All the three VF CWs reached a 100% m/p xylene removal efficiency at day 56. The observed mean o-xylene removal efficiencies upto 100 (± 0.0) % in different setups. The three planted CWs had a range of 50 - 100% removal efficiency for LNAPL contaminants investigated. This removal efficiency seems mainly due to biodegradationof the LANPL compounds within the hybrid duplex-CWs (Ávila et al., 2014). This high removal efficiency of toluene is apparently due to biostimulation or aerobic growth of heterotrophic bacteria as fortified by the findings of Yadav et al. (2014). The high porosity in the gravel zone of the VF was also equally contributing in maintaining the oxygen concentration. The consideration of atmospheric boundary conditions in the simulation domain causes continuous supply of oxygen in CWs, especially in VF CWs. Thus, in this study all three VF CWs were able to maintain the optimal oxygen concentration in the domain and resulted in high benzene and toluene removal efficiencies by the VF CWs. Plant (*P. australis)* grew very well and rapidly too in all the three VF CWs in the course of this study. The supply of nutrients to the treatment systems in this present study may have aided the *P. australis* growth and survival in contaminated medium.

Table 4.3: Performance of 1st stage of the duplex CWs without nutrient supplement (Mean± SD) (%) during the first 21 days of operation.

Parameter	**Unplanted**	VF CW1	HFF1	**Duplex (hybrid) CW1**	VF CW2	HFF2	**Duplex (hybrid) CW 2**	VF CW3	HFF3	**Duplex (hybrid) CW 3**
COD	---	92.4±5.5	8.5±14.8	**80.4±15.3**	82.0±5.3	0±0	**57.1±22.8**	77.3±8.7	46.5±40.6	**88.9±5.4**
DRO	13.0±5.5	78.6±0.2	64.2±1.4	**80.2±0.4**	84.0±0.2	75.8±0.5	**85.4±0.6**	84.0±0.2	75.8±0.5	**85.4±0.6**
Benzene	28±0.02	67.5±0.2	23.8±2.4	**65.0±0.2**	63.1±0.4	22.8±0.2	**62.0±0.2**	62.4±0.5	22.8±0.2	**60.0±0.5**
Toluene	45±5.5	63.1±0.5	32.2±0.2	**72.0±0.2**	75.2±0.5	34.2±0.2	**85.0±0.2**	75.2±0.5	34.2±0.2	**85.0±0.2**
Ethylbenzene	24±1.0	89.0±0.5	14.2±0.2	**90.5±0.2**	85.2±0.5	08.2±0.5	**87.2±0.5**	85.2±0.5	08.2±0.5	**87.2±0.5**
m/p-xylene	25.6±10.5	48.0±0.5	78.0±0.5	**81.5±0.5**	52.5±0.2	72.5±0.5	**83.5±0.5**	50.5±0.2	78.5±0.5	**85.5±0.5**
o-xylene	35±0.05	58.5±0.2	63.2±0.5	**74.5±0.5**	64.5±0.2	61.2±0.5	**78.5±0.5**	64.5±0.2	61.2±0.5	**78.5±0.5**
Ammonium-N	24±0.05	96.5±5.2	11.6±20.2	**88.3±5.4**	82.0±14.1	0±0	**92.5±7.1**	74.1±34.8	16.5±28.5	**78.6±10.7**
Nitrate-N	45±0.05	64.3±55.8	22.9±39.7	**87.5±17.0**	42.8±44.7	0±0	**25.2±42.5**	33.6±50.6	33.3±57.7	**33.3±57.7**
Phosphate-P	12±0.05	32.4±39.7	5.0±8.6	**33.7±40.6**	72.9±12.1	0±0	**53.6±41.4**	69.0±16.1	33.1±57.4	**63.7±32.0**

NA-Not applicable

Table 4.4: Performance of the 2-stage duplex CWs with nutrient supplement (Mean± SD) (%) from day 28 to 56.

Parameter	**Unplanted**	VF CW1	HFF1	**Duplex (hybrid) CW1**	VF CW2	HFF2	**Duplex (hybrid) CW 2**	VF CW3	HFF3	**Duplex (hybrid) CW 3**
COD	----	74.4±9.1	13.3±20.6	**62.4±17.2**	64.2±20.3	0±0	**32.7±20.6**	69.1±17.4	17.4±32.4	**53.8±33.1**
DRO*		97.8±2.8	65.2±31.2	**99.8±0.0**	98.3±2.4	75.5±22.1	**99.8±0.2**	99.9±0.1	NA	**96.6±0.5**
DRO[#]	25±0.05	86.4±2.4	81.9±1.3	**97.6±0.3**	95.5±0.1	90.0±0.5	**99.5±0.0**	91.5±0.4	94.3±0.5	**99.5±0.1**
Benzene*		86.0±24.3	NA	**77.9±3.6**	90.3±10	NA	**62.2±46.8**	93.3±11.5	NA	**53.3±46.2**
Benzene[#]	48±0.05	90.4± 4.5	81.9±6.4	**98.4±0.6**	78.3±2.8	82.5±0.1	**97.4±0.5**	86.3±3.0	81.9±7.9	**96.2±1.7**
Toluene*		91.7±14.4	NA	**58.3±52.0**	89.4±12.9	NA	**89.4±12.9**	88.3±12.6	NA	**88.3±12.6**
Toluene[#]	48±0.05	53.3±5.8	83.3±28.9	**93.3±11.5**	79.3±20.0	NA	**100±0.0**	83.8±14.7	NA	**100±0.0**
Ethylbenzene*		100±0.0	NA	**100±0.0**	64.9±56.3	NA	**91.7±14.4**	95.8±7.2	NA	**88.9±19.2**
Ethylbenzene[#]	50±0.05	80.6±17.3	NA	**100±0.00**	55.6±9.6	NA	**91.7±14.4**	NA	NA	**86.7±23.1**
m/p-xylene*		88.0±12.5	NA	**88.0±12.5**	66.0±57.1	NA	**93.8±9.1**	94.2±6.3	NA	**90.1±13.3**
m/p-xylene[#]	42.5±0.05	50.0±0.0	93.3±11.5	**96.7±5.8**	33.3±0.0	NA	**100.0±0**	92.5±6.6	NA	**100±0.0**
o-xylene*		100±0.0	NA	**100±0.0**	66.7±57.7	NA	**93.3±11.5**	100±0.0	NA	**91.7±14.4**
o-xylene[#]	56.2±0.05	93.3±11.5	NA	**100±0.0**	86.7±23.1	NA	**98.7±2.3**	NA	NA	**NA**
Ammonium-N	15±0.05	97.0±4.0	39.0±53.5	**75.7±32.7**	42.6±8.7	0±0	**59.7±7.5**	74.1±34.8	16.5±28.5	**78.6±10.7**
Nitrate-N	25±0.05	15.6±24.0	19.9±43.3	**39.0±52.4**	55.3±41.4	25.7±35.3	**64.8±38.3**	44.6±29.0	40.0±54.8	**77.1±43.6**
Phosphate-P	32±0.05	44.6±29.0	40.0±54.8	**77.1±43.6**	24.0±14.9	1.5±3.5	**18.0±11.7**	38.3±21.9	0±0	**51.4±18.9**

NA-Not applicable; * Observed; [#] Simulated

4.5 Role of Dynamic Groundwater Table

Tracer experiments were performed to estimate solute transport properties for stable and fluctuating groundwater table conditions. The breakthrough curves (BTCs) of tracer (NaCl) under stable and different groundwater fluctuation cases are presented in figure 4.13 for rapid, general and slow groundwater table fluctuation conditions represented by GWTF-C1, GWTF-C2, GWTF-C3 respectively. The slope of the BTCs shown in figure 4.13 are similar to each other, suggesting that the sand was packed uniformly in each set of experiment without any significant preferential flow paths. The best fit values of dispersion coefficient and respective longitudinal dispersivity are listed in table 4.5 for different groundwater fluctuation cases. The observed values of dispersivity was used to simulate dissolved LNAPL plume in identified domain under corresponding groundwater table case.

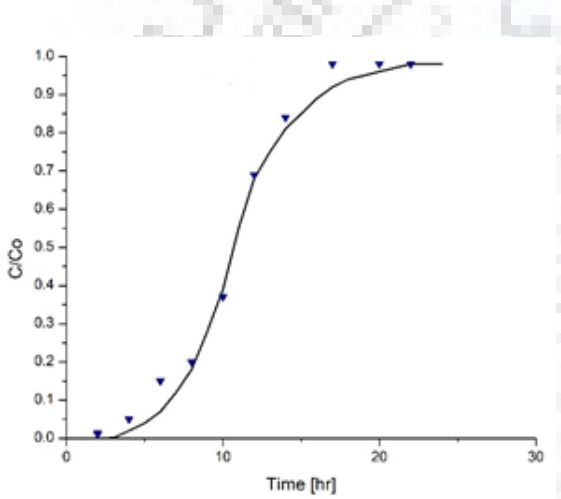

(a) GWTF-C1

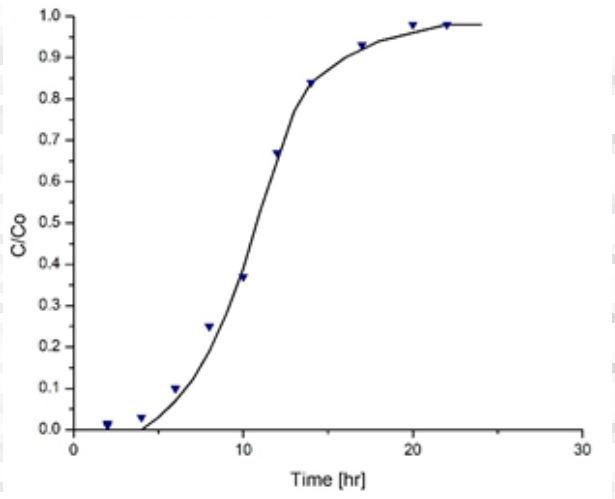

(b) GWTF-C2

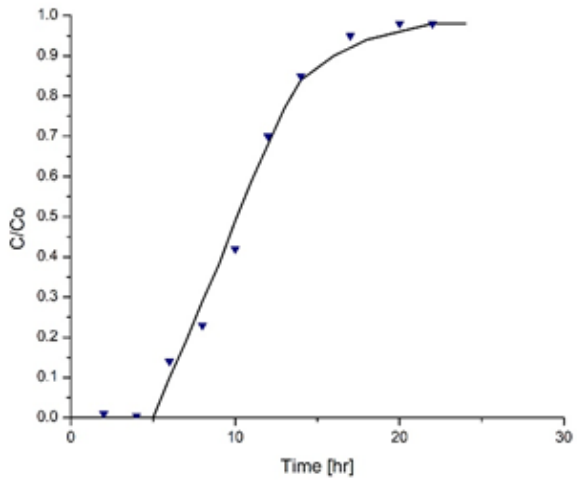

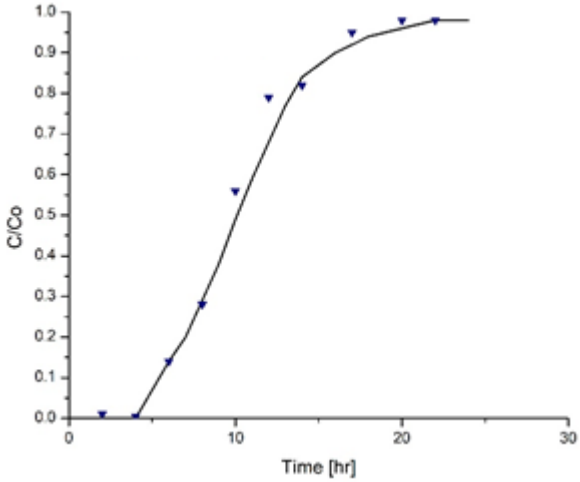

(c) GWTF-C3 **(d) GWTF-C4**

Figure 4.13: BTCs obtained from tracer test analysis for (a) rapid, (b) general, (c) slow and (d) stable groundwater fluctuation conditions.

Table 4.5: The best fitted values of D_L and α_L estimated by tracer BTCs analysis.

Conditions	Longitudinal dispersion coefficient (D_L) [m^2/s]	Longitudinal dispersivity (α_L) [m]
GWTF-C1	0.000246	1.23
GWTF-C2	0.0000171	0.72
GWTF-C3	0.0000108	0.28
GWTF-Stable	0.0000073	0.12

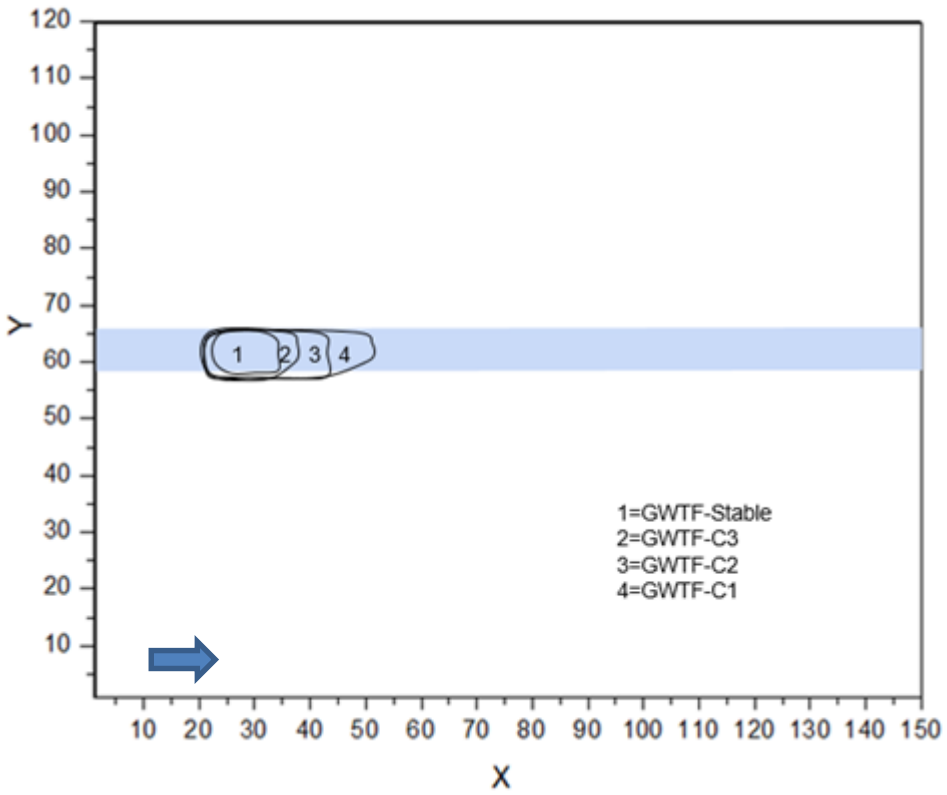

Figure 4.14: Coverage of the LNAPL pool in smear zone subjected to different groundwater fluctuation conditions.

Thereafter, an effort has been made to capture LNAPL pool area in two dimensional sand tank experiments under stable and fluctuating groundwater cases. For this purpose,

periodically soil-water samples were analyzed by GC-MS/IRMS technique (Dempster et al. 1997). The interpreted boundary of pure phase LNAPL pool is presented in figure 4.14 which shows a total area of 250, 200, 160 and 70 cm^2 covered under rapid, general, slow and stable groundwater fluctuation cases, respectively.

Experimentally observed area of pure phase LNAPL pool was used to determine the characteristic length of the pool and for the estimation of dissolution rate. It can be observed from the results that the rapid groundwater fluctuation causes the pure phase LNAPL pool to spread over more area then the stable groundwater case. A high groundwater velocity due to rapid fluctuation in groundwater governs the excess spreading of LNAPL in flow directions. Spreading of pure phase LNAPL over a large area provides more dissolving surface as LNAPL-water interphase to underlying flowing groundwater resulting into more dissolution rates. Similarly, the large LNAPL pool contributes more LNAPL vapour to the overlying unsaturated zone. Further, the volume of water contacting the LNAPL pool surface increases as it spread in large area which also leads to high dissolution rates. This in turn significantly increases dissolved phase concentration load to receiving groundwater and vapor contamination to unsaturated pore air (Dobson et al. 2007; Vasudevan et al. 2014). On the other hand, large coverage of pool contributes more LNAPL mass to capillary ganglia as smaller blobs/fingering, which also play significant role in dissolution under rapid groundwater table conditions. As noted by Sarikurt et al. (2017), the contact time and area of LNAPL-water interphase is significant for dissolution rate and subsequent transport of dissolved LNAPL in subsurface. Similarly, Sulaymon and Gzar (2011) highlighted that length of LNAPL-water interphase plays important role to control the equilibrium concentration of dissolved LNAPL plume. Results of this study confirm that the groundwater table fluctuation causes more spreading of pure phase LNAPL pool itself which ultimately provide more LNAPL-water dissolving area in smear zone. High dissolution rate from large LNAPL pool contributes high concentration of dissolved LNAPL to the downgradient ports. The estimated LNAPL pool coverage area under different cases can be used to forecast dissolved LNAPL plume under dynamic groundwater flow conditions.

The vapor phase LNAPL concentrations are plotted as BTC in figure 4.15. The BTC shows a high LNAPL concentration in case of rapid fluctuating groundwater table followed by general, slow and stable groundwater table case. The vapor equilibrium concentration was observed as 210-230 ppm in fluctuating condition while 180-185 ppm

was observed in stable groundwater case. This means a raising groundwater table carries pure phase LNAPL mass upward and a falling groundwater allows LNAPL to move downward. During dynamics of groundwater level, the trapped LNAPL remain behind in smear zone which creates a large interphase area of air-LNAPL/water (Powers et al. 1992). Therefore, more vapor phase concentration was observed from the residual LNAPL. These results are in line with the findings of study conducted by Oostrom et al. (2006) with 2D experiment under water table dynamic conditions. The study found a considerable residual LNAPL saturation in smear zone. The high vapor concentration can also be attributed to the partition of LNAPL from large dissolved phase plume having high concentration. Further, lowering of groundwater table increases air-filled porosity in smear zone, which eventually affects vapor phase LNAPL partition. The BTC of different groundwater table fluctuation experiments confirms that the vapor intrusion is highly dependent on the nature of groundwater table conditions (Patterson and Davis, 2009). High vapor LNAPL in unsaturated pores may become toxic for the indigenous microorganisms.

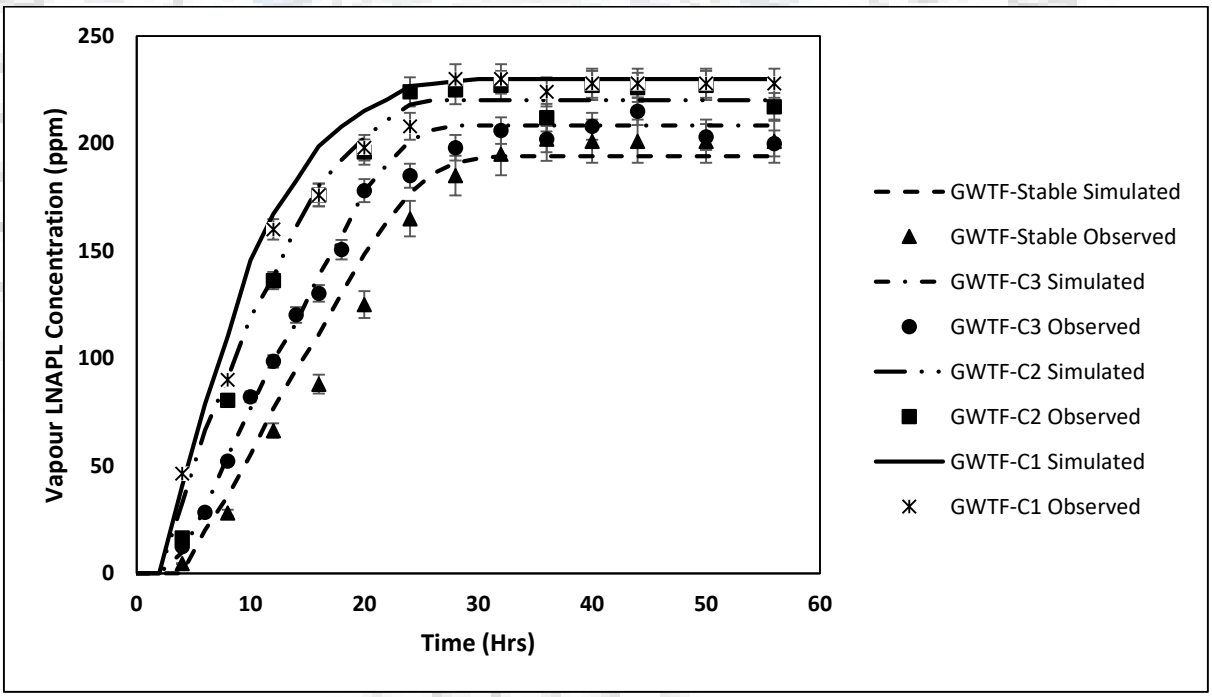

Figure 4.15: BTC representing vapor LNAPL concentration at upper port (UP) in 2D sand tank under stable and fluctuation groundwater table conditions.

The measured pure phase LNAPL pool area was used to estimate its characteristic length of LNAPL pool ($l_{(c)}$) under stable and fluctuating groundwater conditions. The observed

values of $l_{(c)}$ was found 15.81, 14.15, 12.64, and 8.36 cm under rapid, general, slow and stable groundwater fluctuation conditions, respectively. The estimated value of mass transfer coefficient (k^*) are listed in table 4.6. The estimated Sherwood numbers (Sh) were found 0.95, 16.20, 16.95 and 19.30 while Peclet numbers (P_e) were 1.80, 75.47, 80.14, and 95.06 for rapid, general, slow and stable cases respectively. A high value of Sh indicates that dissolution was a dominating process under fluctuating groundwater conditions. The reason for high Sh can be attributed to the large pool spreading, which provides more LNAPL-water interphase under fluctuating groundwater condition. Further, more contact time of underlying groundwater with the large dissolving LNAPL pool also accelerate the dissolution rate. Likewise, high P_e indicates that the advective flow was dominant than the diffusive flow under fluctuating groundwater conditions. However, one cannot ignore the importance of diffusive flux under stable groundwater flow regimes. The correlation Sh with P_e is presented in figure 4.16 with the coefficient of determination (R^2) value of 0.998. This kind of high correlation between Sh and P_e was also reported in a recent study by Sarikurt et al. (2017).

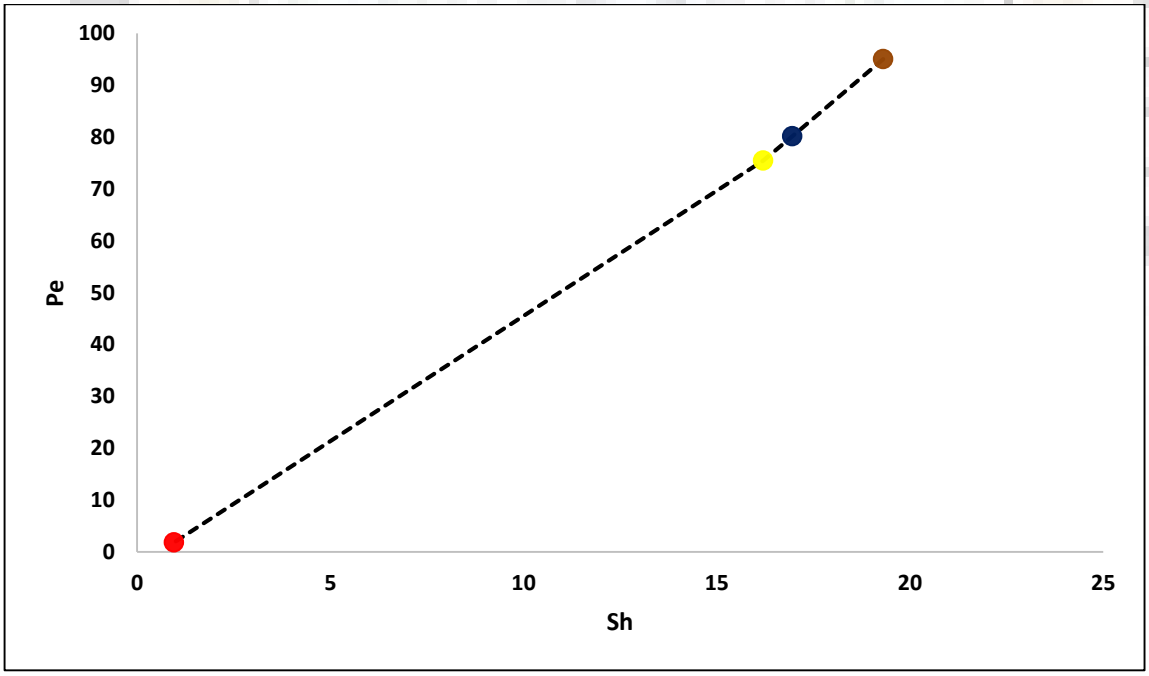

Figure 4.16: Established correlation between Sh and P_e. Red, yellow, blue and green circle represent stable, slow, general and rapid groundwater fluctuation conditions respectively.

Table 4.6: Estimated values of k^* and corresponding values of Sh and P_e under dynamic groundwater table conditions

Conditions	Mass transfer coefficient k^* (m/s)	Sherwood Number Sh (-)	Peclet Number P_e (-)
GWTF-C1	9.50E-02	19.30	95.06
GWTF-C2	5.80E-03	16.95	80.14
GWTF-C3	3.50E-03	16.20	75.47
GWTF-Stable	1.20E-04	0.95	1.80

Dissolved LNAPL concentrations as a function of time for all four cases are presented in figures 4.17-4.18. In figure 4.17a, BTC is presented for port 1 (top sampling layer: X:25cm; Y:60 cm) which was situated just below the water table and nearby LNAPL pool. It shows that toluene concentration starts rising after few hours and increases rapidly and then starts attenuating before reaching to a concentration of 200-230 ppm for rapid fluctuating groundwater case. Similar trends were observed for the remaining fluctuating groundwater cases. The higher concentration in the rapid fluctuation case was due to more dissolving LNAPL pool area than general, followed by slow and stable fluctuation conditions. Likewise, BTCs of port 4 and port 7 of upper layer are presented in figure 4.17b and 4.17c respectively. LNAPL concentration takes 10-12 hours and 20-26 hours to reach port 4 and port 7, which was 55 cm and 115 cm away from pool respectively. However, a significant difference in the final equilibrium concentration (plateau) was observed amongst different groundwater table fluctuation cases. At this stage the supply from the source and the out flux at the observed down-gradient port (port 7) was reaching to an equilibrium condition. A decreasing trend in the equilibrium concentration was observed as plume moves from up gradient location (port 1) to down-gradient locations (Port 4/7) which represents the dependency of biodegradation rate on dissolved LNAPL concentration. In general, the equilibrium concentration of toluene in earlier studies was found quite nearby to its dissolution limit. In this study, the observed concentration of toluene was not able to reach the maximum solubility value of toluene because of (a) limited contact (water-toluene) time of opportunity, (b) the concurrent biodegradation of the dissolved LNAPL in sand tank setup. The study shows that more than 150 ppm dissolved LNAPL concentration was found to start inhibiting metabolic actions of microbes

causing lower degradation rates then its potential rate. Similarly, a concentration less than 100 ppm provides insufficient carbon sources to microbes resulting in comparatively low biodegradation rate of toluene. The optimal biodegradation rate was found in plume area having concentrations ranges from 120-150 ppm, especially under general groundwater condition. While biodegradation rate become quite slow at port 1 due to high dissolved LNAPL concentration (>150 ppm) and causes toxicity to potential microbes. The biodegradation rate in upper layer was accelerated by high diffusion of oxygen from head space by fluctuating groundwater table.

Likewise, the dissolved LNAPL concentrations are presented in figures 4.18a-c for ports 8, 11 and 14 situated in bottom layer. Figure 5.6a shows that the dissolved LNAPL plume takes 10-12 hours to reach at port 8, which is at 30 cm downward from the pool. At port 8, there is very less difference in equilibrium concentrations as compared to port 1. Whereas, a large difference was found in equilibrium concentration of port 11 (Figure 4.18b) and port 14 (Figure 4.18c) in comparison to port 8 (Figure 4.18a). This seems due to high biodegradation rates at port 11 as compared to port 8, even the port 11 is situated in bottom layers where background oxygen level is low.

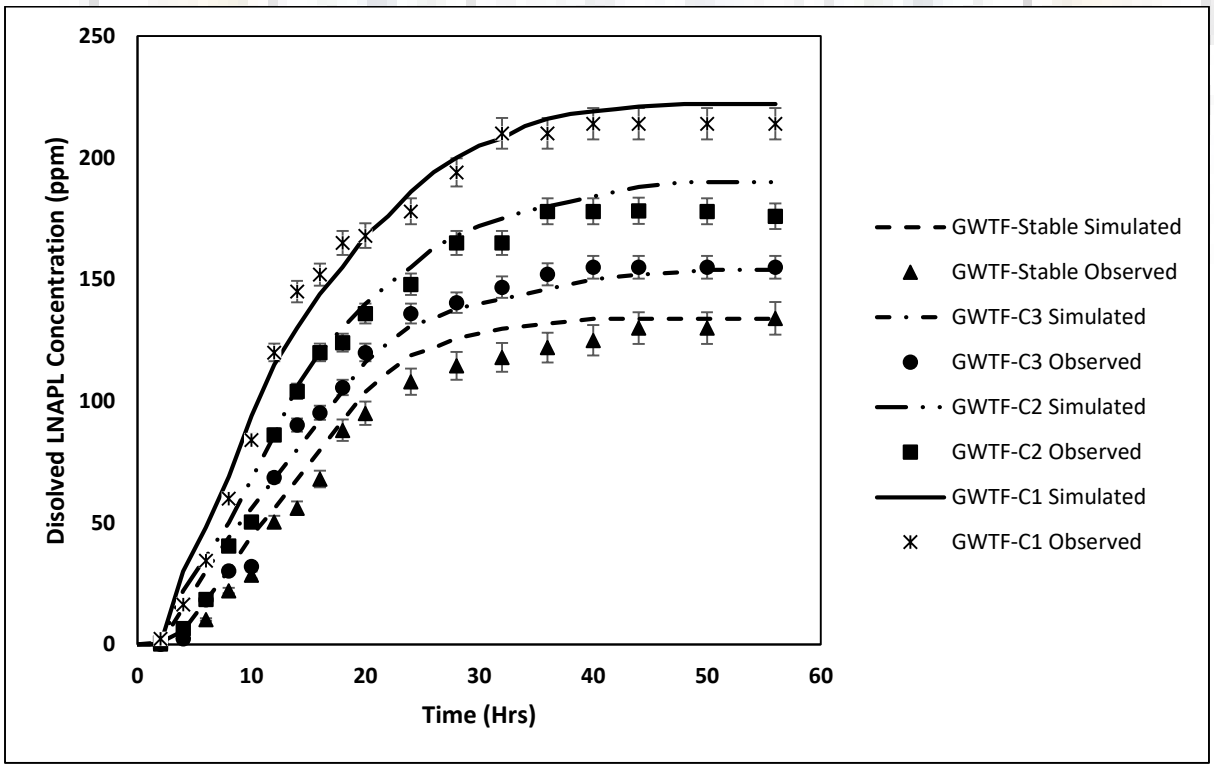

(a) Port 1: X:25; Y60

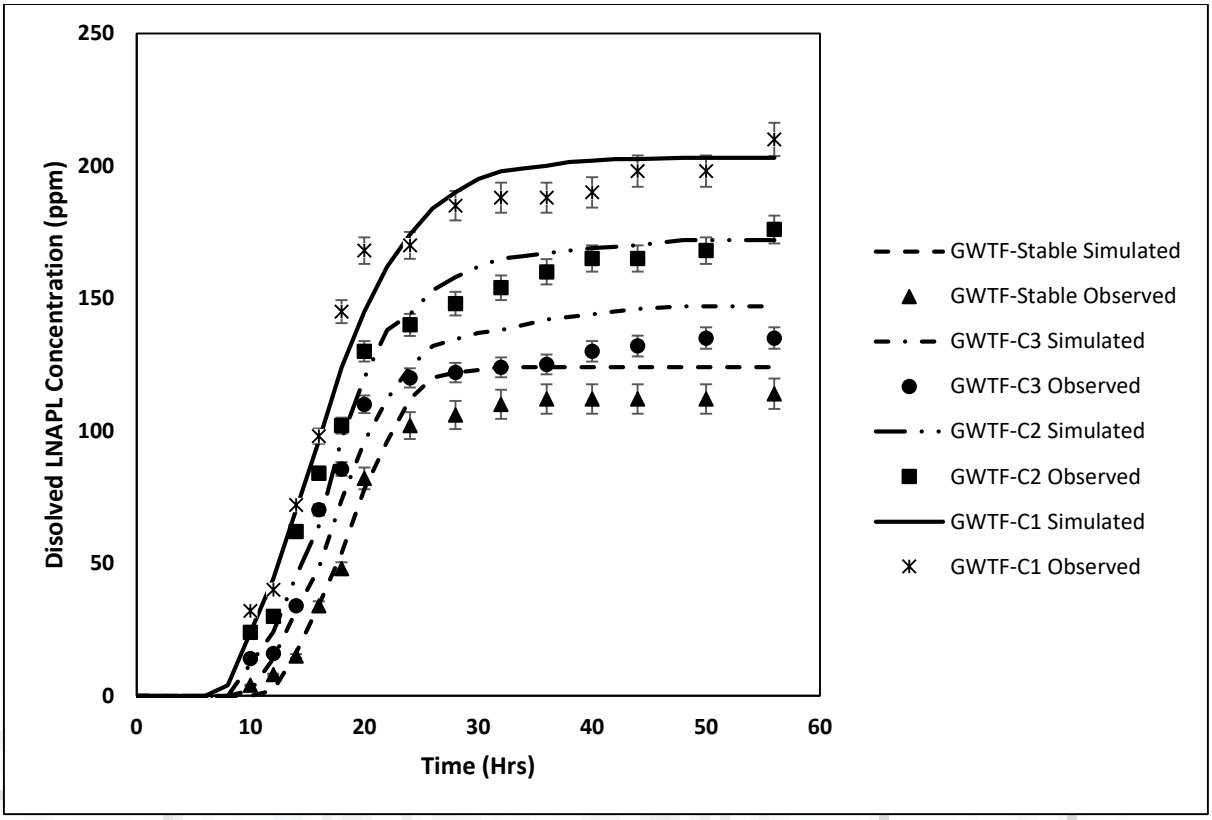

(b) Port 4: X:80; Y60

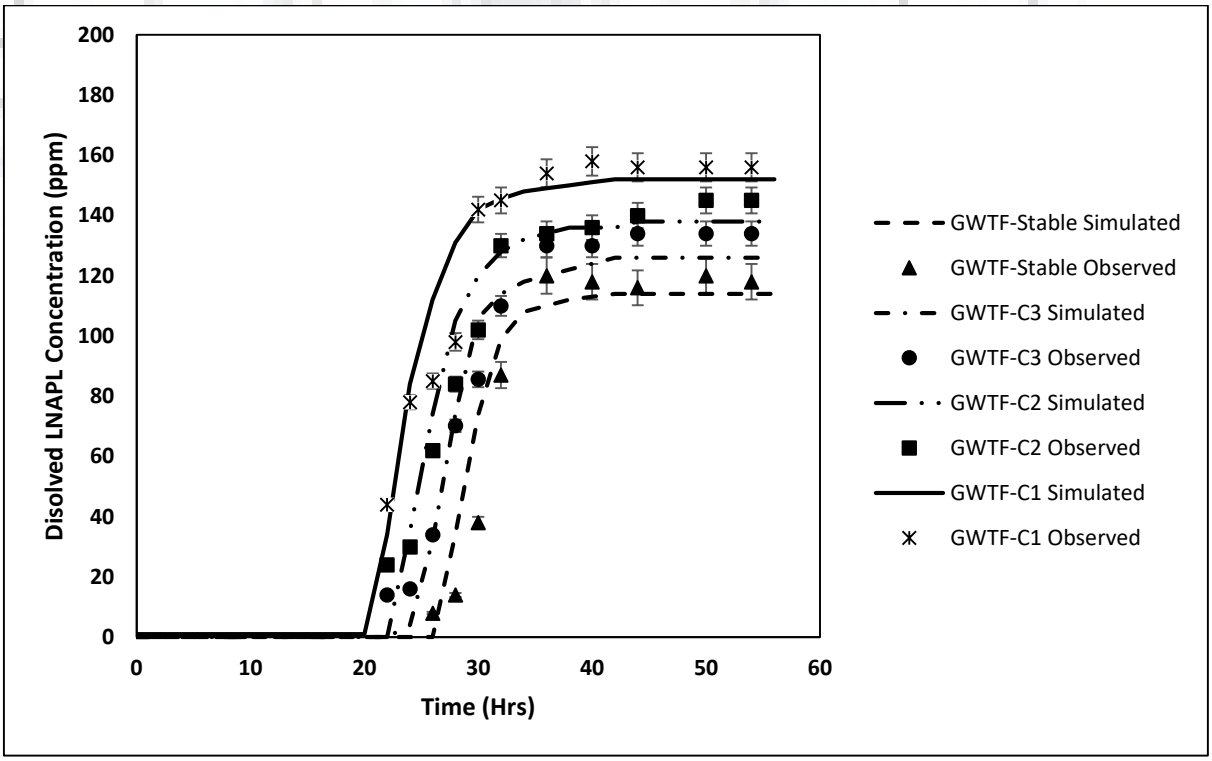

(c) Port 7: X:140; Y60

Figure 4.17: BTCs of (a) port 1, (b) port 4 and (c) port 7 under stable and fluctuating groundwater table conditions.

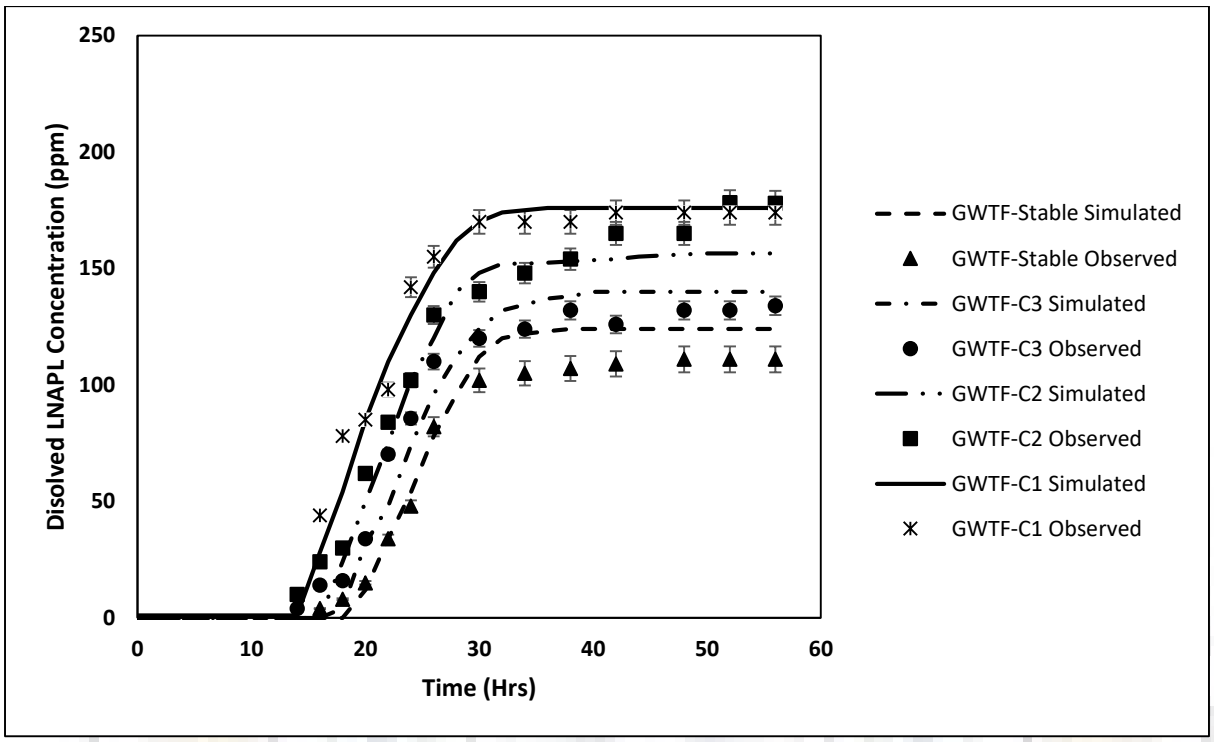

(a) Port 8: X:25; Y30

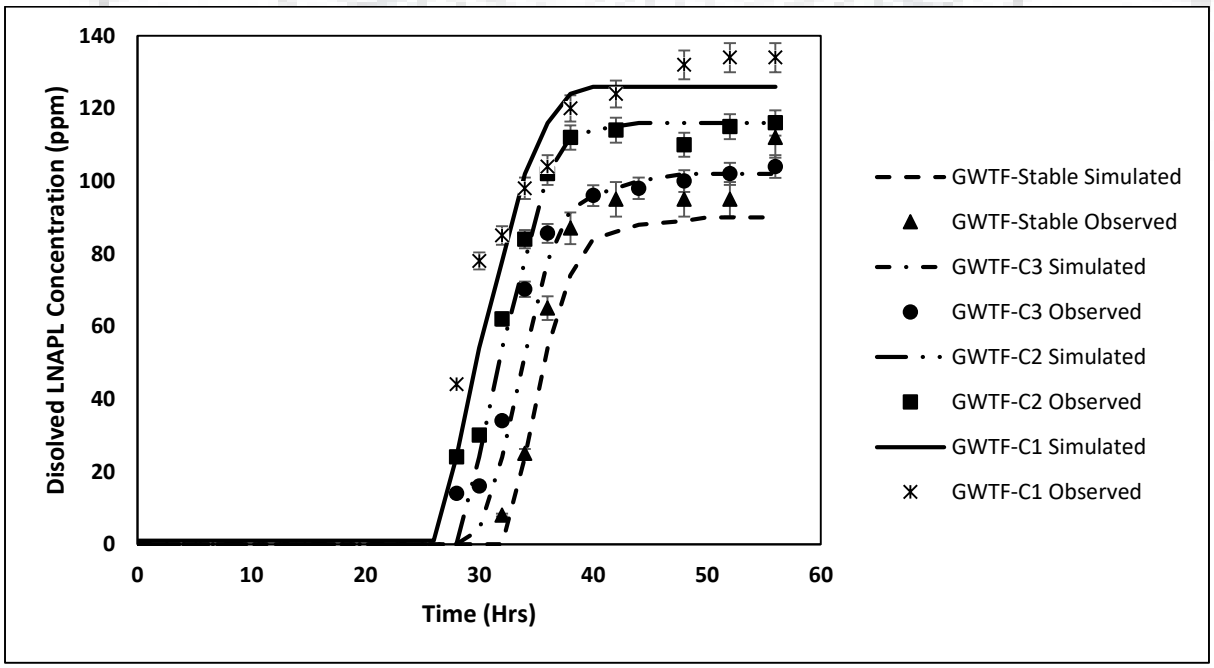

(b) Port 11: X:80; Y30

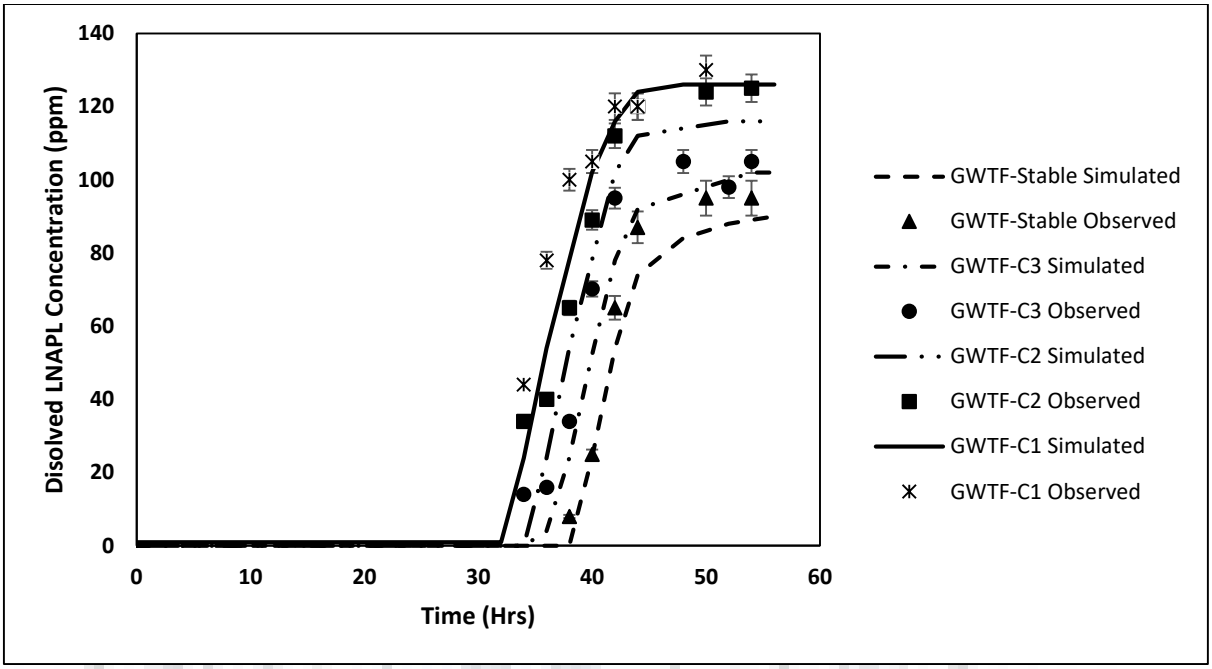

(c) Port 14: X:140; Y30

Figure 4.18: BTCs of (a) port 8, (b) port 11 and (c) port 14 under stable and fluctuating groundwater table conditions.

The experimentally observed dissolved LNAPL concentrations isolines are plotted as a function of space in figures 4.19-4.21. These concentration isolines were plotted using experimentally measured data from all sampling ports (port1-14) including ports situated opposite to flow directions (port RP1-RP2). The objective of these isolines plot is to present different concentration zone originated from LNAPL pool under different selected groundwater table conditions. Figure 4.19 represents concentration isolines originated from large LNAPL pool having 15.81 cm under rapid groundwater table fluctuation condition. Thus, large dissolved plume was created with a concentration ranges from 120-160 ppm in initial 12 hours and later reaches up to 200 ppm nearby the pool location. A large area covered by high concentration i.e. greater than 150 ppm causes toxicity to potential microbes and thus low biodegradation rate was observed in this case. Thus, a closely spaced isolines were observed in rapid fluctuating groundwater conditions. Whereas, figure 4.20 represented isolines of dissolved plume originated from a pure phase LNAPL pool of characteristic length of 14.15 cm under general groundwater table fluctuation condition. In this case, the dissolved plume concentration ranges 110 ppm-140 ppm in initial 12 hours and continuously increases upto 160 ppm. Less concentration (20ppm) of dissolved plume

under general groundwater table fluctuation condition was due to smaller LNAPL pool length then the rapid case. Thus, in general groundwater table fluctuation case, a large area covered by 130-150ppm concentration LNAPL plume become carbon source to potential microbes and causes enhanced biodegradation rates. Similar trends were observed in case of slow groundwater table fluctuation condition as presented in figure 4.21. While, comparatively small dissolved LNAPL plume (figure 4.22) having less concentration (i.e. range of 70 ppm-100 ppm in initial 12 hours and 80-120 ppm in 56 hours) was observed in case of stable groundwater case.

In this study, the concentration isolines clearly show the fast transport of dissolved plume in horizontal direction than its transverse movement under stable and fluctuating groundwater conditions. The horizontal spreading of plume was due to advection dominated flow of the dissolved toluene originating from large contact area between LNAPL pool and water. Dissolved LNAPL plume movement in opposite direction of groundwater flow driven by diffusive flux is comparative very slow. Whereas, the expansion of dissolved LNAPL plume in the vertical direction under fluctuating groundwater shows the crucial role of dispersive flux. The diffusive flux of the dissolved LNAPL can play a crucial role in LNAPL movement under stable groundwater regimes.

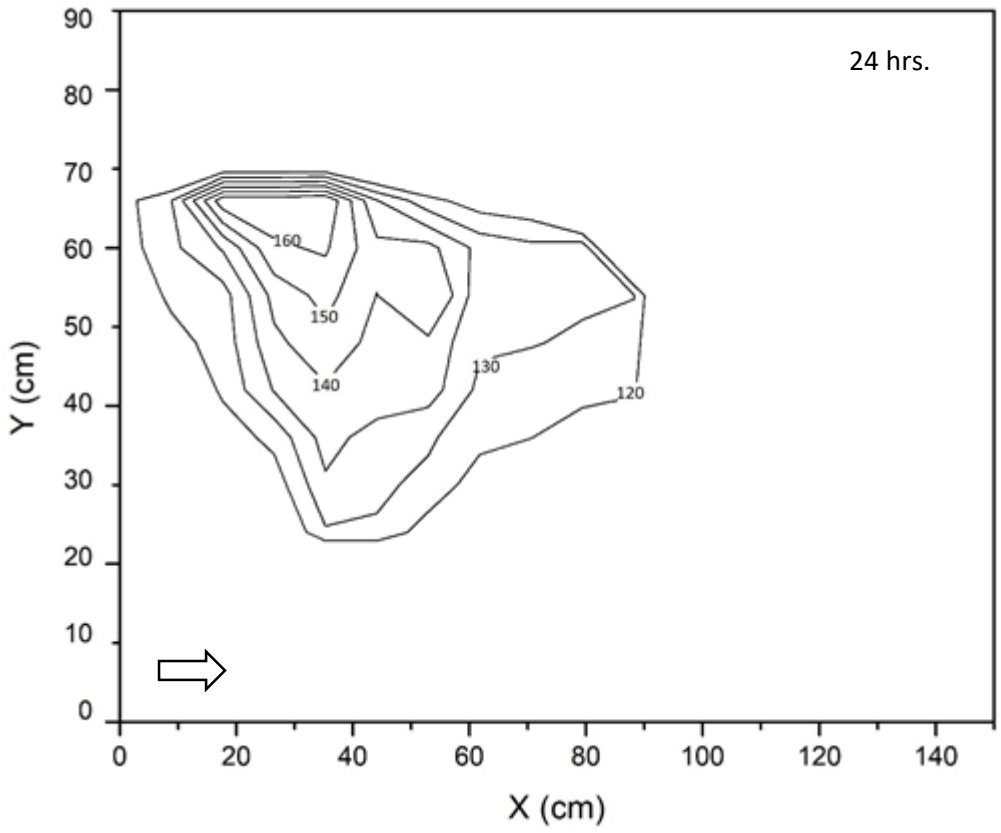

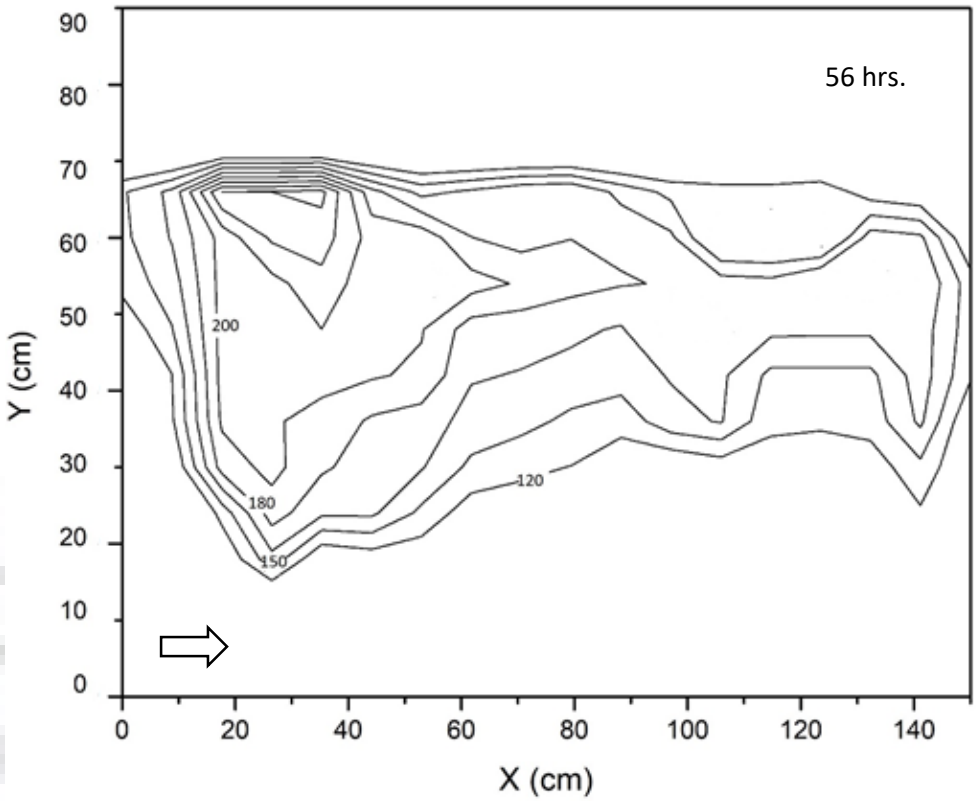

Figure 4.19: Concentration isolines presenting the extension of dissolved LNAPL plume originated from pure phase source under rapid groundwater table condition.

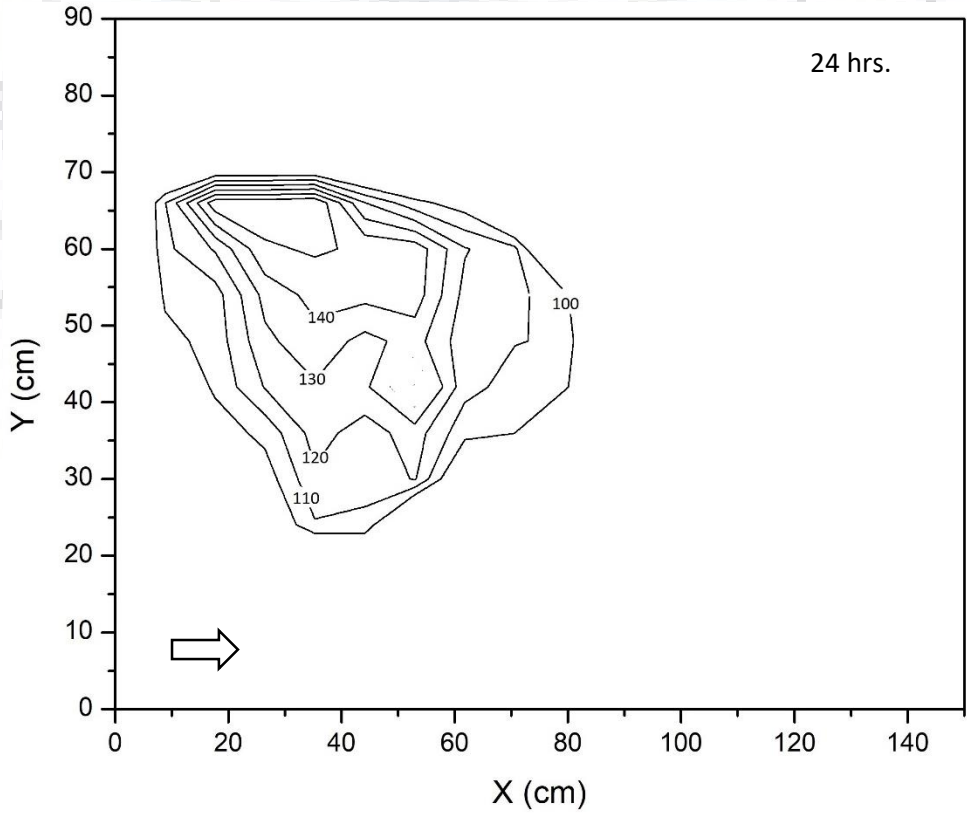

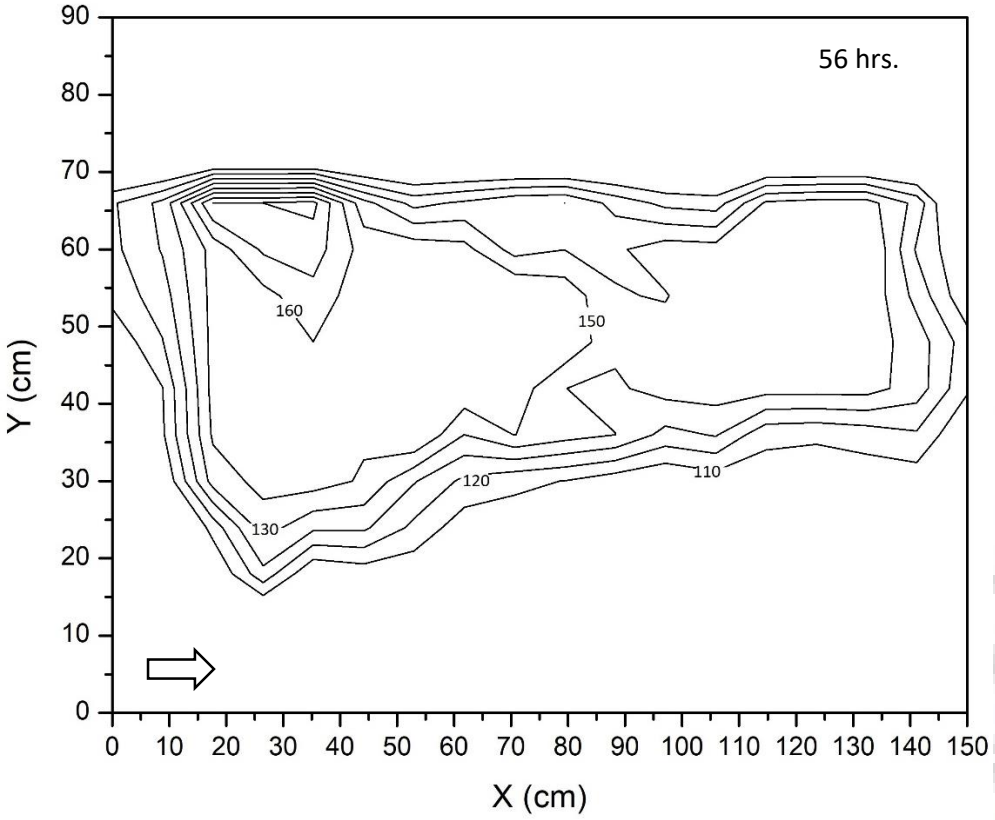

Figure 4.20: Concentration isolines presenting the extension of dissolved LNAPL plume originated from pure phase source under general groundwater table condition.

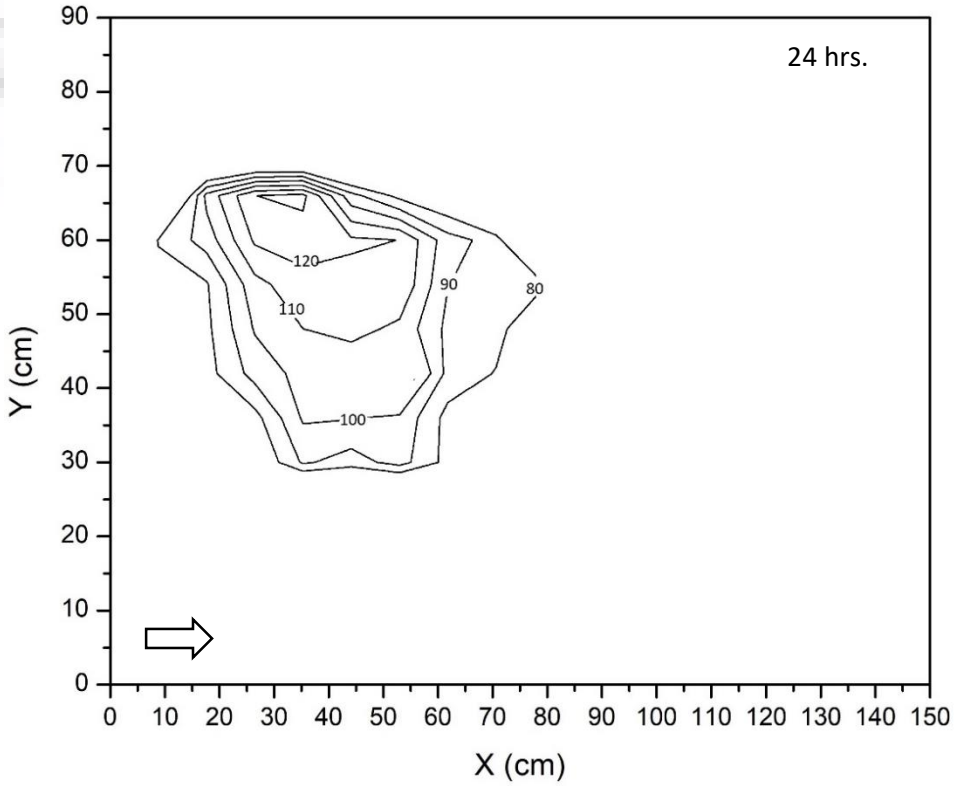

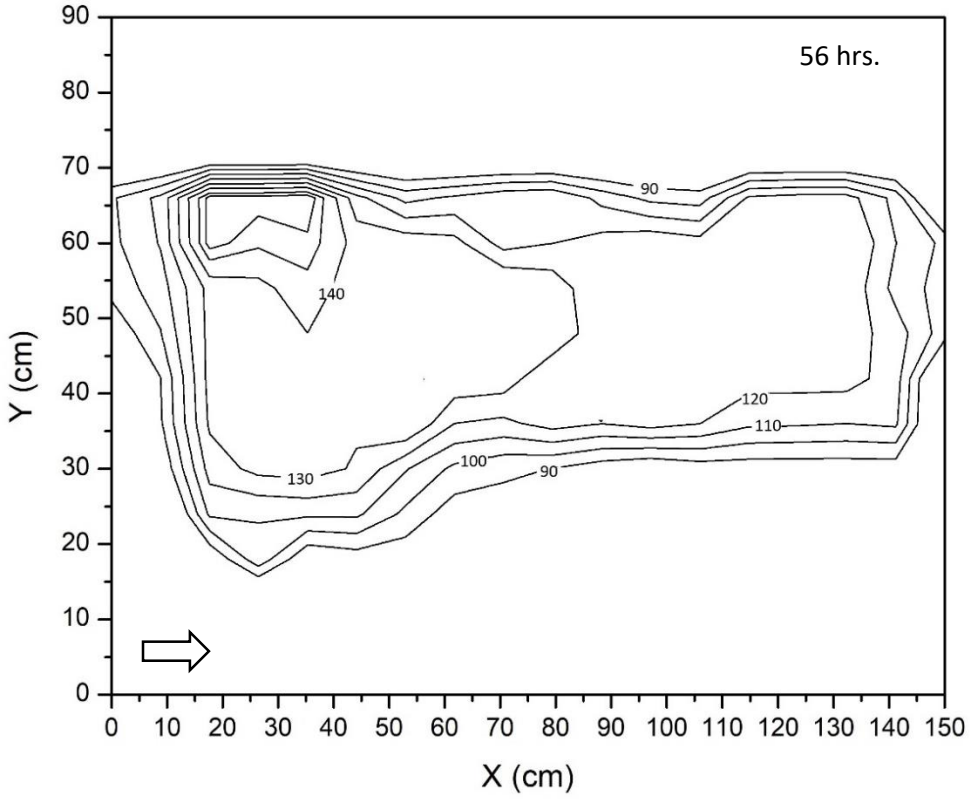

Figure 4.21: Concentration isolines presenting the extension of dissolved LNAPL plume originated from pure phase source under slow groundwater table condition.

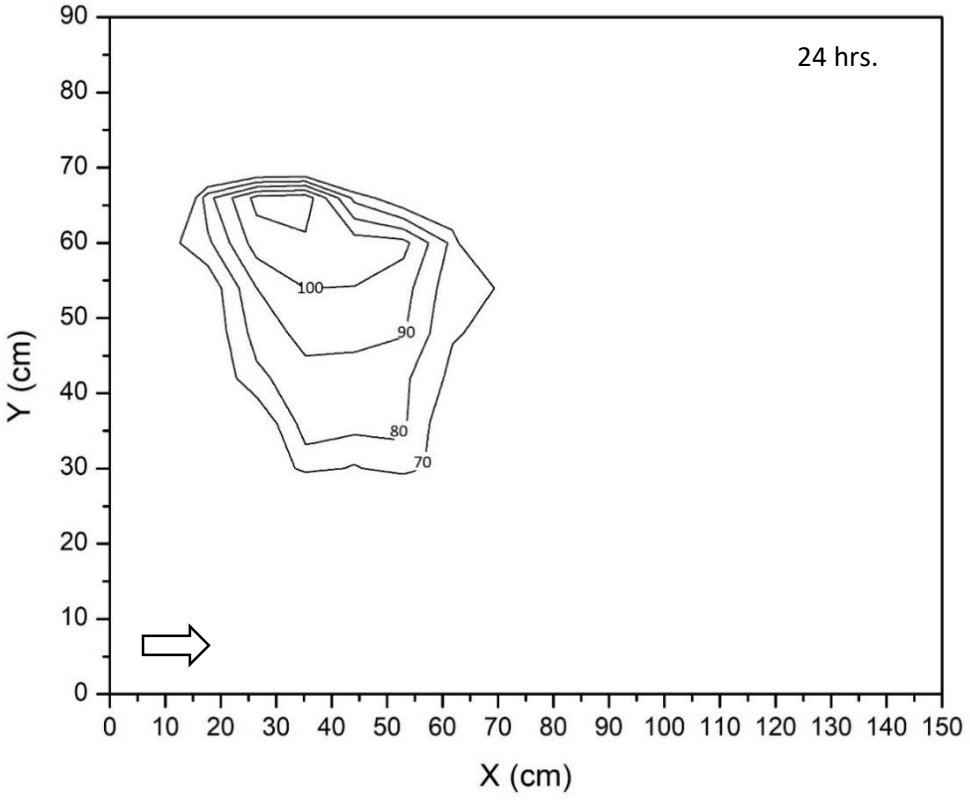

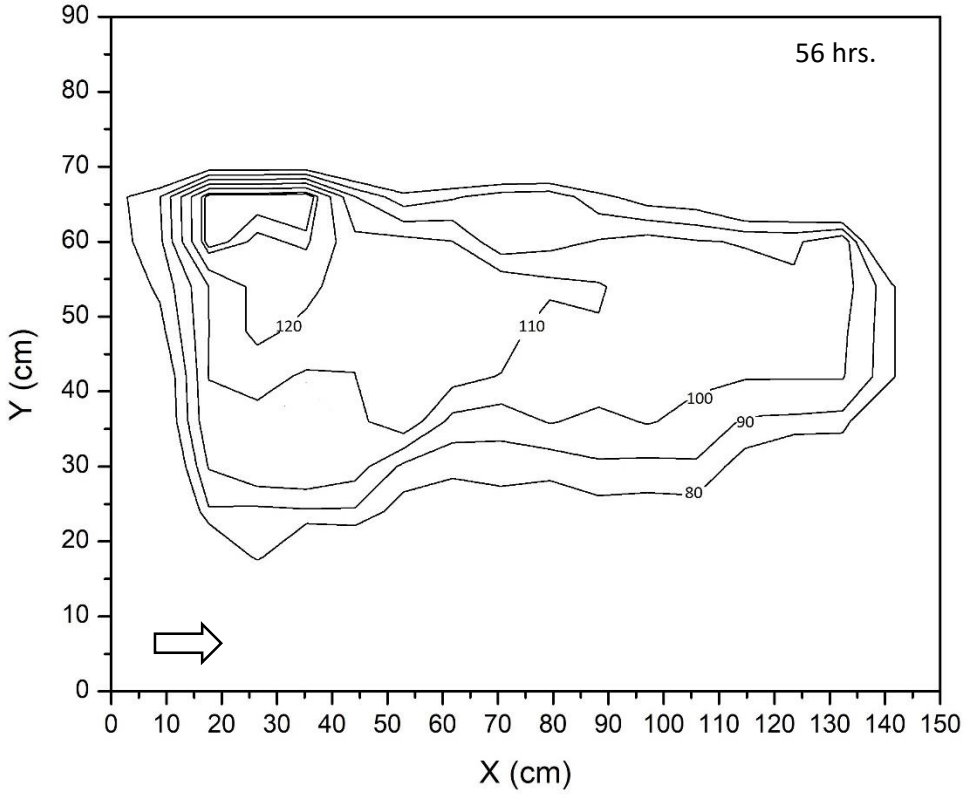

Figure 4.22: Concentration isolines presenting the extension of dissolved LNAPL plume originated from pure phase source under stable groundwater case.

Biodegradation rate of dissolved LNAPL plume originated from pooled LNAPL under stable and fluctuating groundwater conditions was also investigated. For this purpose, spatial biodegradation rates were estimated for port 1 and port 4 of upper sampling layer and port 8 and 14 of lower sampling layer. In figure 4.23, the biodegradation rates were estimated using corresponding values of equilibrium concentration of upward port and subsequent downward port. Figure 4.23a presents biodegradation rate of port 4 situated 55 cm away from LNAPL pool. At this location, biodegradation rates of 0.5 ppm/hour, 0.55 ppm/hour, 0.26 ppm/hour, and 0.13 ppm/hour were observed for dissolved LNAPL zone with the concentration of 180 ppm, 150 ppm, 120 ppm, and 100 ppm under rapid, general, slow and stable groundwater table condition, respectively.

The biodegradation rate was found comparatively low in case of rapid fluctuation than general fluctuation because of large high concentration (>150 ppm) region which causes toxic effects on potential microbes lies in this region. While, the high biodegradation rate in case of general than slow and stable groundwater fluctuation conditions proves the dependency of microbes on dissolved LNAPL concentrations. Figure

4.23b represents biodegradation rates for port 7 of upper layer having dissolved LNAPL concentration in the range of 100 ppm-150 ppm. Similarly, figure 4.23c and 4.23d shows the biodegradation rates for port 8 and port 14 of lower layer respectively. Comparatively low biodegradation rates were observed in lower layer ports under stable groundwater conditions, even if the dissolved LNAPL concentration was in the optimum range of 100 ppm-150 ppm. These low biodegradation rate at lower ports was due to comparatively less populated potential microbes due to low oxygen level. While, the biodegradation rates were also increases at lower port in case of fluctuating groundwater conditions. These accelerated biodegradation rate can attribute to the fact that the additional oxygen to background level was added due to fluctuation in water table, which enhance the microbial growth.

Microbial population was also counted using standard plate count method for periodically collected soil-water samples from port 1 and port 7 of upper layer and port 8 and port 14 of lower layer. The estimated CFU of collected soil-water samples were listed in table 4.7. Initially, microbial count of 216.2-258 $\times 10^4$ CFU/mL and 142.5-147.2 $\times 10^4$ CFU/mL was observed at upper and lower layer respectively. In GWTF-C1 case, the microbial count at port 1 increases upto 305 $\times 10^4$ CFU/mL in 24 hours and then decreases to 78×10^4 CFU/mL in 56 hours. Similarly, at port 7, overgrowth was recorded after 24 hours thereafter decreases to 224×10^4 CFU/mL in 56 hours. Pictures of plates of this study are shown in Appendix-II.

The enhanced microbial growth was observed as dissolved LNAPL concentration reached around 140-150 ppm at this location which provides sufficient carbon source to microbes. However, when the dissolved LNAPL concentration reaches higher than 150 ppm, it become toxic to microbial community. Increasing microbial count was recorded at both port of top layer due to optimum dissolved LNAPL concentration and sufficient oxygen level in general and slow groundwater fluctuation. Microbial count was recorded very low at port 14 of lower layer due to low concentration of dissolved LNAPL and insufficient oxygen level under all groundwater table conditions. Growing population of the microbial community at petroleum hydrocarbon-contaminated groundwater observed due to seasonal groundwater level fluctuations by Zhou et al. (2015). Such microbial analysis may help to implement nutrient and or electron acceptor plan to enhance petrochemical degrading microbes.

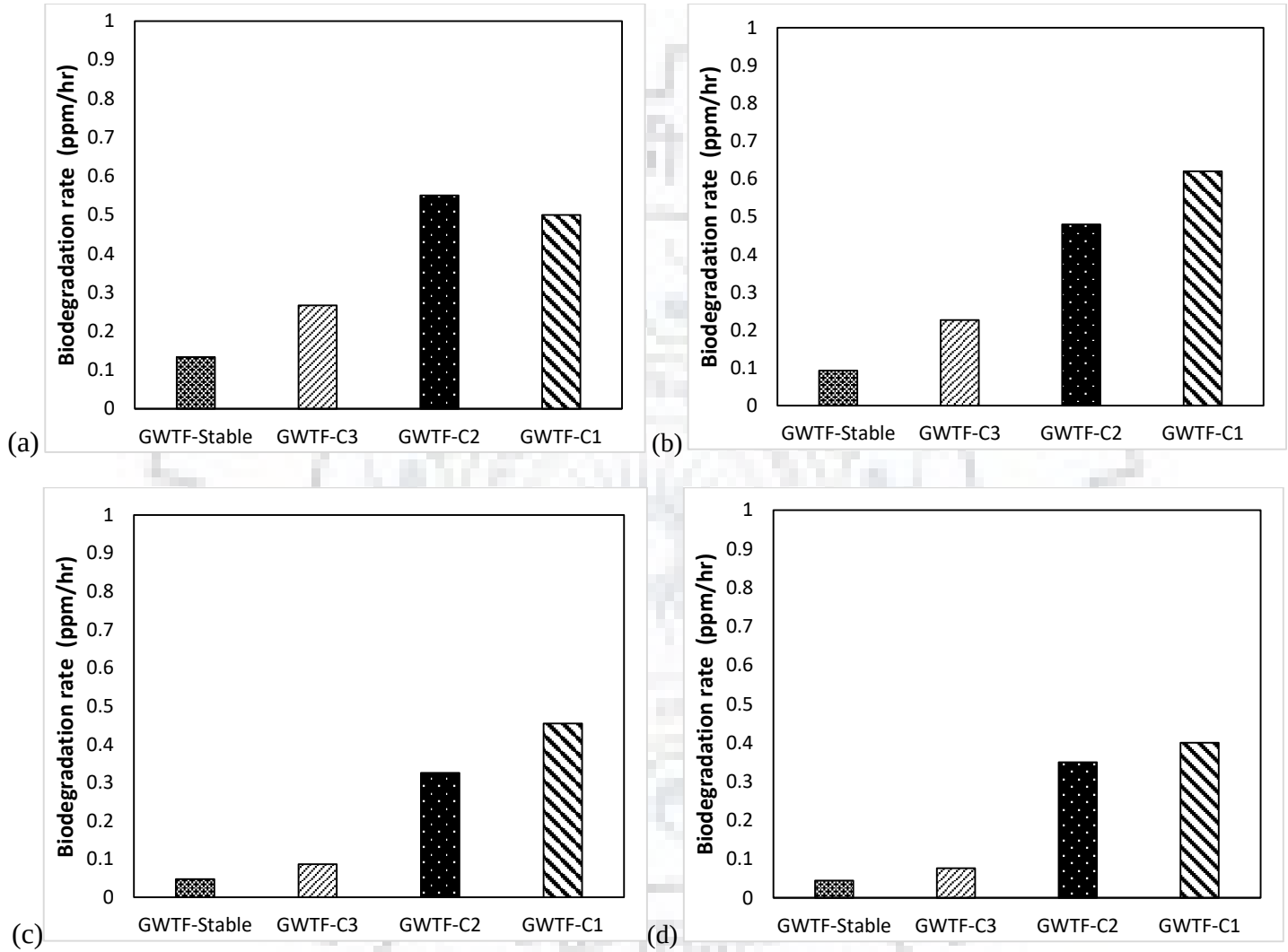

Figure 4.23: Estimated biodegradation rates under stable and fluctuating groundwater conditions observed at (a) port 1 and (b) port 7 of upper sampling layer and (c) port 8 and (d) port 14 of bottom sampling layer of 2D sand tank setup.

Table 4.7: Microbial population count of samples collected from two dimensional sand tank under different groundwater table conditions.

Condition	Port 1			Port 7			Port 8			Port 14		
	10^4 CFU/mL			10^4 CFU/mL			10^4 CFU/mL			10^4 CFU/mL		
	0hr	24hr	48hr	0hr	24hr	48hr	0hr	24hr	48hr	0hr	24hr	48hr
GWFT-C1	254.5	305	78	258.0	O	224.5	147.2	165	135.4	142.5	145.8	165
GWFT-C2	232.1	294.8	304.6	-	285.0	O	145	174.2	235.0	-	164.5	218
GWTF-C3	216.2	285.4	277.5	224.5	288.0	O	144.5	210.5	270.6	-	164.2	235.6

O= Overgrowth

4.6 Role of Groundwater Flow Velocity

To investigate the role of groundwater flow on LNAPL biodegradation and its transport, a series of 3D sand tank experiments were conducted using three different groundwater velocities. A base groundwater velocity of 1.2 m/day was taken in first set of the experiment, thereafter velocity was increased/decreased to two/half fold by adjusting the flow rate using a peristaltic pump without changing the location of the water table in subsequent sets of the experiments. Tracer transport experiments were also performed separately under fast, base and slow groundwater velocities. The hydrodynamic dispersion coefficients were estimated on basis of BTCs obtained from the tracer experiments at these three different velocities (figure 4.24). The values of longitudinal dispersivity corresponding to the respective groundwater velocity are listed in table 4.8.

Lateral spreading of pure phase toluene pool observed during these experiments in smear zone is plotted in figure 4.25 for the considered groundwater velocities. A wide coverage of the LNAPL, mainly in flow direction, under faster groundwater velocity indicates that the pure phase LNAPL was transported around the water table due to the high shear force acting on the water- LNAPL interface.

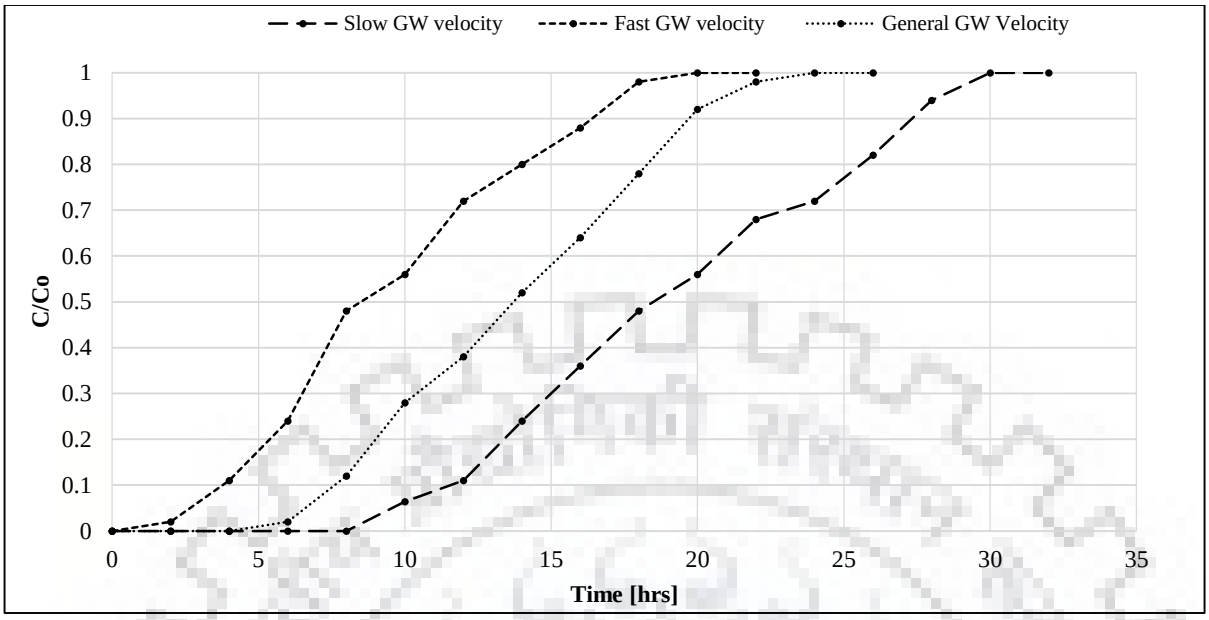

Figure 4:24: Tracer breakthrough curves (longitudinal) observed at *X*=20; *Y*=28; *Z*=15cm under slow, fast and base groundwater velocities.

The length of the pool, $l_{(c)}$, was estimated by plotting the front boundaries of LNAPL pool as shown in the figure 4.25. The pool length was 15, 10, 05 cm under fast, base and slow groundwater velocity cases, respectively. The vertical dispersion coefficient was estimated to be 0.142, 0.215, 0.34 cm^2/hr at the velocities 2.5, 5, 10 cm/hr, respectively. The Sherwood and Peclet numbers (Sh and P_e) represents the ratio of the mass transfer rate and groundwater flow velocity to the rate of diffusive mass transport, respectively. The dissolution rate, k^*, along with these dispersivity coefficients were then used in estimating Sh as suggested by Sulaymon and Gzar (2011). To correlate the advective-dispersive mass transfer in horizontal (x) direction, the P_e was determined as $(P_e)_x = V_x l_{(c)}/D_L$. The obtained P_e using the experimental values of longitudinal dispersion coefficient shows a linear relationship with groundwater velocity as listed in Table 4.8. This relationship confirms the findings of Sulaymon and Gzar (2011) that high mass transfer rates are associated with faster groundwater velocities. Similar effect of groundwater velocity on the mass (name of solute?) transport was reported by Voudrias and Yeh (1994).

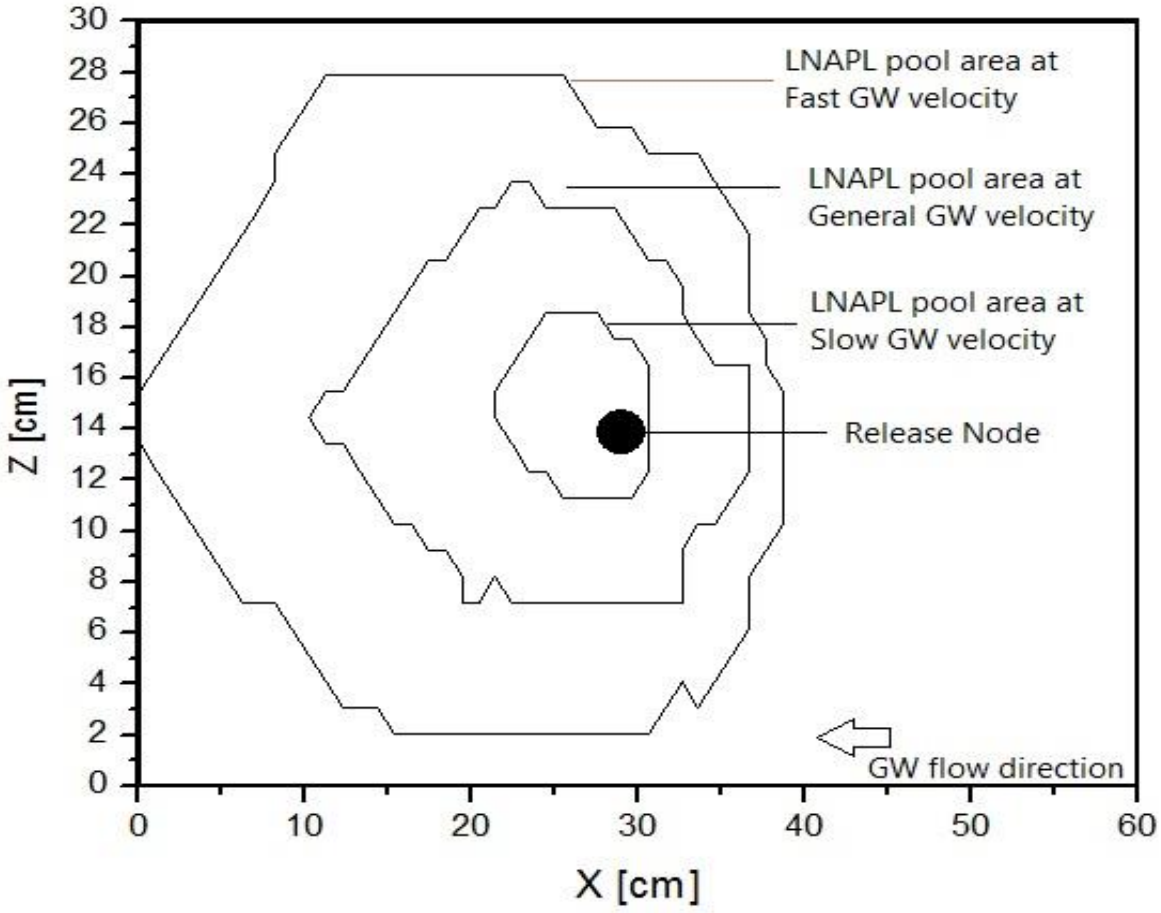

Figure 4.25: Coverage of the LNAPL pool in smear zone subjected to different groundwater velocities.

Table 4.8: Observed values of k^*, S_h, P_e for different groundwater velocities and dispersion coefficients.

$\boldsymbol{V_x}$ (cm/h)	$\boldsymbol{D_L}$(cm^2/h)	k^* (cm/h)	S_h	$P_{e\,(x)}$	$P_{e\,(y)}$
2.5	1.42	0.0838	25.88	12.32	123.20
5	2.15	0.0965	68.10	37.20	372.09
10	3.40	0.1297	160.23	82.35	823.52

The BTCs for different downgradient locations, 05, 10, 15, 20, and 25 cm away from the release point, are presented in figure 4.26 a-e. The BTCs show that the arrival times of

dissolved plume at down-gradient locations is least for the case of fast groundwater velocity followed by the base and slow groundwater velocity cases. A rapid movement of the dissolved phase LNAPL in horizontal i.e. central line of groundwater flow directions under high groundwater velocity indicates that the advective-dispersive transport plays a dominating role in LNAPL transport mechanism as compared to the diffusive flux (Sulaymon and Gzar, 2011). Whereas, the dissolved LNAPL transport in transverse (perpendicular to central line) direction is dominated by flux resulted from diffusion. Toluene concentration starts rising after few hours and increases rapidly and then starts attenuating before reaching to a concentration of 150 -160 ppm for the fast groundwater velocity case. Similar trends were observed for the remaining groundwater velocity cases. However, a significant difference in the final (plateau) concentration is observed in these three cases. At this stage the supply from the source (pure phase toluene pool) and the out flux at the observed downgradient port is reaching to an equilibrium condition. The attenuated value of toluene from its dissolution capacity in water is due to the limited dissolution rate and the biodegradation of the LNAPL.

A decreasing trend in the equilibrium (plateau) concentrations observed as plume moves from an up-gradient port (i.e. *X*=05 cm; *Y*=28 cm; *Z*=15cm; figure 4.26a) to a down-gradient port (*X*=25 cm; *Y*=28 cm; *Z*=15cm; figure 4.26d) fortifies the dependency of biodegradation rate on dissolved LNAPL concentration. The BTCs also indicate the favorable role of groundwater velocity on dissolution rate of the LNAPL. Thus, the equilibrium concentration was higher at all the down-gradient points under faster groundwater velocities. This seems due to large dissolving contact area between pure phase LNAPL pool, having characteristic length of 15 cm, and water as shown in figure 4.25 under the fast groundwater velocity case. Whereas, comparative low concentrations were observed under base and slow groundwater velocity cases due to less characteristic length i.e. 10 cm and 05 cm respectively, for contact between pure phase LNAPL and groundwater. The enhanced dissolution associated with higher groundwater velocity due to large contact area between LNAPL pool and water is also reported by Sulaymon and Gzar, (2011). Furthermore, a slow groundwater velocity allows dissolved LNAPL to have more time of residence to degrade the dissolved LNAPL in the soil-water path resulting in a lesser plateau concentration. The observed and simulated results were compared well for

all the three cases of groundwater flow conditions except some small discrepancies during very initial phase of the experiments (figure 4.26a-e) The estimated spatial degradation rates in horizontal and transverse directions are listed in tables 4.9-4.11. The correlation of these biodegradation rates are also listed in these tables. The results show that the biodegradation rate decreases as the plume move away from the release point under all the groundwater velocity cases. This is because dissolved concentration of the LNAPL decreases with increasing distance towards the downgradient side of the pool. The biodegradation rate was found comparative more under fast groundwater velocity than general groundwater velocity.

Table 4.9: Degradation rate (mg-L/hr) of the dissolved phase LNAPL at different transverse distance from pool under a fast groundwater velocity (10 cm/hr).

Depth of sampling ports from front side glass sheet of 3D-tank	Down-gradient distance			R^2
	05 cm	15 cm	25 cm	
00 cm	1.26	0.74	0.284	0.99
05 cm	0.841	0.602	0.184	0.97
10 cm	0.624	0.41	0.17	0.99
15 cm	0.524	0.38	0.142	0.98

Table 4.10: Degradation rate (mg-L/hr) of the dissolved phase LNAPL at different transverse distance from pool under a base groundwater velocity (5 cm/hr).

Depth of sampling ports from front side glass sheet of 3D-tank	Down-gradient distance			R^2
	05 cm	15 cm	25 cm	
00 cm	0.884	0.62	0.321	0.99
05 cm	0.784	0.462	0.204	0.99
10 cm	0.42	0.282	0.124	0.99
15 cm	0.324	0.18	0.087	0.98

Table 4.11: Degradation rate (mg-L/hr) of the dissolved phase LNAPL at different transverse distance from pool under a slow groundwater velocity (2.5 cm/hr).

Depth of sampling ports from front side glass sheet of 3D-tank	Down-gradient distance			R^2
	05 cm	15 cm	25 cm	
00 cm	0.442	0.321	0.086	0.96
05 cm	0.421	0.287	0.086	0.98
10 cm	0.284	0.145	0.068	0.97
15 cm	0.224	0.12	0.047	0.98

(4.26a) BTC location (cm):*X*=05; *Y*=28; *Z*=15cm

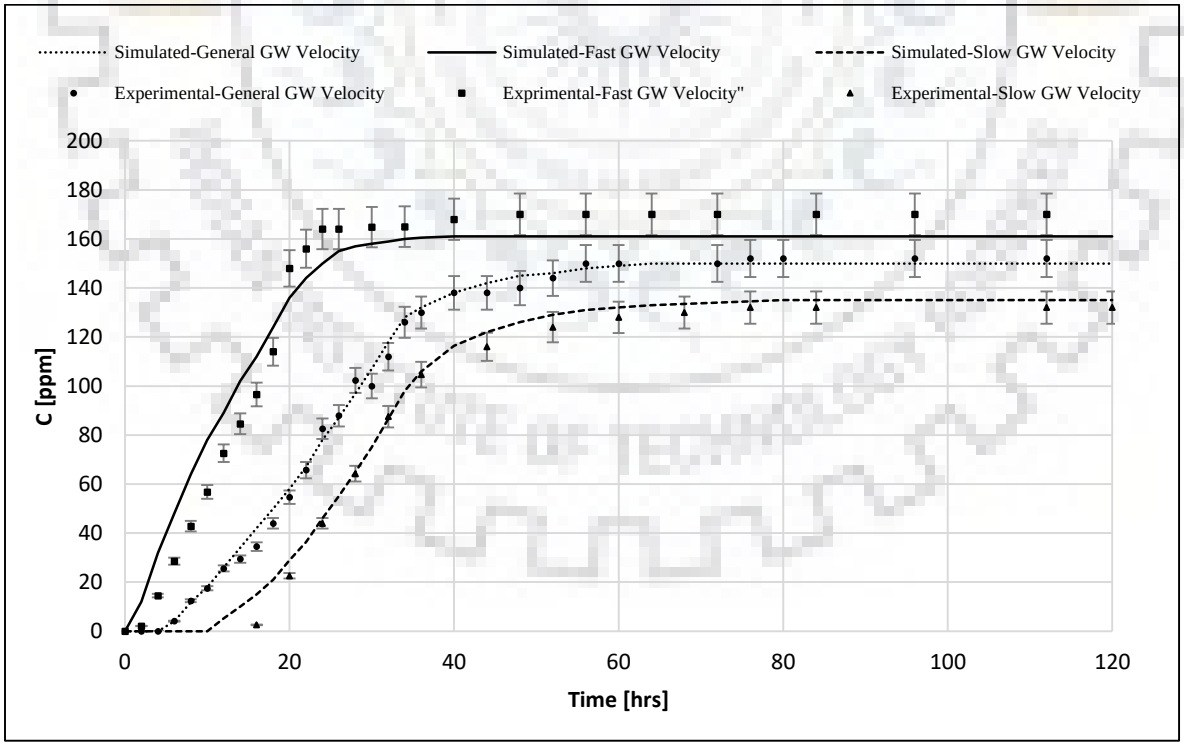

(4.26b) BTC location (cm):*X*=10; *Y*=28; *Z*=15cm

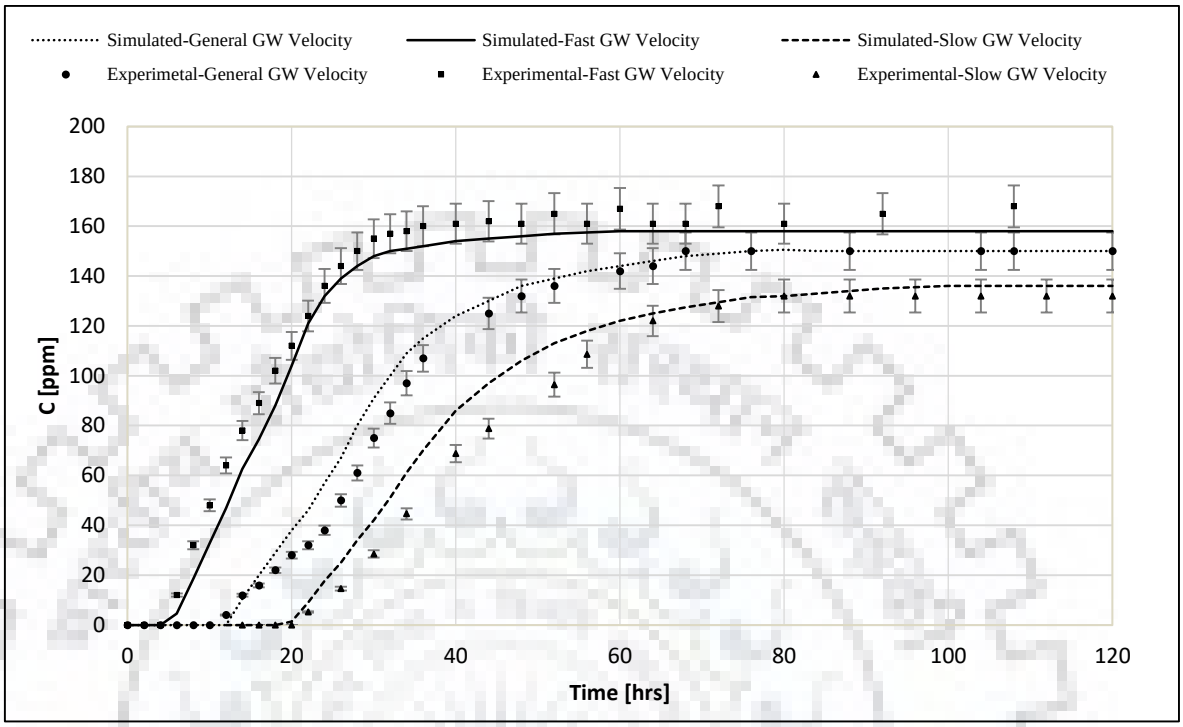

(4.26c) BTC location (cm):*X*=15; *Y*=28; *Z*=15cm

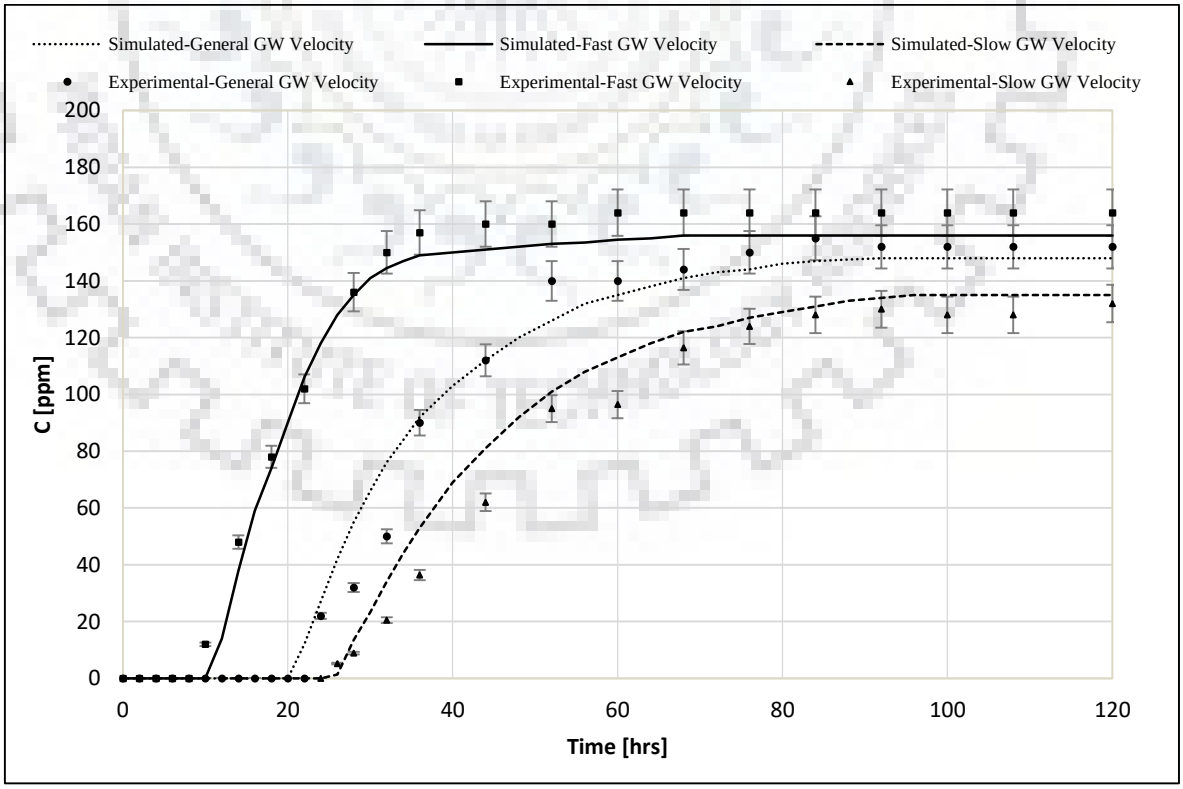

(4.26d) BTC location (cm):*X*=20; *Y*=28; *Z*=15cm

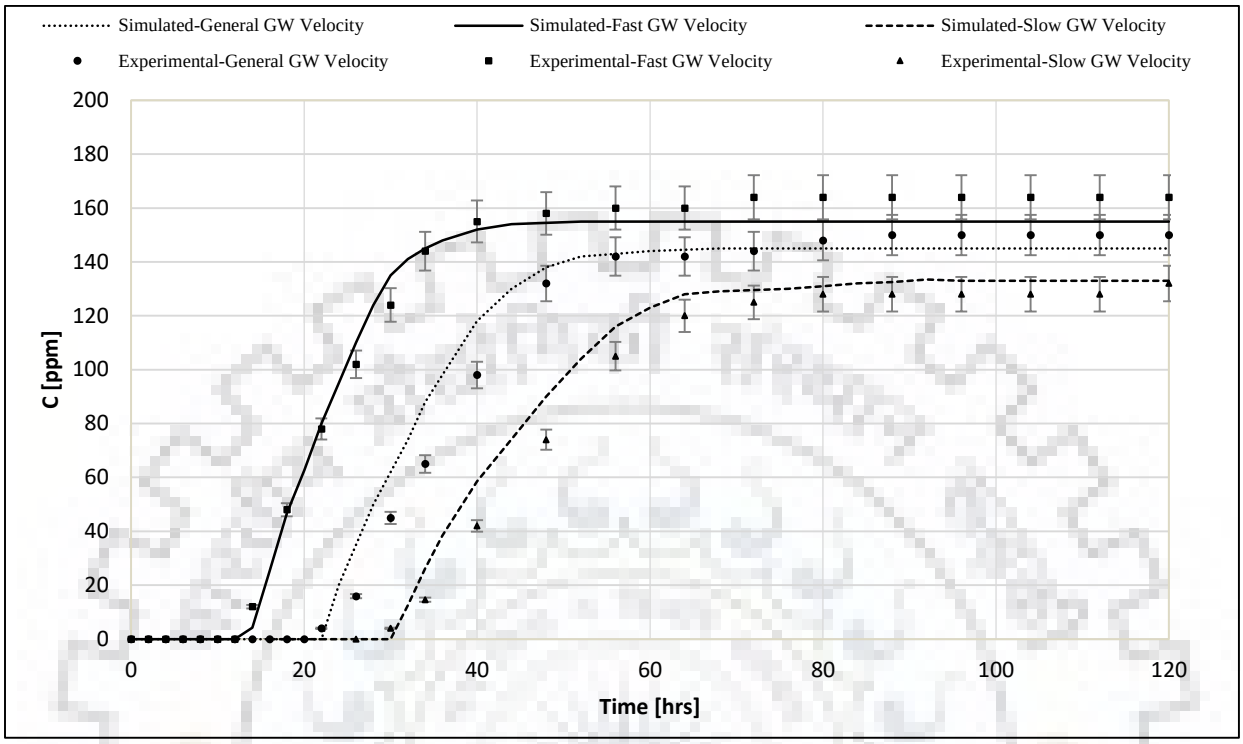

(4.26e) BTC location (cm):*X*=25; *Y*=28; *Z*=15cm

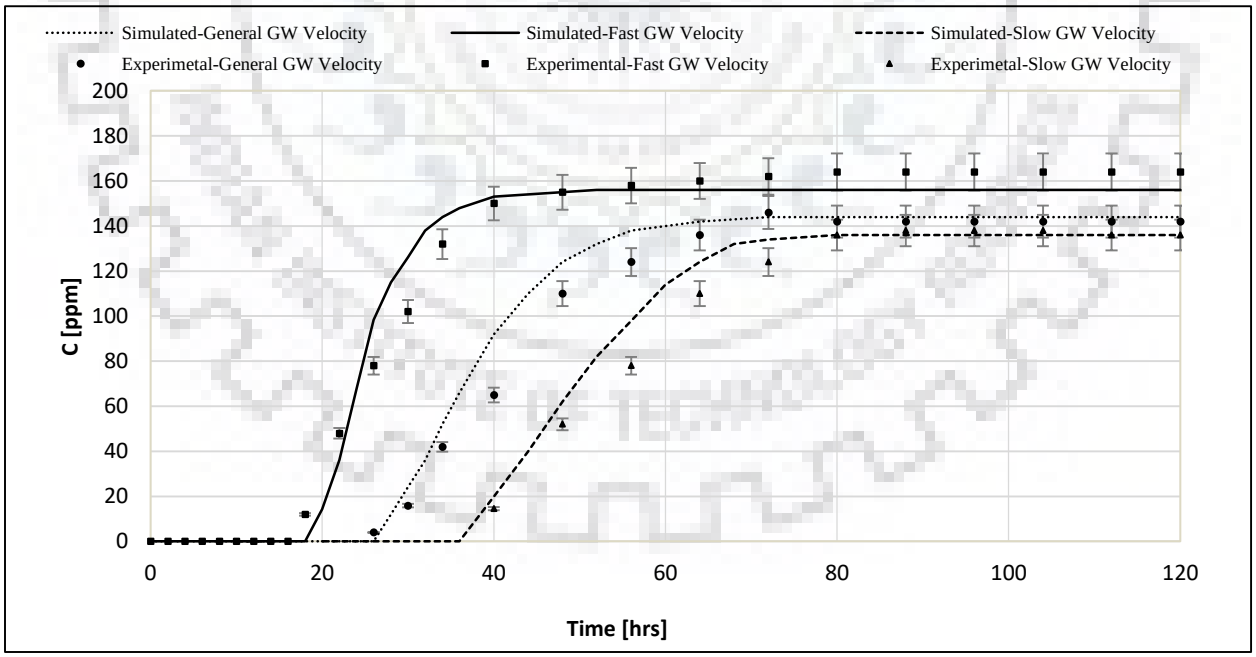

Figure 4.26: The concentration of dissolved LNAPL with time at different down gradient points from LNAPL pool under fast, base and slow groundwater velocities.

Slow groundwater velocity Base groundwater velocity Fast groundwater velocity

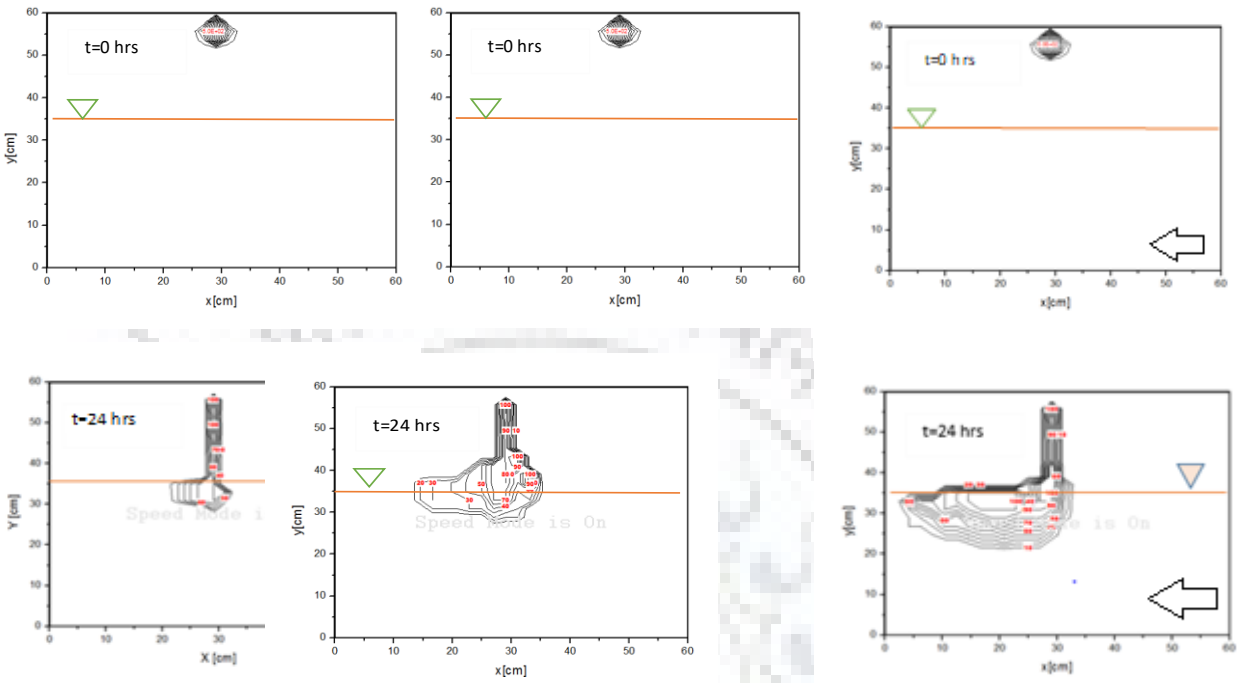

Figure 4.27: The observed concentration isolines of the LNAPL in tank setup under three different groundwater velocities. Soil water samples were analyzed for the saturated zone and soil vapor concentration was converted to water concentration using Henry's coefficient for unsaturated zone.

The dissolved LNAPL concentration as a function of space is plotted in figure 4.27 using concentration isolines. Purpose of the concentration isolines was to analyse spreading patterns of LNAPL in all directions with time. The concentration isolines clearly show the rapid transport of dissolved plume in horizontal direction than its transverse movement under the selected groundwater flow conditions. The horizontal spreading of plume was due to advection dominated flow of the dissolved toluene originating from large contact area between LNAPL pool and water. Dissolved LNAPL plume movement in opposite direction of groundwater flow driven by diffusive flux was comparative very slow. Whereas, the expansion of dissolved LNAPL plume in the vertical direction with an increase in velocity shows the crucial role of dispersive flux. A flushing impact of

groundwater flow in the horizontal direction is illustrated by the closely spaced isolines present in opposite to the flow direction and elongated isolines in down gradient side. Thus, the advective transport play important role than the molecular diffusion under changing groundwater flow regimes having high hydraulic gradient. The marginal expansion of plume in opposite to the flow direction clearly shows the flushing impact (Fagerlund et al. 2008) resulting under fast groundwater velocity. Whereas, the diffusive flux of the dissolved LNAPL can play a crucial role in LNAPL movement under slow groundwater flow regimes. Estimation of corresponding biodegradation rate at different locations during transport experiment can help in designing effective bioremediation techniques in real field conditions.

4.7 Simulation-Optimization Approach for Characteristic Polluted Site

In this section, the results and discussions on simulation and optimization approach are presented for a bioremediation system design for a characteristic polluted site. The designed system was targeted to remediate toluene polluted vadose zone having different soil moisture and temperature conditions along with the polluted saturated zone. For saturated zone treatment, three injection wells were used to provide additional oxygen to polluted saturated zone while one extraction well is to extract groundwater to control LNAPL plume movement and to recharge polluted vadose zone.

The enhanced biodegradation rate of the saturated zone in Figure 4.28 (15 -30 m) with three injections and one extraction well was separately simulated using BIOPLUME III. Concentration isolines of toluene for saturated zone simulated using BIOPLUME III is presented in figure 4.28. The initial concentration of toluene was kept 50 ppm (Figure 4.28a) while the background oxygen concentration was taken as 5 ppm. The supply level of oxygen through injection wells was 8 ppm. The maximum residual concentration of LNAPL in the treatment zone was found 6.6 ppm after three years of remediation period (Figure 4.28b). The biodegradation rate was found to be 0.039 mg-L/day. The biodegradation in the saturated zone is a complex phenomenon and is governed by both aerobic and anaerobic microbes. However, in this study, we have assumed that the aerobic

biodegradation was dominant as the oxygen was supplied from the initial stage till the end of the remediation period. Further, it was also assumed that the rate of biodegradation will be controlled by distribution and availability of electron acceptors (i.e. oxygen) and other factors like temperature, pH and population of microbes will not limit the amount of biodegradation.

The surrogate model based simulation-optimization approach (ELM-PSO) was used to solve a single-objective optimization problem to design an efficient and accurate in-situ bioremediation system for the toluene polluted site. Eight surrogate models were developed for simulation of biodegradation at different soil moisture levels (80, 40, 60 and 20% of saturation level) and temperature (30°C and 10°C) combinations. Further, these trained and tested surrogate models were coupled with PSO to obtain the best feasible remediation strategy with minimum cost. The optimum remediation cost obtained from this approach is listed in table 4.12 for respective combination of soil-moisture level and temperature.

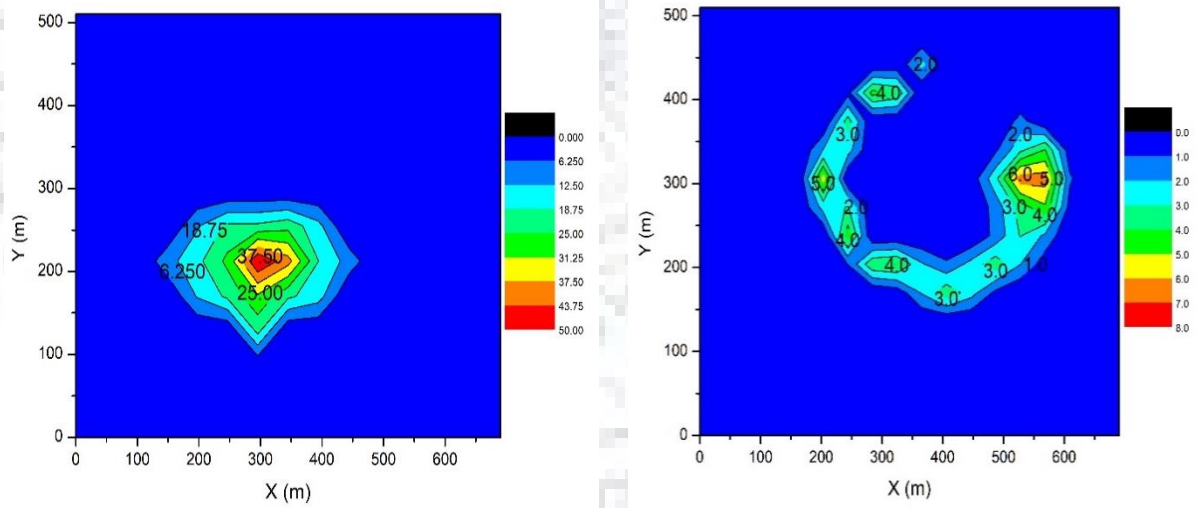

(a) Initially (b) After 3 year

Figure 4.28: LNAPL concentration isolines in saturated zone simulated by BIOPLUME III.

Table 4.12: Comparison of remediation cost for different soil moisture content and temperature conditions.

Soil Moisture Contents	30±2°C		10±0.5°C	
	Remediation Time	Remediation Cost	Remediation Time	Remediation Cost
$0.8\theta_s$	1 year	$ 106570	1 year 6 months	$ 126162
$0.6\theta_s$	1 year	$ 107245	2 years	$ 133755
$0.4\theta_s$	1 year 3 months	$ 120306	3 years	$ 159982
$0.2\theta_s$	1 year 6 months	$ 126905	3 years	$ 161021

Table 4.12 presents the comparison of remediation cost for different soil moisture contents and soil temperature conditions. Further, figure 4.29 shows the optimized pumping rates for three injections and one extraction wells and the remediation system cost at 30°C temperature with soil moisture varying from 80 to 20% of θ_s. It is evident from the figure 4.29 that the minimum cost of $106,570 and $107,245 was achieved when the soil moisture was 80% and 60% of θ_s, respectively. At these soil moisture contents, the designed bioremediation system was able to achieve the clean-up standard of 5ppm in 1 year of remediation period. However, for the lower soil moisture content of 40% and 20%, the remediation period was extended to 1 year 3 months and 1 year 6 months, respectively. The effect of longer remediation period could also be seen on the optimized bioremediation system cost which is $120,306 and $126,905 for $0.4\theta_s$ and $0.2\theta_s$ moisture content, respectively. Similarly, figure 4.30 shows the optimized pumping rates and the remediation cost at 10°C temperature with moisture content varying from 0.8 to $0.2\theta_s$. The remediation costs were $126,162 and $133,755 for 0.8 and $0.6\theta_s$ moisture content in remediation period 1 year 6 months and 2 years, respectively. However, the costs for 0.4 and $0.2\theta_s$ moisture content in 3 years of remediation period were simulated as $159,982 and $161,012. The extension of remediation period for low moisture and the low temperature

combinations was expected as the biodegradation rate for these site conditions was low and the remediation system would require more time to achieve the clean-up level.

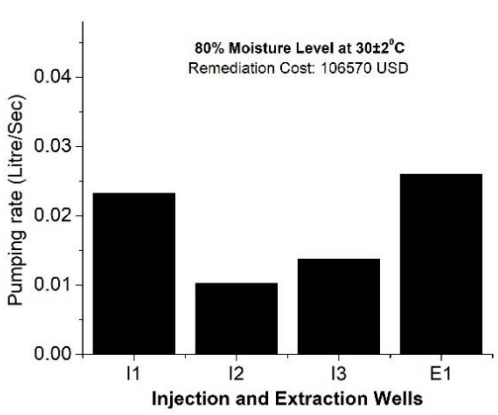

(a) 80% at 30°C

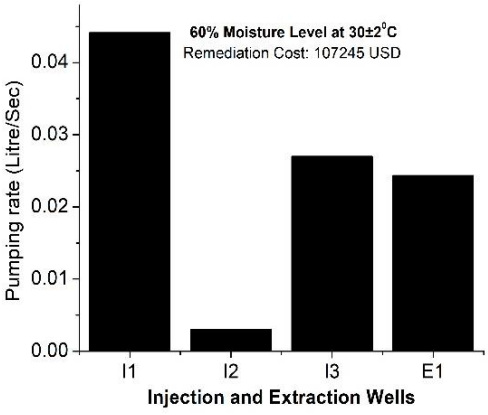

(b) 60% at 30°C

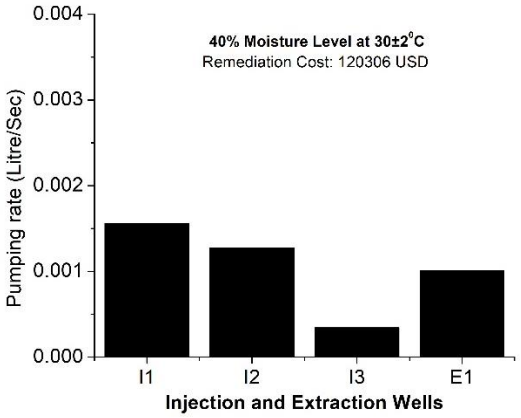

(a) 40% at 30°C

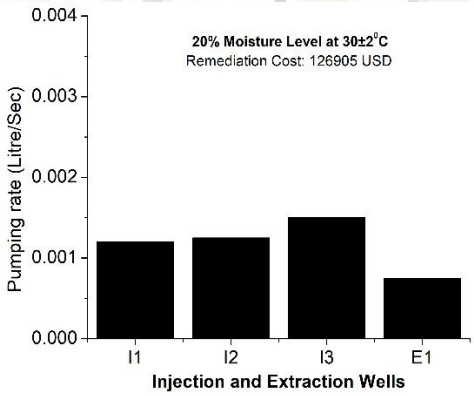

(b) 20% at 30°C

Figure 4.29: Optimized pumping patterns of the three injection and one extraction wells for minimum cost to designed biodegradation system.

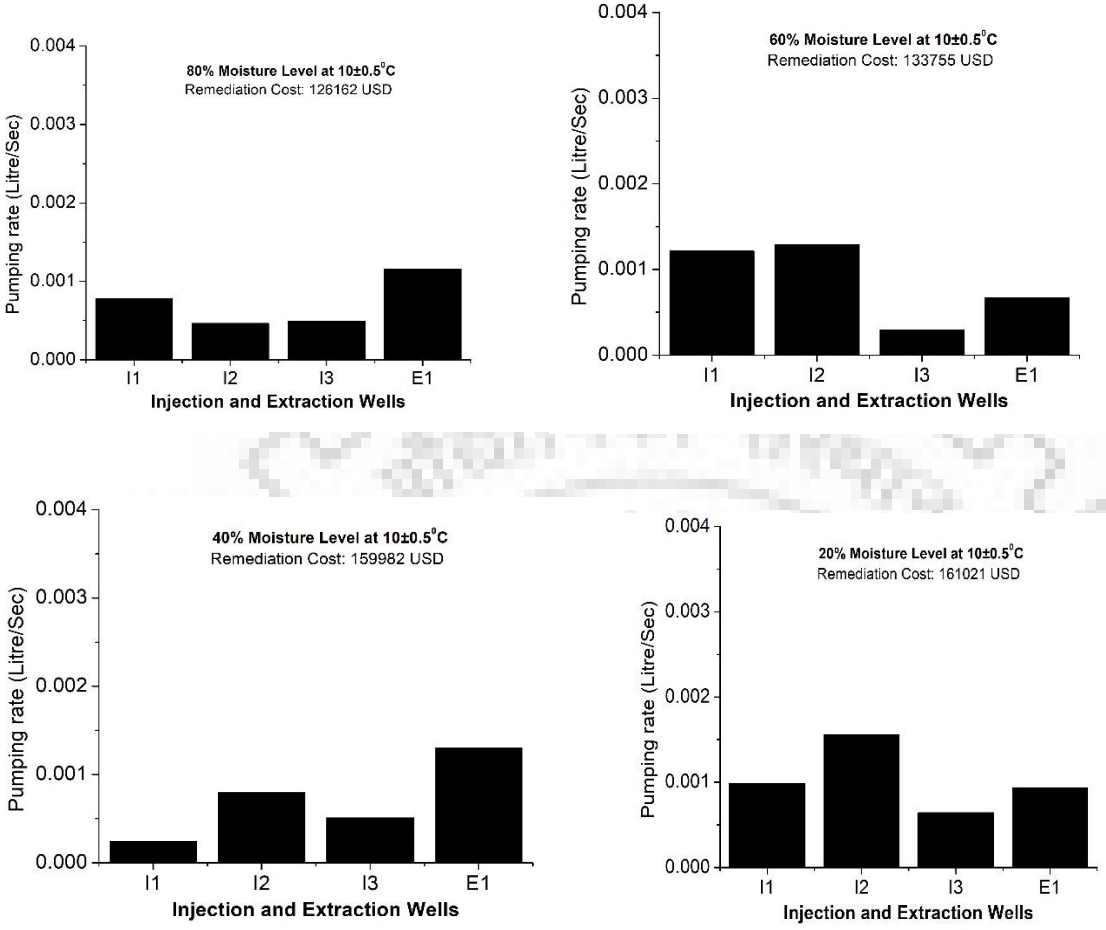

(a) 40% at 30°C (b) 20% at 30°C

Figure 4.30: Optimized pumping patterns of the three injection and one extraction wells for minimum cost to designed biodegradation system.

After obtaining the optimized pumping rates for all the soil moisture-temperature combinations, these pumping rates were validated using HYDRUS 3D model. Figures 4.31-4.34 illustrate the residual contaminant concentration in polluted zones after applying the optimal in situ bioremediation design at 30°C. In case of 80% and 60% moisture content, the clean-up level of 5 ppm was achieved using the optimized pumping rates in one year (Figure 4.31-4.32), however, for the lower moisture content the clean-up level was obtained when the remediation period was extended up to 3 months and 6 months,

respectively (Figures 4.33-4.34). Similarly, in case of 10°C, the clean-up level in the contaminated site was achieved in 1 year 6 months and 2 years while keeping the moisture content at 80 and 60%, respectively (Figure 4.35-4.36). For the lower moisture contents of 40 and 20%, the suggested design took 3 years to degrade the LNAPL up to a pre-defined clean-up level of 5 ppm (figure 4.37- figure 4.38). In case of 30°C-80% and 30°C-60%, the obtained cost is almost same as the remediation period was 1 year, however, the residual concentration was much higher in low moisture content case ranging between 4.3 to 9 ppm (60%) in comparison to 2.9 to 4.5 ppm (80%). This clearly indicates that recharging polluted vadose zone accelerate the biodegradation rate. Similarly, in the cases of 30°C-20% and 10°C-80%, the obtained cost was nearly same pertaining to the constant remediation period. However, figure 4.35- 4.36 show that the residual concentration range was lower for high temperature-low moisture content combination (residual range- 3.9 to 8.6 ppm) than when remediation site had low temperature-high moisture conditions (residual range- 4.5 to 9.9 ppm). This analysis also suggests that for the success of in-situ bioremediation method, the temperature is comparatively a more important factor than the moisture content. Further, in case of constant low temperature (10°C) and varying low moisture content (40% and 20%), the obtained cost differs very less. Results also suggest that the low temperature-high moisture combination in contaminated site degrade the LNAPL more effectively (residual range- 3.3 to 12.5 ppm) than when low temperature-low moisture content maintained (residual range- 3.7 to 13.2 ppm). Furthermore, the concentration isolines of LNAPL in subsurface under varying soil moisture contents and temperature combination suggests that the movement of the plume is restricted if the moisture content is low in the treatment zone.

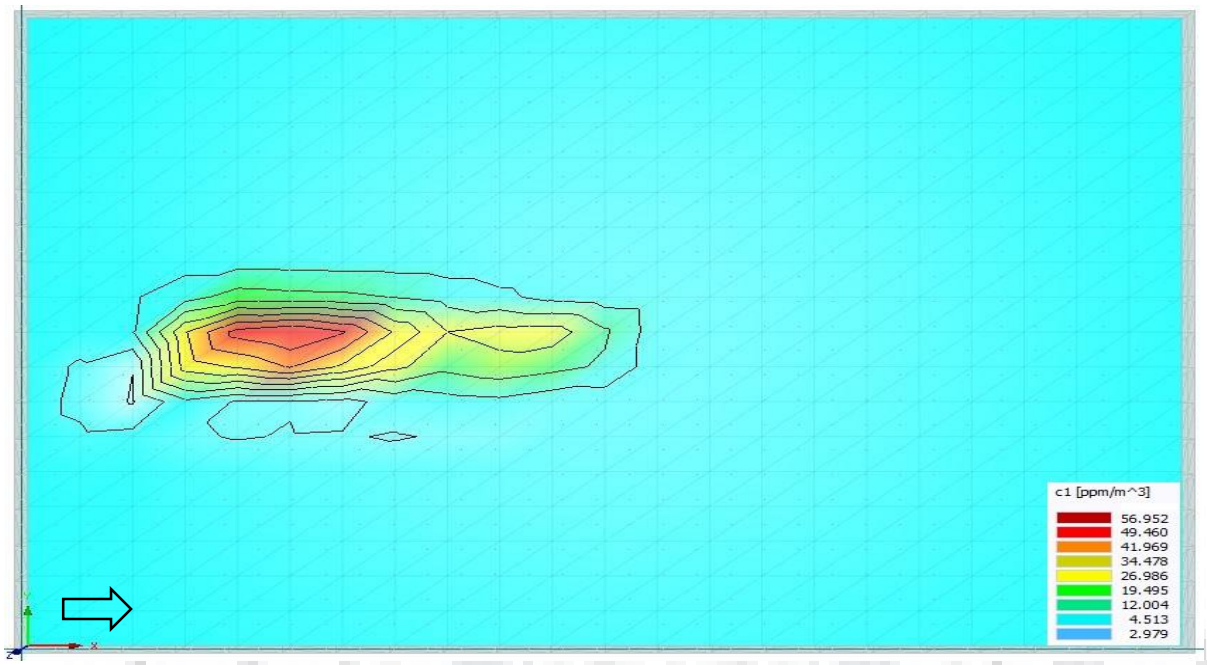

5days

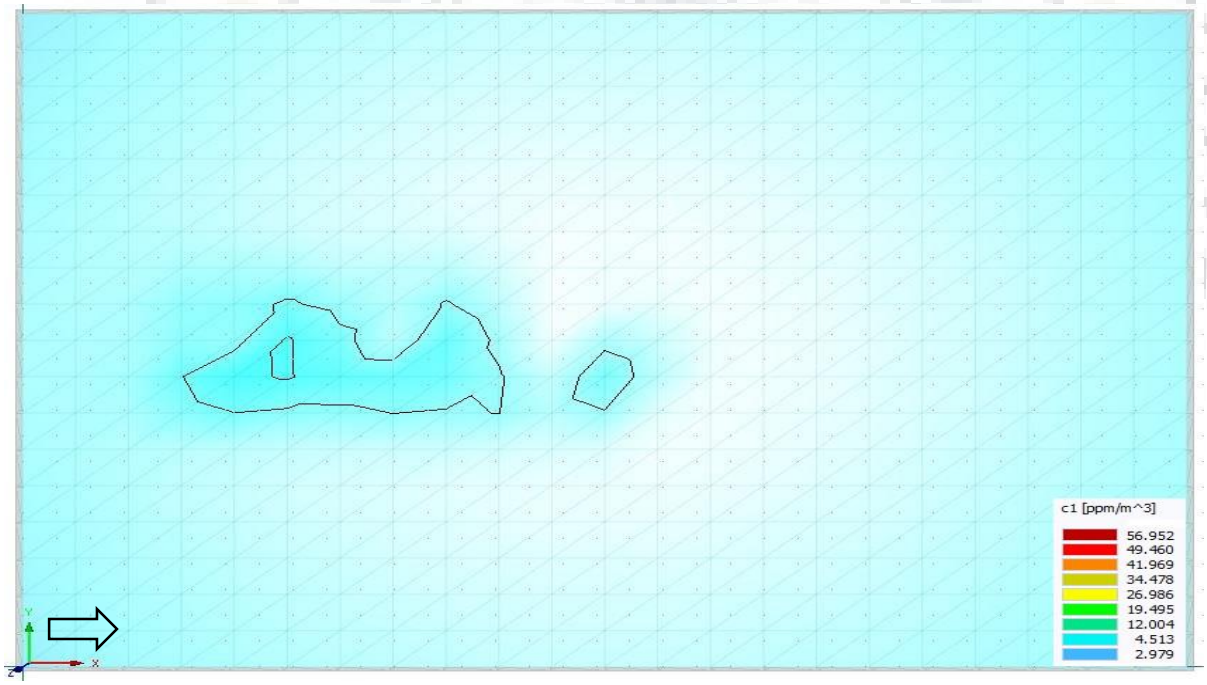

365 days

Figure 4.31: Residual concentration of LNAPL during the remediation period of 1 year with soil moisture 80% and temperature 30°C.

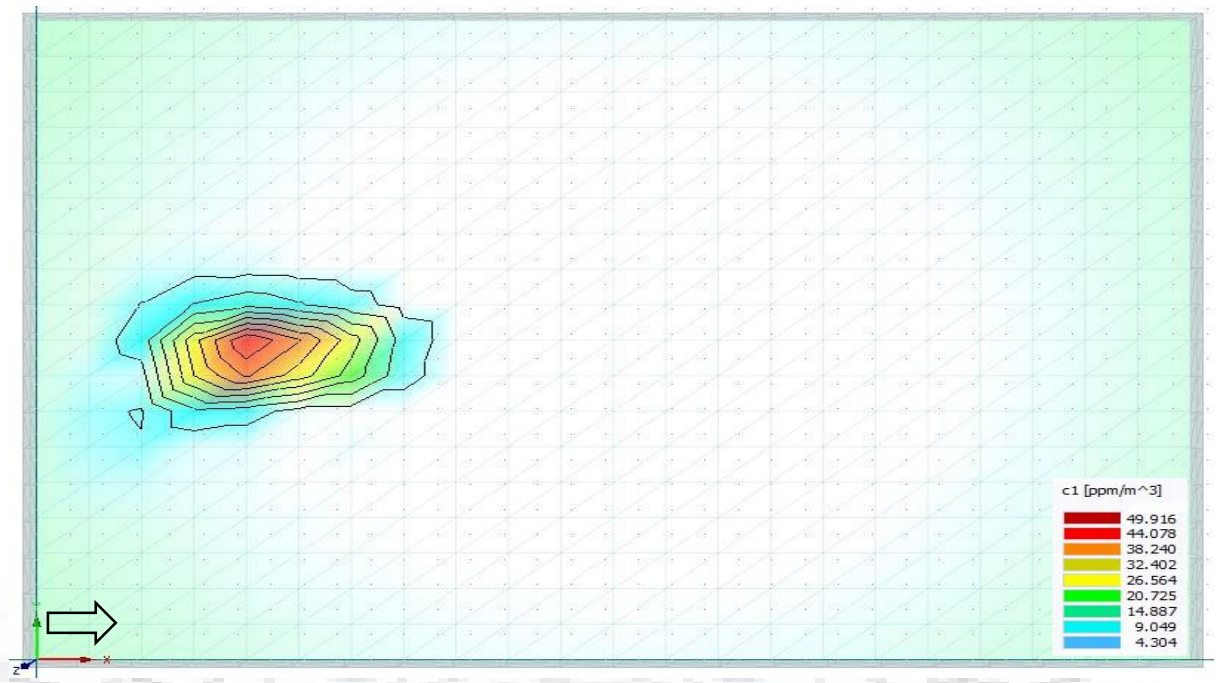

5 days

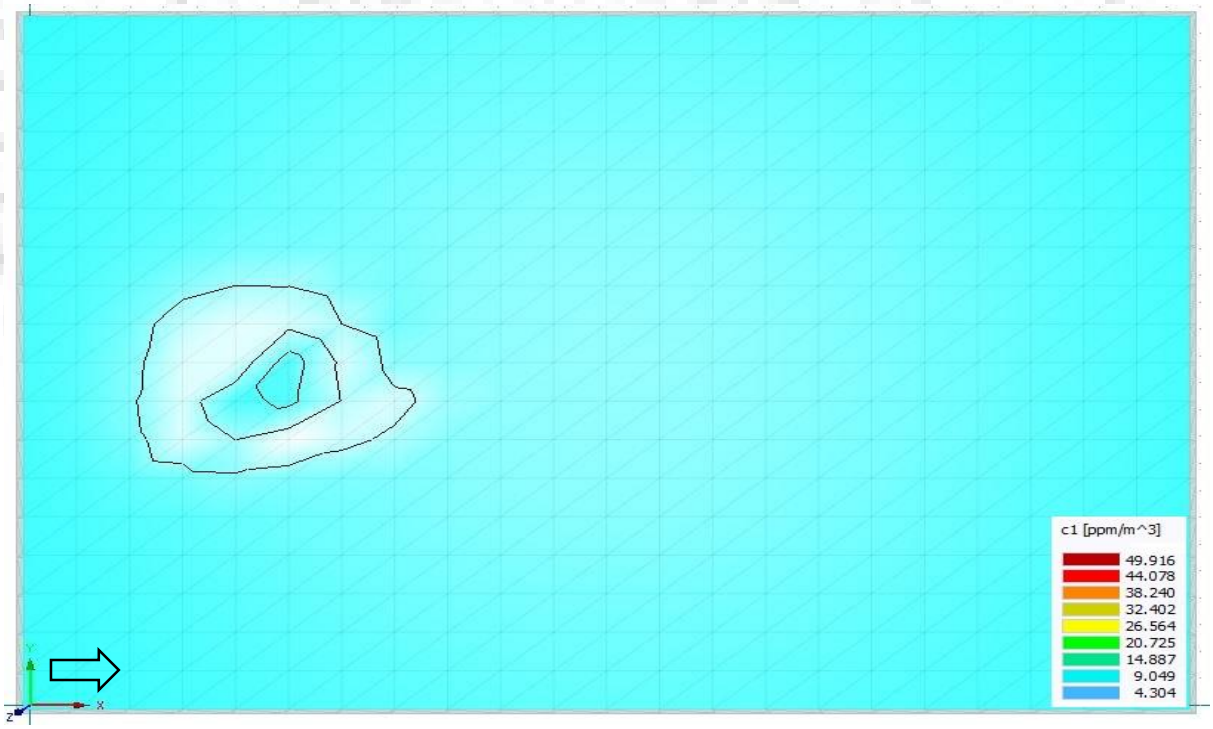

365 days

Figure 4.32: Residual concentration of LNAPL during the remediation period of 1 year with soil moisture 60% and temperature 30°C.

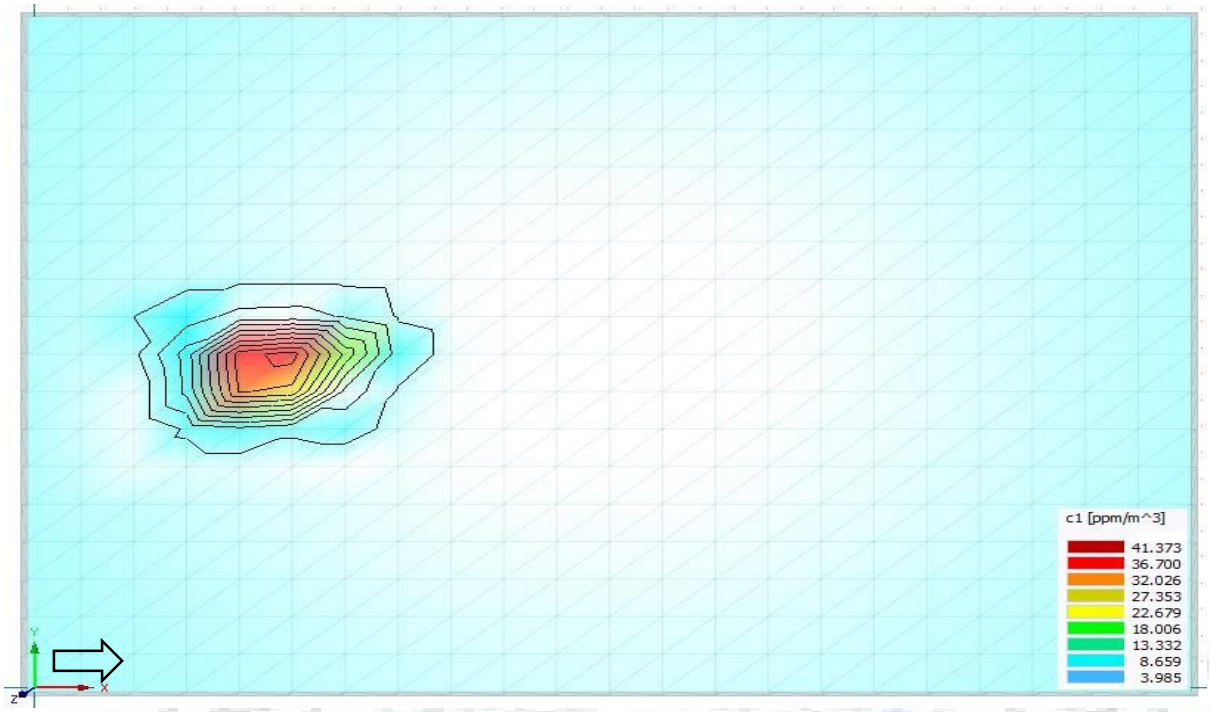

5 days

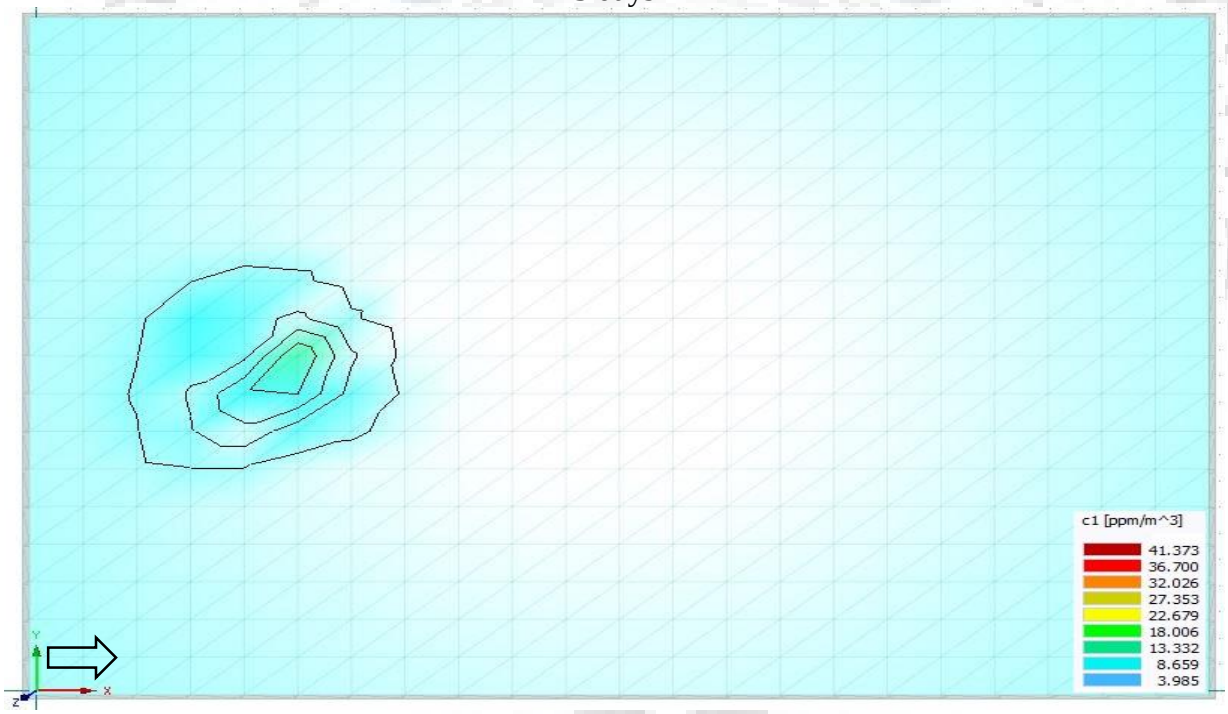

455 days

Figure 4.33: Residual concentration of LNAPL during the remediation period of 1 year 3 months with soil moisture 40% and temperature 30°C.

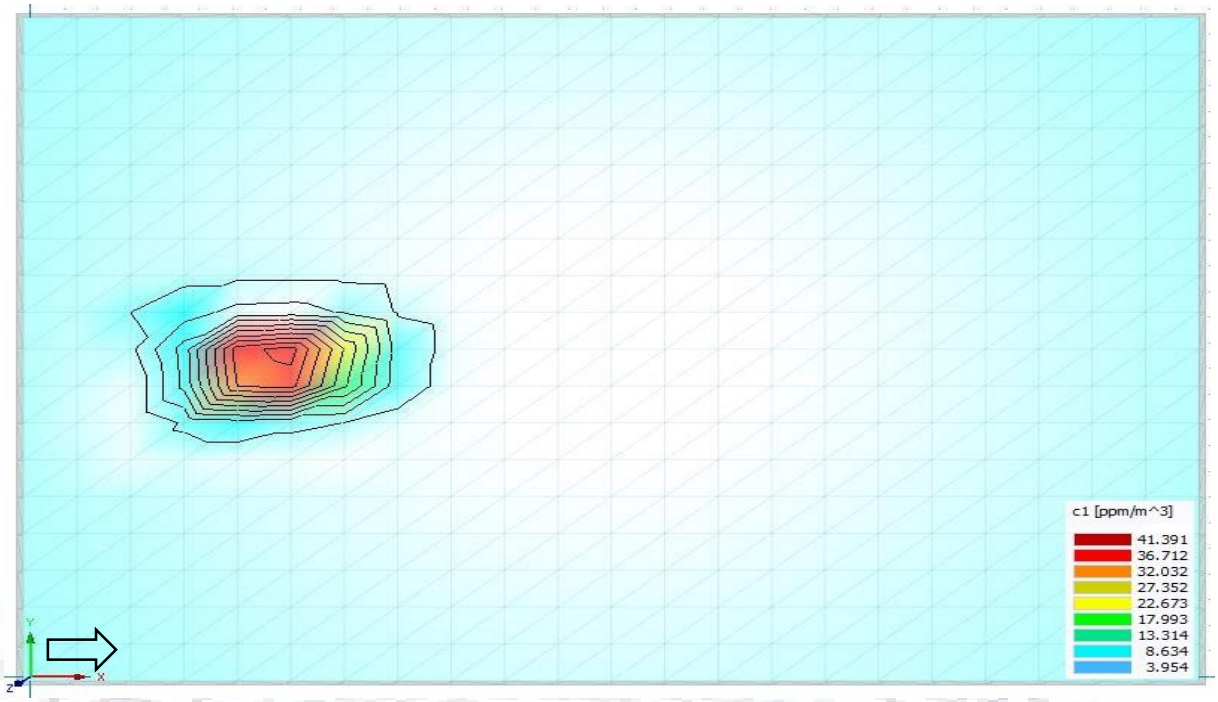

5 days

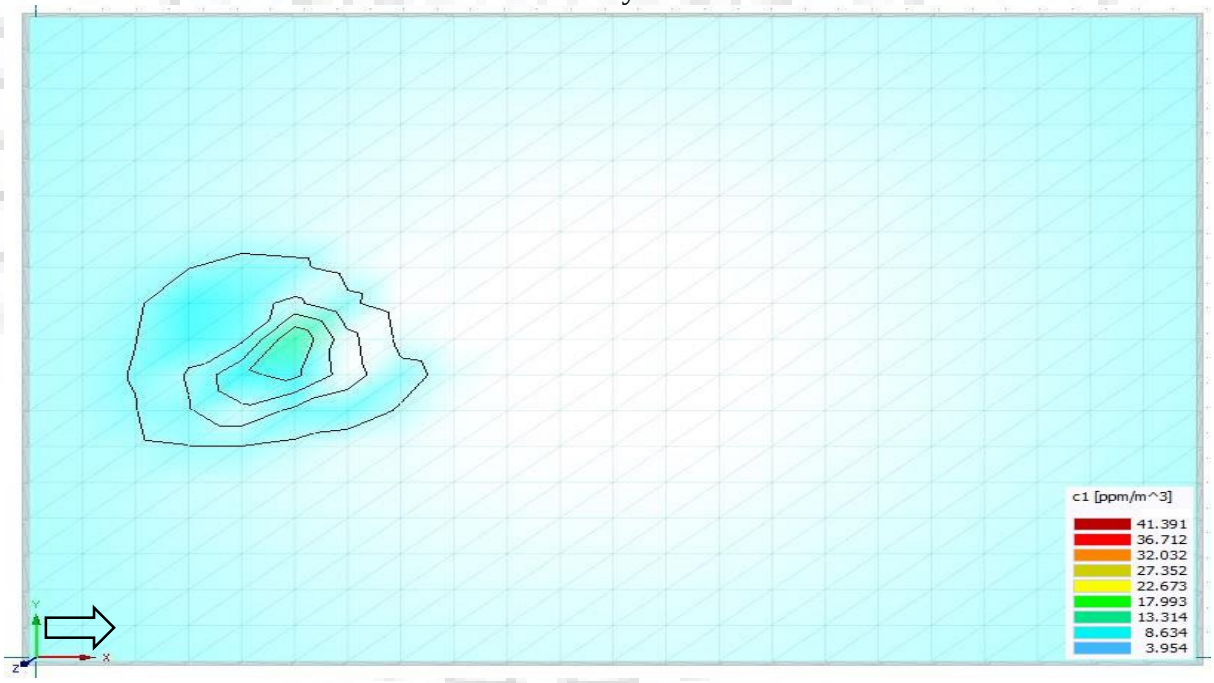

545 days

Figure 4.34: Residual concentration of LNAPL during the remediation period of 1 year 6 months with soil moisture 20% and temperature 30°C.

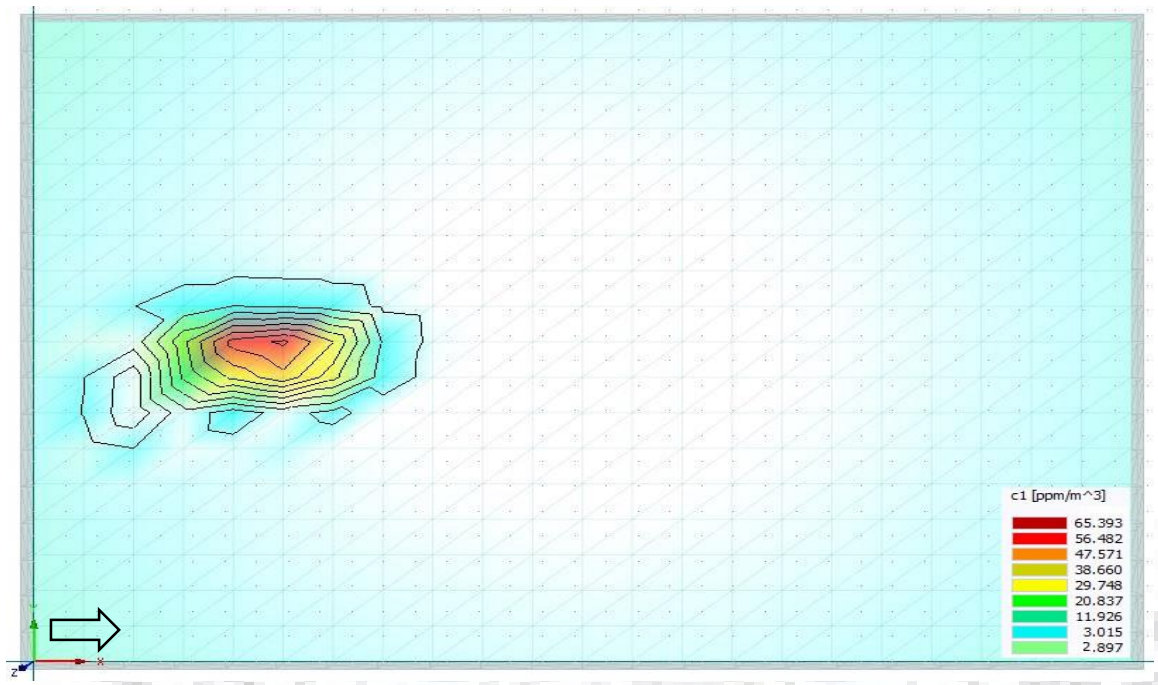

5 days

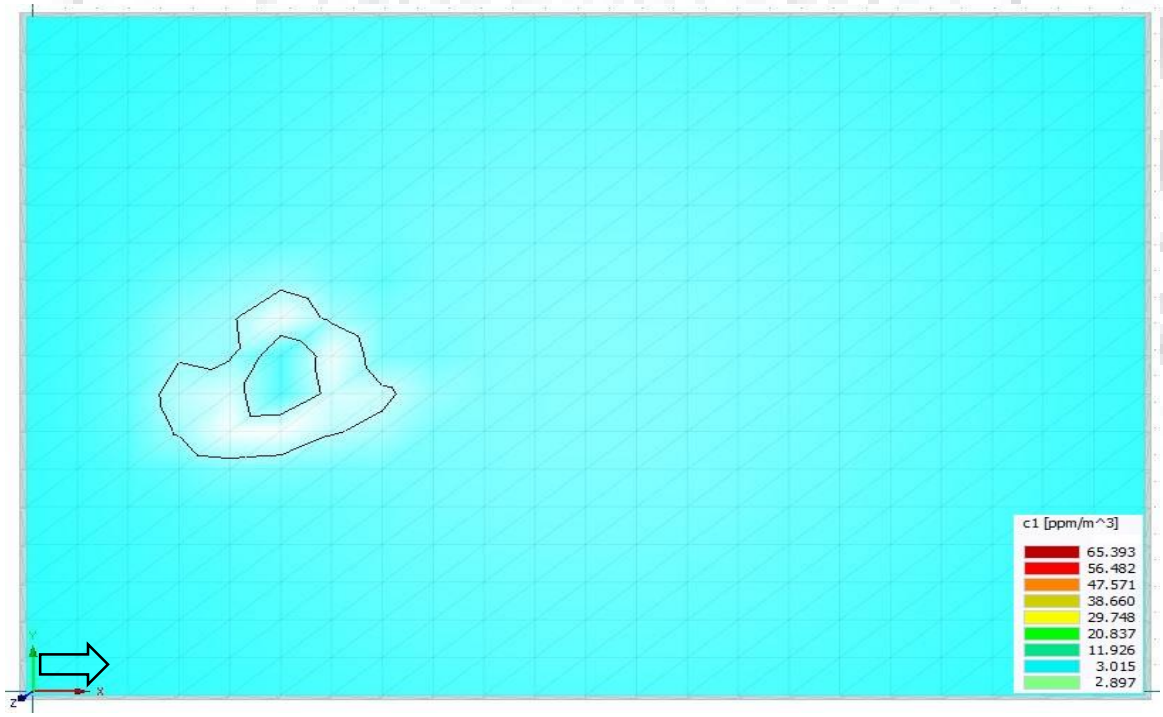

545 days

Figure 4.35: Residual concentration of LNAPL during the remediation period of 1 year 6 months with soil moisture 80% and temperature 10°C.

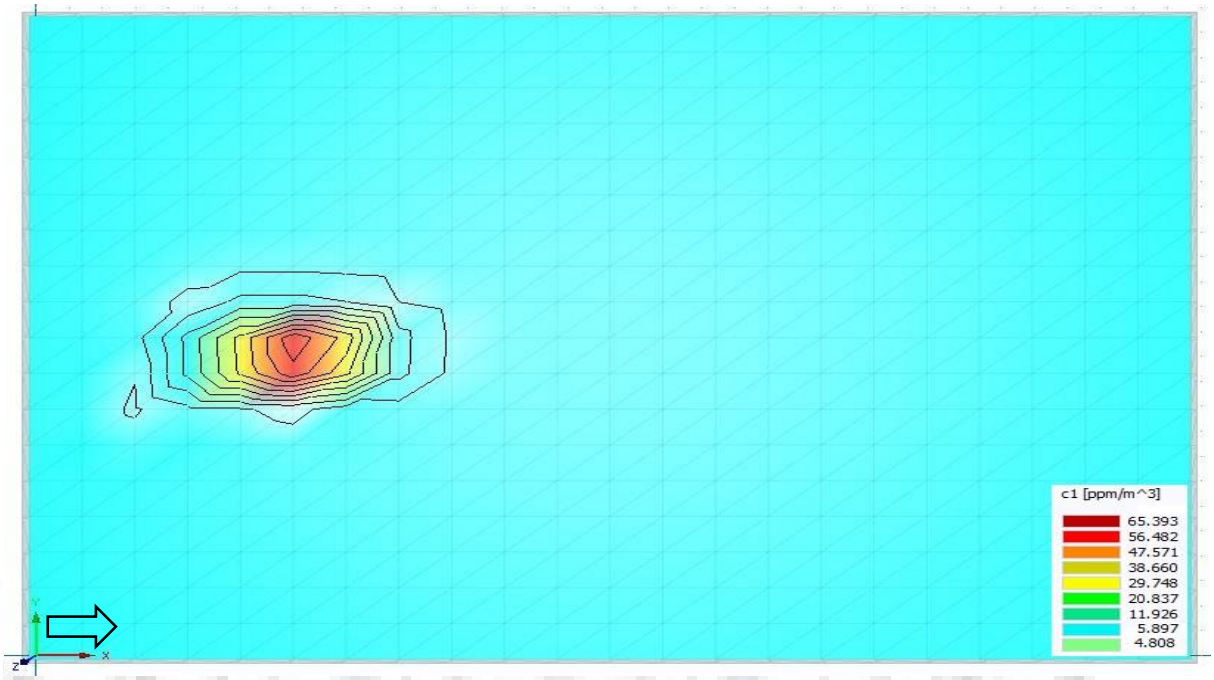

5 days

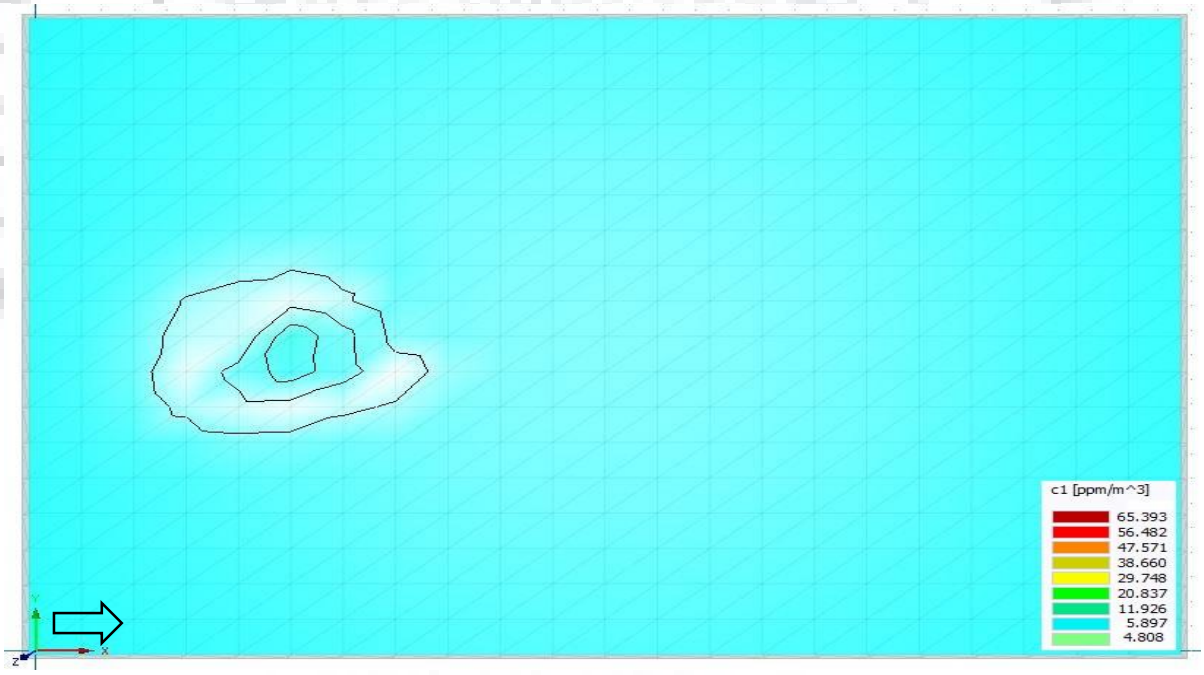

730 days

Figure 4.36: Residual concentration of LNAPL during the remediation period of 2 years with soil moisture 60% and temperature 10°C.

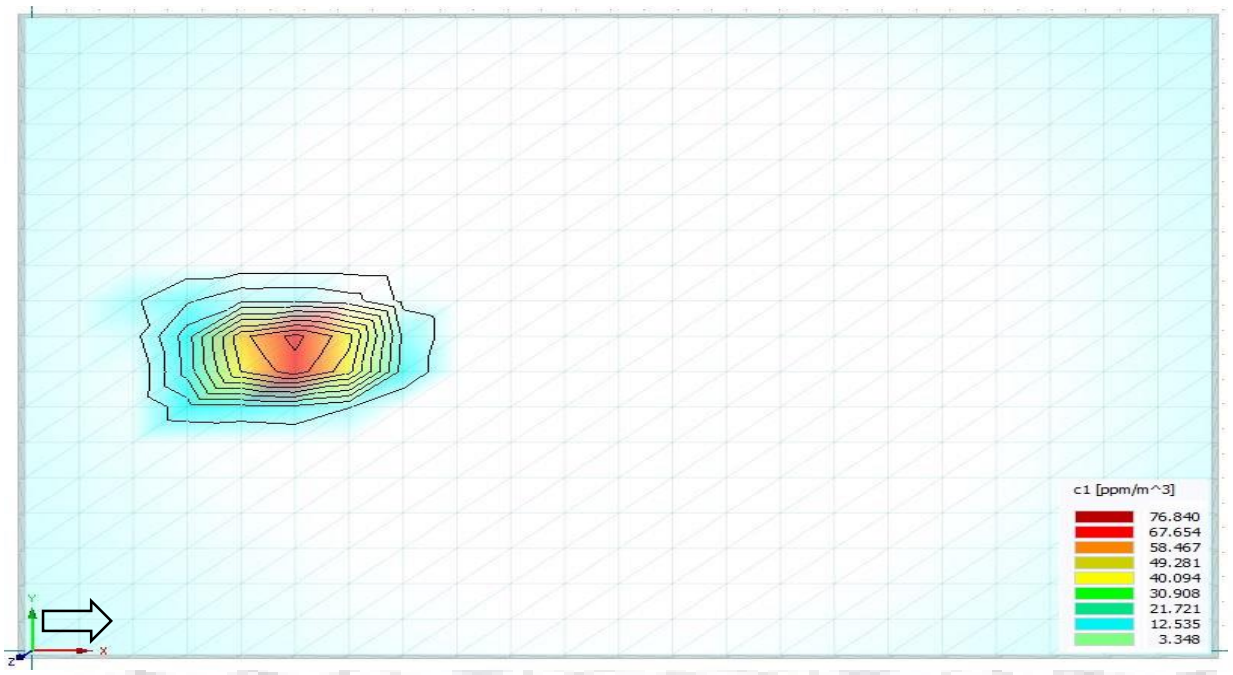

5 days

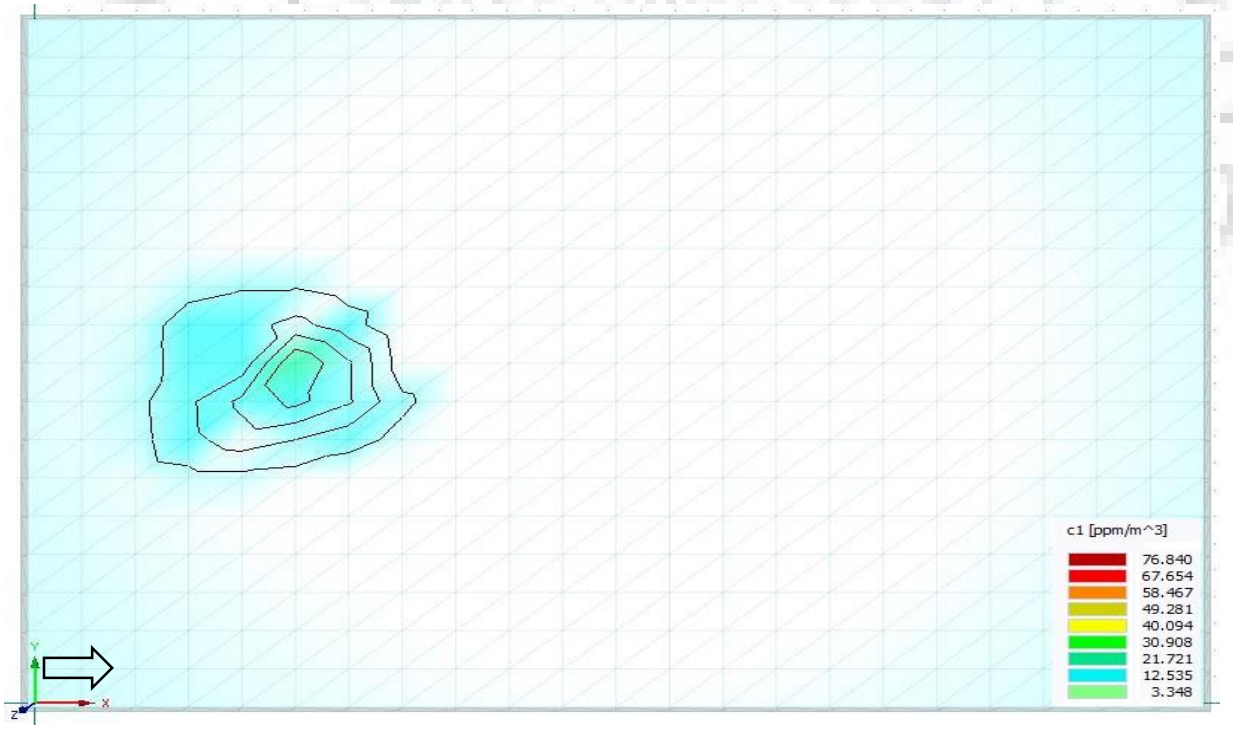

1095 days

Figure 4.37: Residual concentration of LNAPL during the remediation period of 3 years with soil moisture 40% and temperature 10°C.

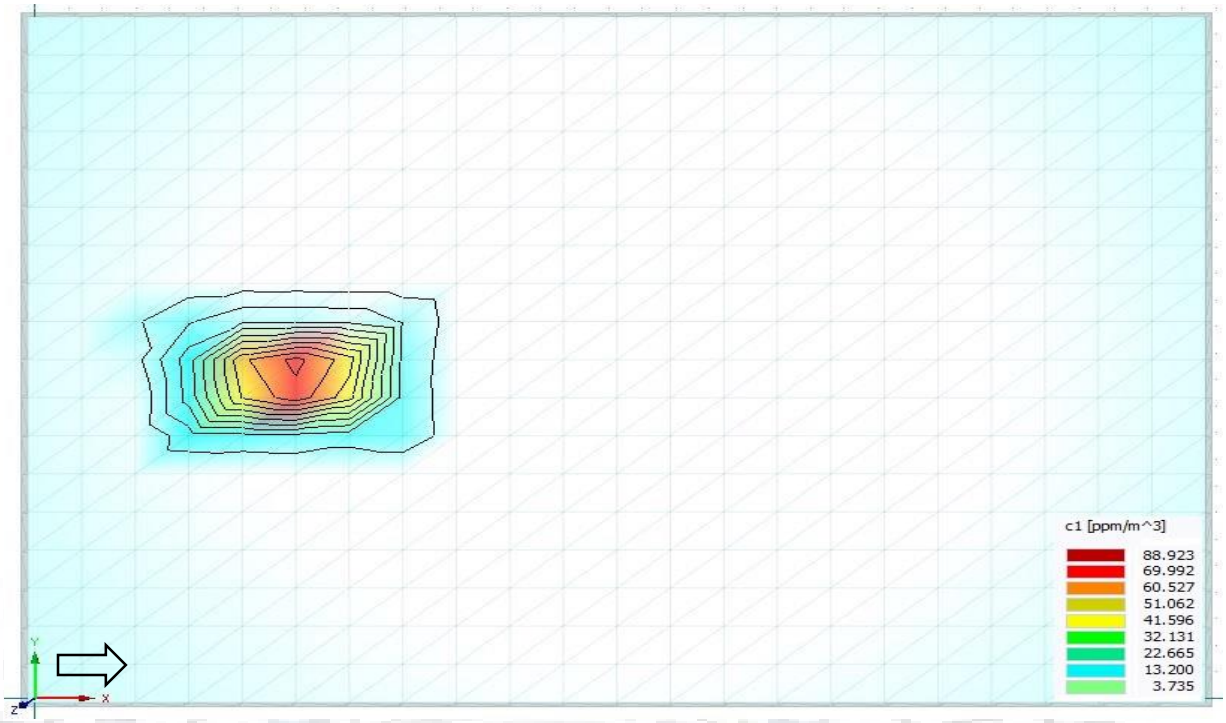

5 days

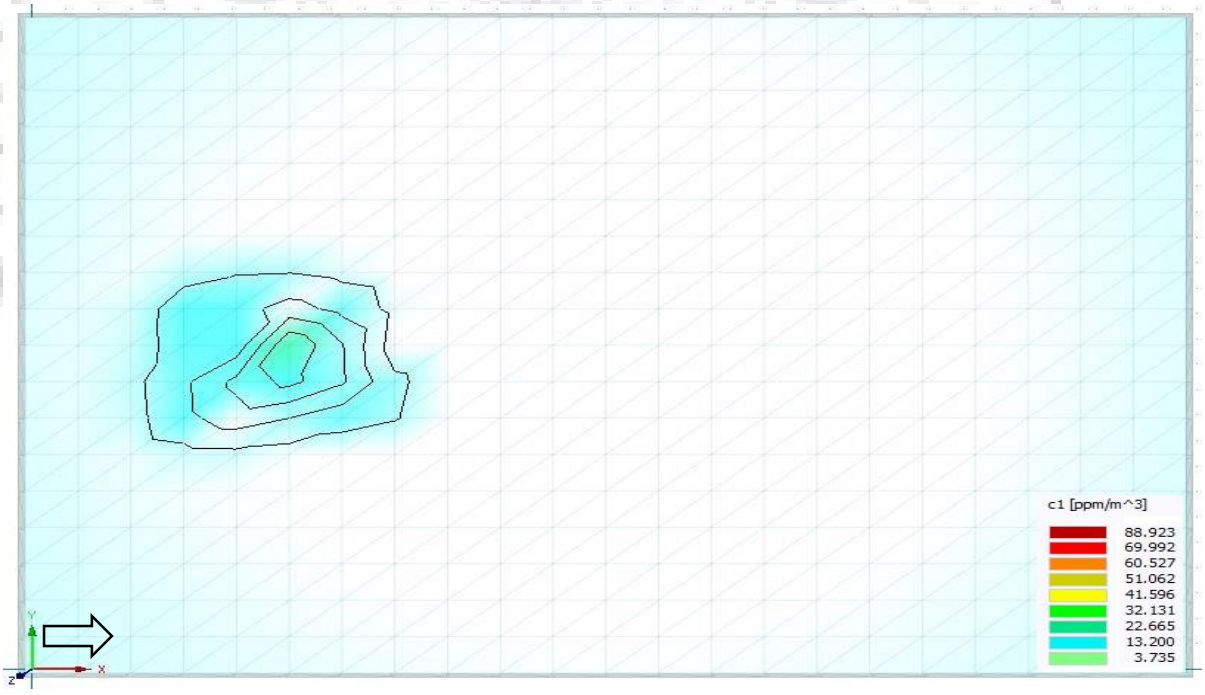

1095 days

Figure 4.38: Residual concentration of LNAPL during the remediation period of 3 years with soil moisture 20% and temperature 10°C.

Chapter 5

Conclusion

The main focus of this Ph.D. research was to investigate the impact of different subsurface factors on fate and transport of LNAPL pollutants. The entire work was conducted in three major steps: i) microcosms and column experiments for investigating impacts of substrate concentration, soil moisture content, temperature, and plant on biodegradation of toluene, a selected representative of LNAPL, ii) two and three dimensional sand tank experiments to analyse the impact of groundwater table dynamics and varying flow regimes on movement of LNAPL in variably saturated zone, iii) simulation-optimization for bioremediation design to decontaminate a characteristic site. A series of microcosms experiments were conducted first to see the impact of initial substrate concentrations on biodegradation of toluene. Results show that LNAPL degradation increases with increasing initial dissolved LNAPL concentration up to about 50 ppm and remain maximum till about 100 ppm before started decreasing with increment in the substrate concentration. A reduced degradation rate of toluene in microcosms having high LNAPL concentration causes toxicity to microbes while very low LNAPL concentration seems due to insufficient carbon source to toluene degraders. A negligible time of acclimatization was observed in all microcosms conducted at fairly high temperature of 28±2ºC. The results of this experiments are helpful in predicting the biodegradation kinetics for different levels of the LNAPL concentration at a polluted site. These results are also useful in designing and selection of suitable concentration zones for the supply of microbes seeding /nutrients/oxygen at a polluted site.

Earlier studies are limited to investigate the impact of individual factors like soil moisture and temperature on LNAPL degradation in subsurface. The combined role of soil moisture and soil temperature conditions on biodegradation of dissolved toluene was thus investigated here using a series of microcosms experiments. It was observed that the biodegradation rate in microcosms having high moisture contents i.e. 60-80% at 30°C was faster than the microcosms having low moisture (40-20%) contents at the same soil temperature level. It was found that temperature of soil-water system is more sensitive to temperature at high moisture content as compared to dry conditions in this experiment. By

keeping the temperature as constant environmental condition, the rate of degradation increases linearly with increment in soil moisture content. However, a nonlinear change in degradation rate was observed by varying the temperature at constant soil moisture level. This results will help to maintain the favourable conditions to enhance the microbial growth at a polluted site.

Impact of groundwater temperature on LNAPL fate and transport is also investigated in a continuous system of column setup. Results show a high dissolution rate of LNAPL at elevated temperature of 28^0C-36^0C resulting in a dissolved LNAPL concentration of about 150 ppm. The biodegradation rates of LNAPL were 0.002, 0.008, 0.012 and 0.015 mg-L/hour at groundwater temperature 4^0C, 20^0C, 28^0C and 36^0C, respectively. This indicates that higher temperature enhanced the biodegradation rate of the LNAPL in subsurface. At this groundwater temperature, a significant increment of microbial actions accelerates the biodegradation rate of LNAPL in subsurface system. Similarly, the role of plant on bioremediation of LNAPL was investigated using a column setup integrated with small scale treatment wetland planted with and without Canna plant. Further, experimental data set of different CWs experiment conducted at IHE Delft were collected and analysed to see the role of *Phragmites australis in* VF and HFF CWs along with impact of nutrient on degradation of LNAPL compounds. The results show that plant play a symbiosis role in removal of LNAPL compounds from polluted root zone. This study confirms plant can treat LNAPL polluted root zone water effectively, where a longer term operation of such units is important to ascertain for the role and benefits of the plants in such systems. The duplex-CW systems offer the advantage of obtaining the highest performance levels for the CW technology with a great reduction in size and land requirement. The laboratory and numerical results show that CWs are highly effective for the removal of hydrocarbons from root zone. The study also shows that availability of different nutrients helps to enhance the treatment process. In order to improve the polluted (ground)-water quality, installation of CWs at the sources zone or pollutant discharge point is strongly recommended.

There is a paucity of knowledge on the impact of dynamic groundwater table conditions and varying groundwater flow regimes on LNAPL behaviors in subsurface. For a better understanding of behaviour of pure phase LNAPL and it dissolved plume under dynamic groundwater table and varying subsurface flow conditions is needed. A series of two

dimensional sand tank experiments was performed to investigate movement of LNAPL under stable and fluctuating groundwater table conditions. Tracer transport experiments were performed to determine the solute transport parameters under rapid, general, slow and stable groundwater table cases. Results show that a large LNAPL pool area was developed under rapid fluctuating groundwater condition which significantly enhance dissolution rate and contributes a high concentration of dissolved LNAPL to downgradient ports. A high biodegradation rate was observed in plume regions having concentration ranges from 140-160 ppm, while it became less in plume regions having low concentration of toluene. A low biodegradation rate was observed in deep layer under stable groundwater condition due to low LNAPL concentration and limited oxygen level. Microbial growth was found to be increasing as plume moves away from the LNAPL pool, which fortifies detrimental impact of toluene on survival of indigenous microorganisms near the LNAPL pool.

To see the impact of groundwater flow regime on LNAPL behaviour in subsurface a 3-D tank se was fabricated. The BTCs show that the arrival times of dissolved plume at down-gradient locations is least for the case of fast groundwater velocity followed by the base and slow groundwater velocity cases. A rapid movement of the dissolved phase LNAPL in horizontal i.e. central line of groundwater flow directions under fast groundwater velocity indicates that the advective-dispersive transport plays a dominating role in LNAPL transport mechanism as compared to the diffusive flux. Toluene concentration starts rising after few hours and increases rapidly and then starts attenuating before reaching to a concentration of 150-160 ppm for fast groundwater velocity case. Similar trends were observed for the remaining groundwater velocity cases. However, a significant difference in the final (plateau) concentration is observed in these three cases. Thus groundwater flow plays significant role in 1) spreading of pure phase LNAPL in capillary zone, 2) accelerating dissolution rates from large pool area, 3) dissolved LNAPL movements and (4) biodegradation of dissolved plume having different varying concentrations. The fact that LNAPL's are highly sensitive to changes in the subsurface conditions in the subsurface zone coupled with their extensive spread and dissolution in the saturated-unsaturated aquifers under varying conditions has led to various groundwater quality issues. Thus, the results of the tank experiments where water table fluctuated and the flow velocity changed will help to estimate future concentration load in area having shallow and coastal aquifer generally impacted by tidal effect may causes dynamic

groundwater table and flow regimes conditions. Gained knowledge will also help to implement the bioremediation plan at a polluted sites located in and around highly dynamic aquifer regions.

In engineered bioremediation techniques like biostimulation, oxygen and nutrients are injected to polluted saturated zone. Most of the earlier studies are focused on bioremediation design for polluted saturated zone while one cannot ignore the role of vadose zone during implementation of such techniques. Thus, simulation-optimization approach was applied to analyse the performance of bioremediation design for polluted vadose zone having different soil moisture and temperature condition along with treatment of polluted saturated zone. The study domain consisted of three injection wells to provide oxygen/nutrients to polluted saturated zone and one extraction well to control toluene plume spreading. The extracted groundwater was used to recharge polluted vadose zone which significantly enhanced the removal of toluene by maintaining optimal soil moisture content. The biodegradation rates estimated in microcosms having different combination of soil moisture and temperature were incorporated as sink of LNAPL in vadose zone. While BIOPLUME III was used to estimate enhanced biodegradation rate in saturated zone by considering additional oxygen and nutrient supply by injection wells. These degradation rates were used in HYDRUS 3D to simulate the saturated and vadose zone soil-moisture flow and toluene transport. The data generated from simulation runs were used in Extreme Learning Machine (ELM)-Particle Swarm Optimization (PSO) tools to achieve the minimum remediation time and cost. The application of *in-situ* bioremediation method in the region of optimal temperature-high moisture content gives the best result as maximum removal efficiency and minimum remediation system design cost. Spreading of toluene was more through vadose zone having soil moisture level higher than 60% at 30°C than 10°C. A minimum cost of $106,570 and $107,245 was achieved when the soil moisture was 80% and 60%, respectively, at 30°C in one year. A small difference of remediation cost clearly demonstrate effect of vadose zone recharge on accelerated biodegradation. However, for the lower soil moisture content of 40% and 20%, the optimized cost was $120,306 and $126,905 in time frame of 1 year 3 months and 1 year 6 months, respectively. The total cost got by the ELM-PSO approach was held to a minimum while effectively fulfilling all the regulatory constraints of the contaminated site. The key findings of this study are as-

a). LNAPL degradation at different combination of soil moisture and temperature conditions can be used for predicting the process of biodegradation and for determining the time needed to remove organic pollutants from polluted sites.

b). Column-scale observation suggests that dissolution and biodegradation of LNAPL are comparatively high under high groundwater temperature conditions. The results of these experiments will help to implement thermally enhanced bioremediation of organic polluted sites using solar based and/or geothermal system.

c). The results of the column experiments performed to investigate the role of plant will help to implement the plant-assisted bioremediation in real field conditions. However, the estimation of LNAPL mass loss due to volatilization from plant and uptake by root will improve these findings.

d). The findings of the 2/3D tank experiments suggest that spreading of the LNAPL plume is governed by mechanisms of dissolution, advection, dispersion and diffusion along with degradation and volatilization rates of the pollutant. The dissolution is highly dependent on the pool size of the LNAPL under varying groundwater table and flow regimes. The results of 2-D/3-D system can be used to forecast the pollution load at surrounding locations and in effective implementation of bioremediation techniques under site prevailing conditions.

e). Vapour phase of LNAPL is highly influenced by rapid fluctuation of groundwater table in 2-D sand tank setup. Thus, one can frame the sound scientific and technical concept to mitigate the risk of vapour intrusion at organic polluted sites to above laying houses and buildings. These findings may help to field practitioners to locate suitable zone for nutrient/ microbial seeding at a hydrocarbon polluted site.

Over all, the integrated experimental, numerical and data based modeling approach addressed in this study is very promising and unique which can contribute immensely in practical designing of remediation strategies for LNAPL polluted subsurface systems. This approach will help to design a suitable location of injection/extraction wells and their optimal operational parameters in minimal cost for a polluted (un)-saturated zones.

Future Recommendations

Consideration of different level of mixed LNAPL concentrations will improve the findings of microcosms experiments. Anaerobic degradation of LNAPL compounds is equally important to incorporate in future studies. Further, the metabolic pathway/daughter compounds of the degradation of LNAPL compounds can be investigated for understanding the geochemical reactions in subsurface. Microcosms experiments at a combination of other environmental factors (pH, Salinity) relevant to a polluted site along with the associated temperature and soil moisture conditions would further improve the site-specific remediation forecast. Additional research could be conducted to examine the role of soil matrix heterogeneity, and subsequent vapour intrusion towards surface under dynamic groundwater flow regimes. Consideration of impact of pressure in saturated zone due to injection and extraction wells will further improve the remediation cost estimation. The density dependent flow is expected nearby the coastal/shoreline area. Therefore, consideration of role of density along with groundwater table dynamic will make this study more widely application. Similarly considering the presence of other hydrocarbons with toluene will further improve the findings of biodegradation rates.

Appendix-I

Photos of Plate used for Microbial Population Counting in Column Setup

➢ At 36˚C

(a) 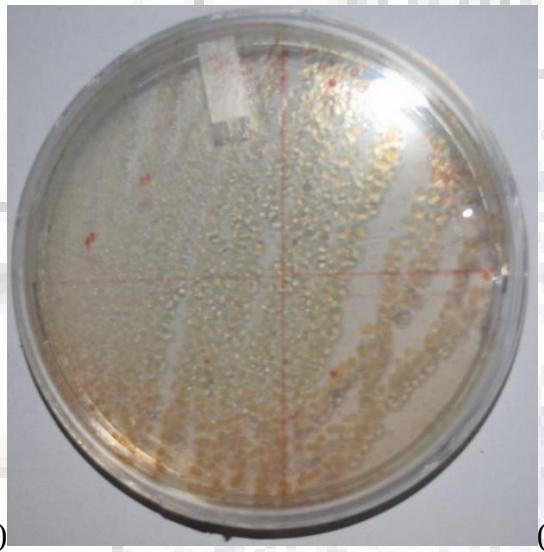 (b) 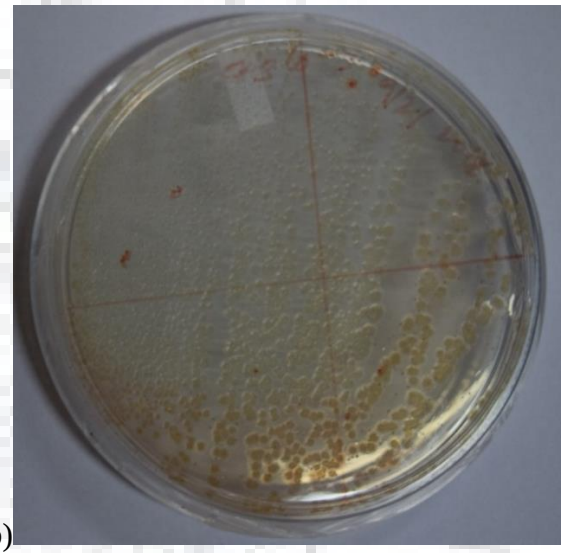

➢ At 28˚C

(c) 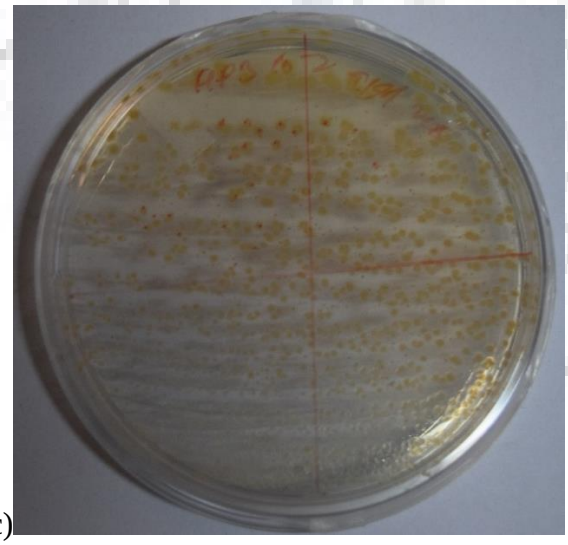 (d) 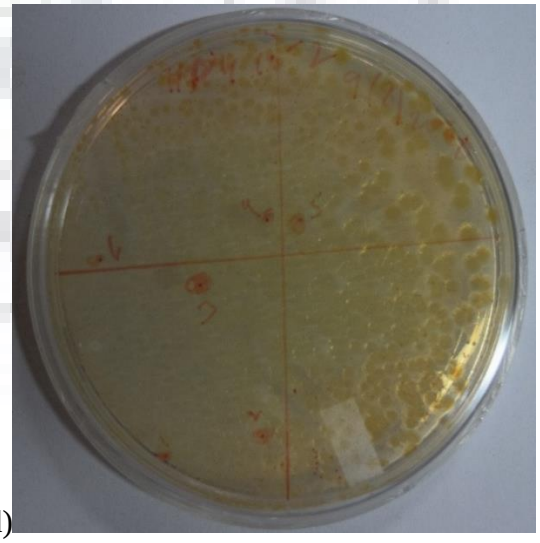

➢ At 20˚C

(e) 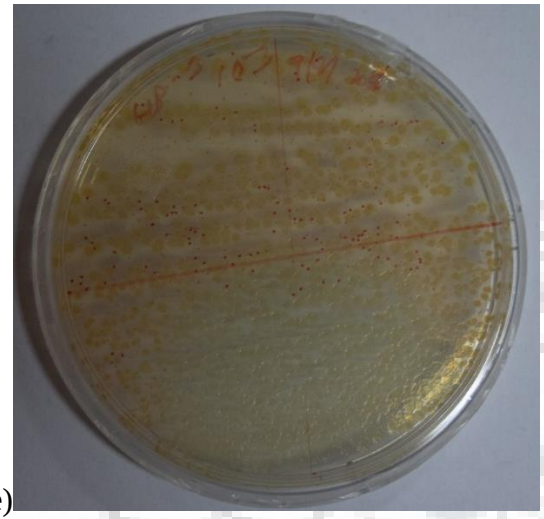 (f) 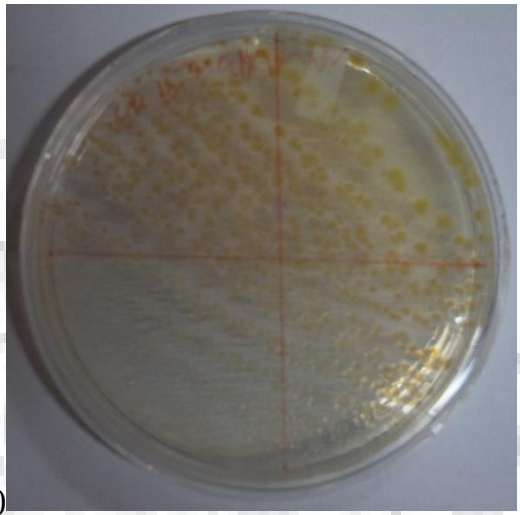

➢ At 4˚C

(g) 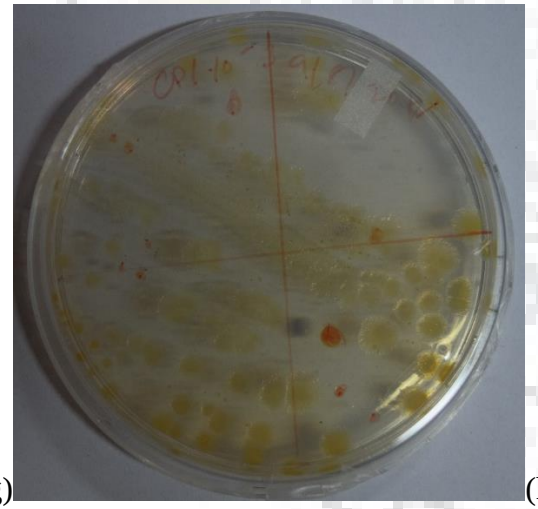 (h) 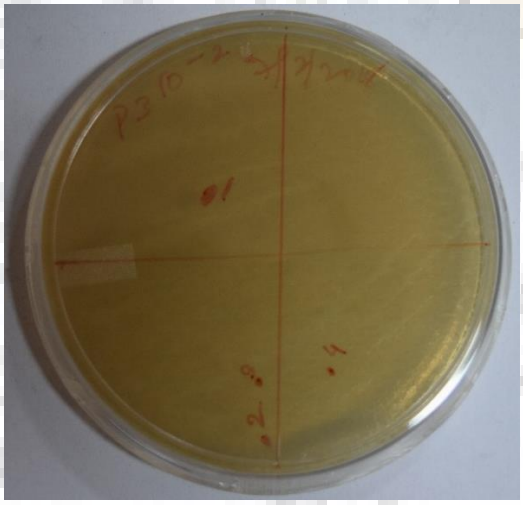

Figure A1: Photos of plates showing microbial growth at 36˚C (a) port P1, (b) port P3; 28˚C (c) port P1, (d) port P3; 20˚C (e) port P1, (f) port P3 and 4˚C (g) port P1; (h) port P3.

Photos of Plate used for Microbial Population Counting in 2D Sand Tank

- Under Rapid Groundwater Table Fluctuation

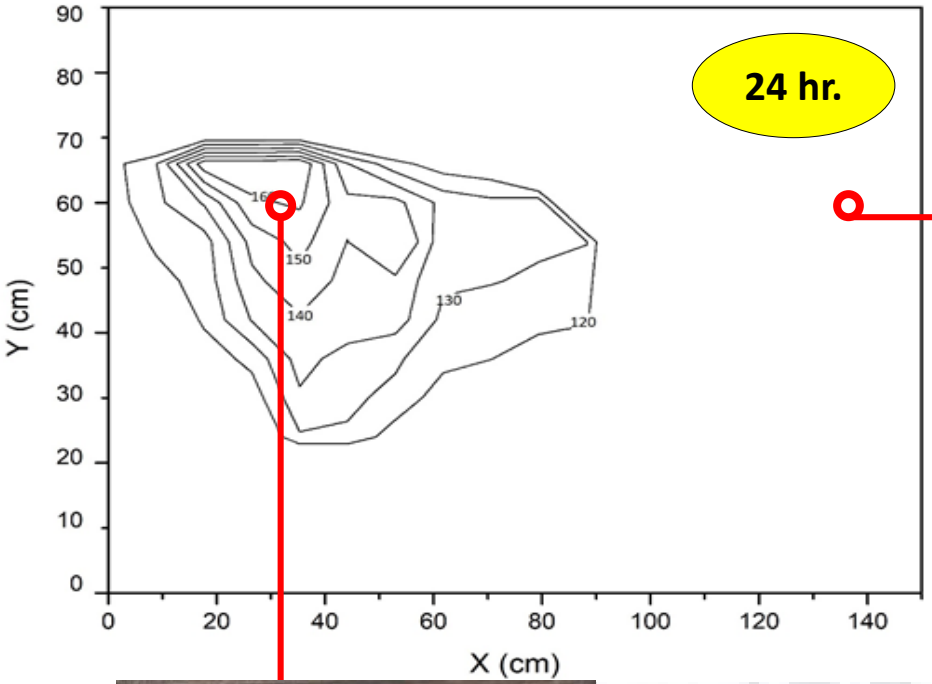

24 hr.

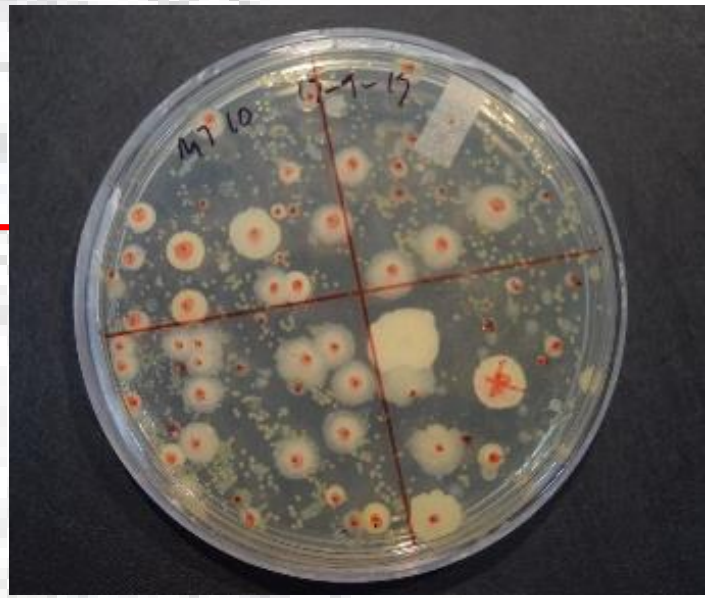

P7: O

P1: 305×10^{4}

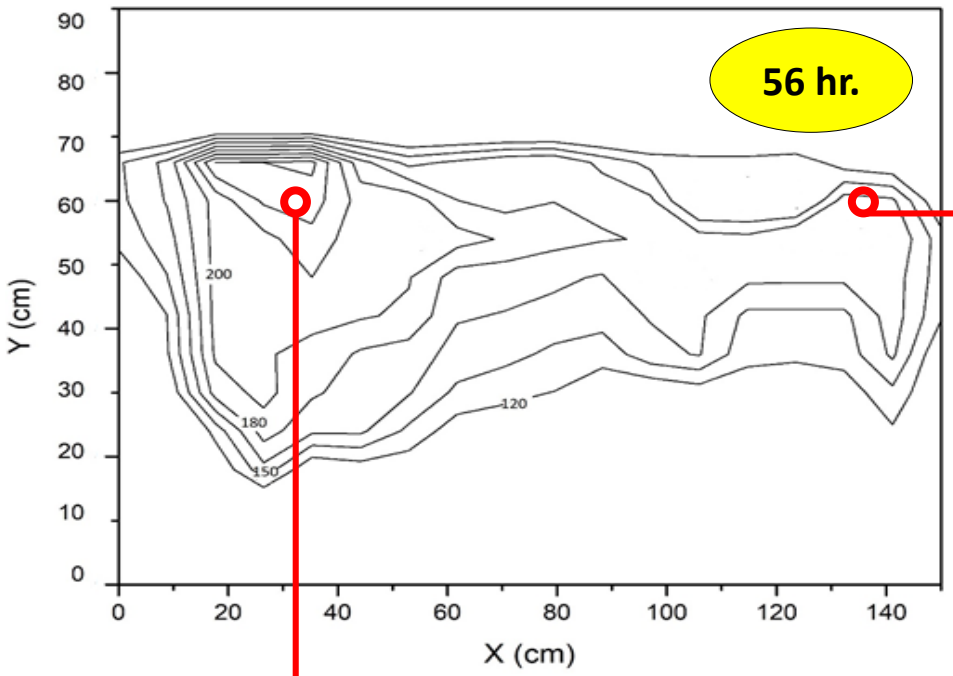

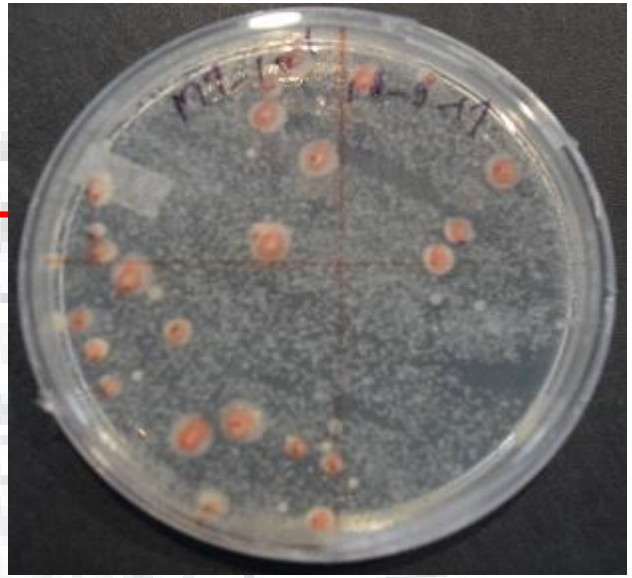

P7:
224×10^4

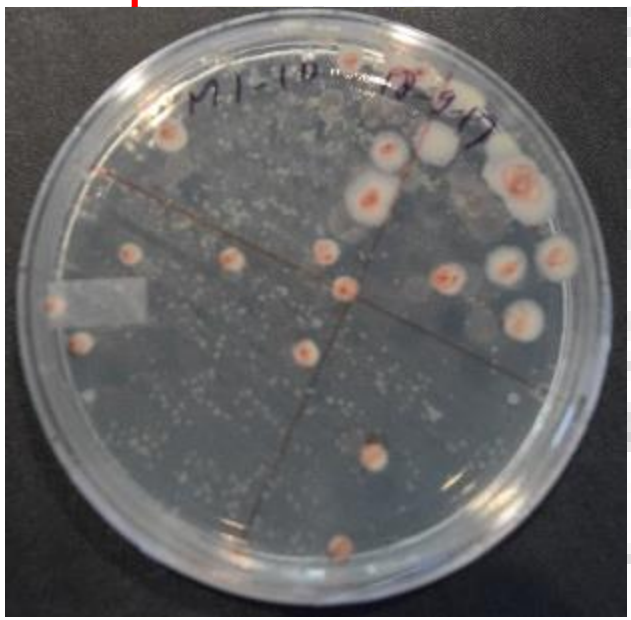

P1:
78×10^4

- Under General Groundwater Table Conditions

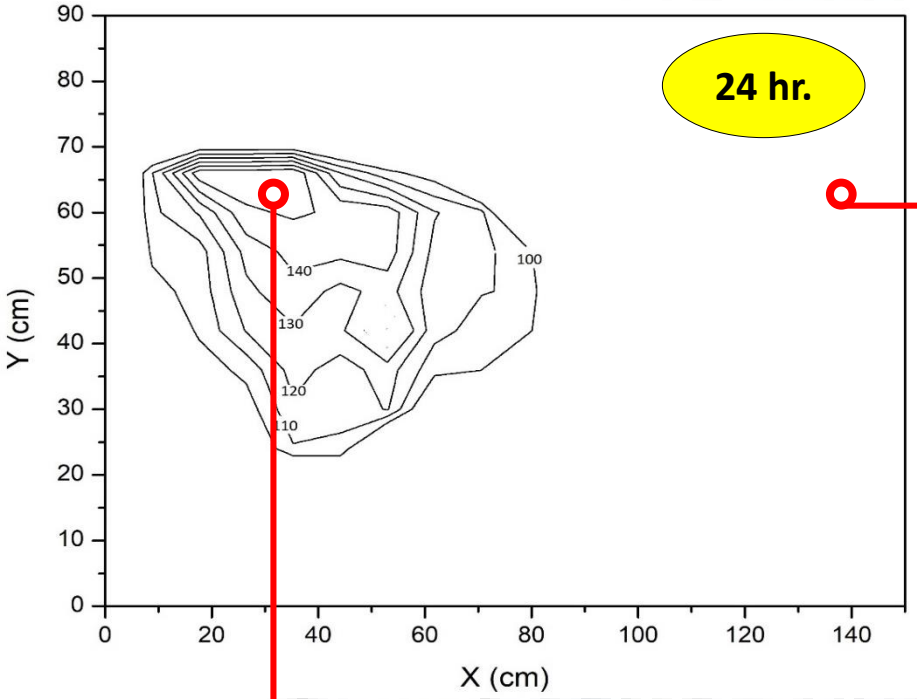

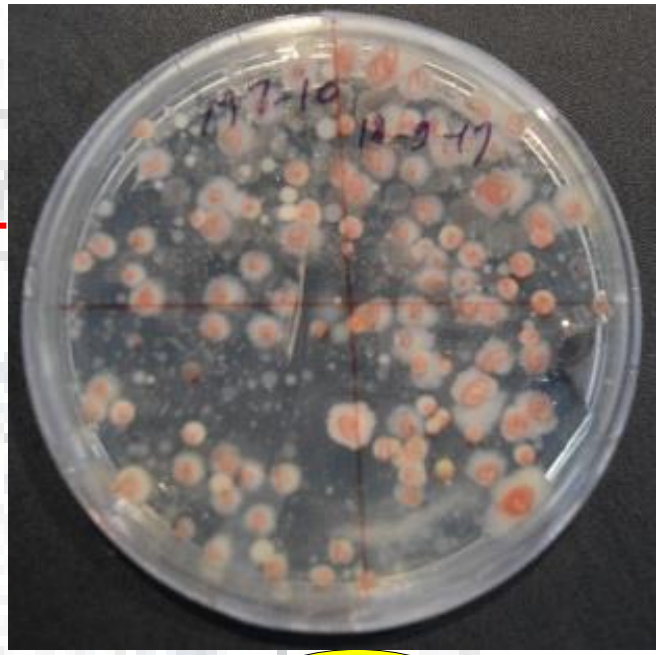

P7:
285×10^4

P1:
294×10^4

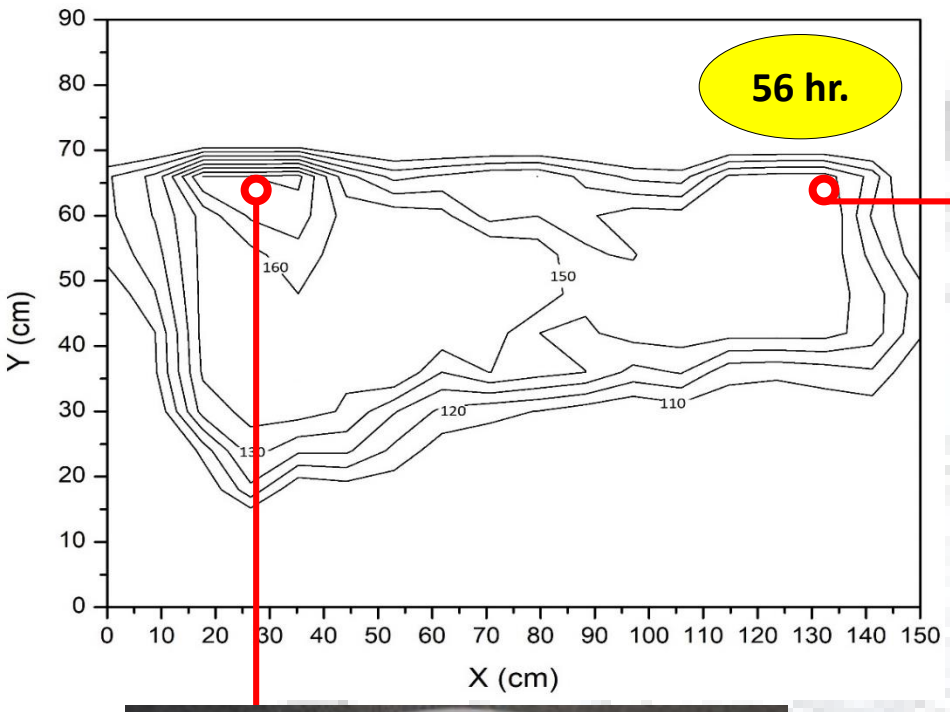

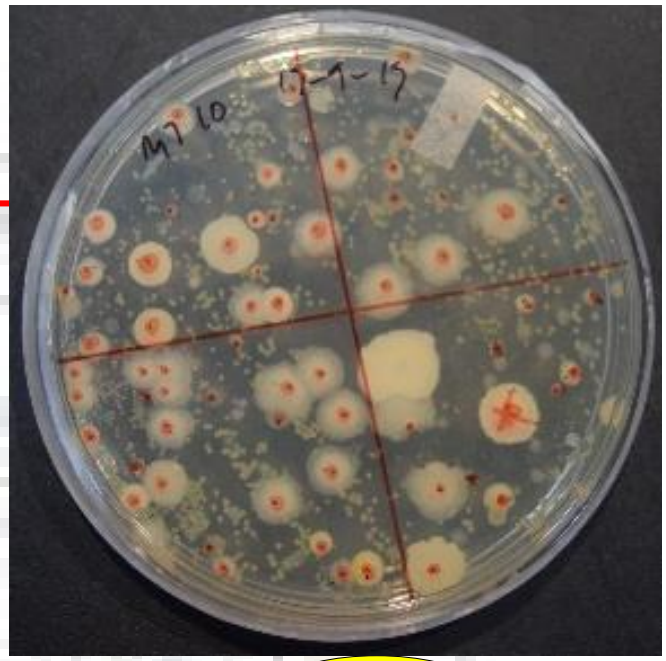

P7: O

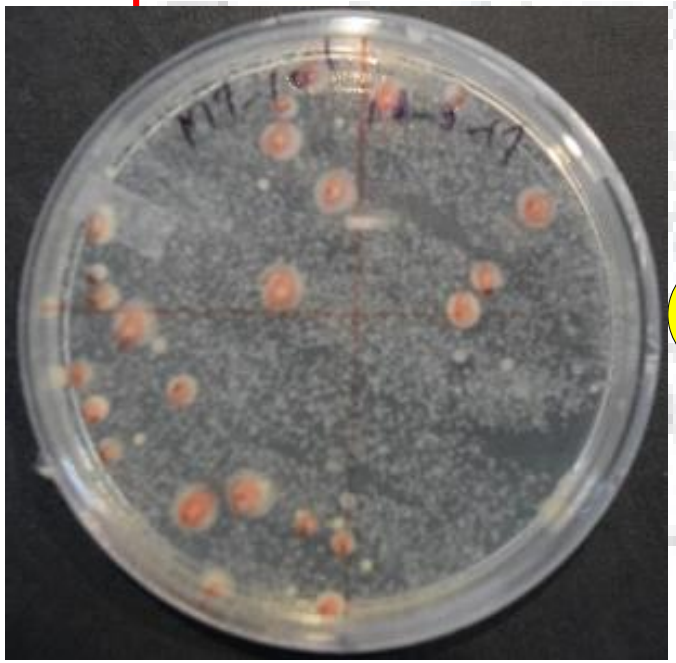

P1:
204×10^4

- Under Slow Groundwater Table Fluctuation

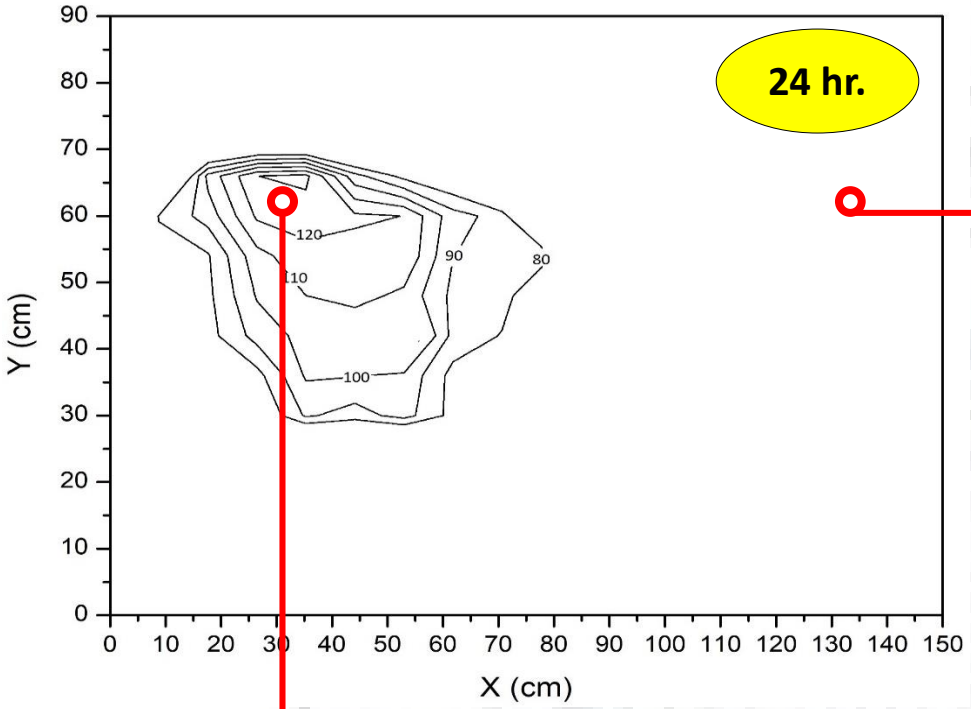

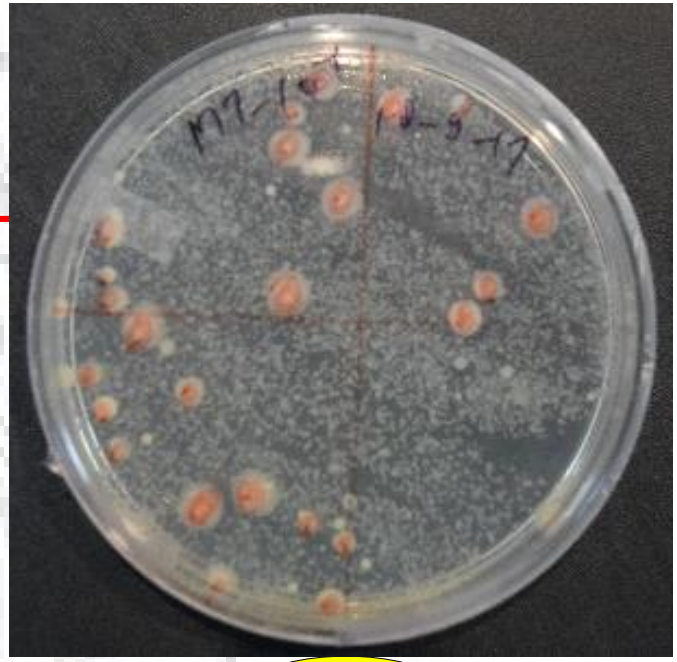

P7:
288×10^{4}

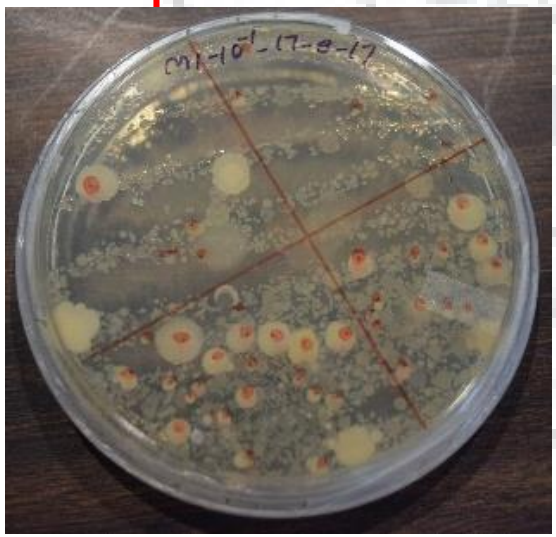

P1:
285×10^{4}

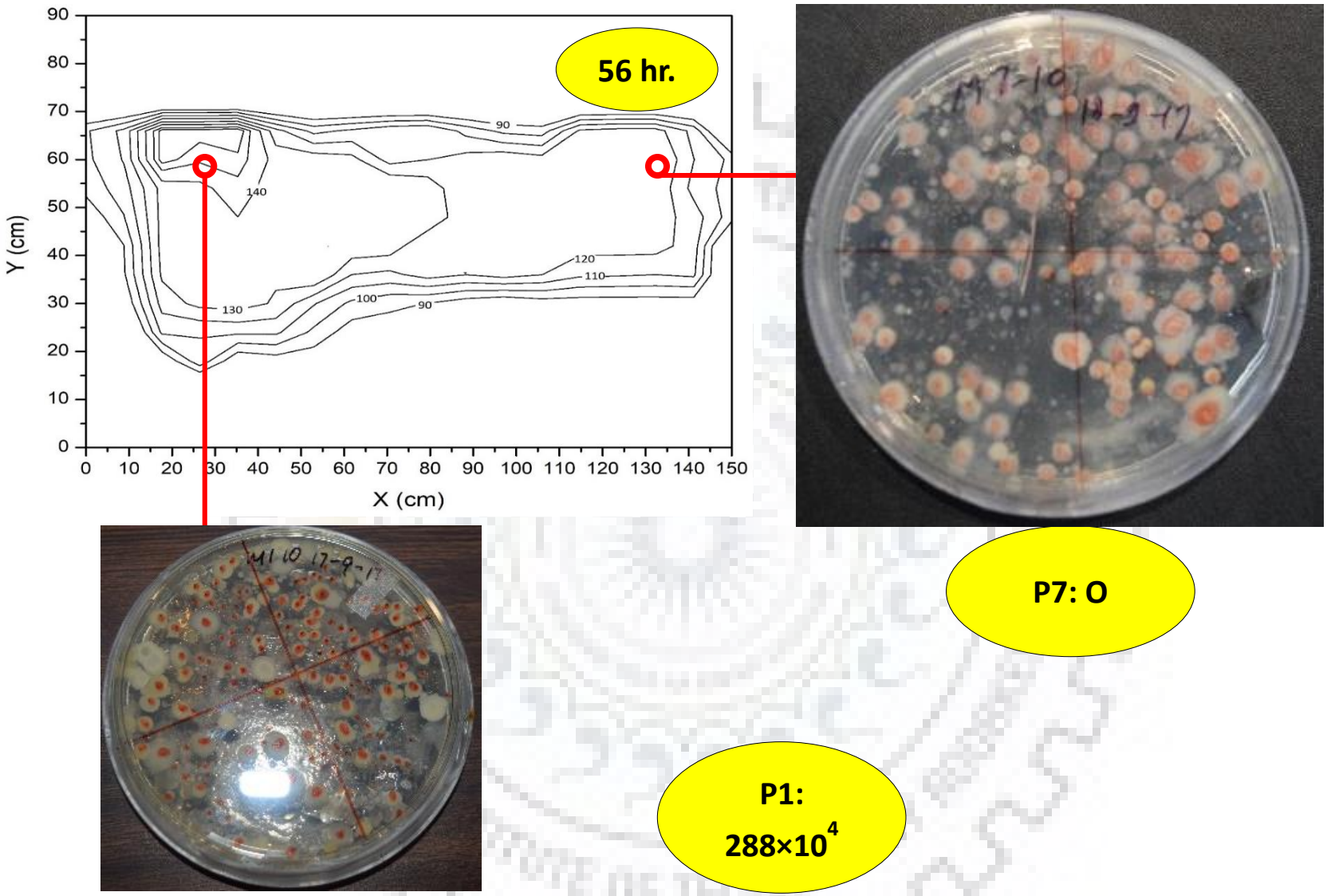

Figure A2: Photos of plat showing microbial growth in different pollutant regions of 2D tank under rapid, general and slow groundwater table fluctuation.

Appendix-III

Numerical Domain of Characteristic Polluted Site

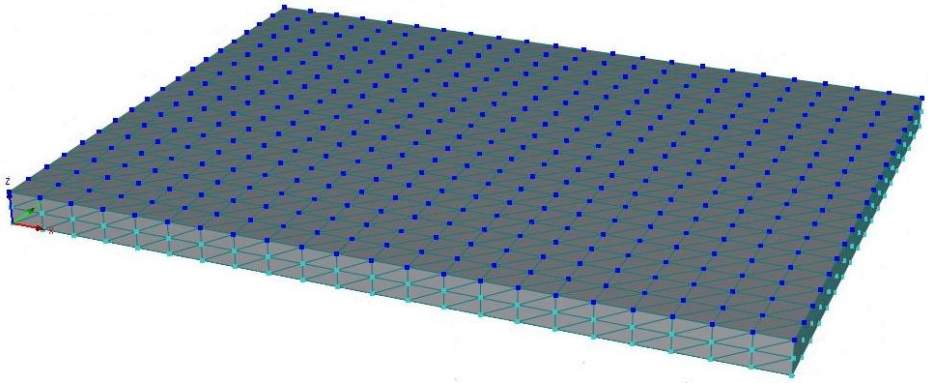

(a) Material Distribution (Whole Mesh)

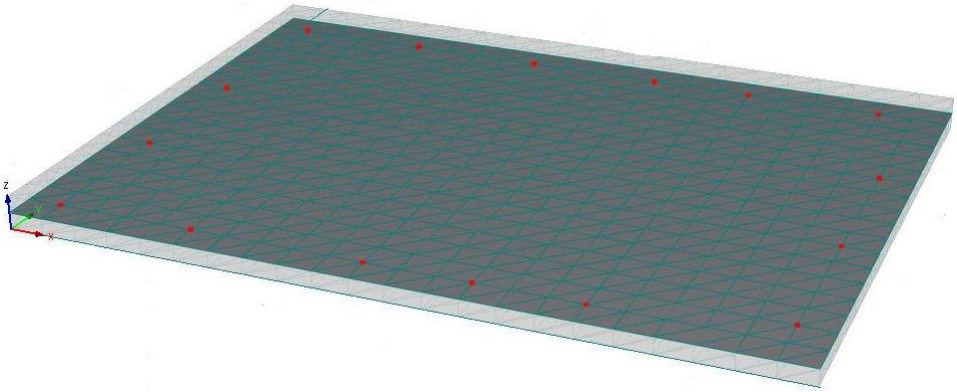

(b) Observation Nodes (Middle Layer)

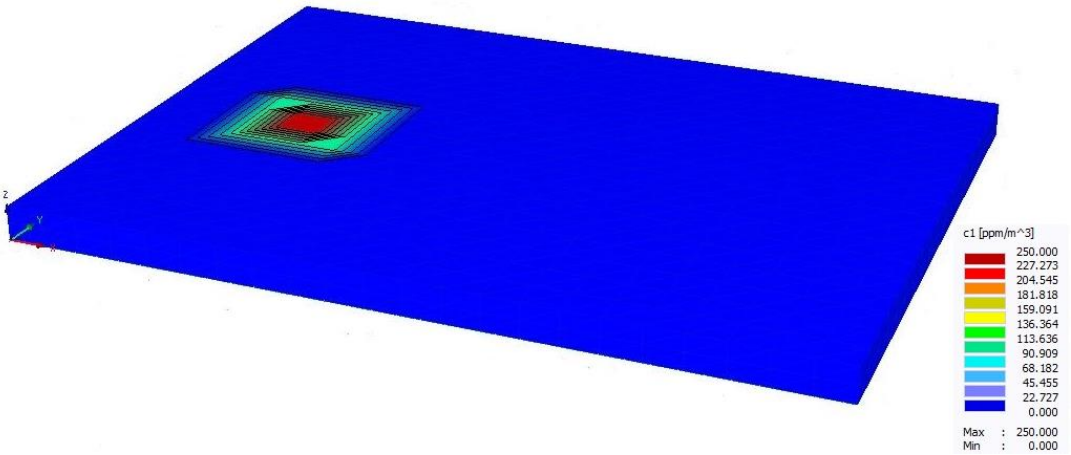

(c) Initial Dissolved LNAPL Concentration

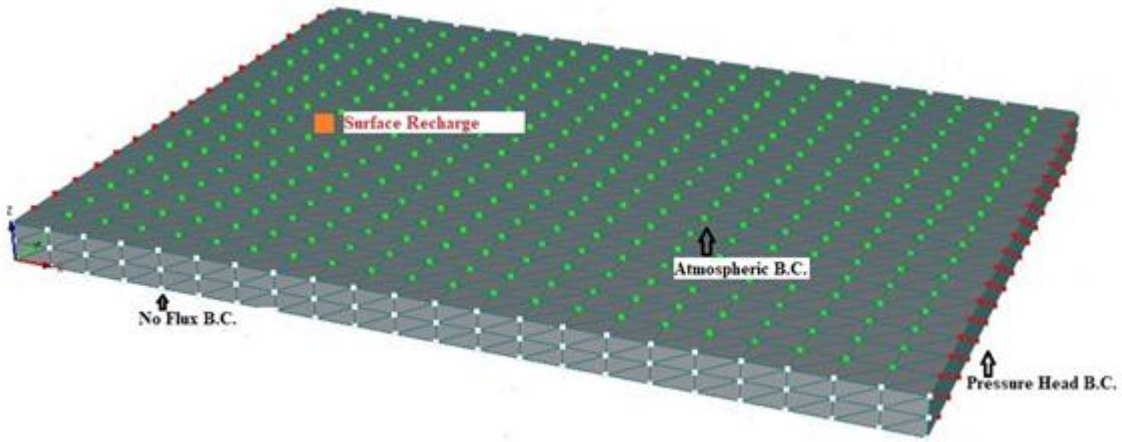

(d) Location of Surface Recharge Peat & Associated Boundary Conditions (B.C.)

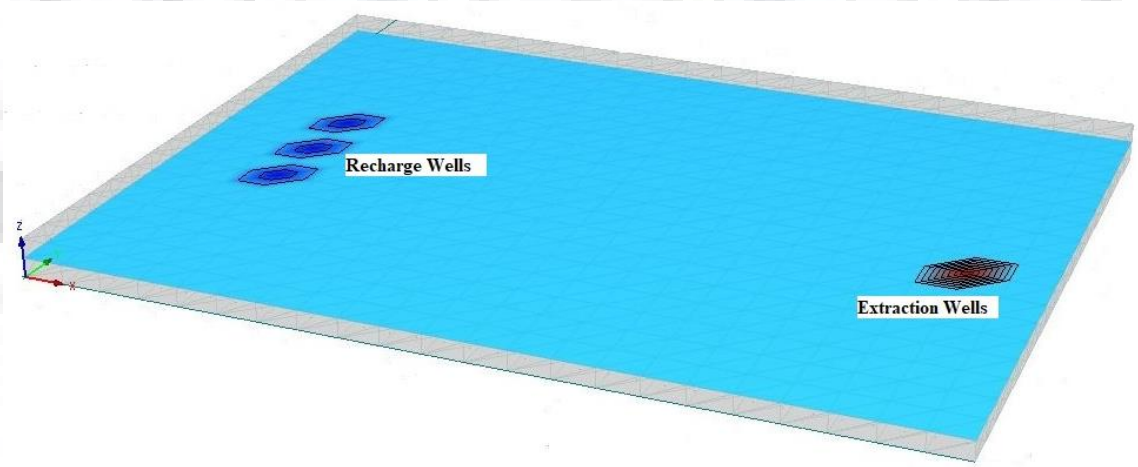

(e) Locations of Recharge Wells and Extraction Wells in Middle Layer

Figure A3. Numerical domain representing different aspects (a - e) considered to investigate the biodegradation system design to remove dissolved toluene from the vadose and saturated zone.

Appendix-IV

Pumping rate (L/s) for injection wells (I1, I2 and I3 and extraction well (E1)

Table A1: Pumping rates for injection wells (I1, I2, and I3 and extraction well (E1) used to evaluate the performance of bioremediation system design.

Sr. No.	Injection wells			Extraction Wells
	I1	I2	I3	E1
1	0.00	0.00	-3.63	2.06
2	-1.71	-3.32	-3.06	0.00
3	-3.31	-2.28	-1.72	1.91
4	0.00	-1.96	-2.78	1.79
5	-2.35	-1.75	0.00	0.00
6	-1.59	-1.91	0.00	2.66
7	-3.64	0.00	0.00	1.98
8	-3.73	0.00	-3.11	0.00
9	-3.19	0.00	-2.98	3.73
10	-2.89	0.00	0.00	0.00
11	-3.13	0.00	0.00	2.47
12	-3.81	-3.32	0.00	3.20
13	0.00	0.00	0.00	0.00
14	0.00	-2.97	-1.53	0.00
15	-2.93	0.00	-3.17	1.72
16	-1.54	-2.98	-2.45	0.00
17	-3.43	0.00	-1.55	0.00
18	-3.66	-2.19	-3.61	2.69
19	-3.27	-2.82	0.00	0.00
20	-3.55	-2.96	-3.40	2.74
21	0.00	0.00	0.00	3.26
22	-1.66	0.00	-1.99	0.00
23	0.00	-3.51	0.00	2.99
24	-3.62	-2.82	0.00	2.33
25	0.00	-3.33	-2.11	3.18
26	0.00	0.00	0.00	0.00
27	-2.70	-3.46	-3.60	2.02
28	0.00	-3.70	-3.49	0.00

29	-3.02	-1.85	-2.61	3.34
30	0.00	-2.27	-2.92	1.68
31	-1.86	0.00	0.00	3.80
32	-3.58	0.00	0.00	0.00
33	-3.37	-3.76	0.00	0.00
34	-1.58	0.00	-2.96	3.78
35	0.00	-3.25	-3.15	3.19
36	-2.54	-3.37	-1.56	2.84
37	-3.30	0.00	-3.34	0.00
38	-1.68	-2.53	-3.11	2.10
39	0.00	-2.28	0.00	1.62
40	0.00	0.00	-1.68	2.31
41	0.00	-2.12	0.00	2.53
42	-2.28	-2.81	0.00	3.67
43	-3.50	-1.85	-2.25	2.11
44	-3.65	-2.87	-2.53	1.68
45	-3.09	-1.93	-1.48	0.00
46	-3.07	0.00	-1.80	0.00
47	-2.77	-2.29	-3.38	0.00
48	-3.55	-2.09	0.00	0.00
49	-1.59	0.00	-3.02	0.00
50	0.00	-3.08	0.00	3.81
51	-1.72	-3.62	-2.45	2.10
52	0.00	-1.84	0.00	1.48
53	0.00	-2.73	-2.30	3.44
54	-2.12	0.00	0.00	0.00
55	-1.54	-2.38	0.00	1.70
56	0.00	-2.40	-1.64	0.00
57	0.00	-3.32	-2.10	0.00
58	0.00	0.00	-2.49	2.91
59	-2.75	-2.40	-2.65	3.67
60	-3.48	0.00	-3.63	2.23
61	-2.38	-2.71	0.00	0.00
62	-2.93	-1.54	-2.74	0.00
63	-3.04	-1.81	-1.87	3.44
64	-2.28	-2.13	-3.62	0.00
65	-3.09	-3.69	0.00	0.00
66	-3.60	-1.51	0.00	3.28
67	0.00	-2.57	-2.06	1.91
68	0.00	0.00	0.00	3.30
69	-3.74	0.00	-3.74	0.00

70	-2.36	-3.04	-3.30	3.41
71	-1.96	-3.68	-3.05	0.00
72	0.00	0.00	0.00	1.63
73	0.00	0.00	-1.97	0.00
74	-3.74	0.00	-3.58	0.00
75	0.00	-3.67	0.00	2.09
76	0.00	-2.01	-3.41	0.00
77	-3.60	-3.61	-2.20	0.00
78	0.00	0.00	-1.83	0.00
79	0.00	-1.91	-1.68	0.00
80	0.00	-1.50	0.00	1.93
81	0.00	0.00	-1.54	0.00
82	0.00	0.00	-2.31	0.00
83	-1.71	-2.95	-1.95	3.31
84	-2.15	-1.91	-1.50	0.00
85	-3.20	-2.22	0.00	1.62
86	0.00	-3.31	0.00	3.79
87	0.00	-3.56	-2.79	3.36
88	-1.84	-2.87	-2.89	2.05
89	-2.50	-3.81	-3.13	0.00
90	0.00	-3.41	0.00	0.00
91	-2.27	-1.70	-2.81	3.21
92	-2.63	-2.84	0.00	3.73
93	0.00	-2.10	0.00	0.00
94	-2.29	-1.76	-3.13	3.17
95	0.00	-2.79	-3.76	2.05
96	-3.36	0.00	-3.07	2.00
97	0.00	0.00	0.00	2.45
98	-1.82	0.00	0.00	3.19
99	0.00	0.00	-1.59	0.00
100	0.00	-2.08	-3.83	2.67
101	-3.01	0.00	-3.83	2.85
102	0.00	0.00	-2.91	2.34
103	-1.88	-3.36	-3.36	1.97
104	-2.08	-3.59	0.00	3.00
105	-1.48	0.00	-1.99	0.00
106	-3.55	0.00	0.00	1.92
107	-2.80	-1.67	-1.76	0.00
108	-3.45	0.00	0.00	2.61
109	-2.74	0.00	-1.56	0.00
110	-2.70	0.00	-3.54	3.55

111	0.00	0.00	0.00	0.00
112	-2.89	-2.32	-2.62	0.00
113	-3.12	-2.69	-2.01	0.00
114	-2.68	0.00	0.00	3.63
115	-3.23	-2.66	0.00	1.86
116	-2.44	-2.47	-3.47	3.78
117	-3.12	-2.92	-1.48	3.08
118	-1.73	-2.24	-2.88	2.44
119	-1.61	-2.21	0.00	0.00
120	0.00	-1.50	-2.52	0.00
121	0.00	-2.45	-3.66	2.25
122	-3.32	0.00	0.00	3.12
123	0.00	-2.01	-3.31	0.00
124	-3.30	-2.69	-2.92	1.83
125	-1.56	0.00	-3.30	2.99
126	-3.47	-3.65	-2.82	1.75
127	-2.02	0.00	0.00	2.74
128	0.00	-2.29	-2.18	2.23
129	-3.59	-1.53	-2.16	0.00
130	-1.97	-3.81	-2.79	2.96
131	-1.90	0.00	-3.21	1.81
132	0.00	0.00	-1.78	2.72
133	0.00	-2.91	0.00	3.79
134	0.00	-2.25	-2.63	2.30
135	-1.65	-2.64	-1.54	2.46
136	-2.83	-1.81	0.00	2.42
137	-1.87	0.00	0.00	2.01
138	-1.95	-2.51	-3.31	0.00
139	-3.46	-1.78	-2.71	3.37
140	-1.88	0.00	-2.04	1.66
141	-3.82	0.00	0.00	0.00
142	0.00	-2.34	-3.00	3.29
143	-1.59	0.00	0.00	3.09
144	0.00	-3.30	-2.68	0.00
145	0.00	0.00	-2.26	3.46
146	-3.23	-2.80	-1.49	2.90
147	0.00	0.00	0.00	3.36
148	-2.75	-2.57	-2.42	1.73
149	0.00	0.00	0.00	0.00
150	-1.62	-2.69	0.00	2.72
151	-3.34	0.00	0.00	2.06

152	-2.46	-2.28	-3.72	2.69
153	0.00	0.00	-1.50	0.00
154	0.00	0.00	-2.04	3.65
155	-2.46	-1.92	-2.65	3.38
156	-2.29	-2.02	0.00	3.43
157	0.00	-3.39	-2.88	0.00
158	-3.44	-2.17	0.00	2.96
159	-1.59	-2.83	0.00	3.70
160	0.00	-2.22	0.00	0.00
161	0.00	0.00	-3.03	0.00
162	-2.05	-1.94	-2.24	2.66
163	0.00	-3.23	0.00	0.00
164	0.00	-2.61	0.00	2.86
165	0.00	0.00	-2.33	2.48
166	-1.57	-2.87	-1.82	3.42
167	-3.26	0.00	0.00	0.00
168	0.00	-2.98	0.00	1.83
169	0.00	-3.45	0.00	3.56
170	0.00	0.00	-2.41	1.63
171	0.00	-2.59	0.00	0.00
172	0.00	-3.07	-2.40	2.37
173	0.00	-2.04	0.00	2.40
174	-2.40	-2.97	0.00	3.16
175	-2.18	0.00	-2.83	1.86
176	-3.47	0.00	-2.57	3.41
177	-2.30	-3.67	-2.69	0.00
178	-3.22	-1.52	0.00	3.10
179	-2.87	-3.68	-1.57	0.00
180	0.00	-2.00	0.00	0.00
181	-2.07	0.00	0.00	2.41
182	-3.09	-2.43	0.00	3.02
183	0.00	-3.40	0.00	2.95
184	0.00	0.00	-2.62	2.74
185	-2.04	-3.76	-3.64	2.00
186	0.00	-2.21	-2.87	3.65
187	-2.01	-2.10	-2.47	0.00
188	0.00	0.00	0.00	2.82
189	-2.08	-2.95	0.00	1.53
190	0.00	-2.00	0.00	0.00
191	-1.48	0.00	-1.93	3.08
192	0.00	0.00	0.00	0.00

193	-2.83	-3.18	0.00	0.00
194	0.00	-3.36	0.00	0.00
195	0.00	0.00	-3.29	0.00
196	-1.58	-2.96	-2.17	2.67
197	0.00	-3.18	-2.34	0.00
198	0.00	0.00	-2.67	2.04
199	0.00	-3.57	0.00	0.00
200	0.00	-2.87	-2.81	0.00
201	-1.77	0.00	0.00	2.27
202	-2.10	-1.75	0.00	2.55
203	-3.39	-2.78	0.00	1.99
204	-1.51	-3.65	0.00	0.00
205	-2.27	0.00	-3.64	2.97
206	-1.90	-2.03	-3.08	0.00
207	-3.28	-2.11	-3.76	3.60
208	-1.69	0.00	0.00	2.84
209	0.00	0.00	-2.63	3.57
210	-2.65	0.00	-3.01	0.00
211	-3.15	-2.22	-2.22	3.32
212	-3.25	-3.49	0.00	0.00
213	0.00	-1.84	-1.54	3.22
214	0.00	-2.19	-1.71	2.55
215	0.00	0.00	0.00	0.00
216	-2.59	-2.09	-2.56	3.01
217	0.00	0.00	-3.17	0.00
218	0.00	-2.05	0.00	2.60
219	-2.80	-3.76	0.00	3.29
220	-3.48	-2.71	0.00	3.41
221	0.00	-3.71	-1.77	2.05
222	-2.63	0.00	-2.37	0.00
223	0.00	0.00	-2.09	2.06
224	-1.80	-3.05	0.00	2.28
225	0.00	0.00	-2.39	0.00
226	0.00	-3.44	0.00	0.00
227	0.00	-2.48	0.00	0.00
228	-1.64	-1.99	-3.28	2.39
229	-2.74	-2.16	-2.63	1.99
230	-1.63	0.00	-1.98	2.56
231	0.00	-2.22	-3.32	0.00
232	-2.14	-1.73	0.00	2.52
233	-2.38	-3.78	-1.58	1.92

234	-3.00	0.00	-1.71	0.00
235	0.00	0.00	-2.67	2.92
236	0.00	-3.14	0.00	2.15
237	0.00	0.00	0.00	0.00
238	-2.20	0.00	-1.95	3.21
239	-2.24	-2.66	-3.06	3.68
240	0.00	0.00	0.00	2.03
241	-1.71	-2.36	0.00	2.18
242	-3.71	0.00	-3.62	2.86
243	-2.14	0.00	-3.28	2.03
244	-3.29	0.00	-1.58	1.79
245	-3.35	-2.42	0.00	2.73
246	0.00	-2.39	0.00	0.00
247	0.00	-2.62	-2.57	1.73
248	-2.99	-1.81	0.00	0.00
249	-3.74	0.00	0.00	2.42
250	0.00	-2.58	-3.10	3.83
251	-1.86	-1.95	-2.27	0.00
252	0.00	-3.67	-3.59	2.53
253	0.00	0.00	0.00	1.56
254	0.00	-3.11	-2.05	3.76
255	0.00	-2.76	0.00	2.49
256	-2.39	-1.99	-2.20	2.26
257	-2.54	-2.96	0.00	2.67
258	0.00	-2.87	-2.57	3.47
259	0.00	0.00	0.00	3.36
260	-2.20	-3.65	-3.05	2.82
261	0.00	-3.02	-2.56	2.39
262	0.00	-3.08	-2.32	2.98
263	0.00	0.00	0.00	0.00
264	-3.74	-2.71	-3.64	1.96
265	-2.98	-3.05	-1.66	3.46
266	-3.71	-3.21	-2.46	2.51
267	-2.07	-1.66	-3.70	2.11
268	-2.06	-3.14	-3.72	0.00
269	-3.04	-3.73	-3.29	0.00
270	-3.27	-3.02	-2.86	0.00
271	-2.57	-3.52	-2.05	0.00
272	-3.62	-2.18	-2.72	3.57
273	-3.35	-2.42	-1.89	1.73
274	-2.92	0.00	-1.48	3.68

275	-2.11	-3.03	-1.48	1.50
276	-3.53	-3.16	0.00	3.62
277	-2.02	0.00	-2.78	2.74
278	-1.67	-2.83	-2.69	3.28
279	-3.41	-3.04	-2.79	0.00
280	0.00	-3.60	-2.26	2.14
281	0.00	0.00	-2.70	0.00
282	0.00	0.00	-3.53	1.58
283	-2.89	0.00	-2.22	0.00
284	0.00	0.00	0.00	0.00
285	-3.22	0.00	-3.18	0.00
286	-2.29	0.00	-2.75	2.82
287	-2.37	-1.57	-1.74	2.10
288	-2.12	-2.03	-3.46	0.00
289	-1.48	-1.85	-2.38	2.00
290	0.00	-3.40	-1.74	0.00
291	-3.23	-3.35	-1.91	1.62
292	-2.30	-2.04	0.00	0.00
293	-2.50	-1.86	0.00	2.20
294	-1.79	-3.13	-3.69	3.52
295	-2.18	0.00	0.00	0.00
296	0.00	0.00	0.00	0.00
297	-1.84	0.00	0.00	0.00
298	0.00	0.00	0.00	3.41
299	0.00	-3.49	-3.82	3.43
300	-2.74	-3.21	-1.62	2.98
301	-2.69	0.00	0.00	3.50
302	-3.23	0.00	0.00	0.00
303	-2.52	-3.79	-2.83	0.00
304	0.00	-1.91	0.00	1.86
305	-2.29	0.00	0.00	0.00
306	0.00	-1.96	-3.73	0.00
307	0.00	-2.93	0.00	3.79
308	-2.14	-1.53	-2.05	0.00
309	-3.45	-2.97	-2.07	1.67
310	0.00	0.00	-3.24	3.33
311	0.00	-3.22	0.00	0.00
312	-2.69	-2.31	-3.17	3.30
313	-2.25	0.00	-2.67	2.00
314	0.00	-2.53	-3.51	1.94
315	0.00	0.00	0.00	0.00

316	0.00	-1.52	0.00	3.04
317	-3.48	-1.79	-3.70	1.72
318	0.00	0.00	0.00	0.00
319	-1.63	0.00	-2.76	1.91
320	-1.57	-2.05	0.00	0.00
321	-3.18	-2.57	-2.17	0.00
322	-2.54	0.00	0.00	2.31
323	-3.65	-2.63	-1.76	1.72
324	-3.66	-2.59	-3.36	3.39
325	-2.42	0.00	0.00	3.80
326	-1.61	-2.81	0.00	2.26
327	-3.01	-1.80	0.00	2.14
328	-3.22	0.00	0.00	1.77
329	0.00	0.00	-1.65	2.60
330	0.00	-3.55	-3.03	0.00
331	0.00	-3.26	0.00	0.00
332	-3.40	-3.46	0.00	2.40
333	-2.39	0.00	-2.16	0.00
334	0.00	-2.71	-1.90	2.96
335	-3.55	0.00	-1.79	0.00
336	-3.61	0.00	-2.12	1.88
337	-1.89	-2.44	0.00	3.48
338	-1.49	-1.99	0.00	2.23
339	0.00	-2.54	-1.68	0.00
340	-2.15	-3.83	-1.57	3.83
341	-2.08	-1.92	0.00	3.44
342	0.00	0.00	-1.49	0.00
343	-3.32	0.00	0.00	0.00
344	-3.46	-3.75	-2.84	2.47
345	-3.78	-3.50	-3.14	3.76
346	0.00	-2.69	-2.14	0.00
347	0.00	-3.27	-2.76	0.00
348	0.00	0.00	0.00	0.00
349	-3.66	-1.93	-3.05	0.00
350	-2.77	0.00	-3.55	0.00
351	-2.59	-2.32	-2.89	1.50
352	0.00	-2.57	-1.54	3.77
353	0.00	-2.06	0.00	0.00
354	-1.56	-3.09	0.00	0.00
355	0.00	0.00	-3.25	2.12
356	-2.73	0.00	0.00	2.81

357	0.00	0.00	-3.25	0.00
358	0.00	-2.04	0.00	1.89
359	-3.33	-2.85	-3.22	1.48
360	-1.51	0.00	-1.54	0.00
361	0.00	0.00	0.00	1.72
362	0.00	-2.39	0.00	2.49
363	-2.90	-2.35	-3.27	2.39
364	-3.00	-3.73	0.00	0.00
365	0.00	-3.05	0.00	1.50
366	0.00	0.00	-3.37	0.00
367	0.00	0.00	-1.73	0.00
368	-3.47	0.00	-3.62	3.21
369	-2.02	-3.52	-2.12	0.00
370	-1.86	-3.40	0.00	0.00
371	-2.70	0.00	-1.96	3.64
372	-3.58	-2.54	-3.19	3.08
373	-1.88	-2.46	-2.07	2.25
374	-3.09	0.00	0.00	2.02
375	-3.74	-1.65	-2.55	1.94
376	-3.07	-2.06	-1.91	0.00
377	0.00	-2.64	-1.59	0.00
378	0.00	-1.79	0.00	3.40
379	0.00	-1.69	0.00	0.00
380	-2.37	-1.85	-3.74	2.25
381	0.00	-3.75	-1.71	0.00
382	0.00	0.00	-2.60	0.00
383	-2.63	-2.72	0.00	0.00
384	-3.61	0.00	-3.57	0.00
385	0.00	-3.45	-1.69	2.53
386	-3.59	-2.68	-3.59	2.51
387	0.00	0.00	0.00	0.00
388	-1.77	-3.34	0.00	3.62
389	-3.80	-1.76	0.00	0.00
390	-3.38	-2.00	0.00	2.13
391	0.00	-3.27	-2.89	2.69
392	-2.36	0.00	-3.36	1.86
393	0.00	-2.50	-3.56	2.62
394	-3.65	0.00	0.00	1.84
395	0.00	-1.80	-3.22	1.66
396	-2.88	-3.27	0.00	0.00
397	-3.75	-1.80	-2.46	1.79

398	0.00	-1.89	-3.57	1.96
399	0.00	-2.93	-1.88	2.80
400	-2.88	-2.70	0.00	0.00
401	-1.86	0.00	-2.38	3.39
402	0.00	-2.83	-3.23	0.00
403	0.00	-1.58	-2.19	0.00
404	-2.96	-2.16	-2.17	2.14
405	0.00	-2.81	0.00	1.93
406	0.00	-3.43	0.00	2.59
407	0.00	-2.37	0.00	3.35
408	-3.78	0.00	0.00	3.39
409	-2.63	-3.40	0.00	3.66
410	-2.05	-3.50	-2.49	0.00
411	-3.70	0.00	0.00	1.89
412	0.00	-2.84	-2.87	1.75
413	0.00	-2.58	-2.55	3.55
414	0.00	-3.00	-3.67	3.45
415	-2.49	-3.72	-1.51	2.84
416	-2.71	0.00	-2.62	0.00
417	-2.24	-3.65	0.00	3.80
418	0.00	-3.10	-2.64	0.00
419	0.00	-3.54	-1.59	0.00
420	0.00	-3.79	-3.07	2.82
421	0.00	-1.49	-2.16	0.00
422	0.00	-2.72	0.00	0.00
423	-3.46	0.00	-2.74	0.00
424	-2.12	0.00	-2.56	1.56
425	-2.42	-1.91	-1.65	2.82
426	-3.43	-2.95	0.00	2.66
427	0.00	0.00	-3.15	0.00
428	-1.64	-3.47	0.00	2.51
429	-3.28	-2.15	-3.68	2.39
430	0.00	-1.73	0.00	2.58
431	-3.29	-2.52	0.00	0.00
432	-3.57	0.00	-1.94	3.26
433	0.00	-3.17	-3.59	1.98
434	-3.13	0.00	0.00	1.47
435	-3.39	-2.10	-2.93	1.65
436	-2.99	-2.10	-1.78	1.58
437	-2.31	-3.20	-3.82	2.09
438	-3.25	0.00	0.00	1.79

439	-1.80	0.00	-3.01	3.84
440	-3.19	0.00	-1.89	2.18
441	-1.70	0.00	-2.58	0.00
442	-2.78	-3.16	-3.83	0.00
443	-3.06	-3.69	-2.61	0.00
444	0.00	-2.33	-2.01	0.00
445	-2.90	-2.67	-3.04	0.00
446	-3.54	-2.64	-1.97	0.00
447	-2.14	0.00	-3.39	2.07
448	-2.70	0.00	-3.79	0.00
449	-3.68	0.00	0.00	1.88
450	-3.72	0.00	0.00	3.52
451	-3.64	0.00	-1.64	3.47
452	0.00	-3.59	-2.72	0.00
453	-3.64	0.00	-3.00	1.55
454	0.00	-2.97	0.00	0.00
455	-3.61	-2.95	-1.74	2.87
456	-2.48	-2.46	-2.95	0.00
457	-2.12	-1.83	0.00	1.58
458	-2.51	-3.75	0.00	3.44
459	-3.67	0.00	-3.45	3.34
460	-2.43	-2.88	0.00	0.00
461	-3.48	0.00	0.00	0.00
462	0.00	-1.77	-3.49	1.79
463	-2.49	-2.95	-2.55	0.00
464	0.00	-2.46	0.00	0.00
465	-1.81	-1.57	0.00	0.00
466	-2.24	0.00	-1.51	0.00
467	-2.33	-3.05	0.00	2.06
468	0.00	-3.44	0.00	0.00
469	-1.88	0.00	0.00	1.91
470	-2.84	-3.65	-3.11	2.23
471	-3.66	-2.06	-1.59	2.02
472	-2.88	-2.51	-3.65	0.00
473	0.00	-1.96	-1.65	3.53
474	0.00	0.00	-3.59	3.33
475	-1.71	0.00	-1.49	3.69
476	-3.08	-2.38	-3.31	2.55
477	0.00	0.00	0.00	0.00
478	-2.08	0.00	-2.86	3.56
479	-1.72	0.00	0.00	3.10

480	-1.85	0.00	-2.92	1.99
481	0.00	-2.63	0.00	0.00
482	0.00	0.00	0.00	2.10
483	0.00	-2.72	0.00	3.38
484	-2.42	-2.59	0.00	2.37
485	-3.54	0.00	0.00	0.00
486	-1.59	-2.92	0.00	2.77
487	-2.47	-2.31	-1.60	1.75
488	-3.41	0.00	0.00	3.32
489	0.00	-2.81	-1.98	3.25
490	-2.25	-2.72	-1.97	2.86
491	0.00	0.00	-2.31	0.00
492	0.00	-3.74	0.00	3.37
493	-1.56	0.00	-2.07	0.00
494	-1.87	-1.62	0.00	1.63
495	-2.78	-1.91	-1.82	2.31
496	-1.58	0.00	-3.66	1.59
497	-2.46	0.00	0.00	3.06
498	-2.53	-1.56	-3.57	2.71
499	0.00	-3.53	-2.02	1.89

Appendix-V

GC-MS Method and Calibration Curve

Table A2: Specification of GC-MS system used for analysis of collected soil-water and soil vapor samples during different experiments of this study.

Sr. No.	Component	Description	Specification
1	Gas Chromatography	Company	Agilent Technologies, Inc.
		Model and Serial No.	Agilent 7890B, Sr. No. CN14133121
		Column type	Chrompack capillary column
		Column dimension	30m×0.25mm
		Column coating	Silicone, 0.25µm
		Column working temperature ranges	-60^0C to 350^0C
		Oven dimension	30×28cm
		Oven temperature ranges	-60^0C to 350^0C
2	Mass spectrometer detector	Model and Serial No.	G7040A/Agilent 5977A/US1416N306
		Mode	SCAN and SIM
		Mass Hunter IP	10.1.1.100
		High Vacuum Pressure	$4.87e^{-05}$
		Turbo pump speed	0-100%
		Operating System	1.2/26T
3	ALV System	Model and Serial No.	CN13500146
		Valve	16
		Wash Valve	02
		Solvent Valve	01
4	Gases	Company	Sigma Gas
	1. Helium (Carrier gases) 2. Nitrogen 3. Hydrogen 4. Air	Purity	99.999%
		Capacity	14 Kg
		Initial Pressure	2000 psi
		Regulator Pressure	100 psi

5	Gas Clean filter	Four filters	Oxygen filter (CP17970); Moisture filter (CP17971), Hydrocarbon filter (CP17972); Carrier gas filter(CP17973)
		Maximum pressure for all filter	15 bar/219 psi
6	Turbo Pump	Model No	X3700-60000 Sr. No. ITI317A055
		Power	50.60 Hz
7	Analysis software	Company	HP
		Windows	7
		Processor	Intel® Xeon ® CPU E3-1225@3.20GHz
		System type	64 bit operating system
		Printer	HP Laser Jet P3015
		Software Installed	Mass Hunter GC/MS Data Acquisition Version B.07.01
			Mass Hunter Qualitative Analysis Version B.07.00, Build 7.0.457.0
			NIST MS Search 2.0 (MS Library)
			MSD ChemStation Data Analysis

Table A3: Input parameters used to develop methods for toluene analysis in GC-MS system.

Sr. No.	Components	Parameter's	Input
1	Oven	Temperature	45^0C
		Temp. Rate	off
		Equilibration time	0.1 min
		Maximum Oven Temp	275^0C
		Hold time	5 min
		Run time	5 min
2	Column	Pressure	5.5 psi Constant Pressure
		Inlet	Aux PCM A
		Outlet	Front Detector
		Heated by	Oven
3	Thermal Aux 1	Type	Nickel Crystal

		Temperature	375^0C
4	Thermal Aux 1	Types	MSD Transfer line
		Temperature	250^0C
5	Inlets	Types	Split-Splitless Inlet
		Liner	Agilent 5183-4692/ 990µL (Split, straight liner with glass wool)
		Heater	250^0C
		Pressure	9.4667 psi
		Total flow	244.2mL/min
		Septum Purge Flow	3 mL/min
		Mode	Split
		Split Ratio	200:1
		Split Flow	240mL/min
6	ALS	Injection Type	Standard
		Injection	10µL Syringe
		Injection Volume	1 µL
		Solvent A Washes	Pre-Injection 1 µL
		Solvent B Washes	Post-Injection 1 µL
		Sample Washes	2
		Sample Pimps	2
		Dwell time	0 min
		Plunger Speed	Fast
		Viscosity Delay	0 Sec
7	MS Parameter	Target mass spectrum [SIM]	92,91
		MS Source Temp	250^0C
		MS Quad Temp	150^0C
		Turbo Speed	100%
		Hi Vacuum	$1.2*10^4$
		Turbo Pump Speed must be increasing upto 100%	
8	Carrier gases	Helium (99.999% pure) at 100 psi regulator pressure.	
9	Spectrum library	NIST Search 2.0 (Japan AIST/NIMC Database-Spectrum MS-NW-67)	
10	Ten largest peak	91 999 | 92 776 | 65 121 | 39 107 | 63 74 | 51 64 | 93 54 | 50 41 | 89 39 | 62 32 |	

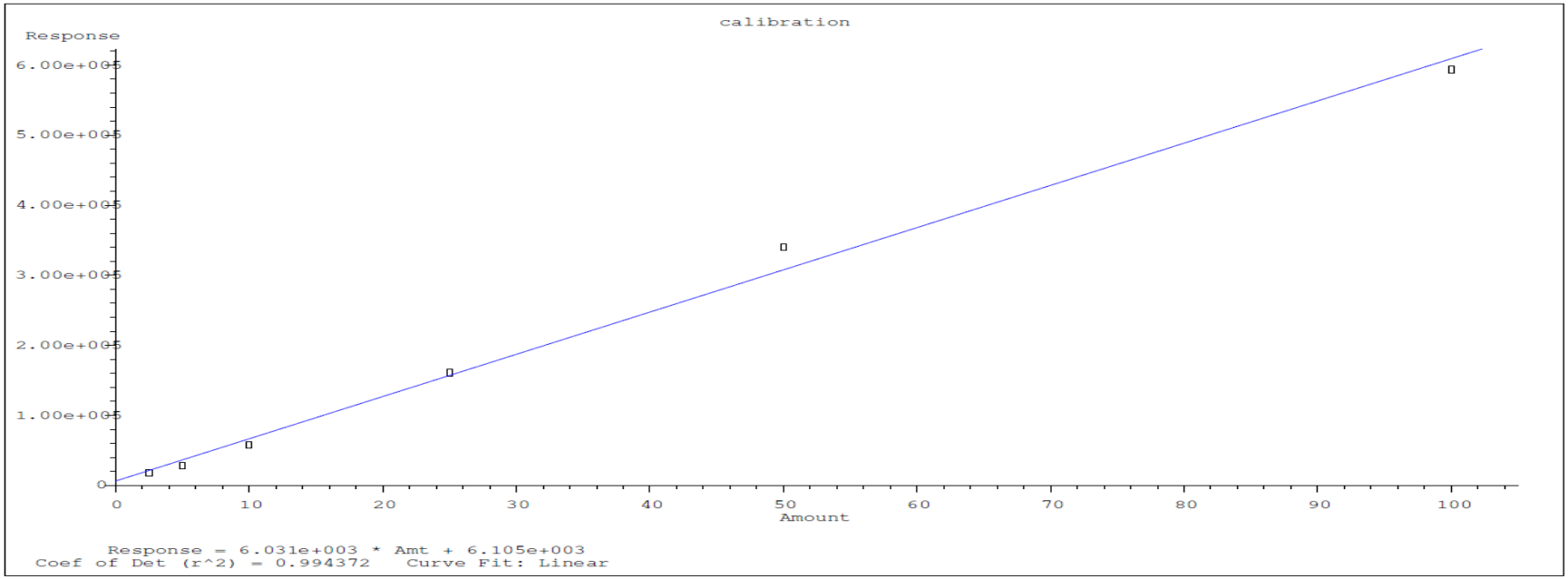

Figure A4: The calibration curve (response vs toluene concentrations) used to calibrate prepared method for toluene analysis in this study.

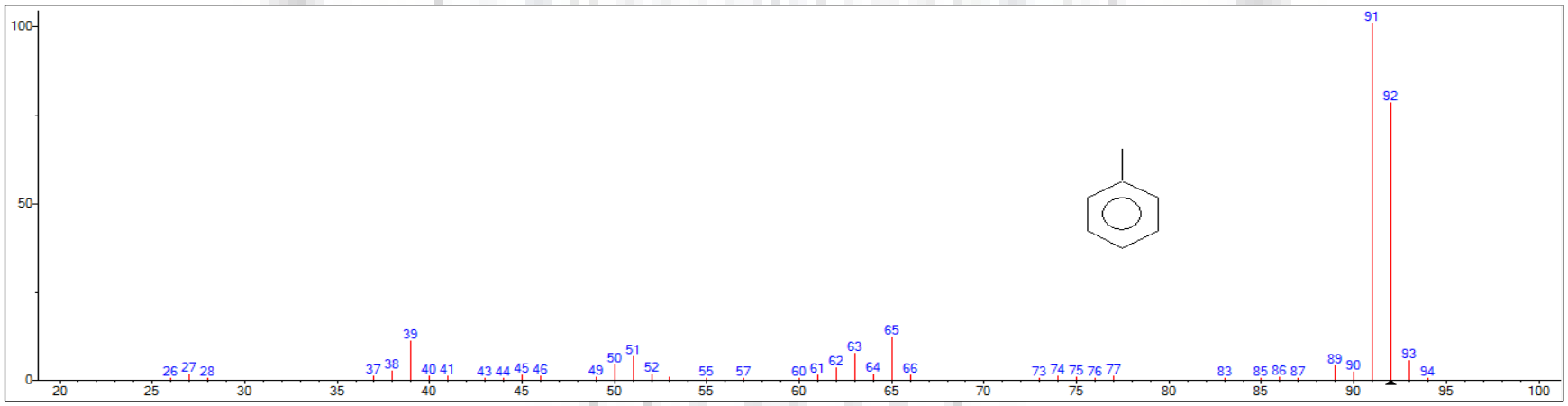

Figure A5: The mass spectrum used to match large peak (91,92) with prepared methods for toluene analysis.

Table A4: The area response with associated bias% obtained during calibration of prepared methods by different concentration of toluene.

Sr.No.	Concentration	Response (ratio)	bias%
1	2.5 ppm	17491.0000	-17.42
2	5 ppm	28421.0000	-21.61
3	10 ppm	57409.0000	-13.55
4	25 ppm	160923.0000	2.58
5	50 ppm	339840.0000	10.47
6	100 ppm	593427.0000	-2.58

References

.

Abou-Elela, S. I., Golinielli, G., Abou-Taleb, E. M., Hellal, M. S., (2013). Municipal wastewater treatment in horizontal and vertical flows constructed wetlands. *Ecoogical. Engginnering.* 61, 460-468. doi:10.1016/j.ecoleng.2013.10.010.

Al-Baldawi, I. A. W., Abdullah, S. R. S., Hasan, H. A., Suja, F., Anuar, N., and Mushrifah, I. (2014). Optimized conditions for phytoremediation of diesel by *Scirpus grossus* in horizontal subsurface flow constructed wetlands (HSFCWs) using response surface methodology. *Journal of Environmental Management*, *140*, 152-159.

Al-Baldawi, I. A. W., Abdullah, S. R. S., Suja, F., Anuar, N., and Mushrifah, I. (2013). Comparative performance of free surface and sub-surface flow systems in the phytoremediation of hydrocarbons using *Scirpus grossus*. *Journal of Environmental Management*, *130*, 324-330.

Al-Baldawi, I. A., Abdullah, S. R. S., Anuar, N., Suja, F., and Mushrifah, I. (2015). Phytodegradation of total petroleum hydrocarbon (TPH) in diesel-contaminated water using *Scirpus grossus*. *Ecological Engineering*, *74*, 463-473.

Albergaria, J. T., Maria da Conceição, M., and Delerue-Matos, C. (2012). Remediation of sandy soils contaminated with hydrocarbons and halogenated hydrocarbons by soil vapour extraction. *Journal of Environmental Management*, *104*, 195-201.

Alvarez, P. J. J., and Illman, W. A. (2006). Bioremediation and natural attenuation, process fundamentals and mathematical models. *Wiley-Interscience*, ISBN-10 0-471-65043-9.

Alvarez, P. J. J., and Vogel, T.M. (1995). Biodegradation of BTEX and their aerobic metabolise by indigenous microorganisms under nitrate reducing conditions. *Water Sciences Technology*, 3,1,15-28.

Alvarez, P. J., and Vogel, T. M. (1991). Substrate interactions of benzene, toluene, and para-xylene during microbial degradation by pure cultures and mixed culture aquifer slurries. *Applied and Environmental Microbiology*, *57*(10), 2981-2985.

Alvarez, P. J., Anid, P. J., and Vogel, T. M. (1991). Kinetics of aerobic biodegradation of benzene and toluene in sandy aquifer material. *Biodegradation*, *2*(1), 43-51.

Alvarez, P. J., Anid, P. J., and Vogel, T.M. (1994). Kinetics of toluene degradation by denitrifying aquifer microorganisms. *Journal of Environmental Engineering*, 120: 1327-1336.

Aly, A.H., Peralta, R. C. (1999). Optimal design of aquifer cleanup systems under uncertainty using a neural network and a genetic algorithm. *Water Resources Research*. 35 (8), 2523–2532.

American Public Health Association, and American Water Works Association. (1989). *Standard methods for the examination of water and wastewater*. American public health association.

Aral, M.M., Liao, B., (2002). Effect of groundwater table fluctuations on LNAPL thickness in monitoring wells. *Environmental Geology*, 42:151-161.

Atlas, R. M. (1991). Microbial hydrocarbon degradation and bioremediation of oil spills. *Journal of Chemical Technology and Biotechnology*, 52, 149–156.

Ávila, C., Garfí, M., and García, J. (2013). Three-stage hybrid constructed wetland system for wastewater treatment and reuse in warm climate regions. *Ecological Engineering*, *61*, 43-49.

Avila, C., Matamoros, V., Reyes-Contreras, C., Piña, B., Casado, M., Mita, L., and Bayona, J. M. (2014). Attenuation of emerging organic contaminants in a hybrid constructed wetland system under different hydraulic loading rates and their associated toxicological effects in wastewater. *Science of the Total Environment*, *470*, 1272-1280.

Azubuike, C.C., Chikere, C.B., and Okpokwasili, G.C. (2016). Bioremediation techniques–classification based on site of application: principles, advantages, limitations and prospects. *World Journal Microbiology Biotechnology*, 32: 180.

Babel, S., and Kurniawan, T. A. (2003). Low-cost adsorbents for heavy metals uptake from contaminated water: a review. *Journal of hazardous materials*, *97*(1-3), 219-243.

Baedecker, M.J., Eganhouse, R.P., Bekins, B.A., Delin, G.N. (2011). Loss of volatile hydrocarbons from an LNAPL oil source. *Journal of Contaminant Hydrology*. 126 (3-4), 140–152.

Baker, R.J., Baehr, A.L. and Lahvis, M.A. (2000). Estimation of hydrocarbon biodegradation rates in gasoline-contaminated sediment from measured respiration rates. *Journal of Contaminant Hydrology*, 41(1), pp.175–192.

Ballesteros, Jr, F., Vuong, T. H., Secondes, M. F., and Tuan, P. D. (2016). Removal efficiencies of constructed wetland and efficacy of plant on treating benzene. *Sustainable Environment Research*, *26*(2), 93-96.

Bao, W.M.J., Vogler, E.T., Chrysikopoulos, C.V. (2003). "Nonaqueous liquid pool dissolution in three-dimensional heterogeneous subsurface formations, *Environ. Geol*. 43 (2003) 968–977.

Basu, S., Yadav, B. K., and Mathur, S. (2015). Enhanced bioremediation of BTEX contaminated groundwater in pot-scale wetlands. *Environmental Science and Pollution Research*, *22*(24), 20041-20049.

Basu, S., Yadav, B. K., and Mathur, S. (2017). Modeling Systems and Processes in Wetlands: A Case Study of Engineered Bioremediation of BTEX-Contaminated Water in Treatment Wetlands. In *Wetland Science* (pp. 463-488). Springer, New Delhi.

Bedessem, M. E., Ferro, A. M., and Hiegel, T. (2007). Pilot-Scale Constructed Wetlands for Petroleum-Contaminated Groundwater. *Water Environment Research*, *79*(6), 581–586.

Bento, F. M., Camargo, F. A. O., Okeke, B. C., and Frankenberger, W. T. (2005). Comparative bioremediation of soils contaminated with diesel oil by natural attenuation, biostimulation and bioaugmentation. *Bioresource Technology*, *96*(9), 1049–55.

Boonsaner, M., Borrirukwisitsak, S., and Boonsaner, A. (2011). Phytoremediation of BTEX contaminated soil by *Canna× generalis*. *Ecotoxicology and Environmental Safety*, *74*(6), 1700-1707.

Borden, R. C., and Kao, C. M. (1992). Evaluation of groundwater extraction for remediation of petroleum-contaminated aquifers. *Water Environment Research*, *64*(1), 28-36.

Borden, R.C., Bedient, P.B., (1986). Transport of dissolved hydrocarbons influenced by oxygen-limited bioremediation. 1. Theoretical development. *Water Resources Research*. 22 (13), 1973–1990.

Borsi, I., Rossetto, R., and Foglia, L. (2015). FREEWAT-FREE and open source software tools for WATer resource management: and Horizon 2020 for promoting innovative ICT tools in water management. *Acque Sotterranee-Italian Journal of Groundwater*, *4*(2).

Bossert, I., Kachel, W. M., and Bartha, R. (1984). Fate of hydrocarbons during oily sludge disposal in soil. *Applied and Environmental Microbiology*, *47*(4), 763-767.

Brusseau, M. L., Zhang, Z., Nelson, N. T., Cain, R. B., Tick, G. R., and Oostrom, M. (2002). Dissolution of nonuniformly distributed immiscible liquid: intermediate-scale experiments and mathematical modeling. *Environmental Science and Technology*, *36*(5), 1033-1041.

Burken, J. G., and Schnoor, J. L. (1998). Predictive Relationships for Uptake of Organic Contaminants by Hybrid Poplar Trees. *Environmental Science and Technology*. *32*(21), 3379–3385.

Calheiros, C. S., Rangel, A. O., and Castro, P. M. (2007). Constructed wetland systems vegetated with different plants applied to the treatment of tannery wastewater. *Water Research*, *41*(8), 1790-1798.

Cardiff, M., Liu, X., Kitanidis, P. K., Parker, J., and Kim, U. (2010). Cost optimization of DNAPL source and plume remediation under uncertainty using a semi-analytic model. *Journal of Contaminant Hydrology*, *113*(1-4), 25-43.

Chabukdhara, M., Munjal, A., Nema, A. K., Gupta, S. K., and Kaushal, R. K. (2016). Heavy metal contamination in vegetables grown around peri-urban and urban-industrial clusters in Ghaziabad, India. *Human and Ecological Risk Assessment: An International Journal*, *22*(3), 736-752.

Chabukdhara, M., Munjal, A., Nema, A. K., Gupta, S. K., and Kaushal, R. K. (2016). Heavy metal contamination in vegetables grown around peri-urban and urban-industrial clusters in Ghaziabad, India. *Human and Ecological Risk Assessment: An International Journal*, *22*(3), 736-752.

Chapelle, F. H. (1999). Bioremediation of petroleum hydrocarbon-contaminated ground water: The perspectives of history and hydrology. *Groundwater*, *37*(1), 122-132.

Chavan, A., Mukherji, S., (2008). Treatment of hydrocarbon-rich wastewater using oil degrading bacteria and phototrophic microorganisms in rotating biological contactor: Effect of N:P ratio. *J. Hazard Mater.* 154, 63–72.

Chen, M. M., Zhu, Y. G., Su, Y. H., Chen, B. D., Fu, B. J., and Marschner, P. (2007). Effects of soil moisture and plant interactions on the soil microbial community structure. *European Journal of Soil Biology*, *43*(1), 31-38.

Chen, Z., Kuschk, P., Reiche, N., Borsdorf, H., Kästner, M., and Köser, H. (2012). Comparative evaluation of pilot scale horizontal subsurface-flow constructed wetlands and plant root mats for treating groundwater contaminated with benzene and MTBE. *Journal of hazardous materials*, *209*, 510-515.

Chrysikopoulos, C. V. (1995). Three-dimensional analytical models of contaminant transport from nonaqueous phase liquid pool dissolution in saturated subsurface formations. *Water Resources Research*, *31*(4), 1137-1145.

Chrysikopoulos, C. V., Voudrias, E. A., and Fyrillas, M. M. (1994). Modeling of contaminant transport resulting from dissolution of nonaqueous phase liquid pools in saturated porous media. *Transport in Porous Media*, *16*(2), 125-145.

Chrysikopoulos, C.V., P. Y., Hsuan, M.M., Fyrillas, K.Y., Lee. (2003). Mass transfer coefficient and concentration boundary layer thickness for a dissolving NAPL pool in porous media. *Journal of Hazardous Materials*. 97 (1) pp. 245-255.

Corseuil, H. X., and Alvarez, P. J. (1996). Natural bioremediation perspective for BTX-contaminated groundwater in Brazil: effect of ethanol. *Water Science and Technology*, *34*(7), 311-318.

Corseuil, H., Weber, W. (1994). Potential biomass limitations on rates of degradation of monoaromatic hydrocarbons by indigenous microbes in subsurface soils. *Water Research*, 28, 1415–1423.

Coulon, F., McKew, B. A., Osborn, A M., McGenity, T. J., and Timmis, K. N. (2007). Effects of temperature and biostimulation on oil-degrading microbial communities in temperate estuarine waters. *Environmental Microbiology*, *9*(1), 177–86.

Cunningham, J. A., Rahme, H., Hopkins, G. D., Lebron, C., and Reinhard, M. (2001). Enhanced In Situ Bioremediation of BTEX-Contaminated Groundwater by Combined Injection of Nitrate and Sulfate. *Environmental Science and Technology*, *35*(8), 1663–1670.

D'Alessio, M. J. Lichwa, D. Vasudevan, S.K. Mohanty, and C., Ray. (2014). Fate and transport of selected endocrine disrupting chemicals in the tropical soils of Hawaii, *Journal of Contaminant Hydrology*, 166: 1-10.

Da Silva, M. L., and Alvarez, P. J. (2002). Effects of ethanol versus MTBE on benzene, toluene, ethylbenzene, and xylene natural attenuation in aquifer columns. *Journal of Environmental Engineering*, *128*(9), 862-867.

Da Silva, M.L.B., Alvarez, P.J.J. (2004). Enhanced anaerobic biodegradation of benzene–toluene–ethylbenzene–xylene–ethanol mixtures in bioaugmented aquifer columns. *Applied Environmental Microbiology*, 70:4720–4726

D'Alessio, M., Yoneyama, B., and Ray, C. (2015). Fate of selected pharmaceutically active compounds during simulated riverbank filtration. *Science of the Total Environment*, *505*, 615-622.

Das, D. B. (2002). Hydrodynamic modelling for groundwater flow through permeable reactive barriers. *Hydrological Processes*, *16*(17), 3393-3418.

Das, D. B., and Mirzaei, M. (2012). Dynamic effects in capillary pressure relationships for two-phase flow in porous media: Experiments and numerical analyses. *AIChE Journal*, *58*(12), 3891-3903.

Das, D. B., and Nassehi, V. (2003). Modeling of contaminants mobility in underground domains with multiple free/porous interfaces. *Water Resources Research*, *39*(3).

Das, D. B., Hassanizadeh, S. M., Rotter, B. E., and Ataie-Ashtiani, B. (2004). A numerical study of micro-heterogeneity effects on upscaled properties of two-phase flow in porous media. *Transport in Porous Media*, *56*(3), 329-350.

Das, D. B., Nassehi, V., and Wakeman, R. J. (2002). A finite volume model for the hydrodynamics of combined free and porous flow in sub-surface regions. *Advances in Environmental Research*, *7*(1), 35-58.

Davis, C., Cort, T., Dai, D., Illangasekare, T. H., and Munakata-Marr, J. (2003). Effects of heterogeneity and experimental scale on the biodegradation of diesel. *Biodegradation*, *14*(6), 373-384.

Davis, J. W., and Madsen, S. (1996). Factors affecting the biodegradation of toluene in soil. *Chemosphere*, *33*(1), 107-130.

Deeb, R. A., and Alvarez-Cohen, L. (1999). Temperature effects and substrate interactions during the aerobic biotransformation of BTEX mixtures by toluene-enriched consortia and *Rhodococcus rhodochrous*. *Biotechnology and Bioengineering*, *62*(5), 526-536.

Dempster, H.S., Sherwood-Lollar, B., Feenstra, S., (1997). Tracing organic contaminants in groundwater: a new methodology using compound-specific isotopic analysis. *Environmental Science and Technology*, 31, 3193–3197.

Di Martino, C., López, N. I., and Iustman, L. J. R. (2012). Isolation and characterization of benzene, toluene and xylene degrading Pseudomonas sp. selected as candidates for bioremediation. *International Biodeterioration and Biodegradation*, *67*, 15-20.

Dibble, J. T., and Bartha, R. (1979). Effect of environmental parameters on the biodegradation of oil sludge. *Applied and environmental microbiology*, *37*(4), 729-739.

Dittmer, U., Meyer, D., and Langergraber, G. (2005). Simulation of a subsurface vertical flow constructed wetland for CSO treatment. *Water Science and Technology*, *51*(9), 225-232.

Dobson, R., M.H., Schroth, and J., Zeyer. (2007). Effect of water-table fluctuation on dissolution on and biodegradation of a multi-component, light nonaqueous-phase liquid. *Journal of Contaminant Hydrology*, 94:235–248.

Dzantor, E. K. (2007). Phytoremediation: the state of rhizosphere 'engineering' for accelerated rhizodegradation of xenobiotic contaminants. *Journal of Chemical Technology and Biotechnology: International Research in Process, Environmental and Clean Technology*, *82*(3), 228-232.

Eckert, P., Appelo, C. A., (2002). Hydrogeochemical modeling of enhanced benzene, toluene, ethylbenzene, xylene (BTEX) remediation with nitrate. *Water Resourse Research*, 38, 5-11. doi:10.1029/2001WR000692.

Eke, P. E., and Scholz, M. (2008). Benzene removal with vertical-flow constructed treatment wetlands. *Journal of Chemical Technology and Biotechnology: International Research in Process, Environmental and Clean Technology*, *83*(1), 55-63.

Essaid, H. I., Bekins, B.A., Cozzarelli, I.M., (2015). Organic contaminant transport and fate in the subsurface: evolution of knowledge and understanding. *Water Resources Research*. 51(7), 4861–4902.

EUGRIS (2007). Further Description: Benzene, Toluene, Ethylbenzene and Xylene http://www.eugris.info/eugrismain.asp?eugrisid=6&Category=Content_Digests.

Fagerlund, F., A., Niemi, and T. H., Illangasekare (2008). Modeling of nonaqueous phase liquid (NAPL) migration in heterogeneous saturated media: Effects of hysteresis and fluid immobility in constitutive relations. *Water Resource Research*, 44, W03409.

Fagerlund, F., Illangasekare, T. H., and Niemi, A. (2007). Nonaqueous-phase liquid infiltration and immobilization in heterogeneous media: 1. Experimental methods and two-layered reference case. *Vadose Zone Journal*, *6*(3), 471-482.

Farhadian, M., Vachelard, C., Duchez, D., and Larroche, C. (2008). In situ bioremediation of monoaromatic pollutants in groundwater: a review. *Bioresource Technology*, *99*(13), 5296–308.

Fetter, C. W. (1994). Applied Hydrogeology (Third ed.). Macmillan College Publishing Company, New York, NY, USA.

Filho, N. I., Vieceli, N. C., Cardoso, E. M., and Lovatel, E. R. (2013). Analysis of BTEX in experimental columns containing neat gasoline and gasoline-ethanol. *Journal of the Brazilian Chemical Society*, *24*(3), 410-417.

Franzetti, a, Di Gennaro, P., Bestetti, G., Lasagni, M., Pitea, D., and Collina, E. (2008). Selection of surfactants for enhancing diesel hydrocarbons-contaminated media bioremediation. *Journal of Hazardous Materials*, *152*(3), 1309–16.

Frutos, F. J. G, Escolano O, Garcı´a S, Mar Babı´n M, Ferna´ndez MD. (2010). Bioventing remediation and ecotoxicity evaluation of phenanthrene-contaminated soil. *Journal Hazardous Material*, 183:806–813.

Fuentes, S, Méndez, V, Aguila, P, and Seeger, M. (2014). Bioremediation of petroleum hydrocarbons: catabolic genes, microbial communities, and applications. *Applied Microbiology and Biotechnology* 98: 4781-4794.

Garg, S., Newell, C. J., Kulkarni, P. R., King, D. C., Adamson, D. T., Renno, M. I., and Sale, T. (2017). Overview of natural source zone depletion: Processes, controlling factors, and composition change. *Groundwater Monitoring and Remediation*, 37(3), 62-81.

Gupta, P.K., and Yadav, B.K. (2017). Bioremediation of non-aqueous phase liquids (NAPLs) polluted soil-water resources chapter 8 in Environmental Pollutants and their Bioremediation Approaches, Bharagava, Ram Naresh, ed. CRC Press, 2017 .

Harms, H. (1996). Bacterial growth on distant naphthalene diffusing through water, air, and water-saturated and nonsaturated porous media. *Applied and environmental microbiology*, *62*(7), 2286-2293.

He, J., Ritalahti, K. M., Aiello, M. R., and Löffler, F. E. (2003a). Complete detoxification of vinyl chloride by an anaerobic enrichment culture and identification of the reductively dechlorinating population as a Dehalococcoides species. *Applied and Environmental Microbiology*, *69*(2), 996-1003.

He, J., Ritalahti, K. M., Yang, K. L., Koenigsberg, S. S., and Löffler, F. E. (2003b). Detoxification of vinyl chloride to ethene coupled to growth of an anaerobic bacterium. *Nature*, *424*(6944), 62.

He, J., Robrock, K. R., and Alvarez-Cohen, L. (2006). Microbial reductive debromination of polybrominated diphenyl ethers (PBDEs). *Environmental Science and Technology*, *40*(14), 4429-4434.

Henrichs, M., Langergraber, G., and Uhl, M. (2007). Modelling of organic matter degradation in constructed wetlands for treatment of combined sewer overflow. *Science of the Total Environment*, *380*(1-3), 196-209.

Höhener, P., Duwig, C., Pasteris, G., Kaufmann, K., Dakhel, N., and Harms, H. (2003). Biodegradation of petroleum hydrocarbon vapors: laboratory studies on rates and kinetics in unsaturated alluvial sand. *Journal of Contaminant Hydrology*, *66*(1-2), 93-115.

Holden, P. A., Halverson, L. J., and Firestone, M. K. (1997). Water stress effects on toluene biodegradation by Pseudomonas putida. *Biodegradation*, *8*(3), 143-151.

Holden, P. A., Hersman, L. E., and Firestone, M. K. (2001). Water content mediated microaerophilic toluene biodegradation in arid vadose zone materials. *Microbial Ecology*, *42*(3), 256-266.

Holman, H. Y., and Tsang, Y. W. (1995). Influence of soil moisture on biodegradation of petroleum hydrocarbons. In situ aeration: air sparging, bioventing, and related remediation processes, Colombus: Battelle. (Eds.) R. E. Hinchee, R. N. Miller, and P. C. Johnson. 323–332.

Horel, A., Schiewer, S., and Misra, D. (2015). Effect of concentration gradients on biodegradation in bench-scale sand columns with HYDRUS modeling of hydrocarbon transport and degradation. *Environmental Science and Pollution Research*, *22*(17), 13251-13262.

Huang, G. B., Zhu, Q. Y., and Siew, C. K. (2006). Extreme learning machine: theory and applications. *Neurocomputing*, *70*(1-3), 489-501.

Huang, X.D., El-Alawi, Y., Penrose, D. M., Glick, B. R., and Greenberg, B. M. (2004). A multi-process phytoremediation system for removal of polycyclic aromatic hydrocarbons from contaminated soils. *Environmental Pollution. 130*(3), 465–76.

Illangasekare, T. H., E. J. Armbruster, D. N. Yates, (1995). Non-aqueous-phase fluids in heterogeneous aquifers - Experimental study. *Journal of Environmental Engineering*, vol. 121, pp. 571-579, 1995.

Imfeld, G., Braeckevelt, M., Kuschk, P., Richow, H. H., (2009). Monitoring and assessing processes of organic chemicals removal in constructed wetlands. *Chemosphere.* 74, 349-362.

Imhoff, P. T., Mann, A. S., Mercer, M., and Fitzpatrick, M. (2003). Scaling DNAPL migration from the laboratory to the field. *Journal of Contaminant Hydrology*, *64*(1-2), 73-92.

Jha, M. K., Chikamori, K., Kamii, Y., and Yamasaki, Y. (1999). Field investigations for sustainable groundwater utilization in the Konan basin. *Water Resources Management*, *13*(6), 443-470.

Jo, M. S., Rene, E. R., Kim, S. H., and Park, H. S. (2008). An analysis of synergistic and antagonistic behaviour during BTEX removal in batch system using response surface methodology. *Journal of Hazardous Materials*, *152*(3), 1276-1284.

Kamaruddin SA, Sulaiman WNA, Rahman NA, Zakaria MP, Mustaffar M, Sa'ari R. (2011). A review of laboratory and numerical simulations of hydrocarbons migration in subsurface environments. *Journal of Environmental Science and Technology*. 4(3), 191–214.

Kechavarzi, C., Soga, K., and Illangasekare, T. H. (2005). Two-dimensional laboratory simulation of LNAPL infiltration and redistribution in the vadose zone. *Journal of Contaminant Hydrology*, *76*(3-4), 211-233.

Kechavarzi, C., Soga, K., Illangasekare, T., and Nikolopoulos, P. (2008). Laboratory study of immiscible contaminant flow in unsaturated layered sands. *Vadose Zone Journal*, *7*(1), 1-9.

Khan, A. M., Wick, L. Y., Harms, H., and Thullner, M. (2016). Biodegradation of vapor-phase toluene in unsaturated porous media: Column experiments. *Environmental Pollution*, *211*, 325-331.

Khan, F. I., Husain, T., and Hejazi, R. (2004). An overview and analysis of site remediation technologies. *Journal of Environmental Management*, 71(2), 95-122.

Khodaei, K., Nassery, H. R., Asadi, M. M., Mohammadzadeh, H., and Mahmoodlu, M. G. (2017). BTEX biodegradation in contaminated groundwater using a novel strain (*Pseudomonas sp*. BTEX-30). *International Biodeterioration and Biodegradation*, *116*, 234-242.

Kim, J., Corapcioglu, M.Y. (2003). Modeling dissolution and volatilization of LNAPL sources migrating on the groundwater table. *Journal of Contaminant Hydrology*, 65, 137–158.

Kruger, A., Ulbrich, U., Speth, P. (2001). Groundwater recharge in Northrhine-Westfalia predicted by a statistical model for greenhouse gas scenarios. *Physics and Chemistry of the Earth, Part B: Hydrology, Oceans and Atmosphere*, 26: 853–861.

Kulkarni, P. R., King, D. C., McHugh, T. E., Adamson, D. T., and Newell, C. J. (2017). Impact of temperature on groundwater source attenuation rates at hydrocarbon sites. *Groundwater Monitoring and Remediation*, 37(3), 82-93.

Kumar K., T. L., van Noorden, and I. S., Pop. (2011). Effective dispersion equations for reactive flows involving free boundaries at the microscale. *Multiscale Modelling Simulation*, 9(1):29–58.

Kumar, A., Datta, M., Nema, A. K., and Singh, R. K. (2016). An improved rating system for assessing surface water contamination potential from MSW landfills. *Environmental Modeling and Assessment*, *21*(4), 489-505.

Kumar, D., Ch, S., Mathur, S., Adamowski, J., (2015). Multi-objective optimization of in-situ bioremediation of groundwater using a hybrid metaheuristic technique based on differential evolution, genetic algorithms and simulated annealing. *Journal of Water and Land Development*. 27 (1), 29–40.

Kumar, D., Prasad, R. K., and Mathur, S. (2013). Optimal design of an in-situ bioremediation system using support vector machine and particle swarm optimization. *Journal of Contaminant Hydrology*, *151*, 105-116.

Kumar, R., Das, A.J., and Lal, S. (2015). Petroleum Hydrocarbon Stress Management in Soil Using Microorganisms and Their Products. In *Environmental Waste Management*, Chandra, R. (Eds.), CRC Press, Taylor and Francis Group, Boca Raton, FL, USA, pp. 525-550.

Kurniawan, T. A., Chan, G. Y., Lo, W. H., and Babel, S. (2006). Physico–chemical treatment techniques for wastewater laden with heavy metals. *Chemical Engineering Journal*, *118*(1-2), 83-98.

Langergraber, G., and Šimůnek, J. (2005). Modeling variably saturated water flow and multicomponent reactive transport in constructed wetlands. *Vadose Zone Journal*, *4*(4), 924-938.

Legout, C., Molenat, J., and Hamon, Y. (2009). Experimental and modeling investigation of unsaturated solute transport with water-table fluctuation. *Vadose Zone Journal*, *8*(1), 21-31.

Lenhard, R. J., Oostrom, M., and Dane, J. H. (2004). A constitutive model for air–NAPL–water flow in the vadose zone accounting for immobile, non-occluded (residual) NAPL in strongly water-wet porous media. *Journal of Contaminant Hydrology*, *71*(1-4), 261-282.

Liang, F., Lu, M., Keener, T. C., Liu, Z., and Khang, S. J. (2005). The organic composition of diesel particulate matter, diesel fuel and engine oil of a non-road diesel generator. *Journal of Environmental Monitoring*, *7*(10), 983-988.

MacDonald, A. M., Bonsor, H. C., Ahmed, K. M., Burgess, W. G., Basharat, M., Calow, R. C., ... and Lark, R. M. (2016). Groundwater quality and depletion in the Indo-Gangetic Basin mapped from in situ observations. *Nature Geoscience*, *9*(10), 762-766.

Machiwal, D., and Jha, M. K. (2015). Identifying sources of groundwater contamination in a hard-rock aquifer system using multivariate statistical analyses and GIS-based geostatistical modeling techniques. *Journal of Hydrology: Regional Studies*, *4*, 80-110.

Margesin, R. (2000). Potential of cold-adapted microorganisms for bioremediation of oil-polluted Alpine soils. *International Biodeterioration and Biodegradation*, *46*(1), 3-10.

Margesin, R., and Schinner, F. (2001). Biodegradation and bioremediation of hydrocarbons in extreme environments. *Applied Microbiology and Biotechnology*, *56*(5-6), 650–663. doi:10.1007/s002530100701.

Martínez-Lavanchy, P. M., Chen, Z., Lünsmann, V., Marin-Cevada, V., Vilchez-Vargas, R., Pieper, D. H., ... and Nijenhuis, I. (2015). Microbial toluene removal in hypoxic model constructed wetlands occurs predominantly via the ring monooxygenation pathway. *Applied and Environmental Microbiology*, AEM-01822.

Mathur, S., and Yadav, B. K. (2009). Phytoextraction modeling of heavy metal (lead) contaminated site using maize (*Zea mays*). *Practice Periodical of Hazardous, Toxic, and Radioactive Waste Management*, *13*(4), 229-238.

Mazzeo, D. E. C., Levy, C. E., de Angelis, D. D. F., and Marin-Morales, M. A. (2010). BTEX biodegradation by bacteria from effluents of petroleum refinery. *Science of the Total Environment*, *408*(20), 4334-4340.

Mercer, J. W. and R. M. Cohen. (1990). A Review of Immiscible Fluids in the Subsurface: Properties, Models, Characterization and Remediation. *Journal of Contaminant Hydrology*, 6, pp. 107-163.

Meyer, D., Chazarenc, F., Claveau-Mallet, D., Dittmer, U., Forquet, N., Molle, P., ... and Campà, R. S. (2015). Modelling constructed wetlands: scopes and aims–a comparative review. *Ecological Engineering*, *80*, 205-213.

Miller, C.T., Poirier-McNeil, M.M., and Mayer, A.S. (1990). Dissolution of trapped nonaqueous phase liquids: Mass transfer characteristics. *Water Resources Research*, 26(11), pp.2783–2796.

Mirzaei, M., and Das, D. B. (2007). Dynamic effects in capillary pressure–saturations relationships for two-phase flow in 3D porous media: Implications of micro-heterogeneities. *Chemical engineering science*, *62*(7), 1927-1947.

Mobile, M. A., Widdowson, M. A., and Gallagher, D. L. (2012). Multicomponent NAPL source dissolution: Evaluation of mass-transfer coefficients. *Environmental Science and Technology*, *46*(18), 10047-10054.

Mohanty, S., Jha, M. K., Kumar, A., and Panda, D. K. (2013). Comparative evaluation of numerical model and artificial neural network for simulating groundwater flow in Kathajodi–Surua Inter-basin of Odisha, India. *Journal of Hydrology*, *495*, 38-51.

Morlett-Chávez, J. A., Ascacio-Martínez, J. Á., Rivas-Estilla, A. M., Velázquez-Vadillo, J. F., Haskins, W. E., Barrera-Saldaña, H. A., and Acuña-Askar, K. (2010). Kinetics of BTEX biodegradation by a microbial consortium acclimatized to unleaded gasoline and bacterial strains isolated from it. *International Biodeterioration and Biodegradation*, *64*(7), 581-587.

Mulkins-Phillips, G. J., and Stewart, J. E. (1974). Distribution of hydrocarbon-utilizing bacteria in Northwestern Atlantic waters and coastal sediments. *Canadian Journal of Microbiology*, *20*(7), 955-962.

Mustafa, A., Azim, M. K., Raza, Z., and Kori, J. A. (2018). BTEX removal in a modified free water surface wetland. *Chemical Engineering Journal*, *333*, 451-455.

Mustapha, H. I., Gupta, P. K., Yadav, B. K., van Bruggen, J. J. A., and Lens, P. N. L. (2018). Performance evaluation of duplex constructed wetlands for the treatment of diesel contaminated wastewater. *Chemosphere*, *205*, 166-177.

Mustapha, H. I., Van Bruggen, J. J. A., and Lens, P. N. L. (2015). Vertical subsurface flow constructed wetlands for polishing secondary Kaduna refinery wastewater in Nigeria. *Ecological Engineering*, *84*, 588-595.

Mustapha, H. I., van Bruggen, J. J. A., and Lens, P. N. L. (2018). Optimization of Petroleum Refinery Wastewater Treatment by Vertical Flow Constructed Wetlands Under Tropical Conditions: Plant Species Selection and Polishing by a Horizontal Flow Constructed Wetland. *Water, Air, and Soil Pollution*, *229*(4), 137.

Nagarajan, K., and Loh, K. C. (2015). Formulation of microbial cocktails for BTEX biodegradation. *Biodegradation*, *26*(1), 51-63.

Nambi, I. M., and Powers, S. E. (2000). NAPL dissolution in heterogeneous systems: an experimental investigation in a simple heterogeneous system. *Journal of Contaminant Hydrology*, *44*(2), 161-184.

Nambi, I. M., and Powers, S. E. (2003). Mass transfer correlations for nonaqueous phase liquid dissolution from regions with high initial saturations. *Water Resources Research*, *39*(2).

Narayanan, M., Tracy, J. C., Davis, L. C., and Erickson, L. E. (1998a). Modeling the fate of toluene in a chamber with alfalfa plants 1. Theory and modeling concepts, *Journal of Hazardous Substance Research*. 1, 1–30.

Narayanan, M., Tracy, J. C., Davis, L. C., and Erickson, L. E. (1998b). Modeling the fate of toluene in a chamber with alfalfa plants 2. Numerical results and comparison study, *Journal of Hazardous Substance Research*. *1*(1994).

Nema, A. K., and Gupta, S. K. (1999). Optimization of regional hazardous waste management systems: an improved formulation. *Waste Management*, *19*(7-8), 441-451.

Nema, A. K., and Gupta, S. K. (2003). Multiobjective risk analysis and optimization of regional hazardous waste management system. *Practice Periodical of Hazardous, Toxic, and Radioactive Waste Management*, *7*(2), 69-77.

Nerantzis, P. C., and Dyer, M. R. (2010). Transport of BTEX vapours through granular soils with different moisture contents in the vadose zone. *Geotechnical and Geological Engineering*, *28*(1), 1-13.

Nesheli, A. S., Haddad, O. B., and Loáiciga, H. A. (2015). Optimal in situ bioremediation design of groundwater contaminated with dissolved petroleum hydrocarbons. *Journal of Hazardous, Toxic, and Radioactive Waste*, *20*(2), 04015021.

Olson, M. R., and Sale, T. C. (2015). Implications of soil mixing for NAPL source zone remediation: Column studies and modeling of field-scale systems. *Journal of contaminant hydrology*, *177*, 206-219.

Oostrom M., Hofstee, C., and Wietsma, T.W. (2000). LNAPLs do not Always Float: An Example Case of a Viscous LNAPL under Variable Water Table Conditions, Hydrology Days. 121.

Oostrom, M., Dane, J. H., and Wietsma, T. W. (2007). A review of multidimensional, multifluid, intermediate-scale experiments: Flow behavior, saturation imaging, and tracer detection and quantification. *Vadose Zone Journal*, *6*(3), 610-637.

Oostrom, M., Hofstee, C., and Wietsma, T. W. (2006). Behavior of a viscous LNAPL under variable water table conditions. *Soil and Sediment Contamination*, *15*(6), 543-564.

Papendick, R. I., and Campbell, G. S. (1981). Theory and measurement of water potential. In 'Water potential relations in soil microbiology'.(Eds JF Parr, WR Gardiner, LF Elliott) pp. 1–22. SSSA Special Publication Number 9. *Soil Science Society of America: Madison, WI*.

Patterson, B. M., and Davis, G. B. (2009). Quantification of vapor intrusion pathways into a slab-on-ground building under varying environmental conditions. *Environmental Science and Technology*, *43*(3), 650-656.

Perfumo, A., Banat, I. M., Marchant, R., and Vezzulli, L. (2007). Thermally enhanced approaches for bioremediation of hydrocarbon-contaminated soils. *Chemosphere*, *66*(1), 179-184.

Petersen, L. W., Rolston, D. E., Moldrup, P., and Yamaguchi, T. (1994). Volatile organic vapor diffusion and adsorption in soils. *Journal of Environmental Quality*, *23*(4), 799-805.

Picone, S., Grotenhuis, T., Van Gaans, P., Valstar, J., Langenhoff, A. and Rijnaarts, H. (2013). Toluene biodegradation rates in unsaturated soil systems versus liquid batches and their relevance to field conditions. *Applied Microbiology and Biotechnology*, 97, 7887-7898.

Poi, G., Shahsavari, E., Aburto-Medina, A., Mok, P. C., and Ball, A. S. (2018). Large scale treatment of total petroleum-hydrocarbon contaminated groundwater using bioaugmentation. *Journal of Environmental Management*, *214*, 157-163.

Popp, N., Schlömann, M., and Mau, M. (2006). Bacterial diversity in the active stage of a bioremediation system for mineral oil hydrocarbon-contaminated soils. *Microbiology (Reading, England)*, *152*(Pt 11), 3291–304. doi:10.1099/mic.0.29054-0.

Power, S.E., and Heermann, S.E. (1999). Potential ground and surface water impacts, appendix B: Modeling interface mass-transfer processes presented in "A critical review: the effect of ethanol in gasoline on the fate and transport of BTEX in the subsurface", Editors Cannon G. and Rice D., UCRL-AR-135949 Vol.4, chapter 2.

Powers, S. E., Abriola, L. M., and Weber, W. J. (1992). An experimental investigation of nonaqueous phase liquid dissolution in saturated subsurface systems: Steady state mass transfer rates. *Water Resources Research*, 28(10), 2691-2705.

Powers, S.E., Abriola, L.M., Weber Jr., W.J. (1994). An experimental investigation of nonaqueous phase liquid dissolution in saturate subsurface systems: transient mass transfer rate. *Water Resource Research*, 30 (2), 321 – 332.

Prado, A. G., and Airoldi, C. (1999). The influence of moisture on microbial activity of soils. *Thermochimica Acta*, *332*(1), 71-74.

Pramer, D., and Bartha, R. (1972). Preparation and processing of soil samples for biodegradation studies. *Environmental Letters*, *2*(4), 217-224.

Prasad, R. K., and Mathur, S. (2007). Groundwater flow and contaminant transport simulation with imprecise parameters. *Journal of irrigation and drainage engineering*, *133*(1), 61-70.

Prasad, R. K., and Mathur, S. (2008). Potential well locations in in situ bioremediation design using neural network embedded Monte Carlo approach. *Practice Periodical of Hazardous, Toxic, and Radioactive Waste Management*, *12*(4), 260-269.

Prasad, R. K., and Mathur, S. (2009). Health-risk-based remedial alternatives for contaminated aquifer management. *Practice Periodical of Hazardous, Toxic, and Radioactive Waste Management*, *14*(1), 61-69.

Prommer, H., Barry, D. A., and Zheng, C. (2003). MODFLOW/MT3DMS-based reactive multicomponent transport modeling. *Groundwater*, *41*(2), 247-257.

Rahman, M. A. (2008). Scale-Up of Perforation Process from Laboratory Model to Bottom Hole Dimensions. *Journal of Porous Media*, *11*(1).

Rahman, M. A., Adane, K. F., and Sanders, R. S. (2013). An improved method for applying the lockhart–martinelli correlation to three-phase gas–liquid–solid horizontal pipeline flows. *The Canadian Journal of Chemical Engineering*, *91*(8), 1372-1382.

Rahman, M. A., Heidrick, T., and Fleck, B. A. (2009). A Critical Review of Advanced Experimental Techniques to Measure Two- Phase Gas/Liquid Flow. *Open Fuels and Energy Science Journal*, *2*, 54-70.

Rahman, M. A., Mustafiz, S., Biazar, J., Koksal, M., and Islam, M. R. (2007). Investigation of a novel perforation technique in petroleum wells—perforation by drilling. *Journal of the Franklin Institute*, *344*(5), 777-789.

Ranck, J. M., Bowman, R. S., Weeber, J. L., Katz, L. E., and Sullivan, E. J. (2005). BTEX removal from produced water using surfactant-modified zeolite. *Journal of Environmental Engineering*, *131*(3), 434-442.

Ranieri, E., Gikas, P., and Tchobanoglous, G. (2013). BTEX removal in pilot-scale horizontal subsurface flow constructed wetlands. *Desalination and Water Treatment*, *51*(13-15), 3032–3039.

Rao, S. M., Joshua, R. E., and Arkenadan, L. (2017). BTEX contamination of Bengaluru aquifers, Karnataka, India. *Journal of Environmental Engineering and Science*, *12*(3), 56-61.

Raoof, A., and Hassanizadeh, S. M. (2012). A new formulation for pore-network modeling of two-phase flow. *Water Resources Research*, *48*(1).

Raoof, A., and Hassanizadeh, S. M. (2013). Saturation-dependent solute dispersivity in porous media: pore-scale processes. *Water Resources Research*, *49*(4), 1943-1951.

Reardon, K. F., Mosteller, D. C., and Bull Rogers, J. D. (2000). Biodegradation kinetics of benzene, toluene, and phenol as single and mixed substrates for Pseudomonas putida F 1. *Biotechnology and Bioengineering*, *69*(4), 385-400.

Rifai, H. S., Newell, C. J., Gonzales, J. R., and Wilson, J. T. (2000). Modeling natural attenuation of fuels with BIOPLUME III. *Journal of Environmental Engineering*, *126*(5), 428-438.

Rifai, H. S., Rittaler, T., (2005). Modeling natural attenuation of benzene with analytical and numerical models. *Biodegradation*. 16, 291–304.

Rifai, H.S., Newell, C.J., Gonzales, J.R., Dendrou, S., Kennedy, L., Wilson, J.T., (1997). BIOPLUME III Natural Attenuation Decision Support System, Version 1.0, User's Manual. Air Force Center for Environmental Excellence (AFCEE), San Antonio.

Rivett, M.O., Wealthall, G.P., Dearden, R.A., McAlary, T.A., (2011). Review of unsaturated-zone transport and attenuation of volatile organic compound (VOC) plumes leached from shallow source zones. *Journal of Contaminant Hydrology*, 123, 130e156.

Rizzo, A., and Langergraber, G. (2016). Novel insights on the response of horizontal flow constructed wetlands to sudden changes of influent organic load: A modeling study. *Ecological Engineering*, *93*, 242-249.

Robledo-Ortíz, J. R., Ramírez-Arreola, D. E., Pérez-Fonseca, A. A., Gómez, C., González-Reynoso, O., Ramos-Quirarte, J., and González-Núñez, R. (2011). Benzene, toluene, and o-xylene degradation by free and immobilized P. putida F1 of postconsumer agave-fiber/polymer foamed composites. *International Biodeterioration and Biodegradation*, *65*(3), 539-546.

Röling, Wilfred F. M. et al. (2002). Robust Hydrocarbon Degradation and Dynamics of Bacterial Communities during Nutrient-Enhanced Oil Spill Bioremediation. *Applied and Environmental Microbiology,* 68.11: 5537–5548. PMC. Web. 9 Oct. 2016.

Rolle, M., Eberhardt, C., Chiogna, G., Cirpka, O. A., and Grathwohl, P., (2009). Enhancement of dilution and transverse reactive mixing in porous media: Experiments and model-based interpretation. *Journal of Contaminant Hydrology*, 110(3-4), 130-142.

Saba, T., Illangasekare, T. H., and Ewing, J. (2001). Investigation of surfactant-enhanced dissolution of entrapped nonaqueous phase liquid chemicals in a two-dimensional groundwater flow field. *Journal of Contaminant Hydrology*, *51*(1-2), 63-82.

Saba, T.A., Illangasekare, T.H., (2000). Effect of ground-water flow dimensionality on mass transfer from entrapped nonaqueous phase liquid contaminants. *Water Resource Research*, 36 (4), 971 – 979.

Sahoo, S., and Jha, M. K. (2013). Groundwater-level prediction using multiple linear regression and artificial neural network techniques: a comparative assessment. *Hydrogeology Journal*, *21*(8), 1865-1887.

Saien, J., and Shahrezaei, F. (2012). Organic pollutants removal from petroleum refinery wastewater with nanotitania photocatalyst and UV light emission. *International Journal of Photoenergy*, *2012*.

Sarikurt, D. A., Gokdemir, C., and Copty, N. K. (2017). Sherwood correlation for dissolution of pooled NAPL in porous media. *Journal of Contaminant Hydrology*, *206*, 67-74.

Schnoor, J. L., Light, L. A., McCutcheon, S. C., Wolfe, N. L., and Carreia, L. H. (1995). Phytoremediation of organic and nutrient contaminants. *Environmental Science and Technology*, 29(7), 318A-323A.

Seagren, E.A., B.E., Rittmann, and A.J., Valocchi. (1999). An experimental investigation of NAPL pool dissolution enhancement by flushing. *Journal of Contaminant Hydrology*, 37(1–2) 111–137.

Seeger, E. M., Kuschk, P., Fazekas, H., Grathwohl, P., and Kaestner, M. (2011). Bioremediation of benzene-, MTBE-and ammonia-contaminated groundwater with pilot-scale constructed wetlands. *Environmental Pollution*, *159*(12), 3769-3776.

Seeger, E. M., Maier, U., Grathwohl, P., Kuschk, P., and Kaestner, M. (2013). Performance evaluation of different horizontal subsurface flow wetland types by characterization of flow behavior, mass removal and depth-dependent contaminant load. *Water Research*, *47*(2), 769-780.

Shaw, L. J., and Burns, R. G. (2003). Biodegradation of organic pollutants in the rhizosphere. *Advances in Applied Microbiology*, *53*, 1-60.

Shieh, H. J., Peralta, R.C. (2005). Optimal in situ bioremediation design by hybrid genetic algorithm-simulated annealing. *Journal of Water Resources Planning and Management*, 131 (1), 67–78.

Shim, H., and Yang, S. T. (1999). Biodegradation of benzene, toluene, ethylbenzene, and o-xylene by a coculture of Pseudomonas putida and *Pseudomonas fluorescens* immobilized in a fibrous-bed bioreactor. *Journal of Biotechnology*, *67*(2-3), 99-112.

Shimp ,J. F. J. C., Tracy, L. C., Davis, E., Lee, W., Huang , L. E., Erickson, and J. L., Schnoor. (1993): Beneficial effects of plants in the remediation of soil and groundwater

contaminated with organic materials, *Critical Reviews in Environmental Science and Technology*, 23:1, 41-77.

Shpiner, R., Liu, G., and Stuckey, D. C. (2009). Treatment of oilfield produced water by waste stabilization ponds: Biodegradation of petroleum-derived materials. *Bioresource Technology*, *100*(24), 6229-6235.

Shuai, X., Green, T. R., Ray, C., and Syrmos, V. L. (2014). Multisection transmission line scatter function theory for measurements of soil dielectric properties. *Soil Science Society of America Journal*, *78*(4), 1139-1145.

Šimůnek, J., M. Šejna, and M.Th. van Genuchten, (2011). The HYDRUS software package for simulating the two- and three-dimensional movement of water, heat, and multiple solutes in variably-saturated media. Tech. Manual, Version 2.0. PC-Progress, Prague, Czech Republic.

Simunek, J., T., Vogel, and M.Th., van Genuchten. (1996). HYDRUS-2D code for simulating water fl ow and solute transport in two-dimensional variably saturated media. Version 1.0. USDA/ARS, U.S. Salinity Lab., Riverside, CA.

Šimůnek, J., Van Genuchten, M. T., and Šejna, M. (2006). The HYDRUS software package for simulating two-and three-dimensional movement of water, heat, and multiple solutes in variably-saturated media. *Technical Manual, Version 1*, 241.

Singh, R. K., Datta, M., and Nema, A. K. (2011). Factoring site age in evaluation of groundwater-contamination hazard rating of abandoned municipal solid-waste landfill sites. *Journal of Environmental Engineering*, 137(11), 1092-1098.

Soga, K., Page, J. W. E., and Illangasekare, T. H. (2004). A review of NAPL source zone remediation efficiency and the mass flux approach. *Journal of Hazardous Materials*, *110*(1-3), 13–27.

Sookhak Lari, K., Davis, G.B., Johnston, C.D. (2016a). Incorporating hysteresis in a multi-phase multi-component NAPL modelling framework; a multi-component LNAPL gasoline example. *Advances in Water Resource*, 96:190-201.

Søvik, A. K., Alfnes, E., Breedveld, G. D., French, H. K., Pedersen, T. S., and Aagaard, P. (2002). Transport and degradation of toluene and o-xylene in an unsaturated soil with dipping sedimentary layers. *Journal of Environmental Quality*, *31*(6), 1809-1823.

Srivastava, P., Sreekrishnan, T. R., and Nema, A. K. (2018). Polyaromatic Hydrocarbons: Review of a Global Environmental Issue. *Journal of Hazardous, Toxic, and Radioactive Waste*, *22*(3), 04018004.

Stefanakis, A. I., Seeger, E., Dorer, C., Sinke, A., and Thullner, M. (2016). Performance of pilot-scale horizontal subsurface flow constructed wetlands treating groundwater

contaminated with phenols and petroleum derivatives. *Ecological Engineering*, *95*, 514-526.

Sudrajat, H., Babel, S., Sakai, H., and Takizawa, S. (2016). Rapid enhanced photocatalytic degradation of dyes using novel N-doped ZrO2. *Journal of Environmental Management*, *165*, 224-234.

Sulaymon, A., and H.A., Gzar. (2011). Experimental investigation and numerical modelling of light non-aqueous phase liquid dissolution and transport in a saturated zone of the soil. *Journal of Hazardous Materials*, 186, 1601–1614.

Susarla, S., Medina, V. F., and McCutcheon, S. C. (2002). Phytoremediation: An ecological solution to organic chemical contamination. *Ecological Engineering*, *18*(5), 647–658.

Sushkova, S., Deryabkina, I., Antonenko, E., Kizilkaya, R., Rajput, V., and Vasilyeva, G. (2018). Benzo [a] pyrene degradation and bioaccumulation in soil-plant system under artificial contamination. *Science of The Total Environment*, *633*, 1386-1391.

Suthersan, S., Koons, B., Schnobrich, M., (2015). Contemporary management of sites with petroleum LNAPL presence. *Ground Water Monitoring and Remediation*, 35(1):23-29.

Tindall, J. A., Friedel, M. J., Szmajter, R. J., and Cuffin, S. M. (2005). Part 1: Vadose-zone column studies of toluene (enhanced bioremediation) in a shallow unconfined aquifer. *Water, Air, and Soil Pollution*, *168*(1-4), 325-357.

Tobiszewski, M., Tsakovski, S., Simeonov, V., and Namieśnik, J. (2012). Chlorinated solvents in a petrochemical wastewater treatment plant: An assessment of their removal using self-organising maps. *Chemosphere*, *87*(8), 962-968.

Tomlinson, D., Thornton, S., Thomas, A., Leharne, S., and Wealthall, G. (2015). An Illustrated Handbook of LNAPL Transport and Fate in the Subsurface. *Environment Agency: Bristol, UK*.

Tormoehlen, L. M., Tekulve, K. J., and Nanagas, K. A. (2014). Hydrocarbon toxicity: a review. *Clinical toxicology*, *52*(5), 479-489.

U.S. Environmental Protection Agency (2006a). In situ and ex situ biodegradation technologies for remediation of contaminated sites. EPA/625/R-06/015.

U.S. Environmental Protection Agency (2006b). Edition of the Drinking Water Standards and Health Advisories. EPA/822/R0, p.18.

Valsala, R., and Govindarajan, S. K. (2018). Interaction of dissolution, sorption and biodegradation on transport of BTEX in a saturated groundwater system: Numerical modeling and spatial moment analysis. *Journal of Earth System Science*, *127*(4), 53.

van Afferden, M., Rahman, K. Z., Mosig, P., De Biase, C., Thullner, M., Oswald, S. E., and Müller, R. A. (2011). Remediation of groundwater contaminated with MTBE and benzene: the potential of vertical-flow soil filter systems. *Water Research*, *45*(16), 5063-5074.

Van Genuchten, M. T. (1980). A closed-form equation for predicting the hydraulic conductivity of unsaturated soils 1. *Soil Science Society of America Journal*, *44*(5), 892-898.

Van Stempvoort, D., and Biggar, K. (2008). Potential for bioremediation of petroleum hydrocarbons in groundwater under cold climate conditions: A review. *Cold Regions Science and Technology*, *53*(1), 16-41.

Vasudevan, M., G., Suresh Kumar, N., and Indumathi M. (2014). Numerical study on kinetic/equilibrium behaviour of dissolution of toluene under variable subsurface conditions". *European Journal of Environmental and Civil Engineering,* 18(9), pp.1070–1093.

Vasudevan, M., Kumar, G. S., and Nambi, I. M. (2015). Numerical studies on kinetics of sorption and dissolution and their interactions for estimating mass removal of toluene from entrapped soil pores. *Arabian Journal of Geosciences*, *8*(9), 6895-6910.

Vogt, C., Gödeke, S., Treutler, H. C., Weiß, H., Schirmer, M., and Richnow, H. H. (2007). Benzene oxidation under sulfate-reducing conditions in columns simulating in situ conditions. *Biodegradation*, *18*(5), 625-636.

Voudrias, E.A., and Yeh, M.-F. (1994). Dissolution of a toluene pool under constant and variable hydraulic gradients with implications for aquifer remediation. *Groundwater*, 32(2), pp.305–311.

Vymazal, J. (2005a). Horizontal sub-surface flow and hybrid constructed wetlands systems for wastewater treatment. *Ecological Engineering*, *25*(5), 478-490.

Vymazal, J. (2009). The use constructed wetlands with horizontal sub-surface flow for various types of wastewater. *Ecological Engineering*, *35*(1), 1–17.

Wang, G., Reckhorn S. P. F., Grathwohl, P. (2003). Volatile organic compounds volatilization from multicomponent organic liquids and diffusion in unsaturated porous media. *Vadose Zone Journal*. 2, 692–701.

Wang, M., and C., Zheng. (1998). Ground water management optimization using genetic algorithms and simulated annealing. *Journal of the American Water Resources Association*, 34(3), 519-530.

Weast, R., and Astle, M. (1981). CRC Handbook of chemistry and physics. CRC Press, Florida

Wipfler, E. L., Ness, M., Breedveld, G. D., Marsman, A., and Van Der Zee, S. E. A. T. M. (2004). Infiltration and redistribution of LNAPL into unsaturated layered porous media. *Journal of Contaminant Hydrology*, *71*(1-4), 47-66.

Wipfler, E.L., van der Zee, S.E.A.T.M. (2001). A set of constitutive relationships accounting for residual NAPL in the unsaturated zone. *Journal of Contaminant Hydrology*, 50: 53-77.

Wolicka, D., Suszek, A., Borkowski, A., and Bielecka, A. (2009). Application of aerobic microorganisms in bioremediation in situ of soil contaminated by petroleum products. *Bioresource Technology*, *100*(13), 3221-3227.

Yadav B.K. and Hassanizadeh S.M., (2011). An overview of biodegradation of LNAPLs in coastal (semi)-arid environment. *Water Air Soil Pollution*. 220, 225-239.

Yadav, B. K., and Mathur, S. (2008). Modeling soil water uptake by plants using nonlinear dynamic root density distribution function. *Journal of Irrigation and Drainage Engineering*, 134(4), 430-436.

Yadav, B. K., Mathur, S., and Siebel, M. A. (2009). Soil moisture flow modelling with water uptake by plants (wheat) under varying soil and moisture conditions. *Journal of Irrigation and Drainage Engineering*, *135*(3), 375-381.

Yadav, B. K., Shrestha, S. R., and Hassanizadeh, S. M. (2012). Biodegradation of toluene under seasonal and diurnal fluctuations of soil-water temperature. *Water, Air, and Soil Pollution*, *223*(7), 3579-3588.

Yadav, B., Ch., S., Mathur, S., and Adamowski, J. (2016). Estimation of in-situ bioremediation system cost using a hybrid Extreme Learning Machine (ELM)-particle swarm optimization approach. *Journal of Hydrology*, *543*, 373-385.

Yadav, B., Mathur, S., Ch., Sudheer, Yadav, B. K. (2017). A simulation-optimization approach for the consideration of well clogging during cost estimation of in-situ bioremediation system. *Journal of Hydrologic Engineering*, doi:10.1061/(ASCE)HE.1943-5584.0001622.

Yadav, B.K., Ansari, F.A., Basu, S., Mathur, A. (2013). Remediation of LNAPL contaminated groundwater using plant-assisted biostimulation and bioaugmentation Methods. *Water Air Soil Pollution*. 225, 1793.

Yadav, B.K., Siebel, M.A., and van Bruggen, J.J.A. (2011). Rhizofiltration of a Heavy Metal (Lead) Containing Wastewater Using the Wetland Plant *Carex pendula*. *CLEAN - Soil, Air, Water* 39:467–474.

Yang, Y., Li, J., Xi, B., Wang, Y., Tang, J., Wang, Y., and Zhao, C. (2017). Modeling BTEX migration with soil vapor extraction remediation under low-temperature conditions. *Journal of Environmental Management*, *203*, 114-122.

Yoon, J. H., and Shoemaker, C. A. (1999). Comparison of optimization methods for ground-water bioremediation. *Journal of Water Resources Planning and Management*, *125*(1), 54-63.

Zhang, Q., Wang, G., Sugiura, N., Utsumi, M., Zhang, Z., and Yang, Y. (2014). Distribution of petroleum hydrocarbons in soils and the underlying unsaturated subsurface at an abandoned petrochemical site, North China. *Hydrological Processes*, *28*(4), 2185-2191.

Zhao, Y., Qu, D., Hou, Z., and Zhou, R. (2015). Enhanced natural attenuation of BTEX in the nitrate-reducing environment by different electron acceptors. *Environmental Technology*, *36*(5), 615-621.

Zheng, Z., Aagaard, P., and Breedveld, G. D. (2002). Sorption and anaerobic biodegradation of soluble aromatic compounds during groundwater transport. 1. Laboratory column experiments. *Environmental Geology*, *41*(8), 922-932.

Zhou, A. X., Zhang, Y. L., Dong, T. Z., Lin, X. Y., and Su, X. S. (2015). Response of the microbial community to seasonal groundwater level fluctuations in petroleum hydrocarbon-contaminated groundwater. *Environmental Science and Pollution Research*, *22*(13), 10094-10106.

Publications

Journals

1. Gupta P.K, Yadav B.K., (2018). "Thermally enhanced biodegradation of dissolved plume originated from pooled LNAPL in subsurface". ***Science of the Total Environment*** (Drafted).

2. Gupta P.K, Yadav B., Yadav B.K., Mathur S., (2018) "Biodegradation system design using a simulation-optimization approach for LNAPL polluted vadose zone along with saturated zone". ***Journal of Contaminant Hydrology*** (In development).

3. Gupta P.K, Yadav B., Yadav B.K., (2018). "Assessment of LNAPL in Subsurface under Fluctuating Groundwater Table using 2D Sand Tank Experiments". ***ASCE Journal of Environmental Engineering*** (Under Review)

4. Gupta P.K, Yadav B.K., (2018). "3D Sand Tank Experiments for Investigating Behavior of LNAPL in Subsurface under Varying Groundwater Flow Regimes". ***Journal of Environmental Quality*** (Under Review).

5. Mustapha I.H., Gupta P.K., Yadav B.K., J.J.A van Bruggen and P. N. L. Lens, (2018). "Performance evaluation of duplex constructed wetlands for the treatment of diesel contaminated wastewater". ***Chemosphere***, https://doi.org/10.1016/j.chemosphere.2018.04.036.

Book Chapters

1. Gupta P.K., Yadav B.K. (2018), "Impact of climatic variability on subsurface water resources". ***In Climate Change and Hydrology-Science, Impacts and Adaptation*** to be published by Springer. (Ed. Dr. Devesh Sharma: Accepted)

2. Gupta P.K., Abhishek, Yadav B.K., (2018), "Impact of hydrocarbon pollutants on partially saturated soil media in batch system: Morphological analysis using SEM techniques". Chapter 5, ***In Water Quality Management; Water Science and Technology Library***, ISBN: 978-981-10-5794-6, Vol. 79, Springer (Eds. V.P. Singh, S. Yadav, R.N. Yadava)

3. Gupta P.K and Yadav B.K., (2017). "Bioremediation of Non-Aqueous Phase Liquids (NAPLS) Polluted Soil and Water Resources". Chapter 8, In ***Environmental Pollutants and their Bioremediation Approaches***, ISBN 9781138628892, CRC Press, Taylor and Francis Group, Florida, USA. (Ed. Dr. R.N.Bhargava).

4. Gupta P.K., Yadav B.K., (2017), "Effects of climatic variation on dissolution of LNAPL pollutants in subsurface environment". Chapter 8, In ***Climate Change Resource Conservation and Sustainability Strategies***, ISBN 9789384871086, DBH Publishers and Distributors, New Delhi. (Ed. Prof. Anubha Kaushik).

Conference proceedings / Presentations

1. Gupta, P.K., Yadav B., Yadav, B.K., (2018). Performance evaluation of in-situ bioremediation system design for toluene polluted subsurface zones under varying soil moisture and temperature conditions. Submitted to AGU Fall Meeting 2018 to be held in Washington DC during 10-14 Dec 2018.

2. Abhishek, Gupta, P.K., Yadav, B.K., Amandeep, Tomar A.S., Kataria, S., Kumar S., (2018). Phytoremediation of toluene polluted groundwater under nutrient loading using constructed wetland. Submitted to AGU Fall Meeting 2018 to be held in Washington DC during 10-14 Dec 2018.

3. Gupta, P.K., Yadav B., Yadav, B.K., (2018). Transport of LNAPL and biofilm growth in subsurface under dynamic groundwater conditions. C001723-Oral presentation in Japan Geoscience Union (JpGU) Chiba-city, Japan, May 20-24 2018.

4. Abhishek, Yadav, B.K., Gupta, P. K., (2018). Morphological Variations in Unsaturated Porous Media due to LNAPL Contamination. Poster in Japan Geoscience Union (JpGU) Chiba-city, Japan, May 20-24 2018.

5. Gupta P.K. and Yadav B.K., (2018), "Modeling dissolution of light non-aqueous phase liquids in subsurface". International Conference on Sustainable Technologies for Intelligent Water Management (STIWM-2018), Feb 16-19, 2018, IIT Roorkee. (Abstract ID: 312).

6. Gupta P.K. and Yadav B.K., (2017), "Role of climatic variability on fate and transport of LNAPL pollutants in subsurface". Session H060: Groundwater Response to Climate Change and Variability, AGU Fall Meeting 2017, New Orleans, USA. (Abstract ID: 220494).

7. Gupta P.K. and Yadav B.K.*, (2017), "Modelling Dissolution of Light Non-Aqueous Phase Liquid (LNAPL) Under Varying Subsurface Flow Conditions". 7th International Groundwater Conferences on Groundwater Vision 2030 (IGWC 2017), December 11-13, New Delhi. (*Corresponding author).

8. Gupta P.K., Yadav B.K., Hassanizadeh S.M., (2017), "Engineered bioremediation of LNAPL polluted soil-water resources under changing climatic conditions". Proceedings of International Conference on Modeling of environmental and water resources systems (ICMEWRS-2017), HBTU Kanpur, 24-26th March, 2017 (ISBN 978-93-85926-53-2).

9. Gupta P.K., Yadav B.K., (2017), "Effects of climatic variation on dissolution of LNAPL pollutants in subsurface environment". Proceedings of National Conference on Climate Change Resource Conservation and Sustainability Strategies: 2017, Guru Gobind Singh Indraprastha University, New Delhi, 16th-17th March, 2017.

10. Yadav B.K., and Gupta P.K., (2016), "Role of groundwater variation on biodegradation and transport of LNAPL pollutants in subsurface". Proceedings of Water Security and Climate Change: Challenges and Opportunities in Asia, Asian Institute of Technology, Bangkok, Thailand, 29 Nov.-01 December, 2016 (Ref.No.G118).

11. Gupta P.K., Yadav B.K., (2016), "Transport of light non-aqueous phase liquids (LNAPLs) under varying subsurface flow conditions". Proceedings of International Conference on Strategies for Environmental Protection and Management (ICSEPM 2016), JNU New Delhi, 11-13 Dec., 2016, p-21-22.

12. Gupta P.K., Yadav B.K., (2016), "Fate and transport of toluene in subsurface under two-dimensional large scale laboratory experiments". Proceedings of Indian National Groundwater Conference (INGWC 2016), Centre for Water Resources, JNTU Hyderabad and AGGS, India, October 5-7, 2016, 440-444, (ISBN 9789352301492).

13. Gupta P.K., Yadav B.K., (2015), "Large scale laboratory investigation and simulation of fate and transport of LNAPL plume in variably saturated subsurface". Proceedings of HYDRO-2015, 20th International Conference on Hydraulics, Water Resources and River Engineering, IIT Roorkee, 17-19 Dec, 2015. (HYD-330).

Hindi Articles

1. पेट्रोकेमिकल प्रदूषित भूजल क्षेत्र के लिए जैविक उपचार, जल चेतना, खंड-6, अंक-2, जुलाई 2017